

August 2022

## Inducible DNA Interstrand Cross-linking Agents: Design, Synthesis, Mechanism, and Biomedical Applications

Muhammad Asad Uz Zaman  
*University of Wisconsin-Milwaukee*

Follow this and additional works at: <https://dc.uwm.edu/etd>

 Part of the [Organic Chemistry Commons](#)

---

### Recommended Citation

Zaman, Muhammad Asad Uz, "Inducible DNA Interstrand Cross-linking Agents: Design, Synthesis, Mechanism, and Biomedical Applications" (2022). *Theses and Dissertations*. 3094.  
<https://dc.uwm.edu/etd/3094>

This Dissertation is brought to you for free and open access by UWM Digital Commons. It has been accepted for inclusion in Theses and Dissertations by an authorized administrator of UWM Digital Commons. For more information, please contact [scholarlycommunicationteam-group@uwm.edu](mailto:scholarlycommunicationteam-group@uwm.edu).

INDUCIBLE DNA INTERSTRAND CROSS-LINKING AGENTS: DESIGN, SYNTHESIS,  
MECHANISM, AND BIOMEDICAL APPLICATIONS

by

Muhammad Asad Uz Zaman

A Dissertation Submitted in  
Partial Fulfillment of the  
Requirements for the Degree of

Doctor of Philosophy  
in Chemistry

at

The University of Wisconsin-Milwaukee

August 2022

## ABSTRACT

### INDUCIBLE DNA INTERSTRAND CROSS-LINKING AGENTS: DESIGN, SYNTHESIS, MECHANISM, AND BIOMEDICAL APPLICATIONS

by

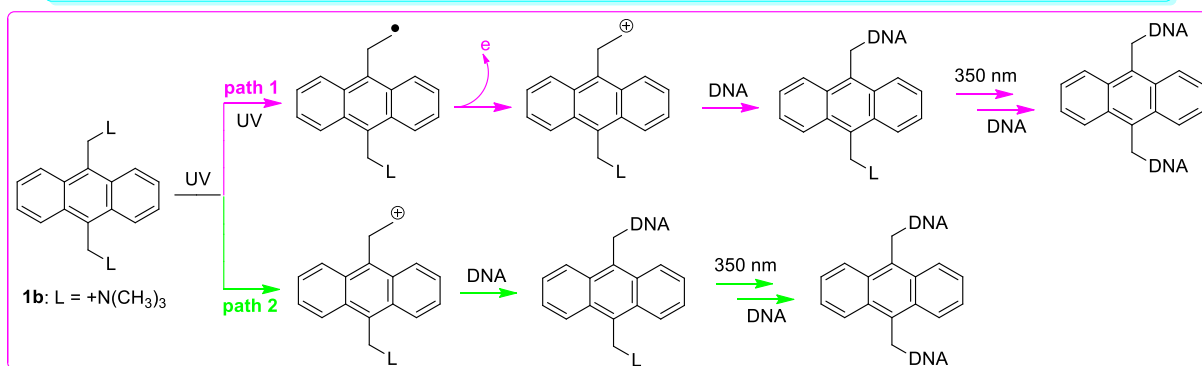
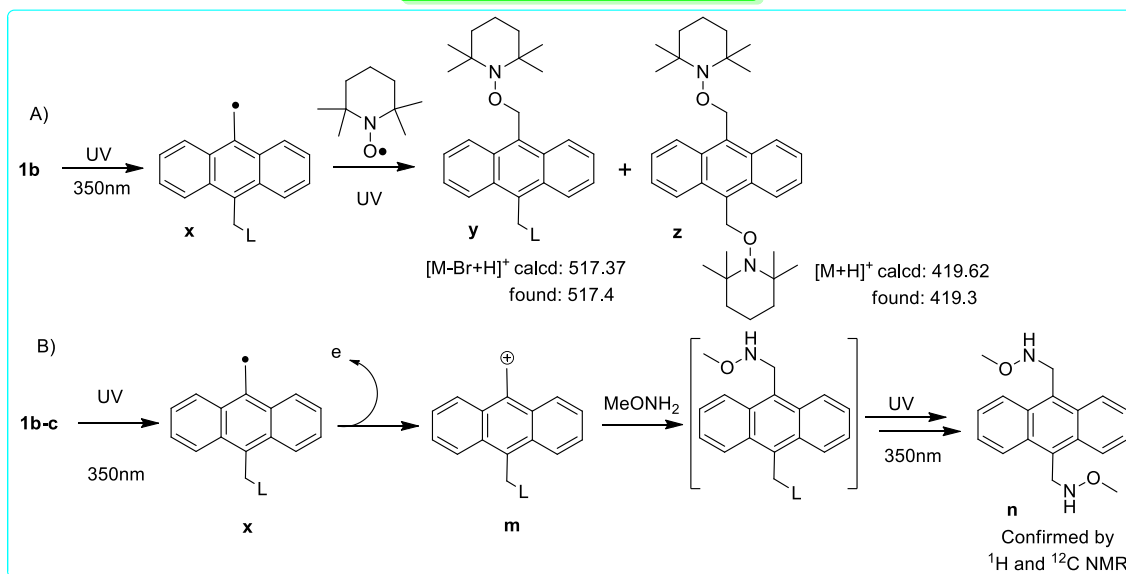
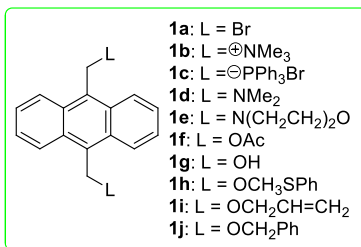
Muhammad Asad Uz Zaman

The University of Wisconsin-Milwaukee, 2022  
Under the Supervision of Professor Xioahua Peng

DNA is the carrier of genetic information, making its chemical reactivity and function extremely important. DNA interstrand cross-links (ICL) leads to covalent bind of two strands, which prevents the separation of double helix. DNA ICLs are the sources of the cytotoxicity of antitumor and anticancer agents. This thesis focuses on investigating the reactivity of a varieties of aromatic compounds towards DNA. Some of these molecules can be activated by photo irradiation to induce DNA ICL formation via alkylation. Others undergo activation by H<sub>2</sub>O<sub>2</sub> to release DNA cross-linking agents. We investigated the mechanism of function of these inducible DNA cross-linking agents as well as their biomedical application.

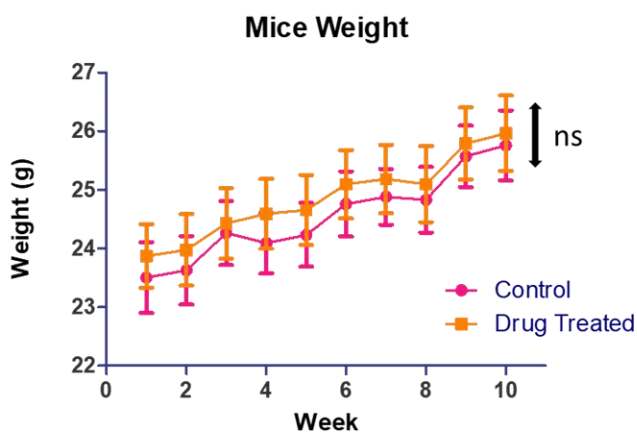
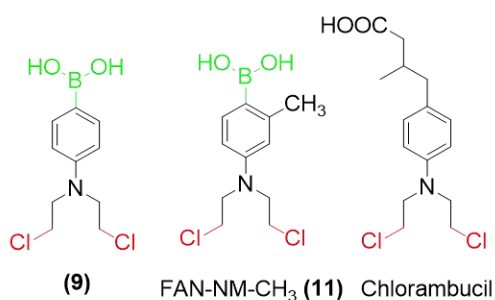
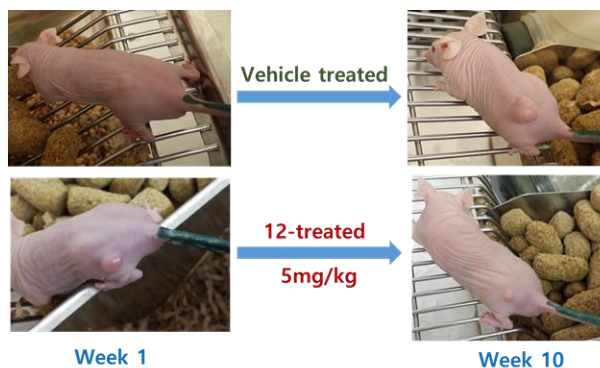
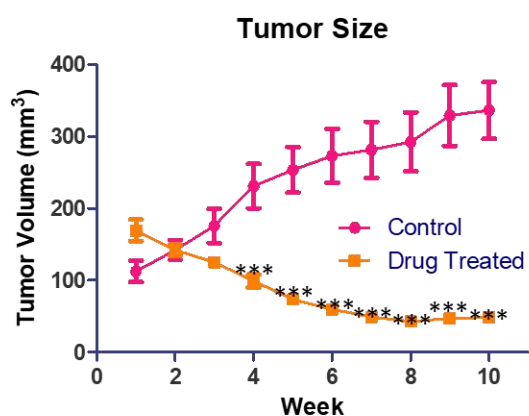
The first part of this thesis is focusing on design, synthesis, and mechanism investigation of the anthracene analogues as photo-inducible DNA cross-linking agents. In an effort to increase the efficiency of photo-inducible DNA cross-linking formation by bifunctional aromatic compounds for biological applications, we used a well-known DNA intercalator anthracene for this study. We synthesized a series of bifunctional compounds containing the 9,10-anthryl core structure, and various benzylic leaving groups and investigated their photo reactivity towards DNA at 350 nm. The efficiency of DNA ICL formation strongly depends on the leaving groups and compound solubility. Compounds **1a-c** with bromo, trimethyl ammonium salts or triphenyl phosphonium salts as leaving groups showed faster reaction rate and higher DNA cross-linking

efficiency than the remaining compounds. Compounds containing amine (**1d** and **1e**), acetate (**1f**), or ether groups (**1g-j**) as leaving groups showed very low DNA ICL efficiency and low reaction rate. DNA ICL formation induced by **1b** was inhibited by both radical and cation trapping agents, indicating that both free radicals and cations are involved in DNA cross-linking process. However, none of the trapping agents was able to inhibit ICL completely even with very high concentration, which might be due to the intercalating interaction between anthracene moiety and duplex DNA. The free radical trapping adducts **y-z** were detected in the photoreaction of **1b** with TEMPO, suggesting the generation of free radicals **x** in photo-induced DNA cross-linking process of **1b-z**. We also observed formation the cation trapping adducts **n** that provide direct evidence for the generation of carbocation **m** in the photo-induced DNA ICL formation induced by **1b-c**. Collectively, these data suggested that both both free radicals and carbo cations may have been involved in photo-induced DNA ICL formation by these anthracene analogues.



The second part of this thesis is focusing on *in vivo* study of H<sub>2</sub>O<sub>2</sub>-activated DNA alkylating agents. We investigated the *in vivo* efficacy and safety of H<sub>2</sub>O<sub>2</sub>-activated nitrogen mustard prodrug **11**. The CD-1 mice and athymic nude mice were used for the safety and *in vivo* efficacy study, respectively. We tested the cytotoxicity of **11** against triple negative breast cancer cell line (MDA-MB-468) and a few renal cancer cell lines (UO-31, SN-12C, A498, TK-10 and CAKI-1). Repeated dose toxicity study was used to identify the safe doses for *in-vivo* efficacy study. The athymic nude mice were xenografted with MDA-MB-468 breast cancer cell line. We observed

that **11** greatly reduced tumor size (>50%) without any obvious side effects such as no obvious weight loss and other unusual behaviors for mice. We did not observe the changes of normal tissues including lung, liver, spleen, brain etc. Pharmacokinetic study showed that duration time of **11** is double of the parent molecule x. In addition, we observed that **11** showed better efficacy but less toxic to mice than the clinically used DNA alkylating agent chlorambucil. Further study suggested that the breast cancer MDA-MB-468 cells showed high H<sub>2</sub>O<sub>2</sub> level and quenching the H<sub>2</sub>O<sub>2</sub> level decreased the anticancer activity of **11**, which indicated that there is a correlation between the anticancer activity of **11** and ROS level in cancer cells. Metabolite extraction study was also conducted on cell culture in an effort to identify activated metabolite.



© Copyright by Muhammad Asad Uz Zaman, 2022  
All Rights Reserved

## TABLE OF CONTENTS

|   |             |
|---|-------------|
| <b>LIST OF FIGURES .....</b>  | <b>ix</b>   |
| <b>LIST OF TABLES .....</b>   | <b>x</b>    |
| <b>LIST OF ABBREVIATIONS .....</b>  | <b>xi</b>   |
| <b>LIST OF SCHEMES.....</b>   | <b>xiii</b> |
| <b>ACKNOWLEDGEMENTS.....</b>  | <b>xv</b>   |
| <b>Chapter 1. Introduction .....</b>  | <b>1</b>    |
| <b>1.1 The structure and functions of DNA.....</b>  | <b>1</b>    |
| <b>1.2 DNA alkylating agents.....</b>   | <b>2</b>    |
| <b>1.3 DNA intercalating agents.....</b>  | <b>7</b>    |
| 1.3.1 Anthracene intercalator and it's derivatives .....  | 8           |
| 1.3.2 Anthracene derivatives used for DNA photo-cleavage studies .....  | 10          |
| 1.3.3 Anthracene derivatives used for DNA binding studies. ....   | 11          |
| 1.3.4 Application of Anthracene derivatives. ....   | 14          |
| <b>1.4 Photosensitive DNA cross-linking agents and their mechanism .....</b>  | <b>16</b>   |
| <b>1.5 DNA Interstrand Cross-linking Induced by Chemical Agents.....</b>  | <b>19</b>   |
| <b>1.6 Reference .....</b>  | <b>26</b>   |
| <b>Chapter 2. Photo-induced DNA interstrand cross-link formation with anthracene as core structure. 30</b>                  |             |
| <b>2.1 Introduction .....</b>   | <b>30</b>   |
| <b>2.2 Anthracene analogues as Photo-inducible DNA Cross-linking Agents .....</b>   | <b>31</b>   |
| 2.2.1 Synthesis of 9, 10-anthryl derivatives contain various leaving groups .....   | 31          |
| 2.2.2 Preparation of DNA Duplex.....  | 34          |
| 2.2.3 DNA interstrand cross-linking assay .....   | 37          |
| <b>2.3 Mechanism of DNA ICL formation and leaving groups effects. ....</b>  | <b>48</b>   |
| 2.3.1 Correlation between UV absorbance and the photo-reactivity.....   | 48          |
| 2.3.2 The effect of the free radical and cation trapping agents on DNA cross-link formation .....                           | 50          |
| 2.3.3 Determination of DNA alkylation sites .....   | 54          |
| <b>2.4 Conclusions .....</b>  | <b>61</b>   |
| <b>2.5 Experiment Section.....</b>  | <b>61</b>   |
| <b>2.6 Reference .....</b>  | <b>69</b>   |
| <b>2.7 Appendix A: Phosphor Image Autoradiograms.....</b>   | <b>70</b>   |
| <b>2.8 Appendix B: Characterization of compounds.....</b>   | <b>91</b>   |
| <b>Chapter 3. In vivo efficacy and selectivity of hydrogen peroxide activated DNA interstrand cross-linking agents.....</b> | <b>114</b>  |
| <b>3.1 Introduction .....</b>   | <b>114</b>  |
| 3.1.1 Reactive oxygen species as activator for prodrug .....  | 114         |



|            |   |            |
|------------|---|------------|
| 3.1.2      | H <sub>2</sub> O <sub>2</sub> -Activated Nitrogen Mustard Precursors .....  | 115        |
| <b>3.2</b> | <b><i>In-vitro</i> toxicity study .....</b>   | <b>118</b> |
| 3.2.1      | Concentration Dependent Cytotoxicity Study. ....  | 118        |
| 3.2.2      | Time Dependent Cytotoxicity Study. ....   | 120        |
| 3.2.3      | MDA-MB-468 Cell Produced a High Level of H <sub>2</sub> O <sub>2</sub> . ....                                     | 121        |
| 3.2.4      | Cytotoxicity inhibition study using ROS blocker. ....   | 122        |
| <b>3.3</b> | <b><i>In-vitro</i> efficacy and selectivity of ROS-activate prodrugs .....</b>                                    | <b>123</b> |
| 3.3.1      | Safety Study with CD-1 Mice.....  | 123        |
| <b>3.4</b> | <b><i>In vivo</i> efficacy study with athymic nude mice xenografted with breast cancer cell lineMDA-MB-468125</b> |            |
| 3.4.1      | Pharmacokinetics and Stability.....   | 128        |
| 3.4.2      | Detection of Drug Metabolites in Cell Culture.....  | 131        |
| <b>3.5</b> | <b>Conclusion .....</b>   | <b>134</b> |
| <b>3.6</b> | <b>Experiment protocol .....</b>  | <b>136</b> |
| 3.6.1      | Protocol for cell preparation.....  | 136        |
| 3.6.2      | Protocol for cell injection to nude mice.....   | 139        |
| 3.6.3      | Protocol for compound injection to nude mice .....  | 140        |
| 3.6.4      | Protocol for Cytotoxicity Assay .....   | 140        |
| 3.6.5      | Extracellular Reactive Oxygen Species Detection Assay .....   | 142        |
| 3.6.6      | Protocol for Inhibition of Cytotoxicity Study Using ROS Production Blocker .....                                  | 143        |
| 3.6.7      | Protocol for Drug Metabolite Extraction to Detect Transformation. ....  | 144        |
| 3.6.8      | Blood Pharmacokinetics and LC-MS/MS Analysis.....   | 144        |
| 3.6.9      | Microsomal Stability Assay Protocol.....  | 145        |
| 3.6.10     | Liver Pharmacokinetic Assay Protocol .....  | 146        |
| 3.6.11     | Brain Pharmacokinetic Assay Protocol.....   | 147        |
| <b>3.7</b> | <b>Reference .....</b>  | <b>149</b> |
| <b>3.8</b> | <b>Appendix A.....</b>  | <b>152</b> |

## LIST OF FIGURES

| Figure #   | Figure title   | Page # |
|------------|--|--------|
| Figure 1-1 | Three types of DNA alkylation  | 3      |
| Figure 2-1 | Time-dependence of DNA ICL formation of duplex <b>3</b> for <b>1a-j</b> upon photo-irradiation | 43     |

## LIST OF TABLES

| Table #   | Table title  | Page # |
|-----------|--|--------|
| Table 2-1 | The solubility of <b>1a-j</b> .....  | 38     |
| Table 2-2 | The optimized conditions, ICL yields and UV absorption data for <b>1a-j</b> .....    | 47     |
| Table 2-3 | Photo-reactivity of <b>1b-c</b> towards dG and dA.....                               | 60     |
| Table 3-1 | Biophysical properties of <b>3-9</b> compared with cytotoxicity and GI <sub>50</sub> | 117    |

## LIST OF ABBREVIATIONS

| A              | Explanation  |
|----------------|--|
| AIBN           | Azobisisobutyronitrile                                       |
| ATP            | Adenosine triphosphate                                       |
| C              | Cytidine   |
| dA             | Deoxyadenosine   |
| dC             | Deoxycytidine  |
| dG             | Dexyguanosine  |
| dT             | Deoxythymidine   |
| DIPEA          | N,N-Diisopropylethylamine                                    |
| DMF            | Dimethylaminomethylene                                       |
| DMSO           | Dimethyl sulfoxide   |
| DMTr           | 4',4'-Dimethoxytrityl  |
| DNA            | 2'-Deoxyribonucleic acid                                     |
| ds DNA         | Double-stranded DNA  |
| EDTA           | Ethylenediaminetetraacetic acid                              |
| ESI            | Electrospray   |
| EtOAc          | Ethyl acetate  |
| EtOH           | Ethanol  |
| G              | Guanosine  |
| HPLC           | High-performance liquid chromatography                       |
| AIBN           | Azobisisobutyronitrile                                       |
| HRMS           | High-resolution mass spectrometry                            |
| ICLs           | Interstrand cross-links                                      |
| LC-MS          | Liquid chromatography–mass spectrometry                      |
| MALDI-TOF      | Matrix-assisted laser desorption/ionization – time of flight |
| MeCN           | Acetonitrile   |
| MeOH           | Methanol   |
| MS             | Mass spectrometry  |
| NBS            | N-Bromosuccinimide   |
| NMR            | Nuclear magnetic resonance                                   |
| ODN            | Oligodeoxyribonucleotide                                     |
| Pac            | Phenoxyacetyl  |
| PAGE           | Polyacrylamide gel electrophoresis                           |
| iPr            | Isopropyl  |
| QM             | Quinone methide  |
| ROS            | Reactive oxygen species                                      |
| RNA            | Ribonucleic acid   |
| T              | Thymidine  |
| TBAF           | Tert-n-butylammonium fluoride                                |
| TEA            | Triethylamine  |
| TEMPO          | 2,2,6,6-Tetramethylpiperidin-1-yl)oxyl                       |
| THF            | Tetrahydrofuran  |
| T <sub>m</sub> | Melting temperature  |
| TMS            | Trimethylsilyl   |

U  
UV  
UVA  
TEA

Uridine  
Ultraviolet  
Ultraviolet A  
Triethylamine

## LIST OF SCHEMES

| Scheme #    | Scheme title   | Page # |
|-------------|--|--------|
| Scheme 1-1  | Structure of DNA double helix and Watson-Crick base pairing.   | 1      |
| Scheme 1-2  | Possible alkylation sites on dA, dG, dC, and dT (dR = 2'-deoxyribose).   | 2      |
| Scheme 1-3  | Monofunctional methylating agents.   | 4      |
| Scheme 1-4  | Commonly used bi-functional alkylating agents as chemotherapeutic agents   | 5      |
| Scheme 1-5  | Cisplatin compounds  | 5      |
| Scheme 1-6  | Nitrogen mustards and the mechanism of action  | 6      |
| Scheme 1-7  | Anthracene intercalator  | 8      |
| Scheme 1-8  | Structure of AMAC  | 10     |
| Scheme 1-9  | Anthracene derivative having DNA photocleaving properties.   | 11     |
| Scheme 1-10 | Structure of AMAC intercalator.  | 12     |
| Scheme 1-11 | Structure of anthryl moiety having DNA binding properties.   | 13     |
| Scheme 1-12 | Structure of anthryl moiety appended with pyrene having DNA binding properties.  | 14     |
| Scheme 1-13 | Structure of anthracenedione analogues having anticancer properties  | 14     |
| Scheme 1-14 | Structure of anthracene analogues reported for chemosensor.  | 15     |
| Scheme 1-15 | Structure of psoralen analog.  | 17     |
| Scheme 1-16 | General structure of three classes of photo-inducible QM precursors  | 18     |
| Scheme 1-17 | Three classes of photo-inducible DNA cross-linking agents via a carboncation mechanism                                       | 18     |
| Scheme 1-18 | H <sub>2</sub> O <sub>2</sub> -activated QM precursors   | 21     |
| Scheme 1-19 | H <sub>2</sub> O <sub>2</sub> -inducible DAN cross-linking agents.   | 22     |
| Scheme 1-20 | Mechanism of action for H <sub>2</sub> O <sub>2</sub> -activated nitrogen mustard precursors                                 | 23     |
| Scheme 2-1  | The structures of <b>1a-j</b>  | 31     |
| Scheme 2-2  | Synthesis of <b>1a-e</b>   | 33     |
| Scheme 2-3  | Synthesis of <b>1f-j</b>   | 34     |
| Scheme 2-4  | The sequence of DNA duplex <b>3</b> .  | 35     |
| Scheme 2-5  | Automated DNA synthesis cycle (1A) and structures of phosphoramidites (2B)   | 36     |
| Scheme 2-6  | Deprotection scheme  | 37     |
| Scheme 2-7  | The structure of [ $\gamma$ - <sup>32</sup> P] ATP.  | 37     |
| Scheme 2-8  | (A) Free radical trapping reaction and (B) cation trapping reaction product obtained with <b>1b-c</b> upon 350nm irradiation | 53     |
| Scheme 2-9  | Cation and free radical trapping products obtained with and upon 350 nm irradiation.   | 53     |
| Scheme 2-10 | Proposed mechanism for DNA ICL formation.  | 54     |

|            |  |     |
|------------|--|-----|
| Scheme 3-1 | Activation of H <sub>2</sub> O <sub>2</sub> -triggered alkylating agents.              | 115 |
| Scheme 3-2 | Chemical structures of modified aromatic nitrogen mustards<br><b>3-11.</b>             | 116 |
| Scheme 3-3 | Structure of antitumor agent <b>12</b> with control drug<br>Chlorambucil and Melphalan | 118 |
| Scheme 3-4 | Activation of <b>12</b> by H <sub>2</sub> O <sub>2</sub>                               | 132 |
| Scheme 3-5 | Possible way of <b>12</b> metabolism.  | 133 |
| Scheme 3-6 | Possible metabolites of <b>12</b> other than activated metabolite.                     | 134 |

## ACKNOWLEDGEMENTS

First of all, I am grateful to my dear advisor Prof. Xiaohua Peng, is an outstanding scholar who has guided me through my research. She has been extremely helpful with the selection of projects, and has helped with troubleshooting them as well. My development as a chemist began with Dr. Peng's profound knowledge, excellent advice, and patient mentoring. It is an honor to be under the supervision of Dr. Peng, and I am greatly appreciative and respectful of her.

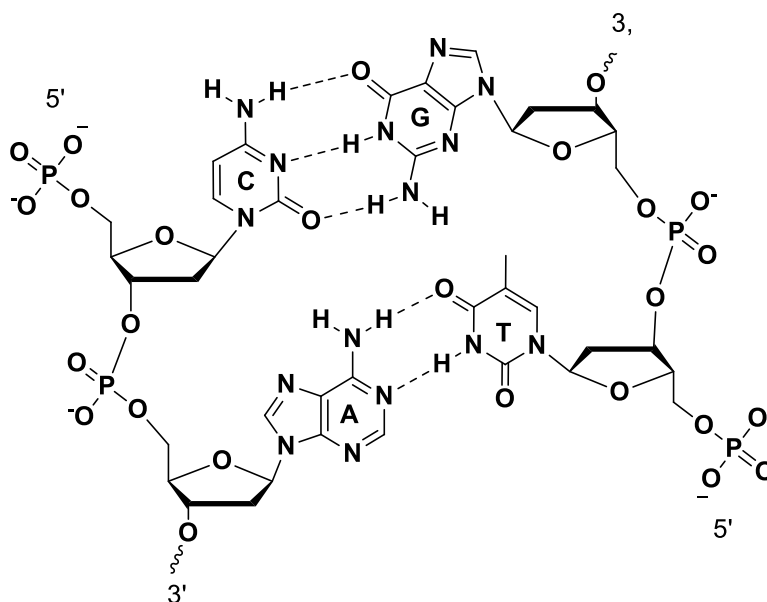
I greatly appreciate my committee members: Prof. James Cook, Prof. Alexander Arnold, Prof. Andy Pacheco, Prof. Shama Mirza for their nice support, encouragement, insightful comments and valuable advice for my research. Having them on my committee is a great honor for me. The talent and expertise they share with us is admirable. I am grateful for their generosity. Especially thank Professor Alexander Arnold for his fruitful collaboration and professionally training in cell culture and animal study. Also special thanks to Prof. James Cook and Prof. Andy Pacheco for their insightful comments and valuable advice for my paper.



## Chapter 1. Introduction

### 1.1 The structure and functions of DNA

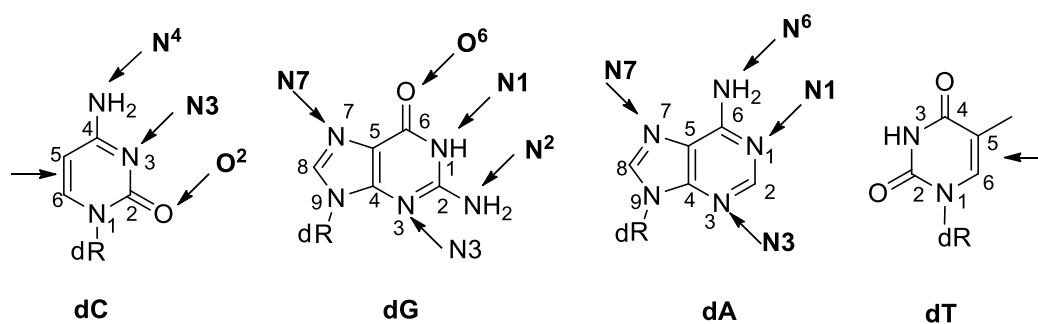
The DNA is a genetic material that carries the genetic information required for the cell's development, function, and reproduction. The structure of DNA was discovered in 1953 by Watson and Crick. DNA has a double helix structure, which consists of two complementary polynucleotide chains<sup>1</sup> (Scheme-1). Each polynucleotide strand is constructed by nucleotides containing a phosphate group, a deoxyribose, and one of four nitrogen-containing nucleobases (adenine [A], thymine [T], guanine [G] and cytosine [C]). Hydrogen bonds bind the complementary strands together, namely A pairs with T and C pairs with G, as part of the Watson-Crick system. The formation of hydrogen bonds allows the temporary separation of two DNA strands that are necessary for DNA replication and transcription, while Watson-Crick base pairs are critical for maintaining high fidelity of DNA replication and transcription.



**Scheme 1-1.** Structure of DNA double helix and Watson-Crick base pairing.

A wide range of chemical agents can react with DNA, as well as photo irradiation, causing it to

lose the normal function. For example, many electrophiles, including alkyl halides, quinone methides, and carbocation precursors, can alkylate DNA bases and phosphate backbones. The cyclic nitrogens, exocyclic amino groups, and carbonyl group in cytosine, guanine or adenine can act as nucleophiles reacting with various alkylating agents (Scheme 1-2). In contrast, the unsaturated C=C bonds located in pyrimidine rings of thymine and cytosine are capable of reacting with other unsaturated molecules by means of the [2+2] cycloaddition mechanism. As a result of all of these reactions, DNA interstrand cross-links are formed, which inhibit DNA replication and transcription. In order to understand how DNA functions and how its chemical reactivity affects genetic information, it is extremely important to understand the reactivity of various chemical agents toward DNA. This thesis focuses on investigating the reactivity of DNA towards two classes of aromatic compounds as novel inducible DNA cross-linking agents, i.e. photo-activatable anthracene analogues and H<sub>2</sub>O<sub>2</sub>-activated arylboronate nitrogen mustard prodrugs. We designed, synthesized, investigated mechanism of function of these molecules and explored their biomedical applications. We utilized the tools of synthetic organic chemistry, physical organic chemistry, biochemistry, molecular biology and medicinal chemistry for this study.



**Scheme 1-2.** Possible alkylation sites on dA, dG, dC, and dT (dR = 2'-deoxyribose).

## 1.2 DNA alkylating agents

Molecular modifications of DNA, such as alkylation, are essential for nucleic acid research and chemotherapy. DNA mono-alkylation, intrastrand cross-links, and interstrand cross-links (ICL)

are the three major types of alkylation. A mono-alkylation modifies a single base on one DNA strand. An intrastrand cross-link is formed when two DNA bases on the same strand are alkylated; and DNA ICL is produced when two bases on the opposite strand are alkylated. DNA ICLs are the sources of the cytotoxicity of many antitumor and anticancer agents.

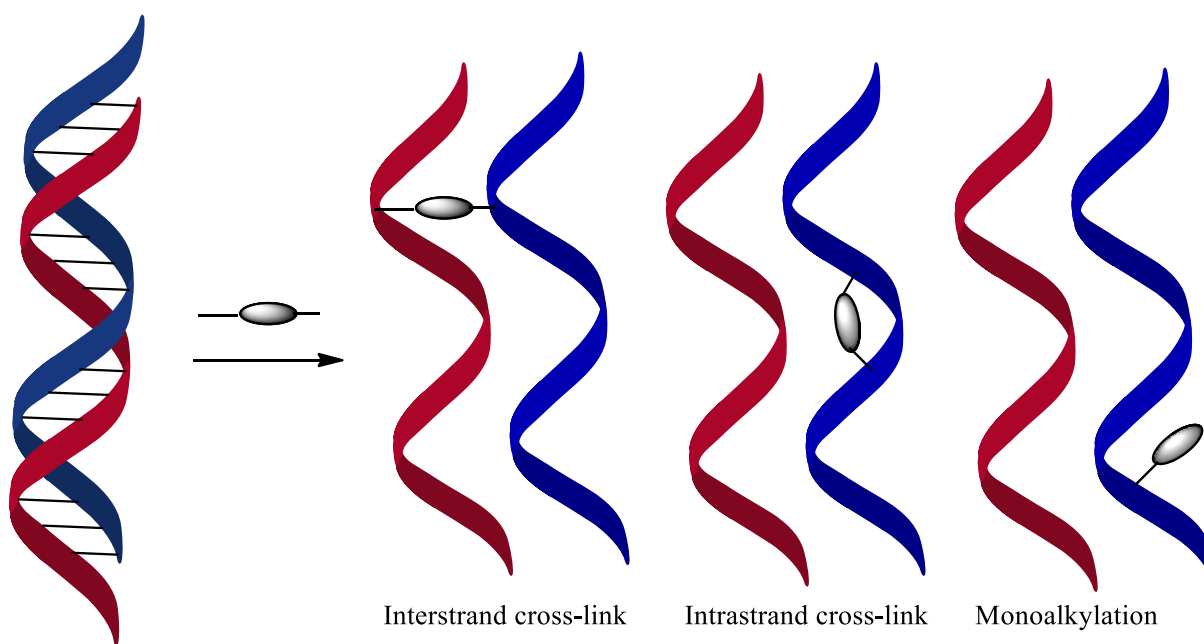
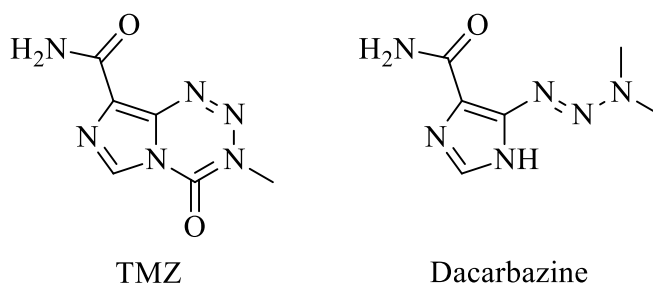


**Figure 1-1.** Three types of DNA alkylation.

Cancer chemotherapy often uses DNA alkylating agents to alter DNA's original structure in order to prevent it from functioning properly. A number of antitumor and anticancer agents showed cytotoxicity through DNA alkylation. Eventually, it can cause DNA mutations and block DNA replication and transcription, leading to cell death. DNA alkylating agents are categorized into two major categories: monofunctional alkylators and bifunctional alkylators. They are one of the significant classes of compounds that have been widely utilized for cancer treatments.

A large variety of DNA alkylating agents have been developed, including methylating agent, quinone methide-based alkylating agents, nitrogen mustard-based alkylators, etc. The simplest alkylating agents are methylating agents that form monoalkylation in DNA such as Temozolomide

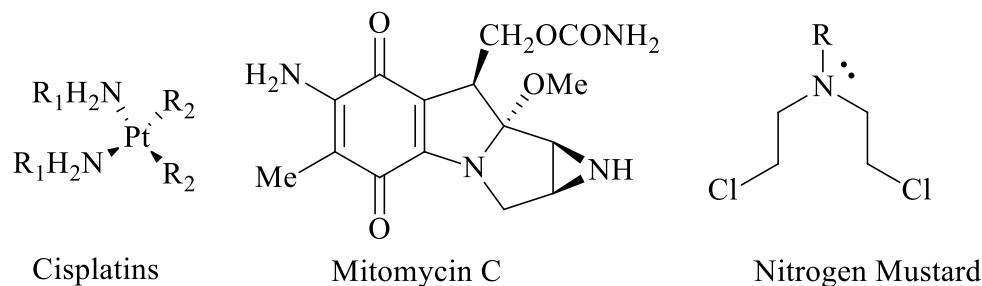
(TMZ) and dacarbazine. They have been studied and used for repairing DNA damage and cancer treatment (Scheme 1-3).<sup>7</sup> In general, methylation occurred either at the N- or O-positions of nucleobases. N-Methylation products are the major adducts formed with methylating agents (~80%). One of the earliest oral alkylating drugs approved for cancer treatment is TMZ. In comparison with other existing drugs, TMZ had two advantages. It is small in size and has good lipophilicity, which makes it efficiently cross the blood-brain barrier and can be used for treating brain cancer. Furthermore, TMZ demonstrated perfect bioavailability (100%) resulting in improved efficacy. The chemotherapeutic agent dacarbazine is used to treat skin cancer melanoma. Dacarbazine damages DNA by methylation at the N7 or O6 of guanine moiety (Scheme 1-3), causing cancer cell death.



**Scheme 1-3.** Monofunctional methylating agents.

As time progressed, bi-functional alkylating agents have been developed, which could form intra- or interstrand cross-links. Interstrand cross-links can induce bends in DNA, affecting how it binds to DNA binding proteins and inhibiting its normal function. Covalent bonds between complementary DNA strands prevent them from separating, inhibiting DNA replication and/or transcription, which ultimately causes cell death. Although DNA ICL is toxic, nucleotide excision repair (NER) can readily repair intrastrand cross-links, which limits its use for cancer treatment. In contrast to intrastrand cross-links, DNA ICLs cannot be easily repaired by NER, making them more toxic. DNA interstrand cross-linking agents have attracted more attention for cancer treatment

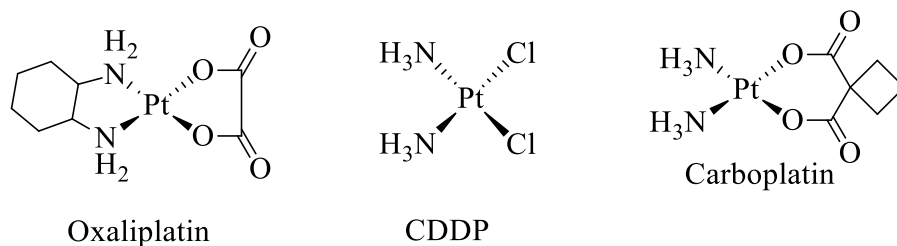
and other biological applications. A wide variety of bi-functional alkylating agents have been used for cancer treatment, including cisplatin, mitomycin C, and nitrogen mustard analogues (Scheme 1-4).



**Scheme 1-4.** Commonly used bi-functional alkylating agents as chemotherapeutic agents

Cisplatin is a well-known anticancer drug approved for medical use. It has been used for half cancer patients who have ever received chemotherapy. For instance,

cisdiamminedichloridoplatinum (II) (CDDP), carboplatin, and oxaliplatin (Scheme 1-5) are anticancer drugs used for the treatment of lung cancer, bladder cancer, germ cell tumors, sarcomas and cervical cancer. These platinum compounds are commonly made up of platinum (II), two neutral ammonium molecules, and two ligands with negative charge. Cisplatin forms both inter- and intrastrand cross-links. However, cisplatin can cause a number of side effects, including kidney damage, hearing loss, bone marrow suppression and vomiting.

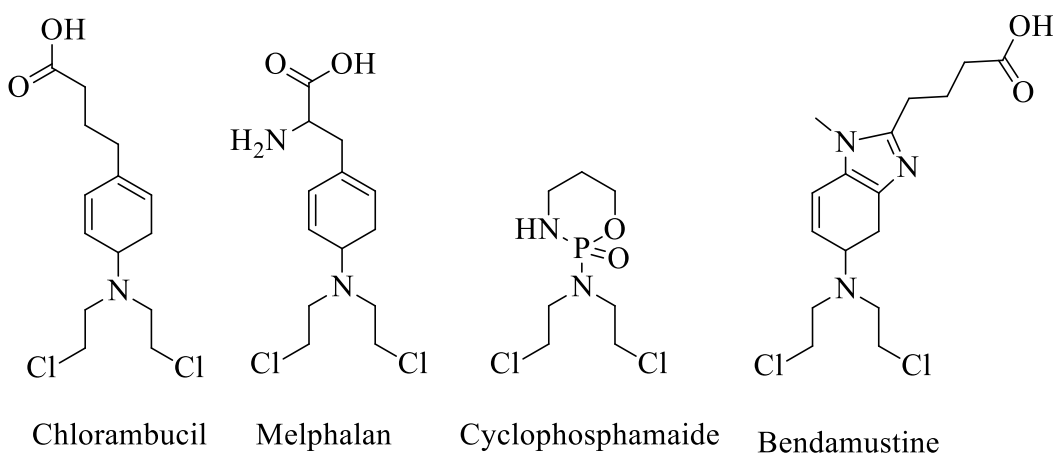


**Scheme 1-5.** Cisplatin compounds.

Mitomycin C, a natural product initially isolated from *Streptomyces caespitosus*, is a quinone methide based prodrug that has been used for treating anal cancers, breast cancers, and bladder

cancers. Mitomycin C is inert towards DNA, but can be activated by enzymatic reduction to form quinone methide intermediates that cross-link DNA via alkylating dGs. However, Mitomycin C showed a series of adverse effects such as nausea, hair loss, mouth sores, and toxicity to the bone marrow.

Nitrogen mustard analogues are another class of DNA alkylating agents which are still widely used for cancer treatment such as chlorambucil, melphalan, cyclophosphamide, and bendamustine (Scheme 1-7). They are featuring a highly reactive *N,N*-bis-(2-chloroethyl)amine functional group that produces DNA ICLs by alkylation. Due to their high reactivity, nitrogen mustards lack of selectivity, which lead to serious side effects, including nausea, hair loss, mouth sores, and loss of fertility due to poor selectivity.



**Scheme 1-6.** Nitrogen mustards and the mechanism of action

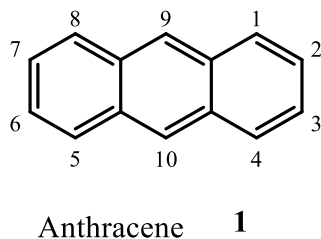
However, most of these traditional chemotherapeutic agents showed poor selectivity even though they are widely used for cancer treatment. Due to their inability to distinguish between cancerous and normal cells, these agents caused serious side effects. Cisplatin, for example, can damage the kidneys, cause hearing loss, suppress bone marrow, and cause vomiting. Side effects of nausea, hair loss, mouth sores, and infertility are all associated with nitrogen mustard analogues.

For better treatment of cancer diseases, we need to improve the selectivity of the DNA alkylating

agents. The development of inducible DNA alkylating agents is an effective way to reduce the toxicity of DNA alkylating agents towards normal cells. These agents are inert to normal cells but can be activated specifically in tumor cells. By targeting the unique conditions of malignant cells, such agents can minimize side effects therefore leaving normal cells untouched. The inducible DNA cross-linking agents are non-toxic and selective, so they can also find other biological applications. Several methodologies have been developed for inducing DNA ICL formation, including photo induction, chemical agent induction, and enzymes induction. This work is focusing on development of efficient photo-inducible DNA cross-linking agents as well as H<sub>2</sub>O<sub>2</sub>-activated DNA alkylating agents. We use a DNA intercalating moiety, anthracene, to improve the binding interaction as well as photosensitivity, therefore enhancing ICL efficiency.

### 1.3 DNA intercalating agents

Molecular interactions with DNA can occur in a variety of ways, including covalent, electrostatic, or intercalation interactions <sup>2</sup>. The intercalation of molecules into DNA lies in the concept of insertion between the planar bases of the DNA molecules. The DNA intercalating agents are substances that bind to DNA and insert themselves into the DNA double helix structure. Intercalation brings molecules close to DNA which is helpful for studying chemical reactivity of DNA towards various organic functional groups. Some DNA intercalating agents are used in cancer treatment to kill cancer cells by preventing them from dividing and inducing DNA damages. Most of these ligands are polycyclic, aromatic, and planar, which makes them good nucleic acid stains. Several DNA intercalators have been studied in depth, including berberine, ethidium bromide, proflavine, daunomycin, doxorubicin, anthracene. Among them, anthracene is a well known DNA intercalator. Part of this thesis focuses on studying the photo reactivity of anthracene analogues towards DNA.



**Scheme 1-7.** Anthracene intercalator.

### 1.3.1 Anthracene intercalator and its derivatives

Anthracene, a solid polycyclic aromatic hydrocarbon, consists of three fused benzene rings. It is a part of coal tar. It is planar, linear, and can overlap with DNA base pairs<sup>3</sup>. A wide variety of closely related derivatives can be prepared using anthracene nucleus' versatile chemistry<sup>4</sup>. Anthracene analogues showed a broad spectrum of biological activities, including anticancer activities<sup>5</sup>, effective against certain conditions of the skin,<sup>6</sup>. One of the first anthracene-based drugs to enter clinical trials was pseudourea.

By spectroscopic methods, anthracene probes can be used to monitor ligand binding to DNA because they absorb moderately in the near-UV region and produce a high fluorescence quantum yield<sup>7</sup>. In DNA, the GC sequences quench the fluorescence of anthracene derivatives while the AT sequences increase anthryl fluorescence. This can be used to identify the binding sites<sup>8</sup>. Anthryl probes also induce DNA damage and strand cleavages due to their long-lived triplet excited states<sup>9-11</sup>. During intercalation of the anthracene moiety into DNA double helix, substituents at the positions 9 and 10 are strategically positioned to occupy the grooves<sup>12</sup>. The anthracenedione moiety is also known to undergo redox processes, which could directly produce cytotoxic effects<sup>13</sup>. There are four naturally occurring anthracenes viz. 1,4,10-trimethoxyanthracene-2-carbaldehyde, (1,4,10-trimethoxy-2-anthracen-2-yl) methanol, 1,4,8,10-tetramethoxyanthracene-2-carbaldehyde,

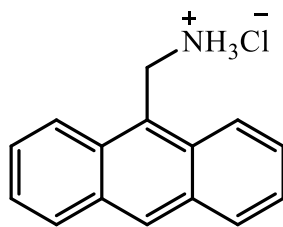


1,4,10-trimethoxyanthracene-2-carboxylic acid and 1,3-dimethoxy-2-methoxymethylantraquinone, which were extracted from a woody plant *Coussarea macrophylla*<sup>14</sup>. Yu et al. reported the bis anthryl compound and its DNA binding and cleavage studies. Bis anthryl compounds have a greater binding constant than monoanthryl compounds<sup>15</sup>. Tolpygin has reported the photo induced electron transfer effect in the amino methyl anthracene derivatives. In the excited state, amino methyl anthracene derivatives may induce photo-induced electron transfer from nitrogen atom lone pairs to anthracene fragments, quenching fluorescence. As a consequence of interactions with metal cations and proton, these compounds inhibit photo-induced electron transfer, causing the sensor to exhibit strong fluorescence<sup>16</sup>. Kraicheva reported the biological activities of anthracene with amino phosphonic acids. These are quite promising as anticancer agents. Due to the fact that the DNA intercalating anthracene ring is the primary pharmacophoric fragment in some cytostatic drugs, amino phosphonates derived from anthracene would be of particular interest here<sup>17</sup>. Phanstiel et al. reported the anthracene containing polyamine compounds. These compounds show a selective drug delivery (cell surface protein)<sup>18</sup>. Metal-free DNA cleaving reagents have been studied by Gobel and co-workers, these compounds are thought of as safer agents for cleaving the P-O bond of phosphodiester in nucleic acids, showing clinical potential<sup>19</sup>. Small organic molecules, such as guanidinium derivatives<sup>20</sup>, cyclodextrin derivatives<sup>21</sup>, dipeptides<sup>22</sup> and especially macrocyclic polyamines<sup>23</sup>, have also been used as cleaving agents of nucleic acids. The anthraquinone group, as a fine intercalator of DNA, has been frequently adopted in certain anticancer drugs, such as doxorubicin, anthracyclines, mitoxantrone and anthrapyrazoles<sup>24</sup>. Teilla et al. reported that the compound formed by conjugating the cis, cis-triaminocyclohexane-Zn<sup>2+</sup> complex (cleaving moiety) with anthraquinone (intercalating moiety) via an alkyl spacer led to a 15-fold increase in DNA cleavage efficiency when compared with the

cis, cis-triaminocyclohexane-  $Zn^{2+}$  complex without the anthraquinone moiety<sup>25</sup>. Yu et al. reported that macrocyclic polyamine bis-anthracene conjugates showed higher DNA binding and photocleaving abilities than their corresponding mono-anthracene conjugates<sup>15</sup>. Roe et al. showed carcinogenic activity of some benzanthracene derivatives in new born mice<sup>26</sup>. Fabbrizzi et al. explained the redox switching of anthracene fluorescence through the  $Cu^{II}/Cu^I$  Couple. Lorente et al. reported concentration dependent interaction studies with DNA and anthracene derivatives<sup>27</sup>.

### 1.3.2 Anthracene derivatives used for DNA photo-cleavage studies

Since Sigman et al. discovered the nuclease activity of the cuprous complex  $(phen)_2 Cu(I)$ , a significant amount of research has been undertaken to identify the mechanism(s) that underlie DNA cleavage<sup>27</sup>. An important property of the anthryl chromophore is its photochemical reactivity and its high singlet excited state energy (76 kcal/mol), which enables photoreactions to be initiated with DNA. It has been shown that the anthracene moiety containing an ammonium salt undergo photochemical reactions with nucleotides and cause DNA strand scission. Thus, (9-anthryl) ammonium chloride has a high potential for DNA cleavage studies<sup>7</sup>.



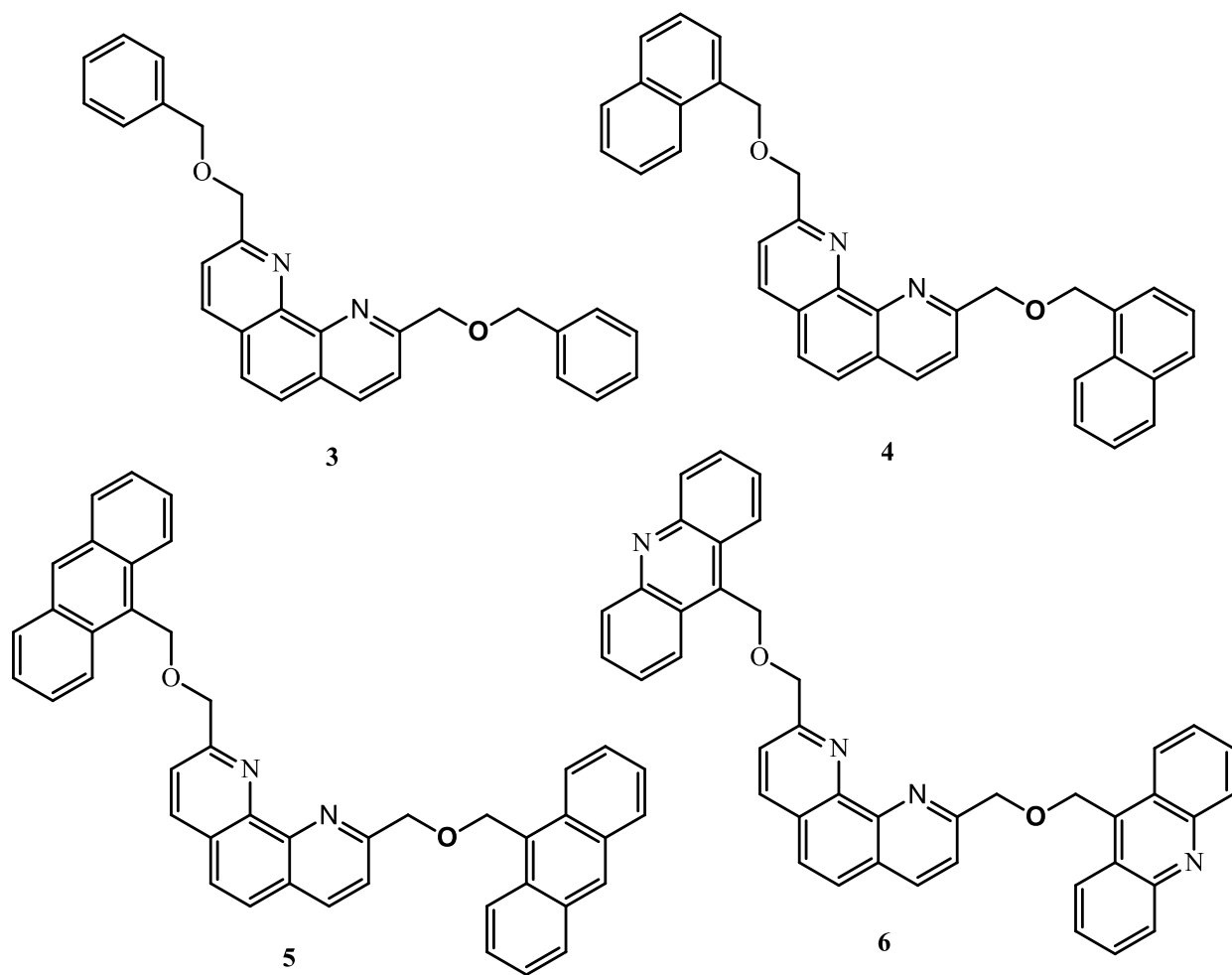
9-Anthryl Methyl Ammonium Chloride  
(AMAC)

2

#### **Scheme 1-8.** Structure of AMAC

A series of compounds based on 1,10-phenanthroline covalently tethered, at the 2 and 9 positions, to either two benzene (**3**), naphthalene (**4**), acridine (**5**) or anthracene (**6**) chromophores were synthesized. Among these acridine and anthracene derivatives were shown to be good DNA

photocleavers (pH=7.0, 22°C, 350 nm), whereas benzene and naphthalene were inactive. Acridine compound showed copper(II)-enhanced photocleaving activity at micromolar concentrations, while only 0.25  $\mu\text{M}$  of anthracene derivatives was required to cleave DNA completely. Moreover, the effect of  $\text{CuCl}_2$  addition to anthracene derivative was shown to be concentration-dependent. Low concentrations of these compounds exhibited cleaving activity that was quenched by addition of the metal salt, while at higher concentrations activity was increased<sup>27</sup>.

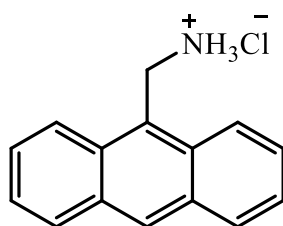


**Scheme 1-9.** Anthracene derivative having DNA photocleaving properties.

### 1.3.3 Anthracene derivatives used for DNA binding studies.

Due to the important functions of DNA in living organisms, studying the interactions between small molecules and DNA is helpful for developing more effective DNA-targeted drugs,

preventing and curing diseases<sup>28, 29, 30</sup>. Binding studies of Anthracene or derivatives have not been explored as well as other simple aromatic hydrocarbons. In general planarity was suggested to be one of the important features needed for efficient intercalation into the DNA helix<sup>15</sup>. Therefore the large planar hydrophobic anthryl moiety is expected to facilitate intercalation of the probe into the relatively nonpolar interior of the DNA helix. The methylene chain functions as a short spacer to separate the chromophore and the charge center to above or below the plane of the anthryl moiety. Thus, when the anthryl moiety intercalates into the helix, the cationic charge is positioned closer to the DNA phosphates for a favorable electrostatic interaction. The strong absorption and fluorescence characteristics of the anthryl group provide a sensitive spectroscopic handle to study its interaction with DNA. The well-resolved vibronic transitions of the anthryl chromophore in the 300-400 nm region of the electronic absorption spectrum provide a spectroscopic signature for the probe environment. Changes in the intensities of these transitions can be used to decipher the nature and the strength of the stacking interactions between the chromophore and the DNA bases. Another interesting feature of the anthryl chromophore is its photochemical reactivity and its large singlet excited state energy (76 kcal/mol). These can be used to initiate photoreactions with DNA<sup>7</sup>.



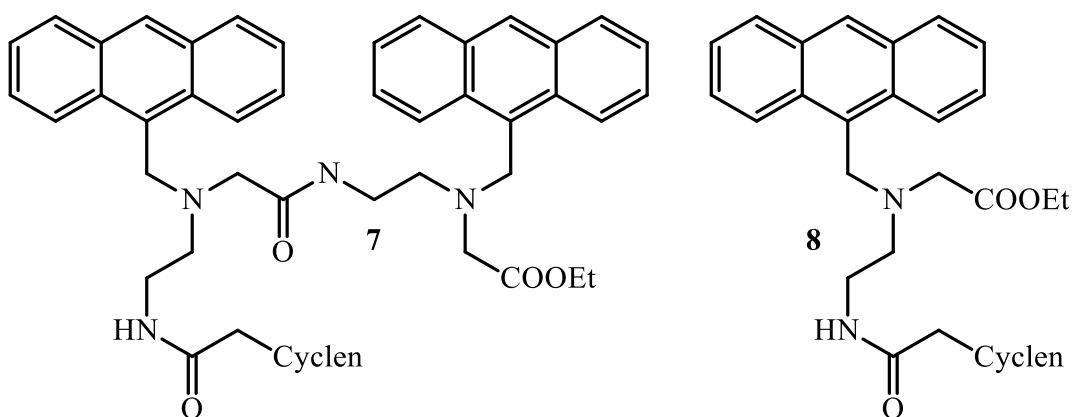
9-Anthryl Methyl Ammonium Chloride  
(AMAC)

2

**Scheme 1-10.** Structure of AMAC intercalator.

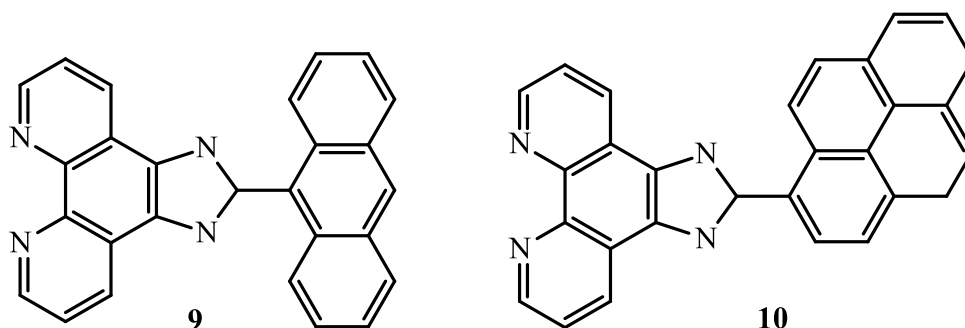
The bis-anthryl compound with multiple peptide backbone, cyclen (1, 4, 7, 10-tetraazacyclododecane) moiety was introduced to enhance water solubility and binding ability

towards DNA. The DNA binding activity of **7** was higher compared with the mono-anthryl compound **8** with similar structure found that DNA binding constant of the bis-anthryl compound is 100 times more than that of monoanthryl compound. On the other hand, mono anthryl compound shows significant CG-selective DNA binding activity<sup>31</sup>. In aqueous solutions, imidazolium anthracene probe exhibited a selective fluorescent quenching effect only with DNA among various anions including the nucleotides investigated. This probe was further applied to monitor the activity of DNase<sup>32</sup>.



**Scheme 1-11.** Structure of anthryl moiety having DNA binding properties.

The anthracene **9** and pyrene **10** chromophore appended polypyridyl ligands and their mixed ligands ruthenium complexes are studied with DNA have revealed that these complexes bind to DNA, mainly in an intercalative mode with moderate strengths. Modification of phen, especially extension of the planarity of the ligand and attaching aromatic chromophores (anthracene) that will increase the strength of interaction of its complexes with DNA<sup>33</sup>.

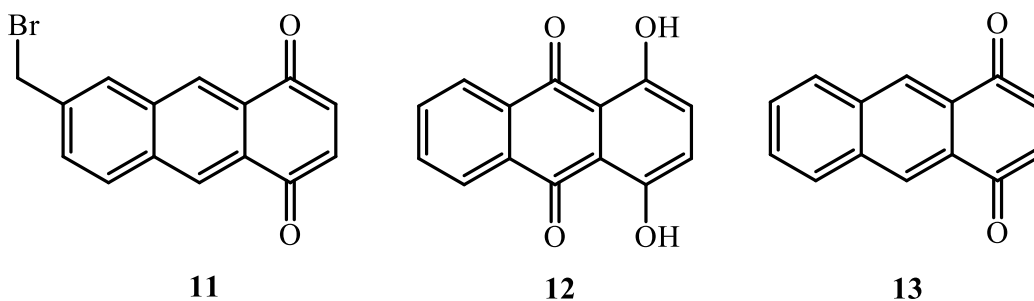


**Scheme 1-12.** Structure of anthryl moiety appended with pyrene having DNA binding properties.

#### 1.3.4 Application of Anthracene derivatives.

##### **Anticancer Activity of Anthracene Derivatives**

Anthracyclines (anthracycline antibiotics) are used in cancer chemotherapy. These anthracyclines inhibit DNA and RNA synthesis by intercalating between base pairs of the DNA/RNA strand, thus preventing the replication of rapidly-growing cancer cells<sup>34</sup>. The anthracenediones represent two latter generation classes of DNA intercalators that show great clinical promise as antitumor drugs<sup>35</sup>. An intermediate, 6-bromomethyl-1,4-anthracenedione **11** was synthesized and converted to various active anti-tumour agents, including a water-soluble phosphate ester pro-drug. Based on their ability to decrease L1210 and HL-60 tumor cell viability, 1,4-dihydroxyanthraquinones **12** are inactive but 1,4-anthracenediones **13** have interesting anti-tumour activity<sup>36</sup>.

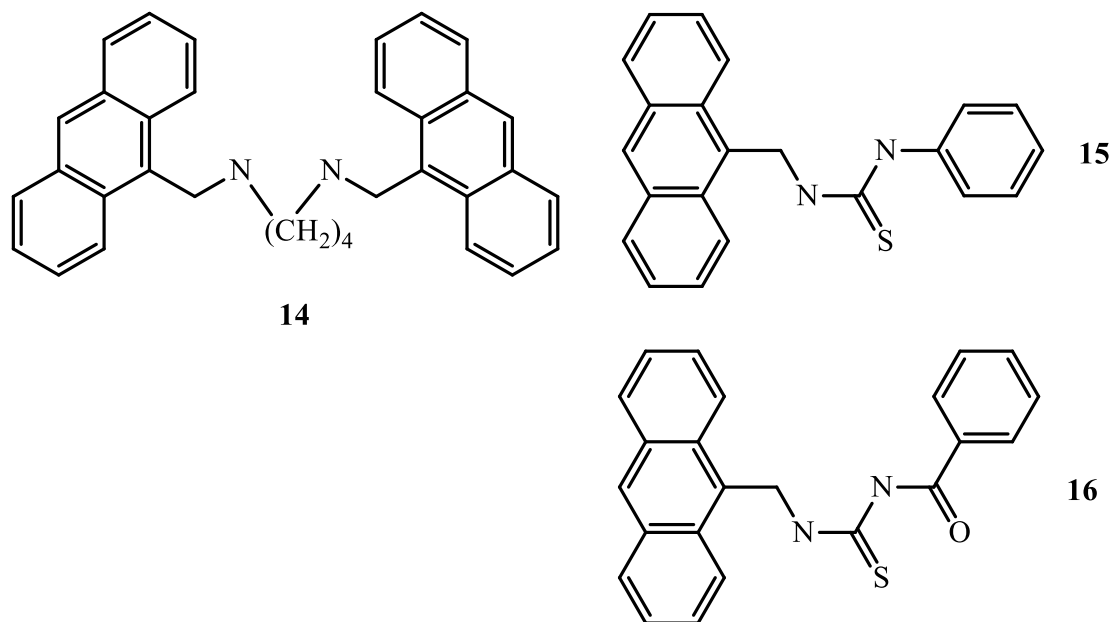


**Scheme 1-13.** Structure of anthracenedione analogues having anticancer properties.

##### **Anthracene Derivatives In Redox Activity**

The anthracene are strong light emitting fragments and chemically stable. The transition metal

based anthracene cyclam rings show a rich and versatile redox chemistry. Profatilova et al. studied the redox activity of potent chemosensors based on anthryl containing diamines **14**, thiourea **15** and urease **16** in the absence and in the presence of complexing metal cations in solution was studied by cyclic and differential pulse voltammetry. The oxidation of compounds under consideration occur in one or two steps involving the anthryl fragment and the donor moiety i.e., amino, thiourea or urea group. It is known that anthracene is reversibly oxidizes via formation of a stable radical cation. Similar oxidation pattern was reported for chemosensors, 9,10-bis(1,3-dithiol-2-ylidene)-9,10-dihydro anthracene derivatives, in which the sulfur containing ionophore was oxidized at about 0.35 V and the oxidation peak of anthracene moiety was observed at 1.62 V.

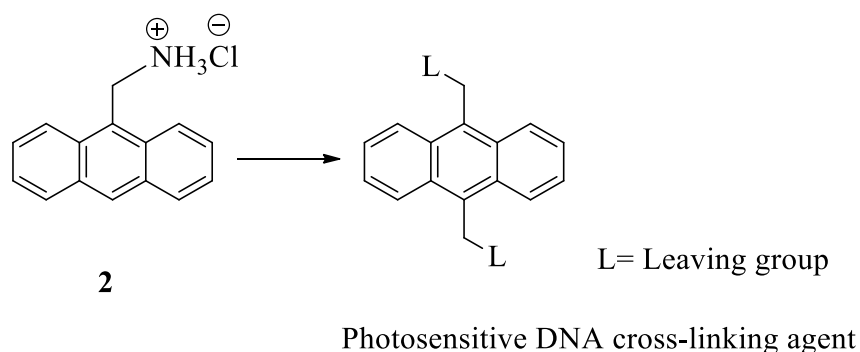


**Scheme 1-14.** Structure of anthracene analogues reported for chemosensor.

Ananthracene chromophores play a crucial role in the development of organic photochemistry. There has been extensive research on anthracene derivatives in many fields, such as material chemistry, thermochromic and photochromic chemistry, and organic light emission. Furthermore,

anthracenes have been used in optical, electronic, and magnetic switches. Anthracene skeletal compounds are also useful for probing DNA cleavage in biological systems. It has been found that anthracene derivatives are capable of acting as good cancer-preventing drugs for humans and are carcinogenic to a wide range of animals.

Anthryl chromophore **2** intercalative binding towards natural and synthetic polynucleotides has also been demonstrated in conjunction with the detailed DNA binding properties of AMAC. Moreover, the anthryl chromophore is highly photochemically reactive and has a relatively high energy of excitation (76 kcal/mol), which is used to initiate photoreactions with DNA. It has been observed in experiments that the AMAC does not show any sequence specificity for binding except for homo AT sequences, but that it does transfer energy from DNA bases to the anthryl chromophore in a sequence dependent manner. It is clear from findings that anthryl chromophore-based molecular systems can bind DNA avidly and thus has a high potential for DNA binding studies. This is why we designed AMAC (**2**) based DNA crosslinking agents for photosensitive DNA cross-linking study.



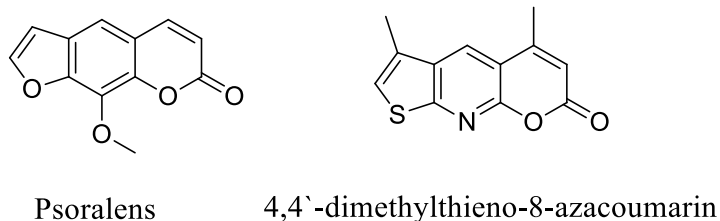
#### 1.4 Photosensitive DNA cross-linking agents and their mechanism

There are two major categories of inducible DNA interstrand cross-linking agents, i.e. photo-induced DNA cross-linking agents and chemical-induced DNA cross-linking agents. Photo-induction has received great attention due to its unique properties, such as its biocompatibility and

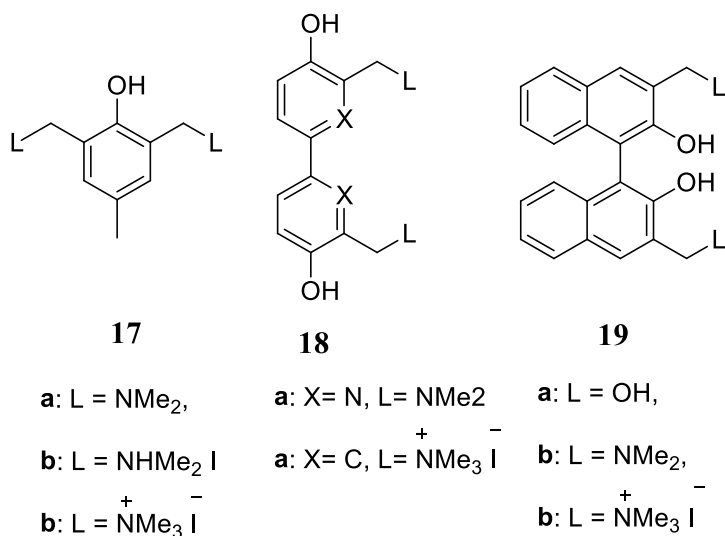


orthogonality. As a clean and noninvasive method, photo-induction can be used without requiring any additional chemical reagents. A number of photo-induced DNA cross-linking agents have been developed for producing DNA ICLs. There are three general mechanisms involved in the photo-induced DNA ICL formation, including [2+2]cylcoadditon, alkylation via quinone methides (QMs), and alkylation via photo-generated carbocations.

Psoralens are the first type of photo-activated DNA cross-linking agents, which can be activated by UVA light (320-410 nm) to form DNA ICLs by a [2+2] cyclo addition reaction with DNA thymidine residues<sup>37</sup>. The combination of psoralens and UVA has been extensively used to treat skin disorders, such as skin cancer and psoriasis<sup>38</sup>. A number of psoralen analogs have been synthesized and studied. Several of them showed good therapeutic properties at low risk of adverse effects<sup>39</sup>. Coumarin moiety also induced DNA ICL formation by a [2+2] cycloaddition reaction (please cite the references here, a few from our group)/ 4-Dimethylthieno-8-azacoumarin, for instance, had an antiproliferative effect in HL-60 cells without causing erythema, which is a common side effect<sup>40</sup> of methoxsalen (8-MOP). Later on, a large number of photo-induced DNA cross-linking agents have been developed, including different coumarin analogues, quinone methide analogues, biaryl functional groups, bifunctional naphthalene compounds, bifunctional benzyl boronates etc .

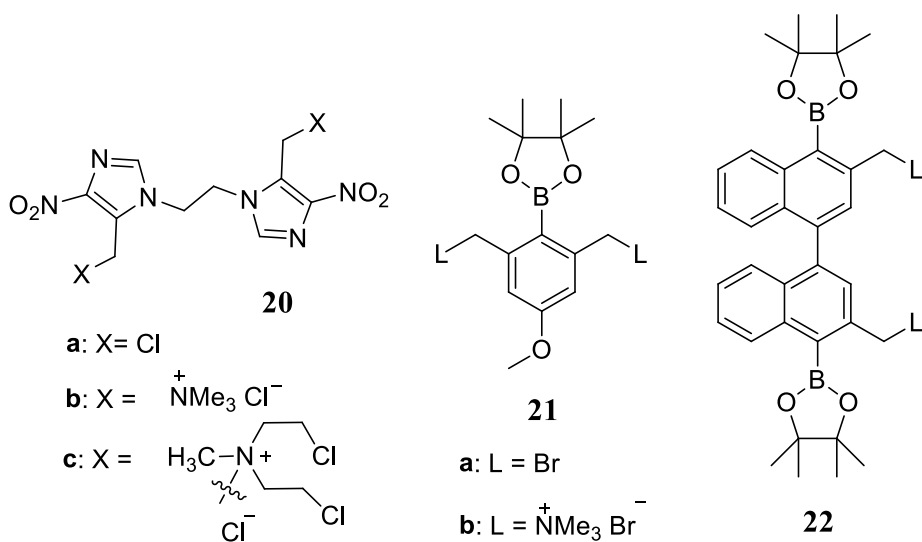


**Scheme 1-15.** Structure of psoralen analog.



**Scheme 1-16.** General structure of three classes of photo-inducible QM precursors.

There are extensive studies on photo-induced DNA cross-linking via [2+2] cycloaddition and QM formation. In contrast, photo-induced DNA ICL formation via a carbocation mechanism has been less explored. A series of biaryl bifunctional compounds IId-j has recently been developed to cross-link DNA with photo-induced activation<sup>41-43</sup>. Upon UV irradiation at 350 nm, all of these compounds cross-linked DNA efficiently. Carbocation plays a key role in DNA cross-linking. It is possible to produce carbocations either by oxidizing the corresponding radicals or by heterolyzing C-L bonds directly.



**Scheme 1-17.** Three classes of photo-inducible DNA cross-linking agents via a carboncation mechanism.

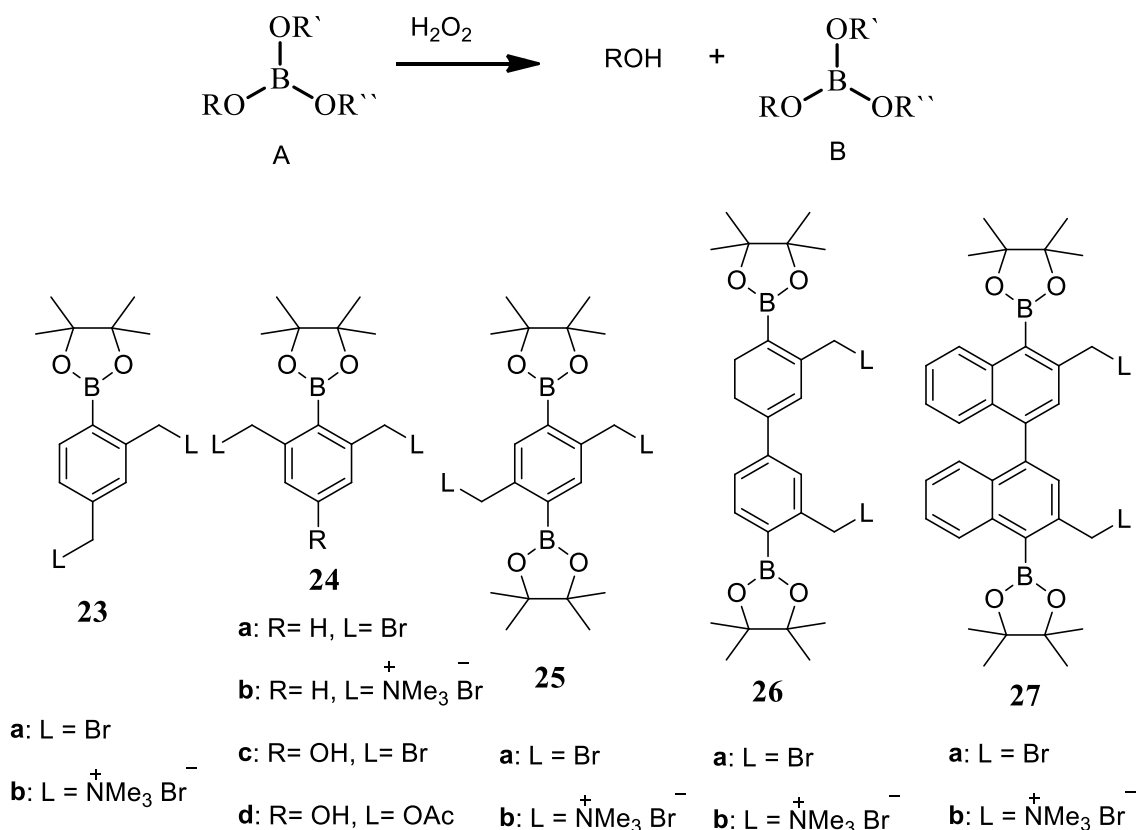
### 1.5 DNA Interstrand Cross-linking Induced by Chemical Agents

A variety of chemical agents were employed to activate DNA ICL precursors, such as fluoride (F<sup>-</sup>), NaIO<sub>4</sub> or <sup>1</sup>O<sub>2</sub>, N-bromosuccinimide (NBS), and hydrogen peroxide (H<sub>2</sub>O<sub>2</sub>). A number of silyl-containing aromatic compounds have been developed as fluoride-inducible DNA cross-linking agents as the silyl protective group can be selectively cleaved by fluoride ions to generate DNA cross-linkers, such as quinone methide or nitrogen mustard. Phenyl selenide-containing compounds have been reported as NaIO<sub>4</sub> or <sup>1</sup>O<sub>2</sub> inducible DNA cross-linking agents.. Some furan-containing nucleosides can be activated by NBS to form enal species, which cross-link DNA. A wide variety of boronate or boronic acid-containing compounds can selectively activated by H<sub>2</sub>O<sub>2</sub> to generate DNA cross-linkers, i.e. QMs or nitrogen mustard. In this thesis, we are focusing on hydrogen peroxide inducible DNA cross-linking agents and their biomedical applications.

**H<sub>2</sub>O<sub>2</sub>-activated prodrugs for targeting cancer cells.** Cancer cells are under oxidative stress due to uncontrolled growth, increased metabolism, mitochondria malfunction or exogenous insults such as chemotherapy<sup>43,44</sup>. Higher level of reactive oxygen species (ROS), including H<sub>2</sub>O<sub>2</sub>, superoxide, and hydroxyl radicals, are observed in many cancer cells than normal cells<sup>45,46</sup>. Increased ROS production is a unique feature of cancer cells, which has been explored for development of targeted cancer therapies. Among various ROS, H<sub>2</sub>O<sub>2</sub> is the most stable one that can accumulate in cancer cells, which is an ideal candidate for targeting cancer. Prodrugs that are specifically activated by H<sub>2</sub>O<sub>2</sub> in tumor cells have the potential to improve tumor selectivity and reduce toxicity to normal tissues. A wide variety of H<sub>2</sub>O<sub>2</sub>-activated prodrugs have been developed for selectively killing cancer cells<sup>47</sup>. Most of these H<sub>2</sub>O<sub>2</sub>-activated prodrugs contain a boronate or

boronic acid group that is responsive to  $\text{H}_2\text{O}_2$ . These boronate-based prodrugs are non-toxic but can be selectively activated by  $\text{H}_2\text{O}_2$  to release cytotoxic species specifically in cancer cells with high level of  $\text{H}_2\text{O}_2$ , of which many have demonstrated in vitro efficacy and selectivity.  $\text{H}_2\text{O}_2$ -Activated prodrugs include DNA alkylating agents, ROS-amplifiers, histone deacetylase inhibitors, therapeutic proteins, and prodrugs of a wide variety of FDA-approved anticancer agents<sup>35</sup>. Our group has developed a wide variety of  $\text{H}_2\text{O}_2$ -activated DNA cross-linking agents that showed in vitro anticancer activity and selectivity. This work focus on determining the in vivo efficacy and selectivity of some of the most promising  $\text{H}_2\text{O}_2$ -activated DNA cross-linking agents.

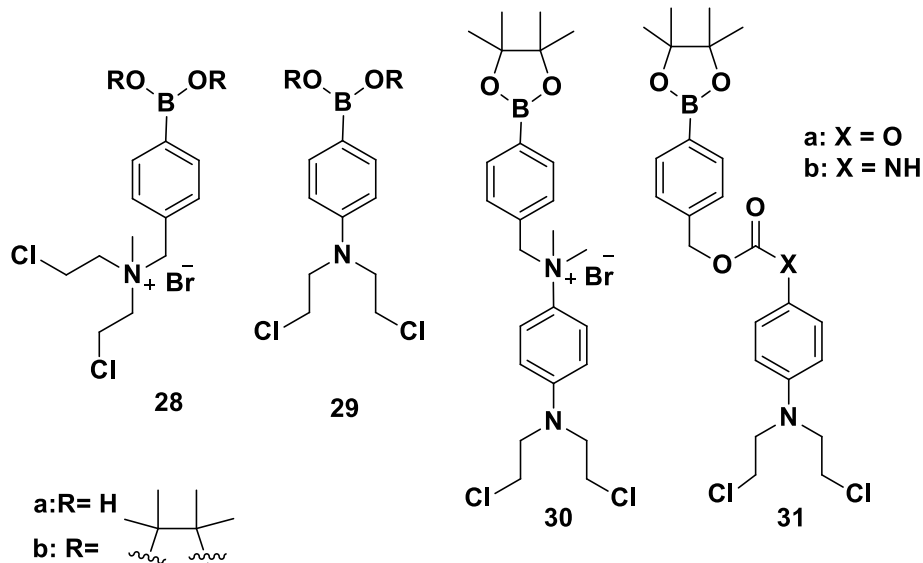
**$\text{H}_2\text{O}_2$ -inducible DNA Cross-linking Agents.** Major problems of DNA cross-linking agents as anticancer drugs are their poor selectivity for cancer cells. Except for being toxic to cancer cells, they are also harmful to normal cells. To enhance the selectivity and reduce the toxicity of DNA cross-linking agents,  $\text{H}_2\text{O}_2$ -activated prodrugs have been developed that are only activated under tumor-specific conditions. It is well known<sup>48</sup> that boronic acid or boronic esters (A) can selectively react with  $\text{H}_2\text{O}_2$  to generate HO-containing compounds (B). The chemical reactivity of compounds can be greatly altered by changing from a boron group that withdraws electrons to a hydroxyl group that donates electrons. This is the foundation for the development of a variety of inducible DNA cross-linking agents that are activated by  $\text{H}_2\text{O}_2$ , with the aim of reducing the toxicity to normal cells, including  $\text{H}_2\text{O}_2$ -activated QM precursors<sup>41,49-51</sup> (scheme 1-18) and  $\text{H}_2\text{O}_2$ -activated nitrogen mustard precursors<sup>52-54</sup> (scheme 1-19). All of these  $\text{H}_2\text{O}_2$ -activated molecules contain a boronic acid or boronate ester as a  $\text{H}_2\text{O}_2$ -sensitive trigger unit. The strong electron withdrawing boron group in the trigger unit deactivates these molecules, but can selectively react with  $\text{H}_2\text{O}_2$  to produce a strong electron donating hydroxyl group, thereby activating the prodrugs to release DNA alkylating agents, QM or nitrogen mustard that cross-link DNA.



**Scheme 1-18.** H<sub>2</sub>O<sub>2</sub>-activated QM precursors.

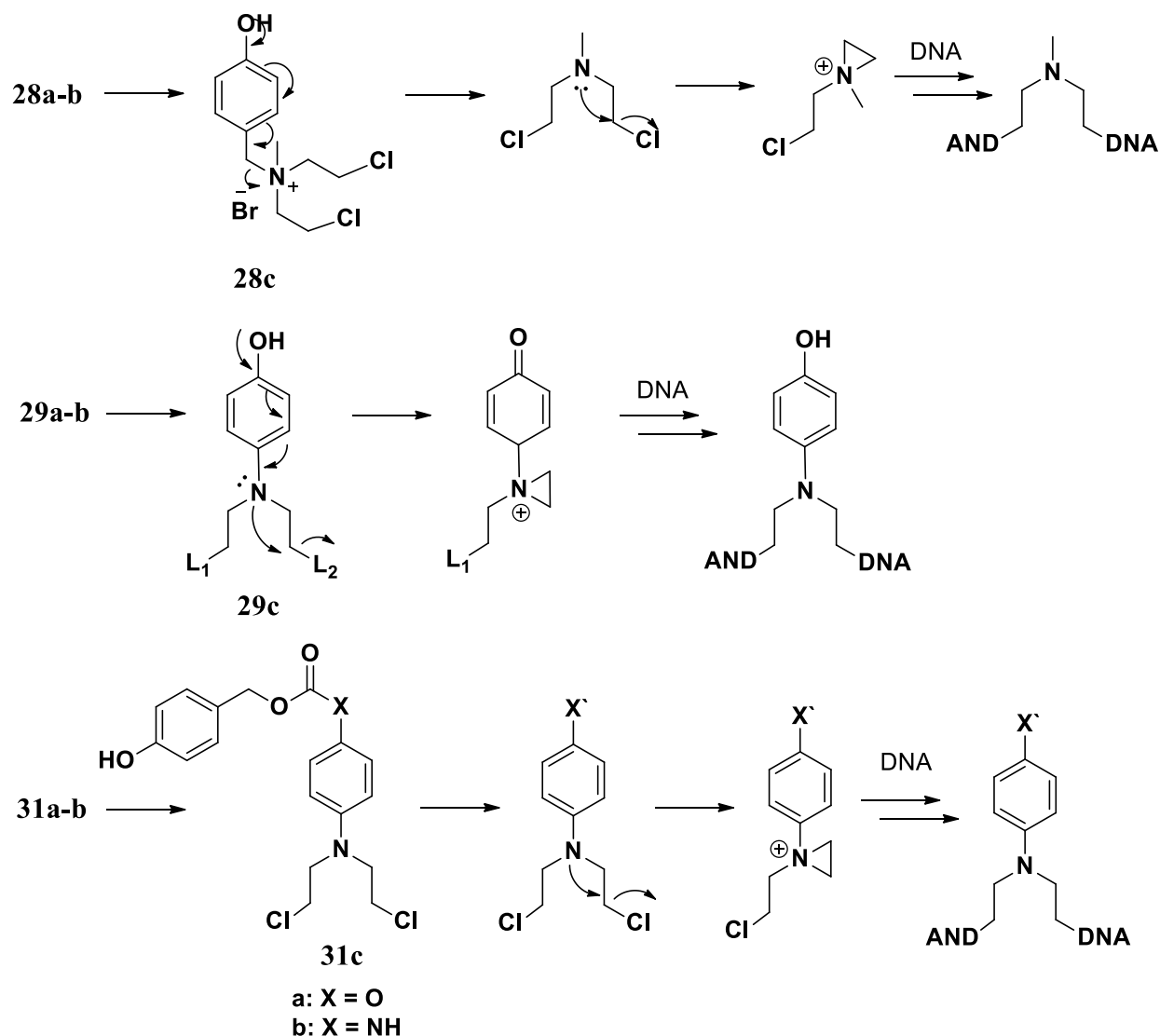
Compounds 23-25 (scheme 1-18) can be activated by H<sub>2</sub>O<sub>2</sub> to form highly reactive QM intermediates that directly cross-link DNA. Among them, 24 showed higher DNA cross-linking efficiency and selectivity as well as anticancer activity and selectivity<sup>51</sup>. We have also developed several classes of H<sub>2</sub>O<sub>2</sub>-activated nitrogen mustard precursors that contain a boronic acid or boronate ester as a trigger unit (scheme 1-29). In order to deactivate the nitrogen mustard, we employed three ways to decrease the electron density of mustard nitrogen that is highly important for its activity, including introducing a positive charge on mustard nitrogen (28),<sup>52</sup> using an electron-withdrawing linker connecting the boronate trigger and nitrogen mustard (30 and 31),<sup>54</sup> or directly attaching mustard nitrogen to the benzene ring of the phenylboronate group (29)<sup>53</sup>. The strong electron withdrawing boron group can deactivate the nitrogen mustard, but selectively react with H<sub>2</sub>O<sub>2</sub> to generate a strong electron donating OH group followed by releasing the highly active

nitrogen mustard.



**Scheme 1-19.** H<sub>2</sub>O<sub>2</sub>-inducible DAN cross-linking agents.

Compounds 28a-b, which contain a boronic acid (or ester) and a nitrogen mustard with a positive charge, were the first generation of H<sub>2</sub>O<sub>2</sub>-activated nitrogen mustard precursors<sup>52</sup>. Because of the positively charged nitrogen, these prodrugs were not active towards DNA, while the presence of boronic acid (or ester) in 28a-b allows their activation by H<sub>2</sub>O<sub>2</sub> to produce the phenol intermediate 28c, which spontaneously releases free nitrogen mustard directly cross-linking DNA. Compounds 28a-b showed good selectivity toward H<sub>2</sub>O<sub>2</sub>. In the presence of H<sub>2</sub>O<sub>2</sub>, high ICL yields were observed, while no ICL formation was observed without H<sub>2</sub>O<sub>2</sub>. The compounds also showed selective cytotoxicity, which inhibited the growth of cancer cells while had minimal effects on normal cells<sup>52</sup>. However, compounds 28a-b were found to have low anticancer activity, likely due to their positive charge that prevented them from passing through the cell membrane.



**Scheme 1-20:** Mechanism of action for H<sub>2</sub>O<sub>2</sub>-activated nitrogen mustard precursors

Later on, two classes of neutral compounds (29, 31) have been developed with the objective of increasing membrane permeability as well as anticancer activity and selectivity. Compounds 29 contain a nitrogen directly bonded to the benzene ring of the trigger unit phenylboronic acid (or ester) at the para-position. The boron group decreases the electron density of nitrogen by both inductive and resonance effects, therefore deactivating nitrogen mustard, while allows activation of nitrogen mustard with H<sub>2</sub>O<sub>2</sub> by generating a phenol intermediate 29c with a strong electron donating OH group which pushes electrons to the nitrogen therefore greatly enhancing its activity.

To study the effect of linker units on the selectivity of these prodrugs against hydrogen peroxide, compounds 30 were designed and synthesized (scheme 1-20). A carboxamide or carbonate linker connected the aromatic nitrogen mustard moiety to the trigger unit, thereby decreasing the electron density of the nitrogen and decreasing its activity. Reaction of 31 with  $\text{H}_2\text{O}_2$  results in the formation of 31c with a strong electron-donating group (OH,  $\text{NH}_2$ ) that induced efficient DNA ICL formation (scheme 1-20). These nitrogen mustard prodrugs formed DNA ICL products by alkylation at dG, dC, and dA sites.

Among these  $\text{H}_2\text{O}_2$ -activated nitrogen mustard prodrugs, **29** showed the best anticancer activity and selectivity, so it served as a lead compound for further optimization. We introduced various substituents in the benzene ring with different electronic properties and/or different size in order to tune its activity towards  $\text{H}_2\text{O}_2$ , anticancer activity and selectivity, as well as drug-like properties. We observed that a strong donating group (OMe) or a withdrawing group ( $\text{NO}_2$ ) decreased the selectivity. The groups with big size inhibit the cross-linking capability even in the presence of  $\text{H}_2\text{O}_2$  possibly due to prevention from interaction with DNA. Finally, compound x with a methyl group showed the best activity and selectivity. We also observed a boronic acid functional group greatly increased the water solubility which is highly important for in vivo study. So, this work focus on evaluating the in vivo efficacy and selectivity of modified 29a (methylated).

Currently, most methods for forming DNA ICL require chemical reagents, which makes in vivo applications quite complicated. Some require additional chemical reagents (CuI) that are highly toxic to the cells, which limited their applications under cellular conditions. In addition to their high toxicity, some require additional chemical reagents, which limits their use in cells. The photo-induction and  $\text{H}_2\text{O}_2$ -induction methods, however, are the most attractive of these methods because



of their bioorthogonal characteristics. A photo-induction method is a green method, which is a non-invasive and clean to use method, which does not require any additional chemicals to be used. In the body,  $H_2O_2$  is produced by endogenous processes. Cancer cells produce higher levels of  $H_2O_2$  than normal cells, which makes it possible to selectively crosslink DNA with  $H_2O_2$ -activated agents to target cancer cells..

## 1.6 Reference

- (1) Watson, J. D.; Crick, F. H. C. Molecular Structure of Nucleic Acids: A Structure for Deoxyribose Nucleic Acid. *Nature* **1953**, *171* (4356), 737–738. <https://doi.org/10.1038/171737a0>.
- (2) Richards, A. D.; Rodger, A. Synthetic Metallomolecules as Agents for the Control of DNA Structure. *Chem. Soc. Rev.* **2007**, *36* (3), 471–483. <https://doi.org/10.1039/B609495C>.
- (3) Becker, H.-C.; Nordén, B. DNA Binding Mode and Sequence Specificity of Piperazinylcarbonyloxyethyl Derivatives of Anthracene and Pyrene. *J. Am. Chem. Soc.* **1999**, *121* (51), 11947–11952. <https://doi.org/10.1021/ja991844p>.
- (4) Wilson, W. D.; Tanious, F. A.; Watson, R. A.; Barton, H. J.; Strekowska, A.; Harden, D. B.; Strekowski, L. Interaction of Unfused Tricyclic Aromatic Cations with DNA: A New Class of Intercalators. *Biochemistry* **1989**, *28* (5), 1984–1992. <https://doi.org/10.1021/bi00431a005>.
- (5) Tanious, F. A.; Jenkins, T. C.; Neidle, S.; Wilson, W. D. Substituent Position Dictates the Intercalative DNA-Binding Mode for Anthracene-9,10-Dione Antitumor Drugs. *Biochemistry* **1992**, *31* (46), 11632–11640. <https://doi.org/10.1021/bi00161a050>.
- (6) Pittillo, R. F.; Woolley, C. Pseudourea, 2,2'-(9,10-Anthrylenedimethylene) Bis-(2-Thio-, Dihydrochloride) Dihydrate: Microbiological Assay and Tissue Distribution Studies in Mice. *Appl. Microbiol.* **1969**, *18* (3), 519–521. <https://doi.org/10.1128/am.18.3.519-521.1969>.
- (7) Kumar, C. V.; Asuncion, E. H. DNA Binding Studies and Site Selective Fluorescence Sensitization of an Anthryl Probe. *J. Am. Chem. Soc.* **1993**, *115* (19), 8547–8553. <https://doi.org/10.1021/ja00072a004>.
- (8) Kumar, C. V.; Asuncion, E. H. Sequence Dependent Energy Transfer from DNA to a Simple Aromatic Chromophore. *J. Chem. Soc. Chem. Commun.* **1992**, No. 6, 470–472. <https://doi.org/10.1039/C39920000470>.
- (9) Kumar, C. V.; Tan, W. B.; Betts, P. W. Hexaminecobalt(III) Chloride Assisted, Visible Light Induced, Sequence Dependent Cleavage of DNA. *J. Inorg. Biochem.* **1997**, *68* (3), 177–181. [https://doi.org/10.1016/S0162-0134\(97\)00089-5](https://doi.org/10.1016/S0162-0134(97)00089-5).
- (10) Rodger, A. [10] Linear Dichroism. In *Methods in Enzymology; Metallobiochemistry Part C: Spectroscopic and Physical Methods for Probing Metal Ion Environments in Metalloenzymes and Metalloproteins*; Academic Press, 1993; Vol. 226, pp 232–258. [https://doi.org/10.1016/0076-6879\(93\)26012-X](https://doi.org/10.1016/0076-6879(93)26012-X).
- (11) Norden, B.; Kubista, M.; Kurucsev, T. Linear Dichroism Spectroscopy of Nucleic Acids. *Q. Rev. Biophys.* **1992**, *25* (1), 51–170. <https://doi.org/10.1017/S0033583500004728>.
- (12) Kumar, C. V.; Punzalan, E. H. A.; Tan, W. B. Adenine-Thymine Base Pair Recognition by an Anthryl Probe from the DNA Minor Groove. *Tetrahedron* **2000**, *56* (36), 7027–7040. [https://doi.org/10.1016/S0040-4020\(00\)00526-3](https://doi.org/10.1016/S0040-4020(00)00526-3).
- (13) Fisher, G. R.; Brown, J. R.; Patterson, L. H. Involvement of Hydroxyl Radical Formation and Dna Strand Breakage in the Cytotoxicity of Anthraquinone Antitumour Agents. *Free Radic. Res. Commun.* **1990**, *11* (1–3), 117–125. <https://doi.org/10.3109/10715769009109674>.
- (14) Chiriboga, X.; Gilardoni, G.; Magnaghi, I.; Vita Finzi, P.; Zanoni, G.; Vidari, G. New Anthracene Derivatives from Coussarea Macrophylla. *J. Nat. Prod.* **2003**, *66* (7), 905–909. <https://doi.org/10.1021/np030066i>.
- (15) Huang, Y.; Zhang, Y.; Zhang, J.; Zhang, D.-W.; Lu, Q.-S.; Liu, J.-L.; Chen, S.-Y.; Lin, H.-H.; Yu, X.-Q. Synthesis, DNA Binding and Photocleavage Study of Novel Anthracene-Appended Macrocyclic Polyamines. *Org. Biomol. Chem.* **2009**, *7* (11), 2278–2285. <https://doi.org/10.1039/B823416G>.
- (16) Tolpygin, I. E.; Bren', V. A.; Dubonosov, A. D.; Minkin, V. I.; Rybalkin, V. P. New Fluorescent Chemosensors on the Basis of 9-Aminomethylantracene. *Russ. J. Org. Chem.* **2003**, *39* (9), 1364–1366. <https://doi.org/10.1023/B:RUJO.0000010232.50792.88>.
- (17) Kraicheva, I. Synthesis and NMR Spectroscopic Study of a New Anthracene Derived Schiff Base and a Bis(Aminophosphonate) Obtained from It. *Phosphorus Sulfur Silicon Relat. Elem.* **2003**, *178*

- (1), 191–197. <https://doi.org/10.1080/10426500307783>.
- (18) Wang, C.; Delcros, J.-G.; Biggerstaff, J.; Phanstiel. Synthesis and Biological Evaluation of N-(Anthracen-9-Ylmethyl)Triamines as Molecular Recognition Elements for the Polyamine Transporter. *J. Med. Chem.* **2003**, *46* (13), 2663–2671. <https://doi.org/10.1021/jm030028w>.
- (19) Scheffer, U.; Strick, A.; Ludwig, V.; Peter, S.; Kalden, E.; Göbel, M. W. Metal-Free Catalysts for the Hydrolysis of RNA Derived from Guanidines, 2-Aminopyridines, and 2-Aminobenzimidazoles. *J. Am. Chem. Soc.* **2005**, *127* (7), 2211–2217. <https://doi.org/10.1021/ja0443934>.
- (20) Piątek, A. M.; Gray, M.; Anslyn, E. V. Guanidinium Groups Act as General-Acid Catalysts in Phosphoryl Transfer Reactions: A Two-Proton Inventory on a Model System. *J. Am. Chem. Soc.* **2004**, *126* (32), 9878–9879. <https://doi.org/10.1021/ja046894v>.
- (21) Anslyn, E.; Breslow, R. Geometric Evidence on the Ribonuclease Model Mechanism. *J. Am. Chem. Soc.* **1989**, *111* (15), 5972–5973. <https://doi.org/10.1021/ja00197a085>.
- (22) Du, J.-T.; Li, Y.-M.; Wei, Wu, G.-S.; Zhao, Y.-F.; Kanazawa, K.; Nemoto, T.; Nakanishi, H. Low-Barrier Hydrogen Bond between Phosphate and the Amide Group in Phosphopeptide. *J. Am. Chem. Soc.* **2005**, *127* (47), 16350–16351. <https://doi.org/10.1021/ja054568p>.
- (23) Wan, S.-H.; Liang, F.; Xiong, X.-Q.; Yang, L.; Wu, X.-J.; Wang, P.; Zhou, X.; Wu, C.-T. DNA Hydrolysis Promoted by 1,7-Dimethyl-1,4,7,10-Tetraazacyclododecane. *Bioorg. Med. Chem. Lett.* **2006**, *16* (10), 2804–2806. <https://doi.org/10.1016/j.bmcl.2006.01.106>.
- (24) Cheng, C. C.; Zee-Cheng, R. K. Y. 2 The Design, Synthesis and Development of a New Class of Potent Antineoplastic Anthraquinones. In *Progress in Medicinal Chemistry*; Ellis, G. P., West, G. B., Eds.; Elsevier, 1983; Vol. 20, pp 83–118. [https://doi.org/10.1016/S0079-6468\(08\)70217-0](https://doi.org/10.1016/S0079-6468(08)70217-0).
- (25) Boseggia, E.; Gatos, M.; Lucatello, L.; Mancin, F.; Moro, S.; Palumbo, M.; Sissi, C.; Tecilla, P.; Tonellato, U.; Zagotto, G. Toward Efficient Zn(II)-Based Artificial Nucleases. *J. Am. Chem. Soc.* **2004**, *126* (14), 4543–4549. <https://doi.org/10.1021/ja039465q>.
- (26) Roe, F. J. C.; Dipple, A.; Mitchley, B. C. V. Carcinogenic Activity of Some Benz(a)Anthracene Derivatives in Newborn Mice. *Br. J. Cancer* **1972**, *26* (6), 461–465. <https://doi.org/10.1038/bjc.1972.63>.
- (27) Gude, L.; Fernández, M.-J.; Grant, K. B.; Lorente, A. Syntheses and Copper(II)-Dependent DNA Photocleavage by Acridine and Anthracene 1,10-Phenanthroline Conjugate Systems. *Org. Biomol. Chem.* **2005**, *3* (10), 1856–1862. <https://doi.org/10.1039/B502485D>.
- (28) *DNA-Ligand Interactions: From Drugs to Proteins*; Guschlbauer, W., Saenger, W., NATO Advanced Study Institute, Federation of European Biochemical Societies, North Atlantic Treaty Organization, Eds.; NATO ASI series; Plenum Press: New York, 1987.
- (29) Suh, D.; Chaires, J. B. Criteria for the Mode of Binding of DNA Binding Agents. *Bioorg. Med. Chem.* **1995**, *3* (6), 723–728. [https://doi.org/10.1016/0968-0896\(95\)00053-J](https://doi.org/10.1016/0968-0896(95)00053-J).
- (30) Tichenor, M. S.; MacMillan, K. S.; Trzuppek, J. D.; Rayl, T. J.; Hwang, I.; Boger, D. L. Systematic Exploration of the Structural Features of Yatakemycin Impacting DNA Alkylation and Biological Activity. *J. Am. Chem. Soc.* **2007**, *129* (35), 10858–10869. <https://doi.org/10.1021/ja072777z>.
- (31) Lerman, L. S. Structural Considerations in the Interaction of DNA and Acridines. *J. Mol. Biol.* **1961**, *3* (1), 18-IN14. [https://doi.org/10.1016/S0022-2836\(61\)80004-1](https://doi.org/10.1016/S0022-2836(61)80004-1).
- (32) Kim, H. N.; Lim, J.; Lee, H. N.; Ryu, J.-W.; Kim, M. J.; Lee, J.; Lee, D.-U.; Kim, Y.; Kim, S.-J.; Lee, K. D.; Lee, H.-S.; Yoon, J. Unique X-Ray Sheet Structure of 1,8-Bis(Imidazolium) Anthracene and Its Application as a Fluorescent Probe for DNA and DNase. *Org. Lett.* **2011**, *13* (6), 1314–1317. <https://doi.org/10.1021/ol103166q>.
- (33) Ghosh, K.; Sarkar, A. R.; Ghorai, A.; Ghosh, U. Design and Synthesis of Anthracene-Based Bispypyridinium Amides: Anion Binding, Cell Staining and DNA Interaction Studies. *New J. Chem.* **2012**, *36* (5), 1231–1245. <https://doi.org/10.1039/C2NJ21024J>.
- (34) de Silva, S. A.; Zavaleta, A.; Baron, D. E.; Allam, O.; Isidor, E. V.; Kashimura, N.; Percarpio, J. M. A Fluorescent Photoinduced Electron Transfer Sensor for Cations with an Off-on-off Proton Switch. *Tetrahedron Lett.* **1997**, *38* (13), 2237–2240. [27](https://doi.org/10.1016/S0040-</a></p></div><div data-bbox=)

- 4039(97)00332-8.
- (35) Weiss, R. B. The Anthracyclines: Will We Ever Find a Better Doxorubicin? *Semin. Oncol.* **1992**, *19* (6), 670–686.
- (36) Fry, D. W. Biochemical Pharmacology of Anthracenediones and Anthrapyrazoles. *Pharmacol. Ther.* **1991**, *52* (1), 109–125. [https://doi.org/10.1016/0163-7258\(91\)90089-5](https://doi.org/10.1016/0163-7258(91)90089-5).
- (37) Rajski, S. R.; Williams, R. M. DNA Cross-Linking Agents as Antitumor Drugs. *Chem. Rev.* **1998**, *98* (8), 2723–2796. <https://doi.org/10.1021/cr9800199>.
- (38) Stern, R. S. Malignant Melanoma in Patients Treated for Psoriasis with PUVA. *Photodermatol. Photoimmunol. Photomed.* **1999**, *15* (1), 37–38. <https://doi.org/10.1111/j.1600-0781.1999.tb00052.x>.
- (39) Kitamura, N.; Kohtani, S.; Nakagaki, R. Molecular Aspects of Furocoumarin Reactions: Photophysics, Photochemistry, Photobiology, and Structural Analysis. *J. Photochem. Photobiol. C Photochem. Rev.* **2005**, *6* (2), 168–185. <https://doi.org/10.1016/j.jphotochemrev.2005.08.002>.
- (40) Via, L. D.; Magno, S. M.; Rodighiero, P.; Gia, O. Synthesis, Photobiological Activity and Photoreactivity of Methyl-Thieno-8-Azacoumarins, Novel Bioisosters of Psoralen. *Bioorg. Med. Chem. Lett.* **2002**, *12* (9), 1253–1257. [https://doi.org/10.1016/S0960-894X\(02\)00152-X](https://doi.org/10.1016/S0960-894X(02)00152-X).
- (41) Han, Y.; Chen, W.; Kuang, Y.; Sun, H.; Wang, Z.; Peng, X. UV-Induced DNA Interstrand Cross-Linking and Direct Strand Breaks from a New Type of Binitroimidazole Analogue. *Chem. Res. Toxicol.* **2015**, *28* (5), 919–926. <https://doi.org/10.1021/tx500522r>.
- (42) Wang, Y.; Lin, Z.; Fan, H.; Peng, X. Photoinduced DNA Interstrand Cross-Link Formation by Naphthalene Boronates via a Carbocation. *Chem. – Eur. J.* **2016**, *22* (30), 10382–10386. <https://doi.org/10.1002/chem.201601504>.
- (43) Wang, Y.; Liu, S.; Lin, Z.; Fan, Y.; Wang, Y.; Peng, X. Photochemical Generation of Benzyl Cations That Selectively Cross-Link Guanine and Cytosine in DNA. *Org. Lett.* **2016**, *18* (11), 2544–2547. <https://doi.org/10.1021/acs.orglett.6b00755>.
- (44) Szatrowski, T. P.; Nathan, C. F. Production of Large Amounts of Hydrogen Peroxide by Human Tumor Cells. *Cancer Res.* **1991**, *51* (3), 794–798.
- (45) Toyokuni, S.; Okamoto, K.; Yodoi, J.; Hiai, H. Persistent Oxidative Stress in Cancer. *FEBS Lett.* **1995**, *358* (1), 1–3. [https://doi.org/10.1016/0014-5793\(94\)01368-B](https://doi.org/10.1016/0014-5793(94)01368-B).
- (46) Zhou, Y.; Hileman, E. O.; Plunkett, W.; Keating, M. J.; Huang, P. Free Radical Stress in Chronic Lymphocytic Leukemia Cells and Its Role in Cellular Sensitivity to ROS-Generating Anticancer Agents. *Blood* **2003**, *101* (10), 4098–4104. <https://doi.org/10.1182/blood-2002-08-2512>.
- (47) Kamiguti, A. S.; Serrander, L.; Lin, K.; Harris, R. J.; Cawley, J. C.; Allsup, D. J.; Slupsky, J. R.; Krause, K.-H.; Zuzel, M. Expression and Activity of NOX5 in the Circulating Malignant B Cells of Hairy Cell Leukemia. *J. Immunol.* **2005**, *175* (12), 8424–8430. <https://doi.org/10.4049/jimmunol.175.12.8424>.
- (48) Cadahía, J. P.; Previtali, V.; Troelsen, N. S.; Clausen, M. H. Prodrug Strategies for Targeted Therapy Triggered by Reactive Oxygen Species. *MedChemComm* **2019**, *10* (9), 1531–1549. <https://doi.org/10.1039/C9MD00169G>.
- (49) Saxon, E.; Peng, X. Recent Advances in Hydrogen Peroxide Responsive Organoborons for Biological and Biomedical Applications. *ChemBioChem* **2022**, *23* (3), e202100366. <https://doi.org/10.1002/cbic.202100366>.
- (50) Kuivila, H. G.; Armour, A. G. Electrophilic Displacement Reactions. IX. Effects of Substituents on Rates of Reactions between Hydrogen Peroxide and Benzeneboronic Acid1-3. *J. Am. Chem. Soc.* **1957**, *79* (21), 5659–5662. <https://doi.org/10.1021/ja01578a020>.
- (51) Cao, S.; Wang, Y.; Peng, X. The Leaving Group Strongly Affects H<sub>2</sub>O<sub>2</sub>-Induced DNA Cross-Linking by Arylboronates. *J. Org. Chem.* **2014**, *79* (2), 501–508. <https://doi.org/10.1021/jo401901x>.
- (52) Cao, S.; Wang, Y.; Peng, X. ROS-Inducible DNA Cross-Linking Agent as a New Anticancer Prodrug Building Block. *Chem. – Eur. J.* **2012**, *18* (13), 3850–3854. <https://doi.org/10.1002/chem.201200075>.

- (53) Wang, Y.; Fan, H.; Balakrishnan, K.; Lin, Z.; Cao, S.; Chen, W.; Fan, Y.; Guthrie, Q. A.; Sun, H.; Teske, K. A.; Gandhi, V.; Arnold, L. A.; Peng, X. Hydrogen Peroxide Activated Quinone Methide Precursors with Enhanced DNA Cross-Linking Capability and Cytotoxicity towards Cancer Cells. *Eur. J. Med. Chem.* **2017**, *133*, 197–207. <https://doi.org/10.1016/j.ejmech.2017.03.041>.
- (54) Kuang, Y.; Balakrishnan, K.; Gandhi, V.; Peng, X. Hydrogen Peroxide Inducible DNA Cross-Linking Agents: Targeted Anticancer Prodrugs. *J. Am. Chem. Soc.* **2011**, *133* (48), 19278–19281. <https://doi.org/10.1021/ja2073824>.
- (55) Chen, W.; Balakrishnan, K.; Kuang, Y.; Han, Y.; Fu, M.; Gandhi, V.; Peng, X. Reactive Oxygen Species (ROS) Inducible DNA Cross-Linking Agents and Their Effect on Cancer Cells and Normal Lymphocytes. *J. Med. Chem.* **2014**, *57* (11), 4498–4510. <https://doi.org/10.1021/jm401349g>.
- (56) Chen, W.; Han, Y.; Peng, X. Aromatic Nitrogen Mustard-Based Prodrugs: Activity, Selectivity, and the Mechanism of DNA Cross-Linking. *Chem. – Eur. J.* **2014**, *20* (24), 7410–7418. <https://doi.org/10.1002/chem.201400090>.

## Chapter 2. Photo-induced DNA interstrand cross-link

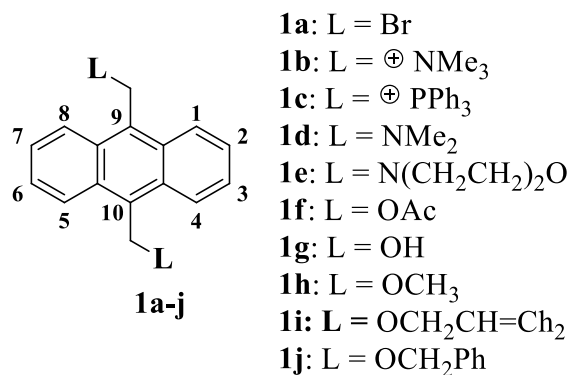
### formation with anthracene as core structure.

#### 2.1 Introduction

Anthracene, a polycyclic aromatic ring, is a well-known DNA intercalator which makes it attractive for DNA interstrand cross-linking study. Planarity of anthracene ring is considered one of the important features for efficient intercalation into the nonpolar interior of the DNA double helix. It has a large binding constant with DNA bases and can be sensitized by DNA which is a unique feature of it. In addition, anthryl chromophore is photo-chemically reactive and has large singlet excited state energy which is good for initiating photochemical reaction. In addition, anthracene has a longer wavelength of maximum absorption which is higher than 350 nm. This is very useful to use it as longer wavelength means lower energy which is less harmful to biological materials such as DNA, RNA, and proteins etc. We designed and synthesized nine anthracene analogues **1a-i** containing different functional groups on the anthracene backbone as leaving groups, investigated the photo reactivities of these molecules towards DNA, and demonstrated the mechanism of function. Many of these analogues efficiently induced DNA ICL formation via a photo-generated carbocation upon 350 nm irradiation. The leaving groups strongly affect the photo-induced DNA cross-linking formation. A trimethyl ammonium salt (**1b**) as a leaving group greatly facilitates the DNA ICL reaction, which is complete within minutes. To make DNA cross-linking agent that can cross-link faster than usual as well as can be activated easily. We designated some anthracene-based analogues to explore the potential of cross-linking by anthryl chromophore. Subsequently, we will improve the ICL formation efficacy by structure modification.

Nine 9,10-anthryl compounds having different leaving groups were synthesized. Interstrand cross-

linking reactions had been conducted under 350 nm UV irradiation and mechanism is studied.



Scheme 2-1. The structures of **1a-j**.

We designed several 9,10 anthracene derivatives based on 9-anthrylmethyl)ammonium chloride (AMAC) which was reported to be efficiently intercalating DNA<sup>1</sup>. Based on their observation we designed bis anthryl compound **1a-j** using bromomethyl, trimethyl amine, triphenylphosphine, dimethyl amine, morpholine, acetate, methanol, oxymethyl, oxy-allyl and oxy-phenyl groups as photoactivable leaving groups.

Bromomethyl, trimethyl amine, triphenylphosphine, dimethyl amine, morpholine, acetate, methanol, oxymethyl, oxy-allyl and oxy-phenyl has already proven to be effective photoinducible leaving groups with different benzyl and naphthalene aromatic hydrocarbons with various substituents. They produce carbocation and/or free radicals upon photoirradiation at 350nm thus making it effective DNA cross-linking agents. We synthesized **1a-j**, tested their DNA cross-linking efficiency upon irradiation at 350nm and tried to characterize the cross-link formation mechanism.

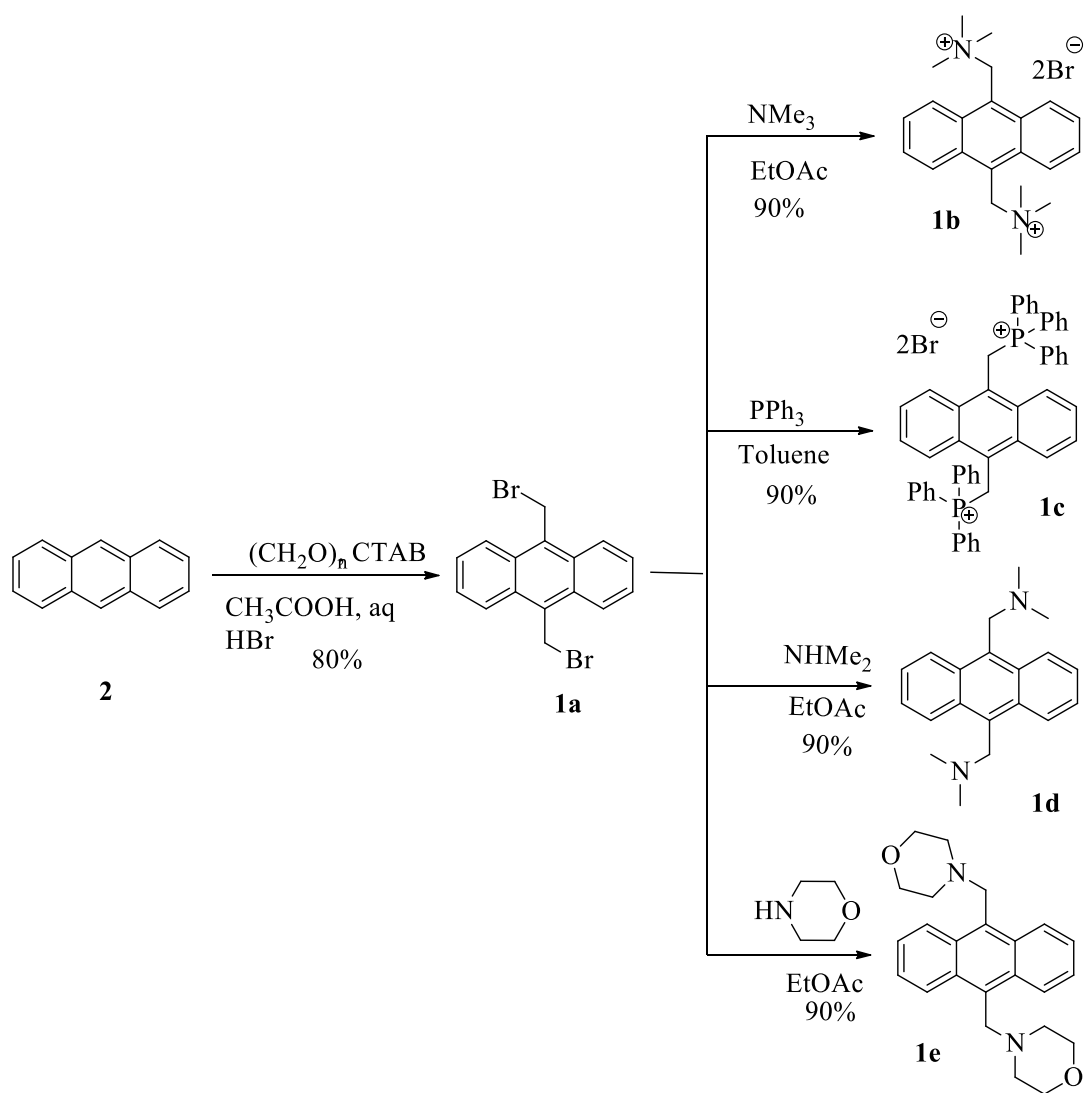
## 2.2 Anthracene analogues as Photo-inducible DNA Cross-linking Agents

### 2.2.1 Synthesis of 9, 10-anthryl derivatives contain various leaving groups

Compounds **1a-e** were synthesized starting from anthracene **2** (Schemes 2-2). As previously described<sup>2</sup>, **2** was treated with paraformaldehyde, cetyltrimethylammonium bromide (CTAB),

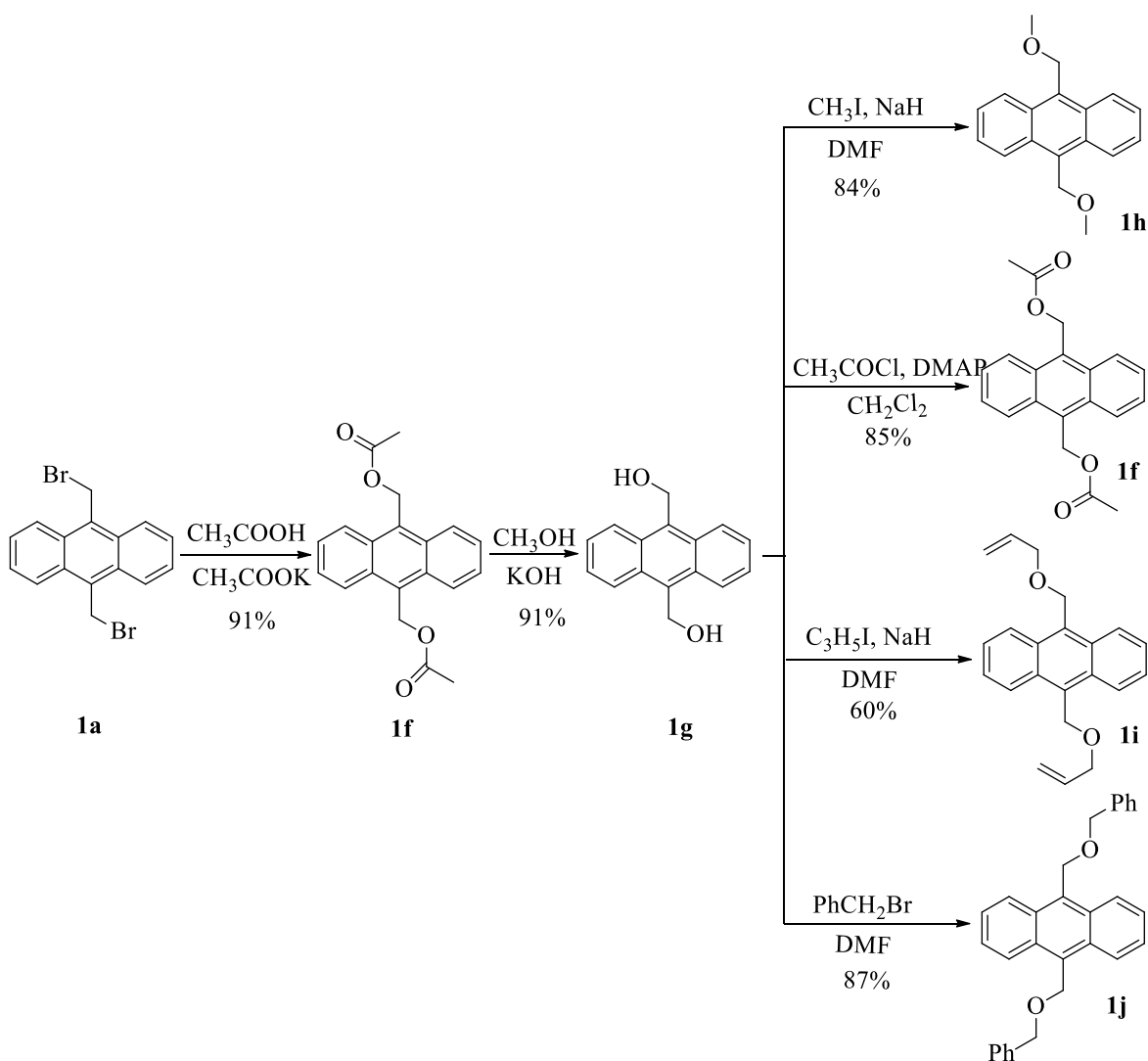
and aq. HBr in acetic acid to generate the bromomethylated product **1a** that was converted to **1b-e** via nucleophilic substitution reaction in almost quantitative yields. Compound **1b** was obtained from **1a** by treating with trimethylamine in ethyl acetate, while **1c**, **1d**, and **1e** were generated by treatment of **1a** with triphenylphosphine, dimethylamine, and morpholine respectively (Scheme 2-2). All compounds are characterized by NMR.





Scheme 2-2. Synthesis of **1a-e**.

Compounds **1f-i** were prepared starting from **1a** that was first converted **1f** containing the acetate as a leaving group by treatment with acetic acid and potassium acetate. Compound **1f** was then hydrolyzed with methanol and potassium hydroxide to generate **1g**. Compounds **1h**, **1i**, and **1j** were obtained by treatment of **1g** with methyl iodide, allyl iodide, and benzyl bromide, respectively.



**Scheme 2-3.** Synthesis of **1f-j**.

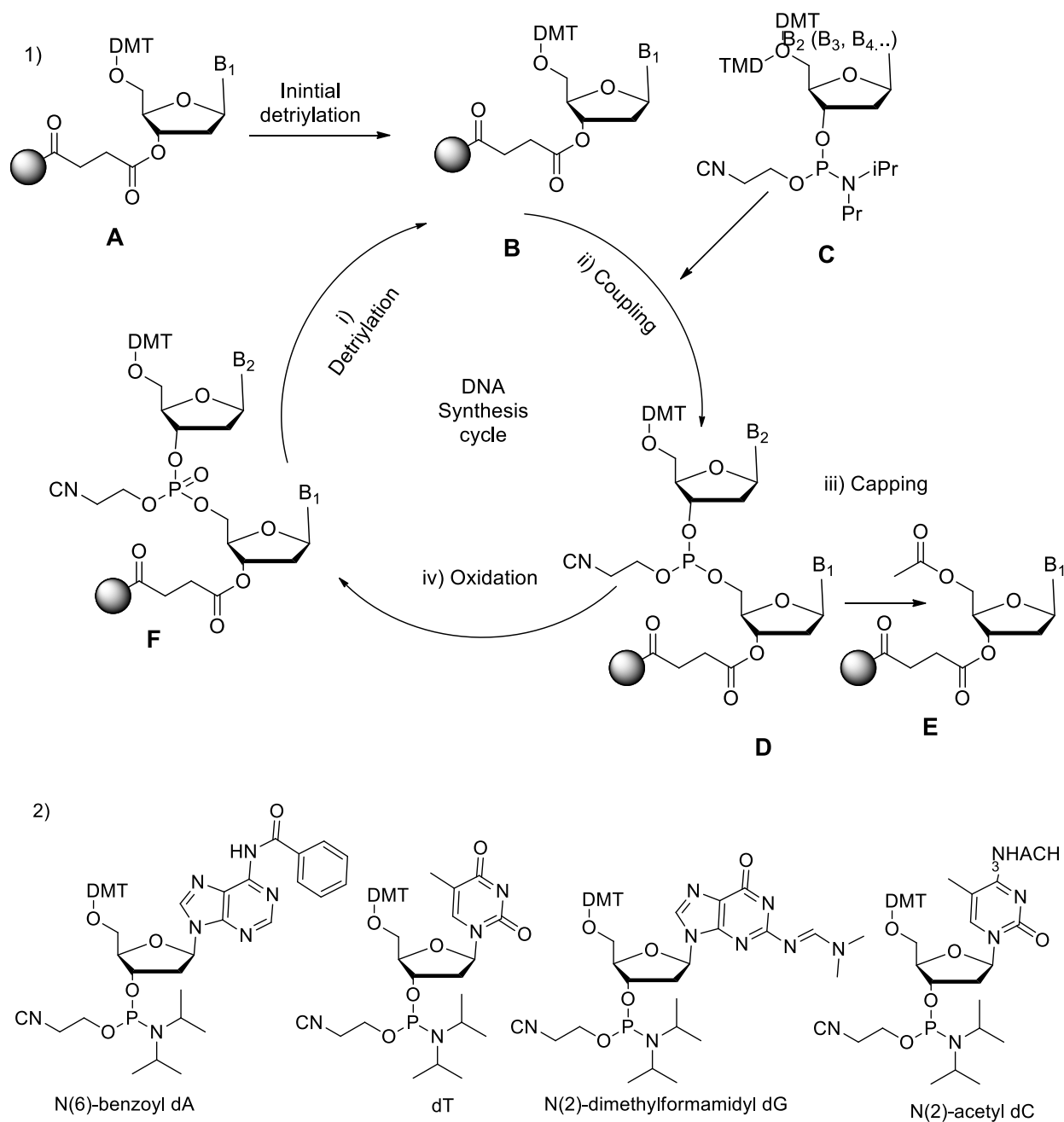
### 2.2.2 Preparation of DNA Duplex

**ODN sequence design.** A 49-mer double helix Oligonucleotide (ODN) **3** was used for studying the photo reactivity of **1a-j** towards DNA. The sequences of duplex **3** is part of p53 genes that have been used in our previous study<sup>3,4</sup> (Scheme 2-4). The DNA damages in p53 gene may result in uncontrolled cell cycles, causing uncontrolled growth of abnormal cells and eventually leading to cancer. There are more than 50% human cancers caused by p53 gene mutation<sup>3,4</sup>.

1            5 6                    14 15    18            22 24 25 27            31                    40    44            49  
 5' -dGCCTAGTTCTTTTAATTACTTGCAATGCAAGTAATTAAAGCTTGATCTG (**3a**)  
 3' -dCGGATCAAGAAAATTAATGAACGTTACGTTCAATTAATTTCGAACTAGAC (**3b**)

**Scheme 2-4.** The sequence of DNA duplex **3**.

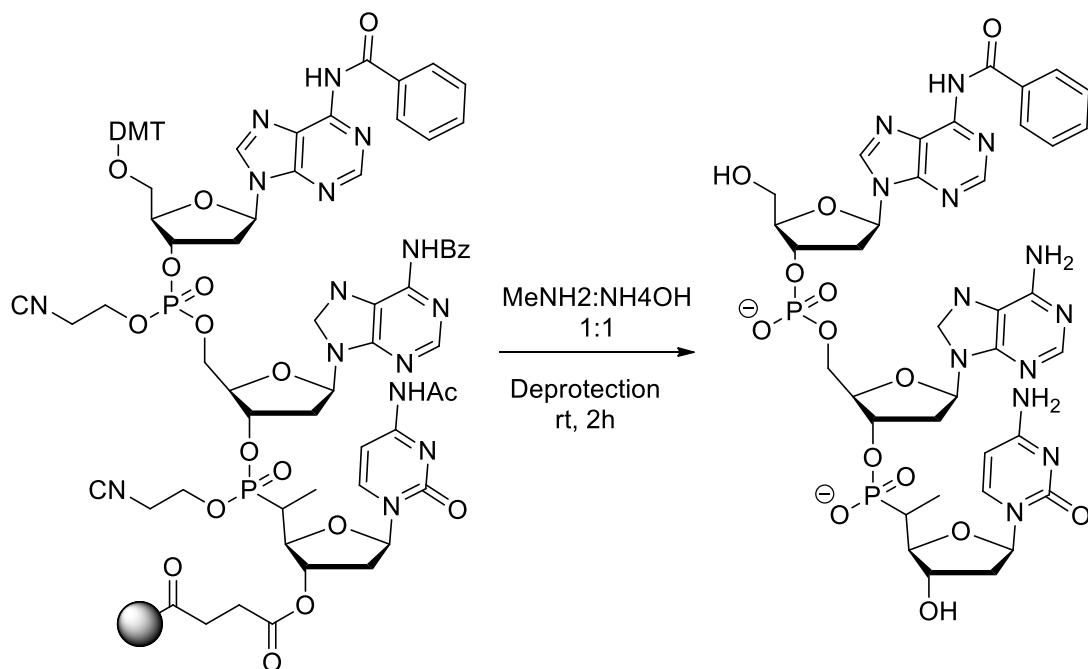
**ODN synthesis.** Oligonucleotides were synthesized via standard solid-phase DNA synthesis techniques using commercially available phosphoramidites (Scheme 2-5). The ODN synthesis goes from the 3'- to 5'-direction. One nucleotide is attached per synthesis cycle. Each cycle contains four steps: (i) detritylation (removal of 4,4'-dimethoxytrityl group), (ii) activation (protonation of diisopropylamine group of the incoming phosphoramidite building block) and (iii) coupling (the terminal 5'-hydroxyl group of the growing ODN chain (**B**) attacks the phosphorus atom of the incoming phosphoramidite building block (**C**) to form a new P-O bond), (iii) capping (block the unreacted 5'-end hydroxyl groups (**E**)), and (iv) oxidation (convert P (III) to P (V)).



**Scheme 2-5.** Automated DNA synthesis cycle (1) and structures of phosphoramidites (2).

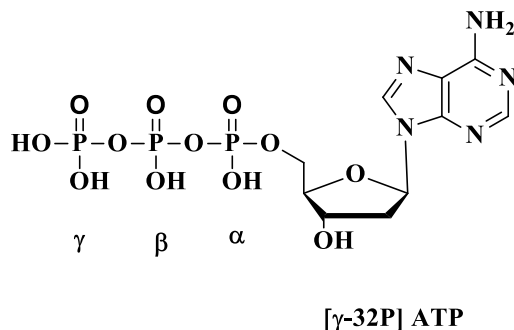
**ODN purification.** The ODNs were deprotected and cleaved from the solid support under mild conditions using a mixture of 40% aqueous  $\text{MeNH}_2$  and 28% aqueous  $\text{NH}_3$  (1:1) at rt for 2 h, then purified by 20% denaturing polyacrylamide gel electrophoresis (PAGE) followed by desalination using the column x. The  $\beta$ -cyanoethyl group was removed by  $\beta$ -elimination reaction. All protecting

groups in the base moieties were removed by hydrolysis.



**Scheme 2-6.** Deprotection scheme..

**<sup>32</sup>P-Labeling at the 5'-end of oligodeoxyribonucleotides.** ODN **3a** was 5'-end labeled using gamma <sup>32</sup>P ATP ([ $\gamma$ -<sup>32</sup>P] ATP) and T4 polynucleotide kinase (T4 PNK) with standard protocol, where T4 PNK transfers the gamma-phosphate from ATP to the 5'-OH group.



**Scheme 2-7.** The structure of [ $\gamma$ -<sup>32</sup>P] ATP.

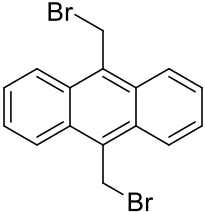
### 2.2.3 DNA interstrand cross-linking assay

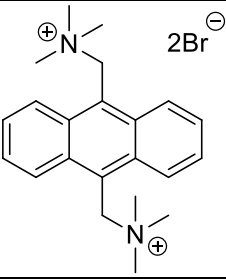
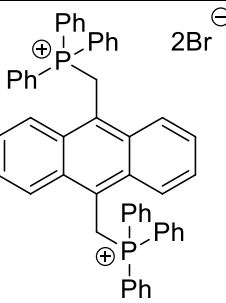
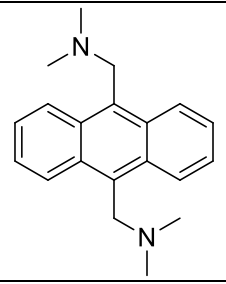
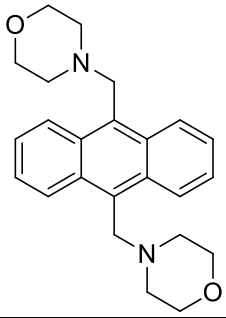
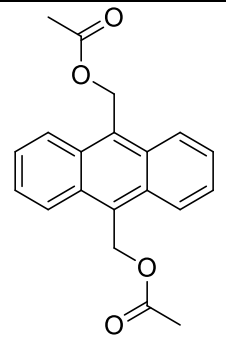
After having synthesized **1a-j**, we studied their photo reactivities towards DNA using a 49-mer

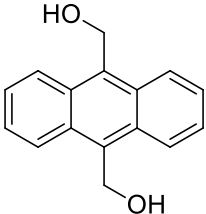
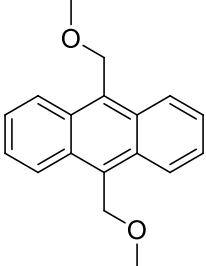
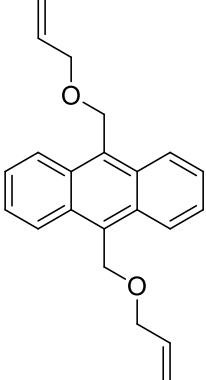
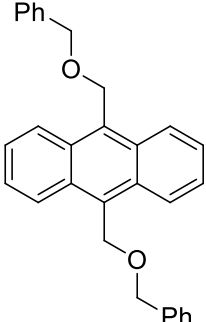
DNA duplex (**3**) in a phosphate buffer (pH 8.0) upon 350 nm irradiation by assessing DNA ICL formation<sup>5,6</sup>. PAGE was used for DNA ICL analysis. The cross-linked and the single-stranded DNA can be distinguished by PAGE because they migrate differently in the polyacrylamide gel due to different molecular size. The cross-linked products with larger molecular size migrate slower than the single-stranded ODN. Molecular Dynamics phosphorimager (ImageQuant, version 5.2) was used for quantification of DNA ICL yields, where the ICLs and the single strands show different bands on the image plate. Origin 8.0 software was used for data plot and curve fitting.

**Solubility:** Initially we tested the solubility of **1a-j** in an aqueous solution as well as different organic solvents. It showed that **1b** has excellent solubility in water while **1c** has only slight water solubility. Other analogues **1a** and **1d-j** are insoluble in water and only slightly soluble in organic solvents used for DNA ICL study, such as CH<sub>3</sub>CN..... Compounds **1b-e** are soluble in methanol while **1a** and **1f-j** have better solubility in chloroform. It was observed that all compounds (**1a** and **1c-j**) except for **1b** showed better solubility in DMSO than any other organic solvents. Thus, we decided to do DNA cross-linking study of **1b** with water and **1a** and **1c-j** with DMSO. Besides we studied the effect of solvent ratio (DMSO:phosphate buffer) on the photo-induced ICL formation of **1b**.

**Table 2-1.** The solubility of **1a-j**.

| Compound  | Structure   | Solvents with good solubility |
|-----------|---|-------------------------------|
| <b>1a</b> |  | DMSO, CHCl <sub>3</sub>       |

|           |   |   |
|-----------|---|---|
| <b>1b</b> |    | H <sub>2</sub> O, MeOH  |
| <b>1c</b> |    | DMSO, MeOH, H <sub>2</sub> O                                      |
| <b>1d</b> |   | DMSO, MeOH  |
| <b>1e</b> |  | DMSO, MeOH  |
| <b>1f</b> |  | CHCl <sub>3</sub> , CH <sub>2</sub> Cl <sub>2</sub> , EtOAc, DMSO |

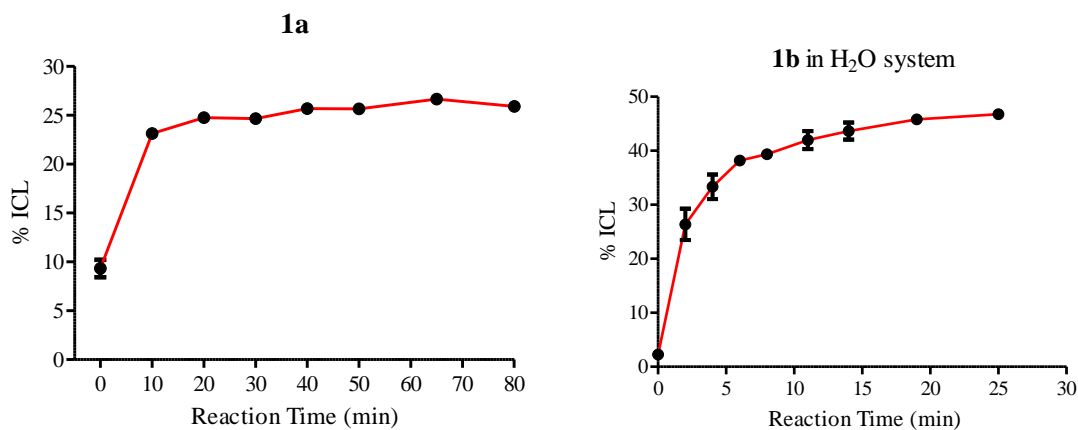
|           |   |   |
|-----------|---|---|
| <b>1g</b> |    | DMSO, MeOH  |
| <b>1h</b> |    | CHCl <sub>3</sub> , CH <sub>2</sub> Cl <sub>2</sub> , EtOAc, DMSO |
| <b>1i</b> |   | CHCl <sub>3</sub> , CH <sub>2</sub> Cl <sub>2</sub> , EtOAc, DMSO |
| <b>1j</b> |  | CHCl <sub>3</sub> , CH <sub>2</sub> Cl <sub>2</sub> , EtOAc, DMSO |

We tested the DNA cross-linking ability of **1a-j** in the presence or absence of 350 nm light. These compounds did not induce DNA ICL formation without photo irradiation while efficient DNA cross-linking was achieved upon UV irradiation at 350 nm. Previous study showed that the DNA cross-linking efficiency strongly depended on the irradiation time and the concentration of the substrates<sup>5</sup>. To fully understand how the anthracene ring and various leaving groups affect the

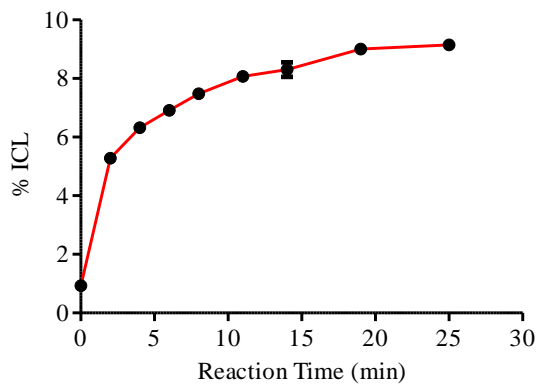


DNA cross-linking ability, we first optimized the reaction time and compound concentration to obtain optimal DNA cross-linking efficiency for **1a-j**.

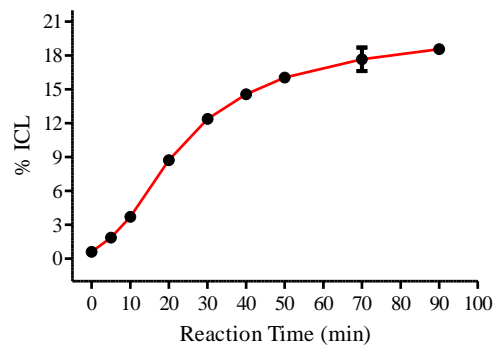
**Time-dependent DNA cross-link study.** We carried out the time-dependent DNA cross-linking study of **1a-j** with a concentration of 500  $\mu\text{M}$  to determine the time needed to achieve the highest DNA ICL yield. In general, the DNA ICL yields gradually enhanced with the increased reaction time, and then reached a balance at specific time points. Further increase of the reaction time did not enhance the ICL yields. This time was then defined as optimal reaction time for the compound. The optimal reaction time for **1b** in buffer only and in buffer:DMSO system (Buffer: DMSO= 7:3 ratio) was found to be 5 min and 20 min approximately. The optimal time for **1a** and **1c-j** in buffer:DMSO system (7:3 ratio) is 55 min, 50 min, 360 min, 480 min, 600 min, 240 min, 300 min and 300 min respectively (Figure 2-1 and Table 2-2).



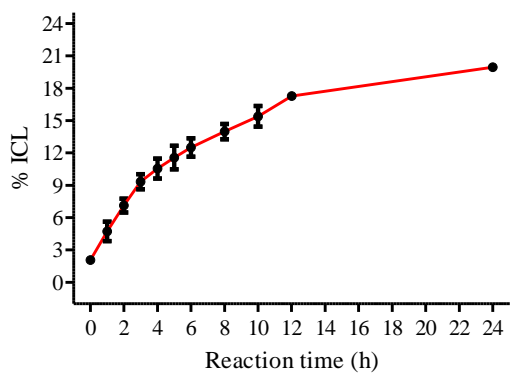
**1b** in H<sub>2</sub>O:DMSO system



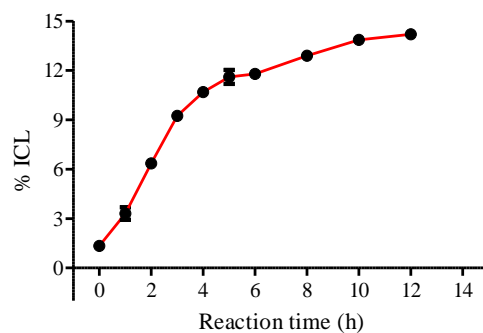
**1c**



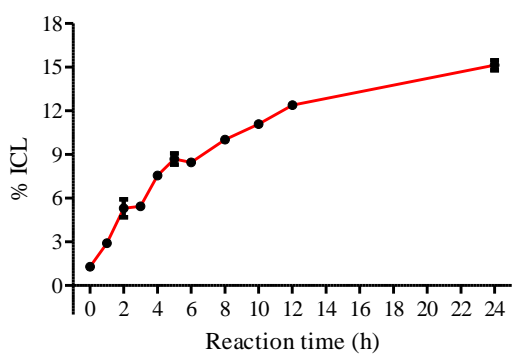
**1f**



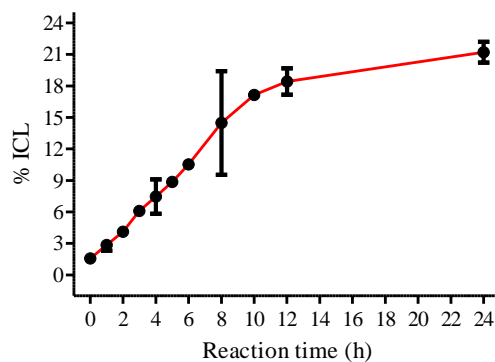
**1d**



**1g**



**1e**



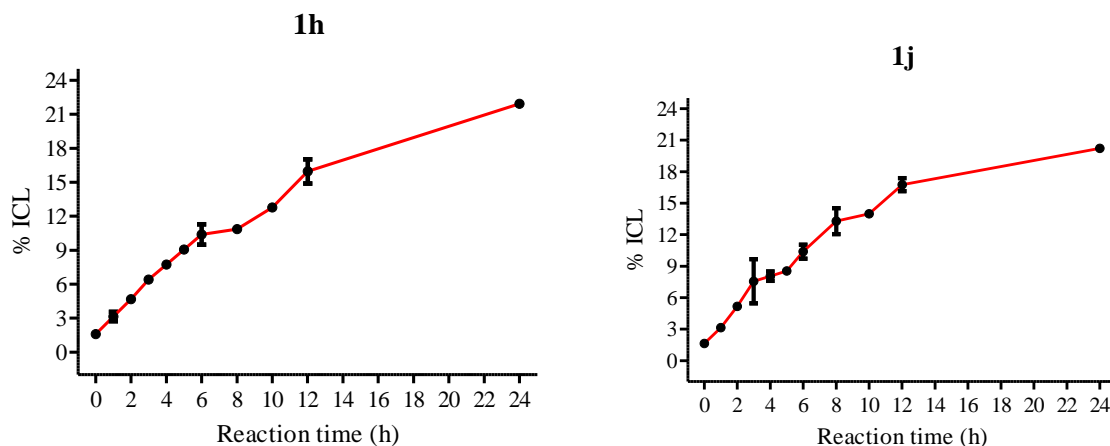


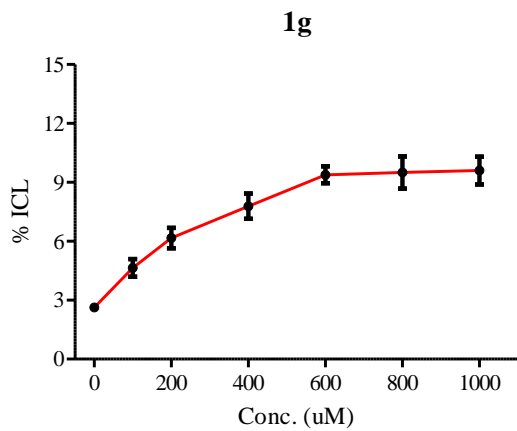
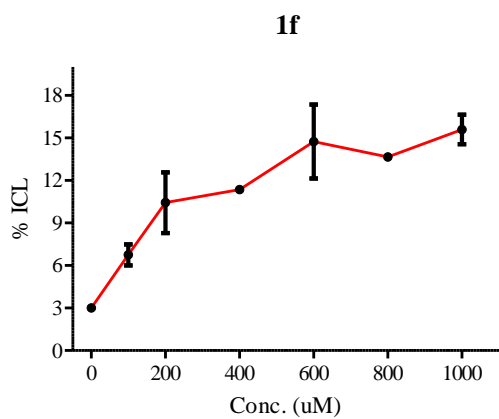
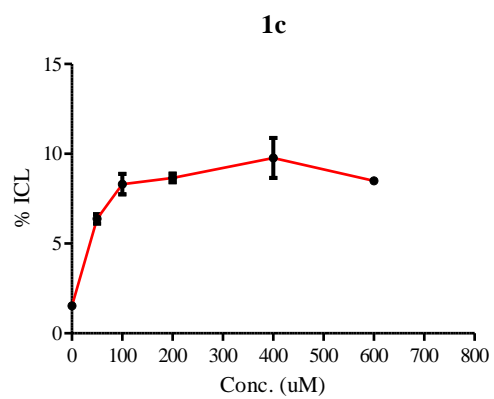
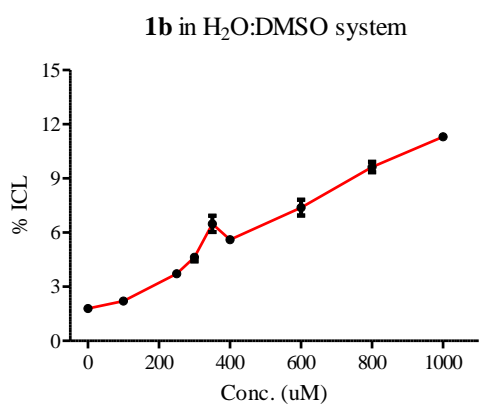
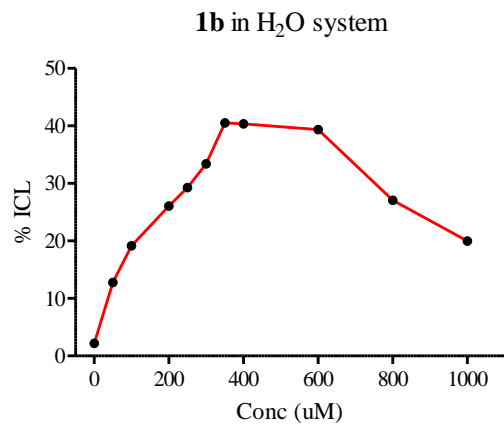
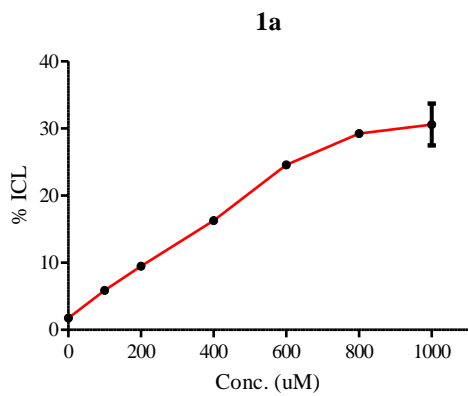
**Figure 2-1.** Time-dependence of DNA ICL formation of duplex **3** for **1a-j** upon photo-irradiation.

Solvent ratio for all compounds tested was H<sub>2</sub>O:DMSO = 7:3, except for **1b** which was tested in both H<sub>2</sub>O only and H<sub>2</sub>O:DMSO system. **1a** at time points 0', 10', 20', 30', 40', 50', 65' and 80 min. [**1a**] = 500 μM; **1b** (Solvent: H<sub>2</sub>O only) at time points 0, 2, 4, 6, 8, 11, 14, 19, 25 min [**1b**] = 500 μM; **1b** (Solvent: H<sub>2</sub>O:DMSO) at time points 0, 2, 4, 6, 8, 11, 14, 19, 25 min [**1b**] = 500 μM; **1c** at time points 0, 5, 10, 20, 30, 40, 50, 70, 90 min, [**1c**] = 500 μM; **1d** at time points 0, 1, 2, 3, 4, 5, 6, 8, 10, 12 h. [**1d**] = 500 μM; **1e** at time points 0, 1, 2, 3, 4, 5, 6, 8, 10, 12, 24 h. [**1e**] = 500 μM; **1f** at time points 0, 1, 2, 3, 4, 5, 6, 8, 10, 12, 24 h. [**1f**] = 500 μM; **1g** at time points 0, 1, 2, 3, 4, 5, 6, 8, 10, 12, 24 h. [**1g**] = 500 μM; **1h** at time points 0, 1, 2, 3, 4, 5, 6, 8, 10, 12, 24 h. [**1h**] = 500 μM; **1j** at time points 0, 1, 2, 3, 4, 5, 6, 8, 10, 12, 24 h. [**1j**] = 500 μM. Reaction mixtures were irradiated with UV at 350 nm.

It was observed that salts (**1b-c**) generally have much faster reaction rate than all other leaving groups (**1a, 1d-j**) regardless of nature of leaving groups (Table 2-2). However, it was also observed that the trimethyl ammonium salt (**1b**) showed faster photo-induced DNA cross-linking reaction rate, when reacted in buffer only instead of DMSO:buffer mixture (3:7) (Figure 2-1 and Table 2-2) ICL yield also decreased greatly when reacted in DMSO:buffer system compared to

buffer only.

**Concentration-dependent DNA cross-linking study.** Having determined the optimal reaction time for **1a-j**, we performed the concentration-dependent DNA cross-linking study to determine the optimized concentration to reach the highest DNA cross-linking yields. In general, the DNA ICL yields were gradually enhanced by increasing the concentration of compounds except for **1b-c**. For **1b-c**, it appears that they showed the highest ICL yields at low concentration: 350 $\mu$ M and 300 $\mu$ M respectively. Concentrations higher than x mM of 1b and y mM of 1c did not lead to higher ICL yields but on the other hand caused DNA damages. The DNA cross-linking reaction reached a balance at specific concentrations, and further increase of compounds concentration did not increase the ICL yields. This concentration was defined as optimal concentration for the compound. For example, the DNA ICL yield reached the highest at approximately 0.35 mM concentration for **1b** (when dissolved in water), and the concentration higher than 0.35 mM did not further increase the DNA ICL yield. On the other hand, increasing the concentration caused noticeable DNA damage. Thus, 0.35 mM was the optimal concentration for **1b**. Finally, the optimal concentrations for all compounds were determined, 0.8 mM for **1a and 1d-e**, 0.35 mM and 1 mM for **1b** when dissolved in H<sub>2</sub>O and DMSO respectively, 0.35 mM for **1c**, 0.6 mM for **1g**, and 0.7 mM for **1h-j** (Figure 2-2 and Table 2-2).



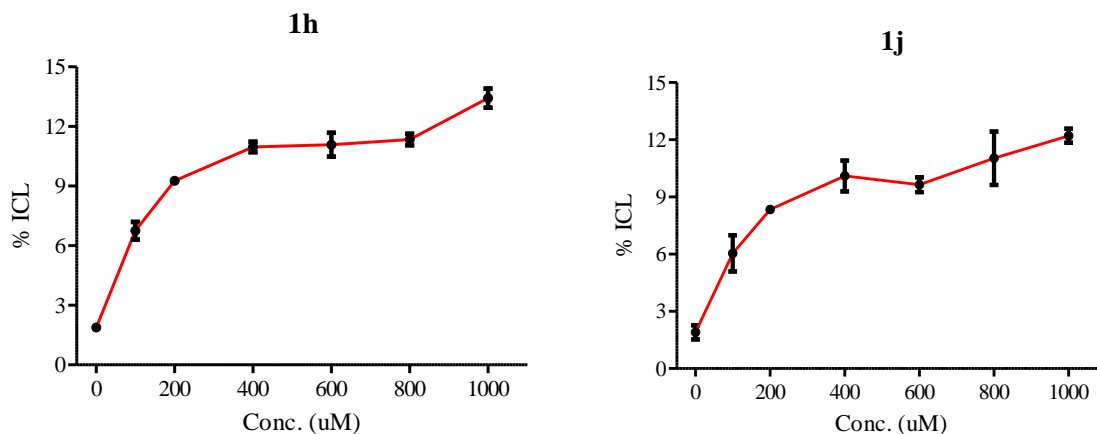


**Figure 2-2.** The concentration dependence of DNA ICL formation of duplex **3** for **1a-j** upon 350 nm irradiation. Solvent ratio for all compounds tested was H<sub>2</sub>O:DMSO = 7:3, except for **1b** which was tested in both H<sub>2</sub>O only and H<sub>2</sub>O:DMSO system. **1a** with an irradiation of 55 min; **1b** with an irradiation of 5 min and 20 min in H<sub>2</sub>O system only and H<sub>2</sub>O:DMSO system respectively; **1c** with an irradiation of 50 min; **1d** with an irradiation of 360 min; **1e** with an irradiation of 480 min; **1f** with an irradiation of 600 min; **1g** with an irradiation of 240 min; **1h** with an irradiation of 300 min; **1j** with an irradiation time of 300 min.

These data suggested that compounds **1a-c** with bromo, trimethyl ammonium salts or triphenylphosphonium salts as leaving groups showed faster ICL reaction rate and higher ICL yields than **1d-j**. Acetate or ether functionalities are not good leaving groups for the photo-induced ICL formation induced by the anthracene moieties.

**Table 2-2.** The optimized conditions, ICL yields and UVabsorption data for **1a-j**.

| Compound         | Reaction Time (min) | Conc. (mM) <sup>[b]</sup> | ICL (%) <sup>[c]</sup> | $\lambda_{350}$ (nm) | $\mathcal{E}_{350}$ (M <sup>-1</sup> cm <sup>-1</sup> ) | K (10 <sup>-5</sup> S <sup>-1</sup> ) |
|------------------|---------------------|---------------------------|------------------------|----------------------|---|---------------------------------------|
| <b>1a</b> (R=Br) | 55                  | 0.8                       | 26±2                   | 394                  | 3055.4  | 4                                     |

|   |      |      |                  |     |        |      |
|---|------|------|------------------|-----|--------|------|
| <b>1b</b> (R= +NMe <sub>3</sub> ) in H <sub>2</sub> O system  | 5.0  | 0.35 | 40 <sub>±2</sub> | 379 | 3525.9 | 94.1 |
| <b>1b</b> (R= +NMe <sub>3</sub> ) in DMSO:H <sub>2</sub> O system   | 20.0 | 1.0  | 10 <sub>±1</sub> |     |        | 4.3  |
| <b>1c</b> (R= +PPh <sub>3</sub> )   | 49.8 | 0.3  | 21 <sub>±1</sub> | 389 | 3812.8 | 6    |
| <b>1d</b> (R= N(CH <sub>3</sub> ) <sub>2</sub> )  | 360  | 0.8  | 13 <sub>±1</sub> | 373 | 2011.6 | 0.5  |
| <b>1e</b> (R= O(C <sub>2</sub> H <sub>4</sub> ) <sub>2</sub> NH)  | 480  | 0.8  | 15 <sub>±1</sub> | 377 | 5786.2 | 0.44 |
| <b>1f</b> (R = OAc)   | 600  | 0.6  | 12 <sub>±2</sub> | 373 | 2080.7 | 0.52 |
| <b>1g</b> (R = OH)  | 240  | 0.7  | 11 <sub>±1</sub> | 369 | 4443.3 | 0.36 |
| <b>1h</b> (R = OCH <sub>3</sub> )   | 300  | 0.7  | 13 <sub>±2</sub> | 372 | 4989.5 | 0.44 |
| <b>1j</b> (R = OCH <sub>2</sub> Ph)   | 300  | 0.7  | 15 <sub>±2</sub> | 374 | 4221.5 | 0.42 |
| <sup>a</sup> The DNA cross-linking reaction was performed in a pH 8 phosphate buffer with 50nM DNA duplex <b>3</b> upon 350 nm irradiation.   |      |      |                  |     |        |      |
| <sup>b</sup> The minimum compound concentration needed to obtain the highest DNA cross-linking efficiency.                                    |      |      |                  |     |        |      |
| <sup>c</sup> The maximum DNA ICL yield obtained for each compound under optimized conditions (all data are the average of three experiments). |      |      |                  |     |        |      |

Finally, we performed DNA cross-linking assay under the optimum concentration and optimized reaction time for each compound (Figure 2-3). Among all compounds teste, **1b** is the most efficient photo-activated DNA cross-linker with the highest ICL yield and the shortest reaction time

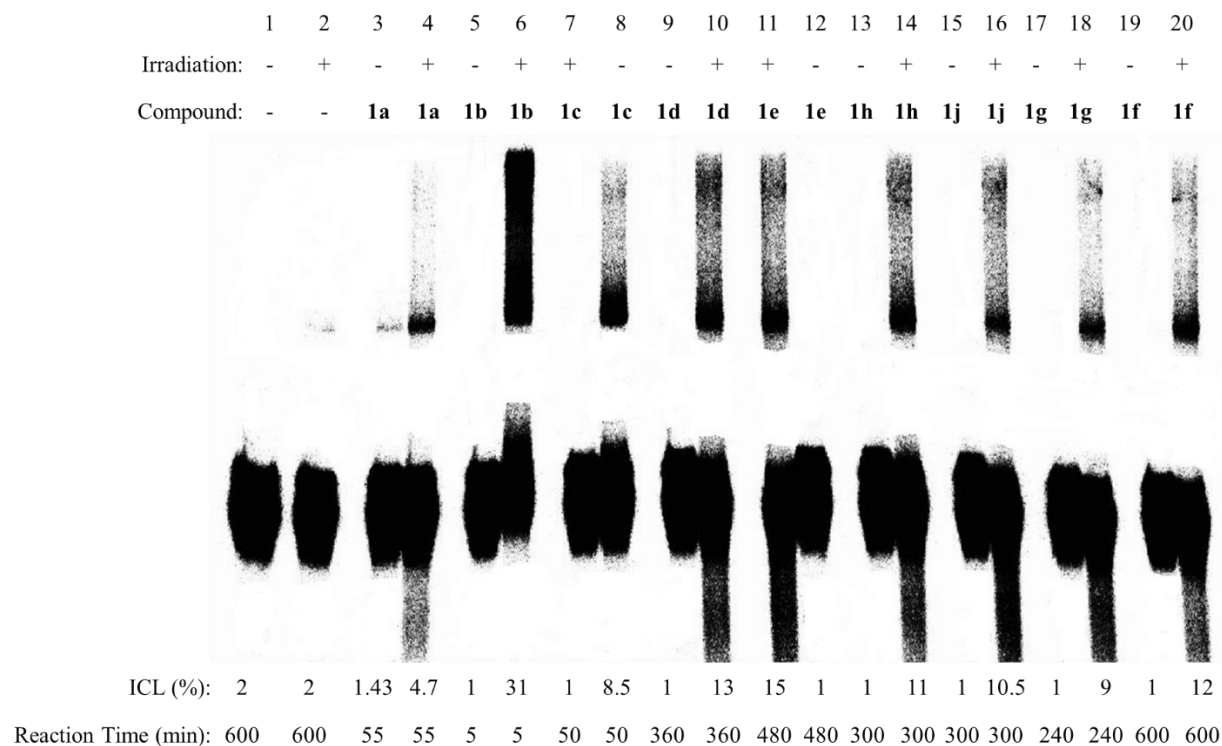


**Figure 2-3.** Photo-induced DNA ICL formation induced by **1a-j**. Lane 1: DNA without UV irradiation; lane 2: DNA with 10 h UV irradiation at 350 nm; lanes 3, 5, 7, 9, 12, 13, 15, 17, 19: DNA with the compound but no UV irradiation at 350 nm for respective optimum time; lanes 4, 6, 8, 10, 11, 14, 16, 18, 20: DNA with the compound upon 350 nm irradiation for respective optimumtime: lane 4: **1a** (ICL yield, 4.7%); lane 6: **1b** (ICL yield, 31%) ; lane 8: **1c** (ICL yield, 8.5%); lane 10: **1d** (ICL yield, 13%); lane 11: **1e** (ICL yield, 15%); lane 14: **1h** (ICL yield, 11%); lane 16: **1j** (ICL yield, 11%); lane 18: **1g** (ICL yield, 9%); lane 20: **1f** (ICL yield, 12%). All DNA ICL yields were obtained by duplicate experiments and shown as average  $\pm$  standard deviation.

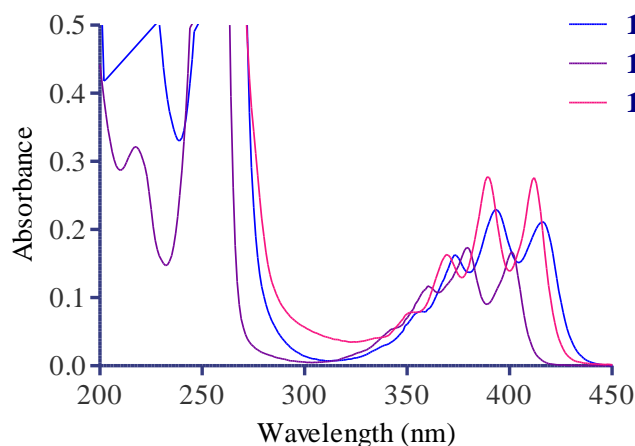
## 2.3 Mechanism of DNA ICL formation and leaving groups effects.

### 2.3.1 Correlation between UV absorbance and the photo-reactivity

Apart from the electronic effect, As the leaving groups could also affect the UV absorption which may in turn influence the photo reactivity of these molecules towards DNA, we measured their UV



absorbance (Figure 2-4). UV-Vis spectra of **1a-j** were determined at 20.0 uM concentration in water (**1b**), methanol (**1c-e**) or chloroform (**1a** and **1f-j**). There is no clear correlation between the UV absorption and the photo reactivity of these compounds. All compounds showed hypsochromic or blue shift (~400 nm) for maximum UV absorption compared to the parent compound **2**. However, **1a-c** showed higher shift than the remaining analogues. In general, compounds with a UV absorption closer to 350 nm (maximum output for rayonet photo reactor used in the study) exhibited lower DNA cross-linking reactivity than compounds with a UV absorption away from 350 nm. For instance, **1a**, **1b-c** showed higher blue shift whereas at the same time they showed higher DNA cross-linking efficiency than the remaining groups in general. However, the photo-induced DNA ICL reaction rate for different compounds did not correlate well with the order of the hypsochromic shift.



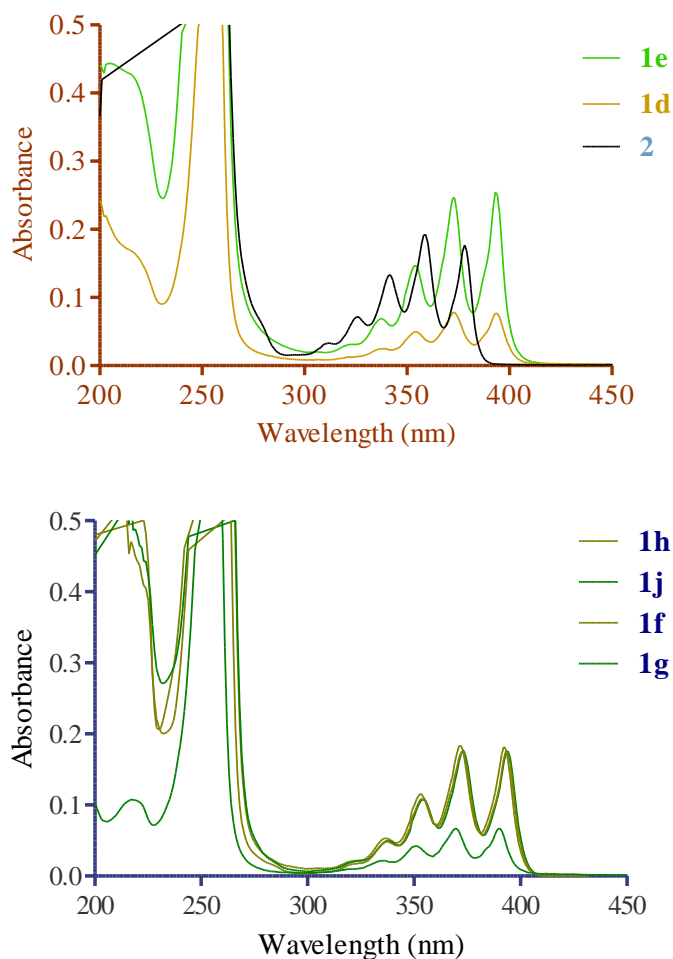


**Figure 2-4.** UV absorption spectra for **1a-e** and **1f-j** at 20.0  $\mu\text{M}$  concentration.

### 2.3.2 The effect of the free radical and cation trapping agents on DNA cross-link formation

Our previous study showed that the leaving groups, as well as the aromatic substituents affect the pathways for photo-induced carbon cation formation<sup>6</sup>. For phenyl boronate esters with bromo as a leaving group, carbocations were formed via free radical oxidation, while for those with trimethyl ammonium as a leaving group, they were formed via direct heterolysis of C-N bonds. However, due to the limited literature data, it is difficult to conclude that this is a common phenomenon. Few compounds have been reported to cross-link DNA by a carbocation mechanism upon photoirradiation with a limited structure variation. There is no report about photo-inducible

DNA ICL formation by anthracene analogues.

To better understand the mechanism and how different leaving groups affect the DNA cross-link mechanism, radical and cation trapping experiments were carried out for **1b-c** under the optimized DNA cross-linking conditions. Compounds **1b-c** were chosen for this study as they showed faster reaction rate as well as higher ICL yields in comparison to other compounds. The 2,2,6,6-tetramethylpiperidin-1-oxyl (TEMPO) was used as a radical trap, methoxyamine used as a carbocation trapping agent, whereas betamercapto ethanol was used as both radical and carbocation trapping agent. The results are shown in Figure 2-5

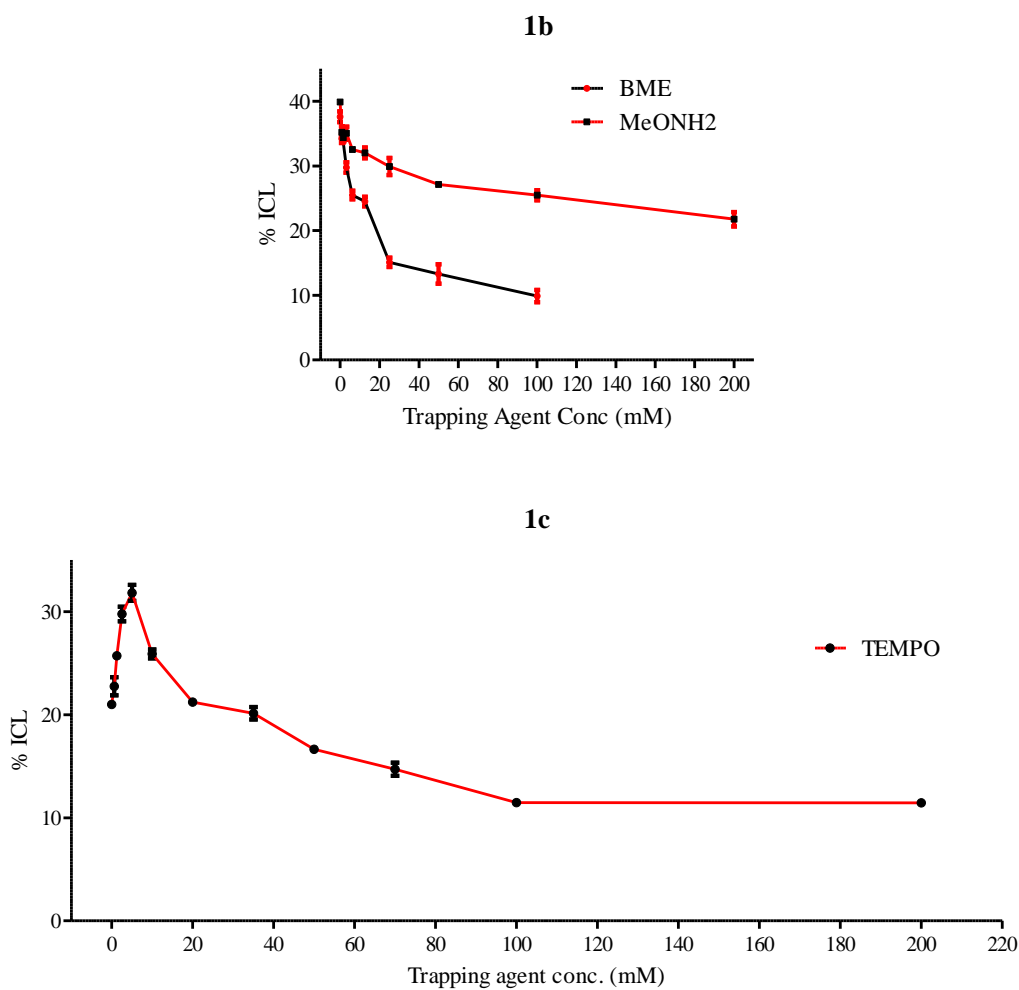


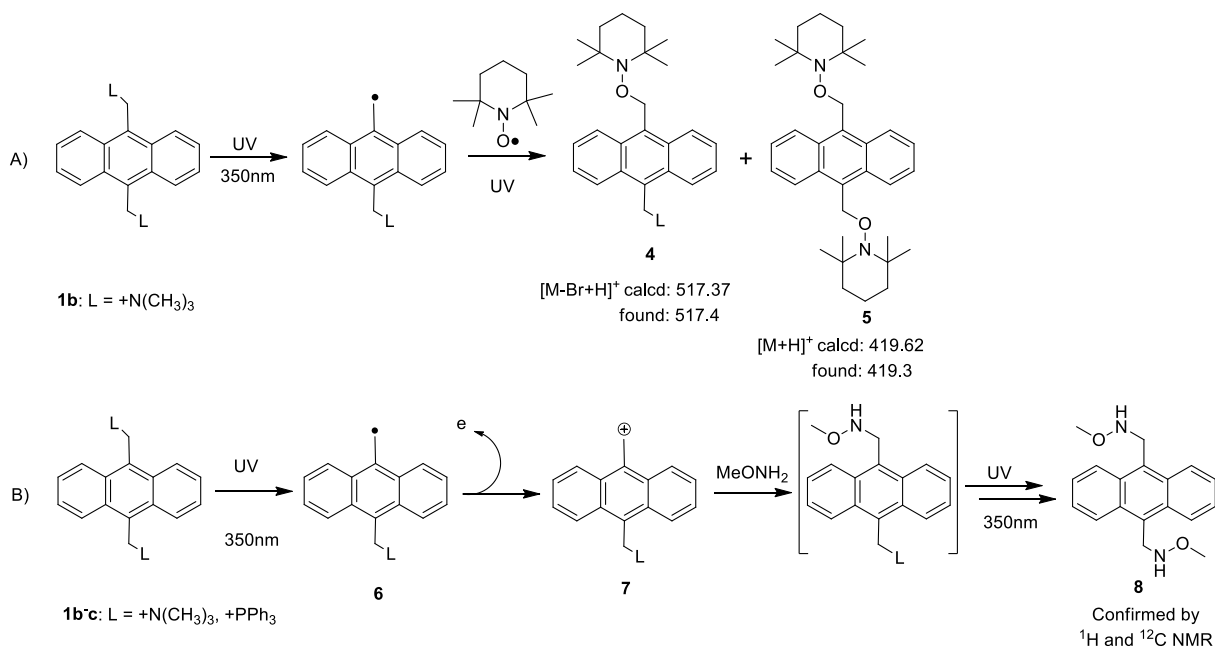
**Figure 2-5.** Carbocation and radical trapping with DNA ICL formation for **1b-c**.

In general, the DNA ICL yields gradually decreased for **1b** with increased concentration of methoxyamine and BME. The inhibition of ICL formation with methoxyamine indicated that carbocations were involved in the photo-induced DNA ICL process. Carbocation can be generated from radical oxidation or direct heterolysis of C-X bonds. We performed radical trapping experiments using TEMPO as a trapping agent to figure out if radicals were involved in the process. For **1c** an unusual trend of DNA ICL yield inhibition was found where ICL yield increased initially with increasing concentration of TEMPO but decreased afterwards (after 5 mM TEMPO). This indicated that DNA ICL formation maybe of radical-cation pathway (defined as first to generate radicals, then the radicals were converted to cations via free radical oxidation) where the radicals were first formed upon photo irradiation of these compounds, then oxidized to cations that directly crosslink DNA. However, surprisingly none of the trapping agents was able to inhibit the DNA ICL yield completely even with very high concentration (100 mM or 200 mM). At this point, we don't have explanation of that but we assume intercalation of these compounds in the DNA may have some effect with it.

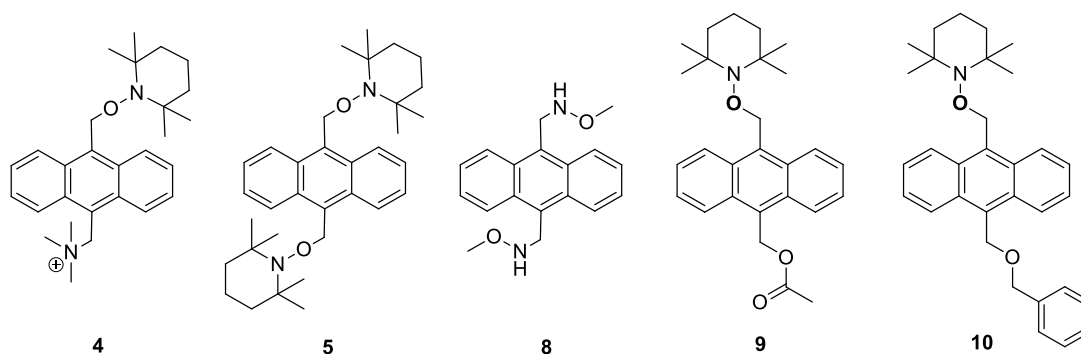
We were not able to get a perfect ICL formation inhibition trend for **1b** with TEMPO or **1c** with Methoxyamine and BME. Thus, we propose that the DNA ICL formation might be of both free radical way (**1c**) as well as carbocation way (**1b**).

In order to provide direct evidence for free radicals and carbocations formation, the carbocation and radical trapping reactions were carried out with monomers of **1b-c**, **1f**, and **1j** using large excess of methoxyamine and TEMPO as trapping agents, respectively. The cation and radical trapping adducts (**4-8**) were obtained for **1b**, **1c**, **1f** and **1j** upon 350 nm irradiation, which was confirmed by LC-MS and/or NMR analysis. The departure of two leaving group in **1b** took place in a stepwise manner since the mono-trapping adduct **4** as well as di-trapping adduct **5** were

detected in the trapping reaction. Radical trapping adduct for electron withdrawing leaving groups were obtained for **1f**, **1j**. The biscation trapping adduct **6** was obtained for **1a-c**.

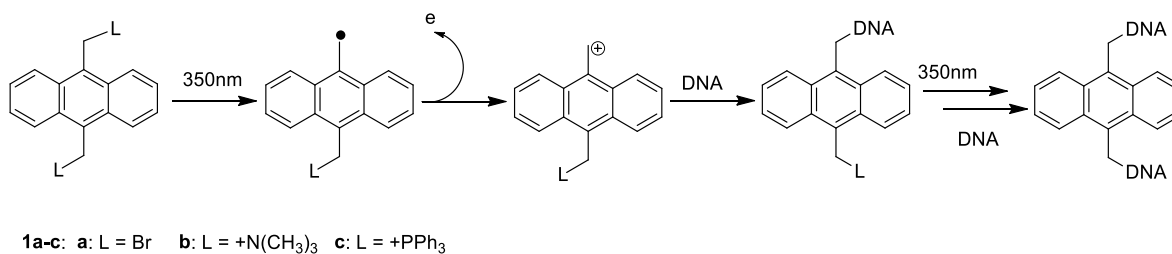


**Scheme 2-8.** (A) Free radical trapping reaction and (B) cation trapping reaction product obtained with **1b-c** upon 350 nm irradiation.



**Scheme 2-9.** Cation and free radical trapping products obtained with and upon 350nm irradiation.

Overall, these results showed that the mechanism pathway for photo-induced DNA cross-link formation by these compounds was complex and not only influenced by the leaving groups but also maybe by the intercalation of anthracene moiety into DNA.

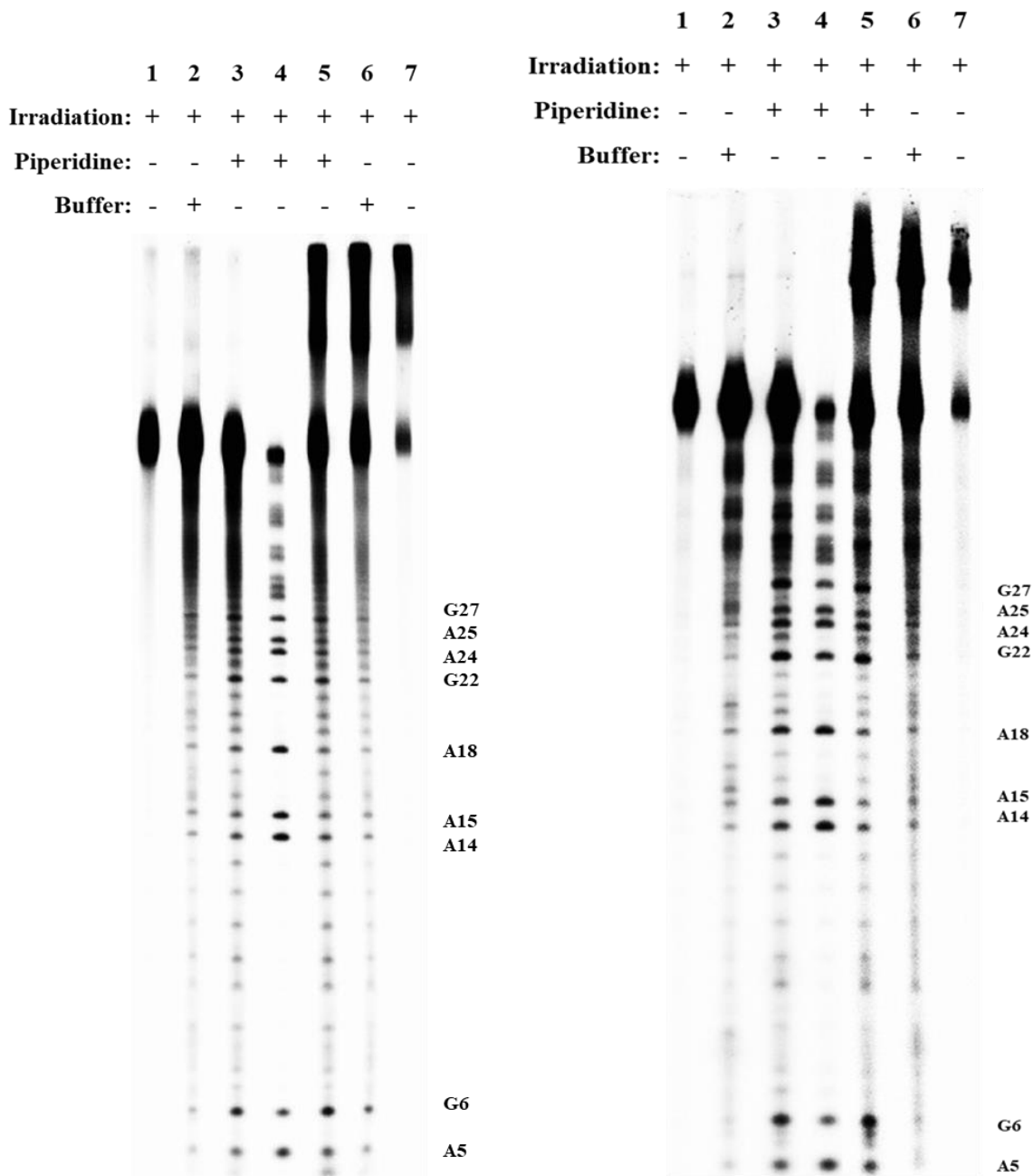


**Scheme 2-10.** Proposed mechanism for DNA ICL formation.

### 2.3.3 Determination of DNA alkylation sites

As the N7-alkylated purine nucleosides can be cleaved upon heating in the presence of piperidine, studying the heat stability of the cross-linked DNA has been used to determine whether ICL formation occurs with dG or dA<sup>7,8</sup>. Thus, we performed the heat stability study with DNA ICL products formed with **1b** and **1c**. We isolated both single-stranded ODNs (p32-ODN) as well as the ICL products formed with DNA duplex **3**, which were heated in pH 7 phosphate buffer or piperidine at 90 °C for 30 min. The heat stability data of the isolated single-stranded ODNs and ICL products for **1b-c** are demonstrated in Figure 2-6. All ICL products were relatively stable upon heating under neutral conditions (pH 7.0 phosphate buffer), while obvious cleavage bands were observed under basic conditions (1.0 M piperidine).

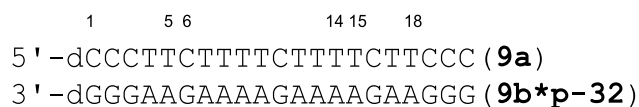
The reaction sites of **1b-c** upon 350 nm irradiation was examined by testing the stability of the DNA ICL products upon heating under neutral or basic conditions. All DNA ICL products formed with **1b-c** were destroyed by heating in 1.0M piperidine for 30 min, whereas they were subjected to heating in a phosphate buffer.



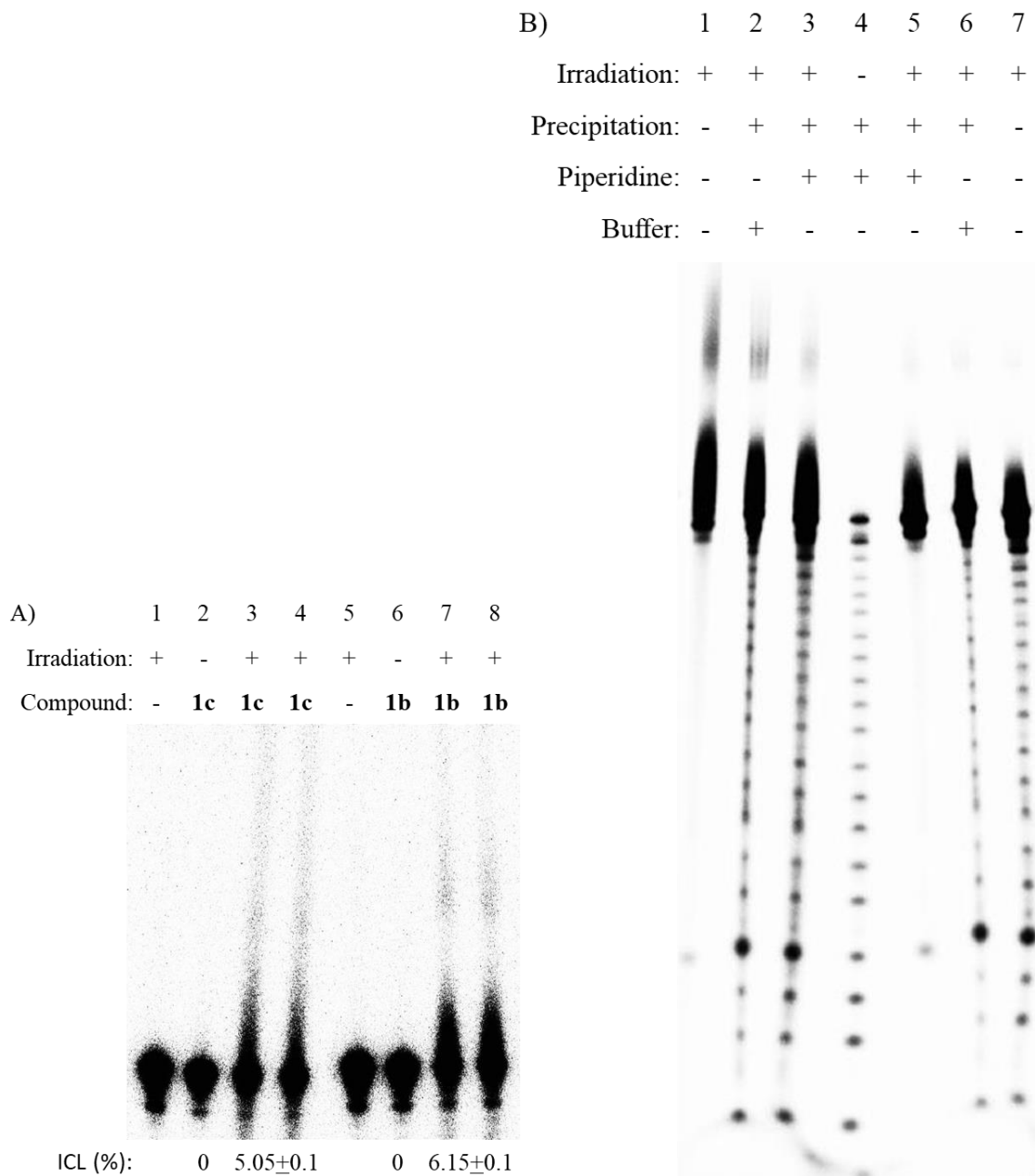
**Figure 2-6.** Determination of the cross-linking site of **1b-c** with 49-mer DNA duplex (**3**). Phosphor-image autoradiogram of 20% denaturing PAGE analysis of the isolated ICL products and alkylated single-stranded ODN. Lane 1: isolated alkylated single-stranded ODN (control); lane 2: single-strand ODN heated in pH 7 phosphate buffer at 90°C for 30min; lane 3: single-strand ODN heated in 1.0M piperidine at 90°C for 30min; lane 4: G+A sequencing; lane 5: DNA ICL

products heated in 1.0M piperidine at 90°C for 30min; lane 6: DNA ICL products heated in a pH 7 phosphate buffer at 90°C for 30min; lane 7: isolated DNA ICL products (control).

The piperidine heat stability study can identify alkylated purines but not alkylated pyrimidines. To investigate whether the alkylation could occur with pyrimidines, we tested the ICL reaction with duplex containing dCs/dTs in one strand (**9a**) and dGs/dAs in the complimentary strand (**9b**). ICL formation was observed when duplex was treated with **1b** and **1c** (approximately 6%) which suggested that dC and/or dT are possible alkylation sites.



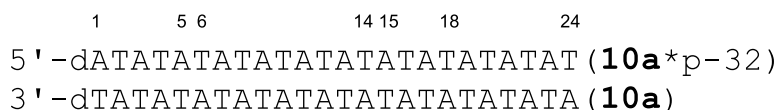




**Figure 2-7.** A) Photo-induced DNA ICL formation for **1b-c** with CT labeled 21mer duplex **9**. Phosphorimage autoradiogram of 20% denaturing PAGE analysis of the ICL reaction mixture. B) Determination of the cross-linking site of **1b-c** with GA labeled 21mer duplex (**9**). Phosphor-image autoradiogram of 20% denaturing PAGE analysis of the isolated ICL products and alkylated single-stranded ODN. Lane 1: isolated precipitated single-stranded ODN; lane 2: single-strand ODN

heated in pH 7 phosphate buffer at 90°C for 30min; lane 3: single-strand ODN heated in 1.0M piperidine at 90°C for 30min; lane 4: G+A sequencing; lane 5: isolated precipitated single-stranded ODN; lane 6: single-strand ODN heated in pH 7 phosphate buffer at 90°C for 30min; lane 7: single-strand ODN heated in 1.0M piperidine at 90°C for 30min.

To determine whether cross-linking reaction takes place with dT, we synthesized one self-complementary dAT sequences (**10a**) that was treated with **1b** upon 350 nm irradiation. The DNA ICL formation was not observed, however tailing duplex was clearly observed indicating that ICL reaction did not take place between dA and opposing dT but mono alkylation may have occurred with dA and dT (Figure 2-8 A). However, the cleavage bands were observed with dAs when the single-stranded ODN **10a** was isolated from the cross-linking reaction mixture and heated in 1.0M piperidine at 90°C for 30 min (Figure 2-8 B). This indicated that mono-alkylation occurred with dAs.



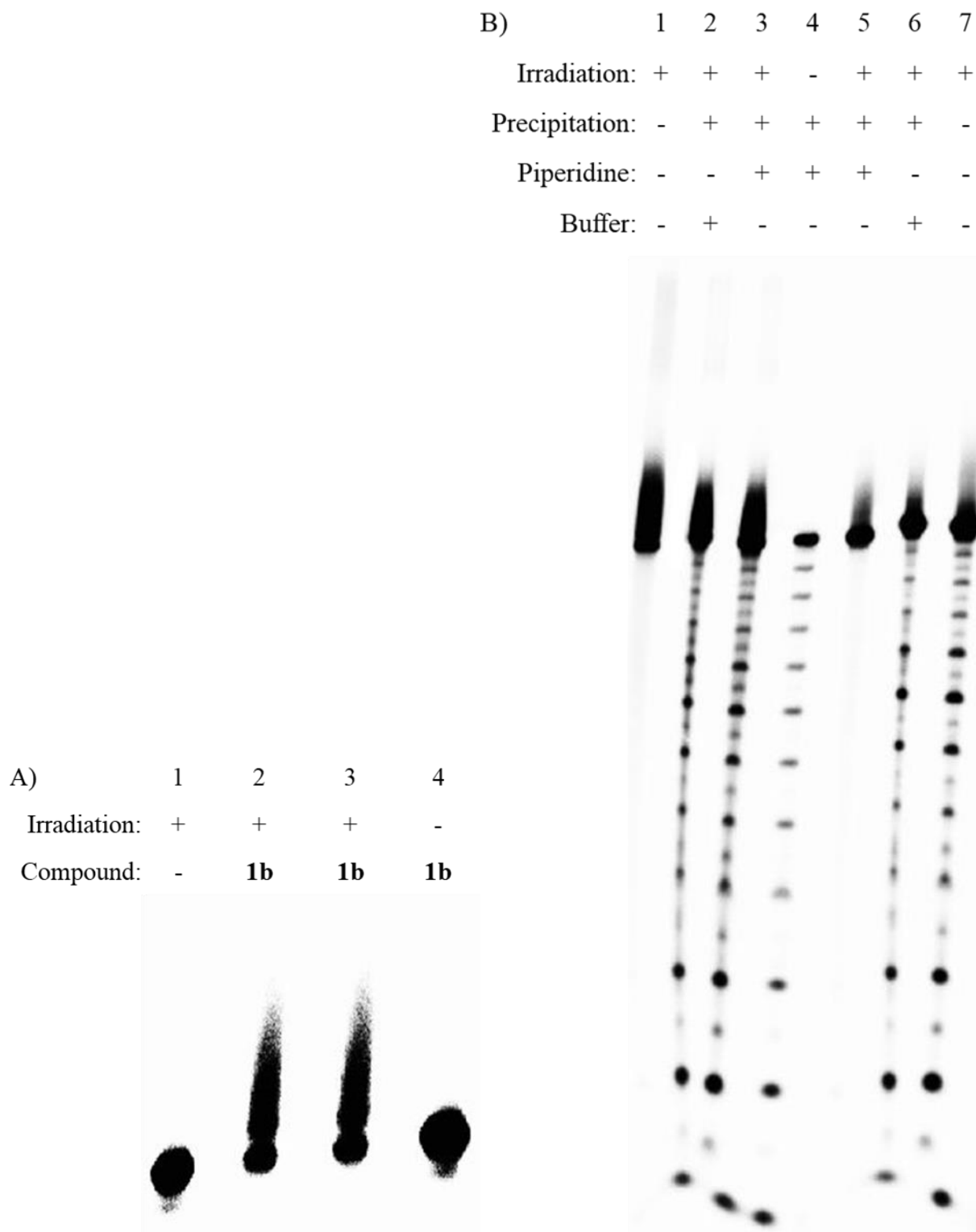


Figure 2-8. A) Photo-induced DNA ICL formation for **1b** with duplex 10. Phosphorimage autoradiogram of 20% denaturing PAGE analysis of the ICL reaction mixture. B) Determination

of the cross-linking site of **1b-1c** with AT labeled 24mer duplex. Phosphor-image autoradiogram of 20% denaturing PAGE analysis of the isolated ICL products and alkylated single-stranded ODN. lane 1: isolated precipitated single-stranded ODN; lane 2: single-strand ODN heated in pH 7 phosphate buffer at 90°C for 30min; lane 3: single-strand ODN heated in 1.0M piperidine at 90°C for 30min; lane 4: G+A sequencing; lane 5: isolated precipitated single-stranded ODN; lane 6: single-strand ODN heated in pH 7 phosphate buffer at 90°C for 30min; lane 7: single-strand ODN heated in 1.0M piperidine at 90°C for 30min.

For comparison of the photo-reactivity of these compounds towards dG and dA, we estimated the cleavage ratio of dG<sub>27</sub>+dG<sub>22</sub> to dA<sub>25</sub>+dA<sub>24</sub> (Cleaved dG/dA). Both compound **1b-c** showed major cleavage at dG sites with a cleavage ratio of dG/dA of approx. ~1.5, indicating that dGs were the preferred alkylation sites for these compounds (Table 3). Compound **1b** showed less selectivity towards dG compared to **1c**.

| Table 3. Photo-reactivity of <b>1b-c</b> towards dG and dA evaluated from the ratio for cleavage at dG <sub>27</sub> , dG <sub>22</sub> , dA <sub>25</sub> and dA <sub>24</sub> . <sup>[a]</sup>  |                                    |                                    |
|---|------------------------------------|------------------------------------|
| Compound  | <b>1b</b> (R = +NMe <sub>3</sub> ) | <b>1c</b> (R = +PPh <sub>3</sub> ) |
| Cleav. <sup>[b]</sup><br>(dG/dA)  | 1.28                               | 1.53                               |
| [a] The DNA cross-linking reaction was performed in a pH 8 phosphate buffer with 50 nm DNA duplex upon 350 nm irradiation. The ICL products were isolated and heated in 1.0 M piperidine at 90°C for 30 min. The cleavage bands at dG <sub>27</sub> , dG <sub>22</sub> , dA <sub>25</sub> , and dA <sub>24</sub> were quantified. [b] Ratio of cleavage at dG <sub>27</sub> + dG <sub>22</sub> to that at dA <sub>25</sub> + dA <sub>24</sub> . |                                    |                                    |

Collectively, these data demonstrated that ICL reactions took place with opposing dG/dC while mono-alkylation occurred with dAs. As DNA duplexes contain multiple dG/dC base pairs, it is likely that a variety of cross-linked duplexes are formed by irradiation depending on the position and the amount of crosslinks introduced in the duplex.

## 2.4 Conclusions

We have developed a novel type of 9,10-anthryl analogues as efficient photo-sensitive DNA cross-linking agents. These compounds can contain variety of leaving groups that can be activated by 350nm irradiation to generate anthryl cations directly producing DNA interstand cross-linking products. For all these five compounds tested, the formation of anthryl cations was through oxidation of the corresponding anthryl radicals generated from photo-induced cleavage of C-L bonds. Leaving groups did not affect the formation of anthryl cations. However, DNA ICL efficiency and cross-linking reaction rate strongly depended on the leaving groups as well as solubility. ICL reaction rate was very faster with **1b** containing trimethyl ammonium group compared to the others (when dissolved in water). It also appears that analogues with salt leaving groups (**1b-c**) have higher reaction rate than remaining (**1a, 1c-d**). The anthryl cations generated from **1b-c** alkylated dG, dC and dA while cross-linking reaction took place with opposing dG/dC and with dA/dT as well. Monoalkylation with dA also occurred. Like previous compounds, these also showed dGs as the most preferred site of alkylation. This study provides novel example of very fast photo-inducible DNA cross-linking agents. It also sets examples and guidelines for development of fast photoactivable probes and agents for various biological applications.

## 2.5 Experiment Section

**General Information.** All chemicals from commercially available source were directly used without further purification. Oligonucleotides were synthesized via standard automated DNA synthesis techniques. Deprotection of the synthesized DNA were performed under mild deprotection conditions using a mixture of 40% aqueous MeNH<sub>2</sub> and 28% aqueous NH<sub>3</sub> (1:1) at room temperature for 2 h. 20% denaturing polyacrylamide gel electrophoresis was used for DNA purification. [ $\gamma$ -<sup>32</sup>P] ATP was used for DNA labeling with standard method. Quantification of

radiolabeled oligonucleotides was carried out using a Molecular Dynamics phosphorimager equipped with ImageQuant, version 5.2, software.  $^1\text{H}$  NMR and  $^{13}\text{C}$  NMR spectra were taken on a Bruker DRX 300 MHz spectrophotometer with TMS as internal stander. High-resolution mass spectrometry IT-TOF was used for molecular measurement.

***Anthracene, 9,10-bis(bromomethyl)- (1a)***. A mixture of anthracene (10 g, 0.056 mmol, 1 equiv), paraformaldehyde (0.056 mmol), cetyltrimethylammonium bromide (0.224 g), and glacial acetic acid (14 mL) were stirred at rt. Next, 35 mL of aqueous HBr (48% w/v) was slowly added drop wise to the reaction mixture over a period of 1h. The reaction mixture was stirred and heated to 80°C for 5 h, cooled. Solid was filtered, washed with water, then dried. Recrystallization from toluene furnished pure 9,10-bis(bromomethyl)anthracene. Yield 16.35g (80%). (the NMR spectra were in agreement with those reported<sup>9</sup>).

$^1\text{H}$  NMR (500 MHz,  $\text{CDCl}_3$ ):  $\delta$  ppm 8.31 (dd,  $J = 6.81, 3.21$  Hz, 4H), 7.61 (dd,  $J = 6.98, 3.05$  Hz, 4H), 5.46 (s, 4H).

$^{13}\text{C}$  NMR ( $\text{CDCl}_3$ , 500 MHz):  $\delta$  25.58 (2C, s), 123.36 (5C, s), 125.68 (4C, s), 128.59 (2C, s), 129.26 (1C, s).

$^{13}\text{C}$  NMR (DMSO, 500 MHz):  $\delta$  28.83 (2C, s), 125.26 (4C, s), 127.2 (5C, s), 129.54 (2C, s), 131.34 (1C, s).

***1,1'-(anthracene-9,10-diyl)bis(N,N,N-trimethylmethanaminium) dibromide (1b)*** . To a mixture of **1a** (100mg, 0.275 mmol) in ethyl acetate, trimethylamine solution (0.36 ml, 1.375 mmol) was added through syringe. The mixture was stirred for 5 hour. After reaction completion, solid was filtered, washed with ethyl acetate and then dried to give **1b** as a solid.

$^1\text{H}$  NMR (DMSO, 500 MHz):  $\delta$  3.10 (s, 18H), 5.85 (s, 4H), 7.75 (dd,  $J =$  , 4H), 8.90 (dd,  $J =$  ,

4H).

$^1\text{H}$  NMR (300 MHz, DMSO):  $\delta$  ppm 3.11 (s, 18H), 5.83 (s, 4H), 7.76 (q,  $J = \text{Hz}$ , 4H), 8.90 (dd,  $J = 6.80, 3.20 \text{ Hz}$ , 4H).

$^{13}\text{C}$  NMR (DMSO, 500 MHz):  $\delta$  53.30 (8C, s), 53.68 (1C, s), 58.67 (2C, s), 124.94 (1C, s), 126.18 (3C, s), 127.49 (5C, s), 132.91 (2C, s).

**9,10-Anthrylenebismethylenebis(triphenylphosphonium bromide) (1c)** . To a solution of **1a** (100mg, 0.275 mmol) in toluene, triphenyl phosphine solution (0.36 ml, 1.375 mmol) was added through syringe. The mixture was refluxed for 5 hour and cooled down leading to solid precipitate, which was filtered, washed with toluene, and dried to give **1c** as a solid.

$^1\text{H}$  NMR (MeOD, 500 MHz):  $\delta$  5.95 (4H, d), 7.54-7.77 (30H, dddd), 7.04 (4H, ddd), 7.90 (4H, ddd).

$^1\text{H}$  NMR (300 MHz, MeOD) ppm 5.99 (s, 4H), 7.05 (dd,  $J = 6.96, 2.94 \text{ Hz}$ , 4H), 7.92 (dd,  $J = 6.73, 3.21 \text{ Hz}$ , 4H), 7.52 (dd,  $J = 13.14, 5.90 \text{ Hz}$ , 24H), 7.78 (dd,  $J = 8.44, 4.71 \text{ Hz}$ , 6H).

$^{13}\text{C}$  NMR (MeOD, 500 MHz):  $\delta$  24.3 (2C, q), 117.3 (3C, q), 121.8 (1C, t), 124.6 (4C, s), 125.8 (5C, s), 129.8 (13C, sx), 130.7 (2C, s), 134.2 (14C, s), 134.8 (7C, q).

**$N^9, N^9, N^{10}, N^{10}$ -Tetramethyl-9,10-anthracenedimethanamine (1d)**. Into a solution of **1a** in ethyl acetate was added dimethylamine solution (2.0M in Methanol). The reaction mixture was stirred at rt overnight. After evaporating solvent, the residue was purified by column chromatography (ethyl acetate: methanol = 5:1) to afford **1d** as a yellow solid.

$^1\text{H}$  NMR (DMSO, 300 MHz):  $\delta$  2.36 (12H, s), 4.59 (4H, s), 7.59 (4H, ddd), 8.57 (4H, ddd) (the NMR spectra were in agreement with those reported<sup>10</sup>).

**4,4'-[9,10-Anthracenediylbis(methylene)] bis[morpholine] (1e).** Into a solution of **1a** in ethyl acetate, morpholine was added. The resulting mixture was stirred at rt overnight. Solvent was removed and the precipitate was collected by filtration, purified by column chromatography (ethyl acetate:methanol = 5:1) to yield **1e** as a solid product (2.1 g, 70%).

<sup>1</sup>H NMR (CDCl<sub>3</sub>, 500 MHz): δ 2.56 (8H, s), 3.57 (8H, s), 4.39 (4H, s), 7.46 (4H, ddd), 8.47 (4H, ddd).

<sup>13</sup>C NMR (CDCl<sub>3</sub>, 500 MHz): δ 52.61 (5C, s), 53.65 (2C, s), 66.14 (5C, t), 124.15 (4C, s), 124.5 (4C, s), 130.1 (2C, s).

**anthracene-9,10-diylbis(methyl) diacetate (1f).** Compound **1a** and potassium acetate were mixed in acetic acid and refluxed at 120°C overnight. Then, the mixture was poured into cold water and the precipitate was filtrated and dried in vacuum. The residue was purified by column chromatography (Hexane: Dichloromethane = 10:1) to give **1h** as a light yellow solid.

<sup>1</sup>H NMR (DMSO, 300 MHz): δ 2.08 (6H, s), 6.15 (4H, s), 7.66 (4H, ddd), 8.43 (4H, ddd).

**9,10-bis(hydroxymethyl)anthracene (1g).** A mixture of **1f** and KOH in methanol was refluxing overnight. Then, the solution was cooled to rt, leading to the formation of the solid product that was filtered and washed with water.

<sup>1</sup>H NMR (DMSO, 300 MHz): δ 5.43 (4H, s), 7.56 (4H, ddd), 8.44 (4H, ddd).

**9,10-bis(methoxymethyl)anthracene (1h).** Into a solution of **1m** in DMF at 0°C, NaH was added. The reaction mixture was stirred for 10 min at 0°C, then CH<sub>3</sub>I was added. The reaction mixture was allowed to warm to rt, stirred overnight, quenched with water, diluted with ethyl acetate, washed with brine and dried over anhydrous Na<sub>2</sub>SO<sub>4</sub>. Solvent was removed and the residue was purified by column chromatography (Hexane: DCM = 10:1).



**9,10-Bis-(benzyloxymethyl)-anthracene (1j).** Compound **1m** in DMF was cooled to 0°C, followed by the addition of NaH. The resulting mixture was stirred for 10 min. Then benzyl bromide was added. The reaction mixture was allowed to warm to rt and stirred overnight, quenched with water, diluted with ethyl acetate, washed with brine and dried over anhydrous Na<sub>2</sub>SO<sub>4</sub>. Solvent was removed and the residue was purified by column chromatography (Hexane: DCM = 10:1) to afford **1j** as a solid.

#### **Free radical trapping adducts.**

**9,10-bis(((2,2,6,6-tetramethylpiperidin-1-yl)oxy)methyl)anthracene (5).** A solution of **1a**, **1b**, or **1c** (1 equiv) in CH<sub>3</sub>CN (2 mL) was added TEMPO (10 equiv) at rt while stirring. The resulting mixture was irradiated with 350 nm light for (how long?) until all starting material was consumed. Solvent was removed and the residue was purified by chromatography (hexane/DCM=10:1 for **1a**; DCM/methanol=10:1 for **1b–c**) to afford the trapping adducts **4**, **5**, and **6**, respectively. Trapping adducts were confirmed using LC-MS.

#### **Cation trapping adducts.**

**N,N'-(anthracene-9,10-diylbis(methylene))bis(O-methylhydroxylamine) (6).** To a solution of MeONH<sub>2</sub>·HCl (40 equiv) in DMF (2 mL) was added trimethylamine (44 equiv). After stirring at rt for 30 min, **1b** or **1c** (1 equiv) in DMF were added. The resulting mixture was stirred for 20 min, then irradiated with 350 nm light until the starting material was consumed (about how long?). The reaction was quenched with water and the mixture extracted with ethyl acetate (3x3 mL). The combined organic phases were washed with brine and dried over anhydrous Na<sub>2</sub>SO<sub>4</sub>. After removing solvent, the residue was purified by column chromatography (hexane: methanol = 10:1) to provide the corresponding trapping adduct **6** which was confirmed by NMR.

<sup>1</sup>H NMR (CDCl<sub>3</sub>, 500 MHz): ppm 8.31 (dd, *J* = 6.81, 3.21 Hz, 4H), 7.61 (dd, *J* = 6.98, 3.05 Hz,

4H), 5.46 (s, 4H)

$^1\text{H}$  NMR (500 MHz, Solvent)  $\delta$  ppm 8.36 (t,  $J = \text{Hz}$ , 4H), 7.49 (t,  $J = \text{Hz}$ , 4H), 5.38 (s, 4H), 3.47 (s, 6H)

$^{13}\text{C}$  NMR ( $\text{CDCl}_3$ , 500 MHz):  $\delta$  57.3 (2C, s), 65.7 (3C, s), 123.8 (5C, s), 124.7 (5C, s), 129.2 (1C, s), 129.7 (2C, s).

**Photoreaction of oligonucleotides.** The photoreactions of **1a-j** with DNA duplex **3** (50-100 nM) were carried out in 10 mM potassium phosphate (pH 7) and 100 mM NaCl buffer in Pyrex tubes in a Rayonet photochemical chamber reactor (Model RPR-100) fitted with 16 lamps having an output maximum at 350 nm..

**ICL formation with duplex DNA 3:** The  $^{32}\text{P}$ -labelled oligonucleotide (0.5  $\mu\text{M}$ ) was annealed with 1.5 equiv of the complementary strand by heating to 90°C for 5 min in potassium phosphate buffer (pH 7, 10 mM), followed by cooling to rt. The  $^{32}\text{P}$ -labeled ODN duplex (2  $\mu\text{L}$ , 0.5  $\mu\text{M}$ ) was then mixed with 1M NaCl (2  $\mu\text{L}$ ), 100 mM potassium phosphate (2  $\mu\text{L}$ , pH 8), and **1a-j** (concentration range: 50  $\mu\text{M}$  to 1 mM in 6 mL DMSO and  $\text{H}_2\text{O}$  mixture) and autoclaved distilled water to give a final volume of 20  $\mu\text{L}$ . The reaction was irradiated with 350 nm light until the reaction was completed, followed by quenching with an equal volume of 90 % formamide loading buffer. The resulting mixture was then subjected to 20 % denaturing polyacrylamide gel for electrophoresis.

**Trapping assay of oligodeoxynucleotides:** The  $^{32}\text{P}$ -labeled oligonucleotide duplex (2  $\mu\text{L}$ , 0.5  $\mu\text{M}$ ) was mixed with 1M NaCl (2 $\mu\text{L}$ ) and 100 mM potassium phosphate (2 $\mu\text{L}$ , pH 8). The stock solution of  $\text{MeONH}_2\cdot\text{HCl}$  (2M) was titrated with 5M NaOH to adjust the pH to  $\sim 7.0$ , which was diluted to the desired concentration (100/3  $\mu\text{M}$  to 2000/3 mM). Then, 3  $\mu\text{L}$  was added to the reaction mixture as appropriate for the desired concentration (final  $\text{MeONH}_2$  concentration: 50

$\mu\text{M}$  to 100 mM). Similarly, 3 $\mu\text{L}$  or 6 $\mu\text{L}$  of TEMPO in DMSO (100/3  $\mu\text{M}$  to 2000/3 mM) was added to the reaction mixture as appropriate for the desired concentration (final TEMPO concentration: 50  $\mu\text{M}$  to 100 mM). Compounds **1a-1c** (0.5mM in 6  $\mu\text{L}$  DMSO or H<sub>2</sub>O) and the appropriate amount of autoclaved water were added to give a final volume of 20  $\mu\text{L}$  (DMSO/H<sub>2</sub>O: a final ratio of 3:7). The reaction was irradiated with 350 nm light for optimized time for each compound and quenched with an equal volume of 90% formamide loading buffer, then subjected to 20% denaturing polyacrylamide gel electrophoresis.

**Piperidine Treatment with DNA ICL Product Formed with Duplex 3/9/10 and 1b-c.** The <sup>32</sup>P-labeled oligonucleotide duplex **3a/3b** (0.5  $\mu\text{M}$ ) was mixed with 1 M NaCl, 100 mM potassium phosphate (pH 8), and 5/3 mM **1b-c** (dissolved in DMSO). The solution was irradiated with 350 nm light (5min for **1b** or 50 min for **1c**) and purified by 20% denaturing PAGE. The band containing cross-linked product was cut, crushed and eluted with 200 mM NaCl and 20 mM EDTA. The crude product was further purified on a C<sub>18</sub> column eluting with H<sub>2</sub>O (4  $\times$  1.0 mL) followed by MeOH/H<sub>2</sub>O (3:2, 1.0 mL). The dry product was dissolved in H<sub>2</sub>O (35  $\mu\text{L}$ ) and divided into three portions. One portion (15  $\mu\text{L}$ ) was incubated with piperidine (10M, 5  $\mu\text{L}$ ) at 90°C for 30min, the second portion (15  $\mu\text{L}$ ) was incubated with 1M NaCl and 10mM potassium phosphate buffer (pH 7) mixture (1:1) under the same condition, and the third portion (5  $\mu\text{L}$ ) was used as a control sample. Next, the samples were subjected to 20% denaturing PAGE analysis.

#### **General Procedure for the trapping assay.**

**Radical Trapping.** A reaction mixture of **1a-c** (200 mg, 0.23 mmol, 1 equiv) and TEMPO (360 mg, 10.0 equiv) in CH<sub>3</sub>CN (2 mL) was irradiated with 350 nm UV light for around 24 hours until there was no more new products formed. The solvent was removed, and the residue was purified by column chromatography (hexane/Dichloromethane =10/1) and analyzed by the liquid

chromatography mass spectrometry ion-trap time-of-flight (LCMS-IT-TOF).

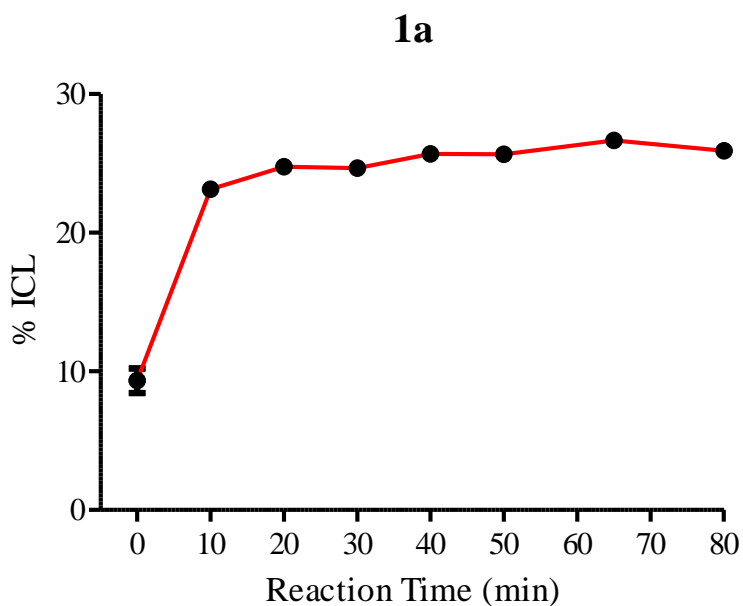
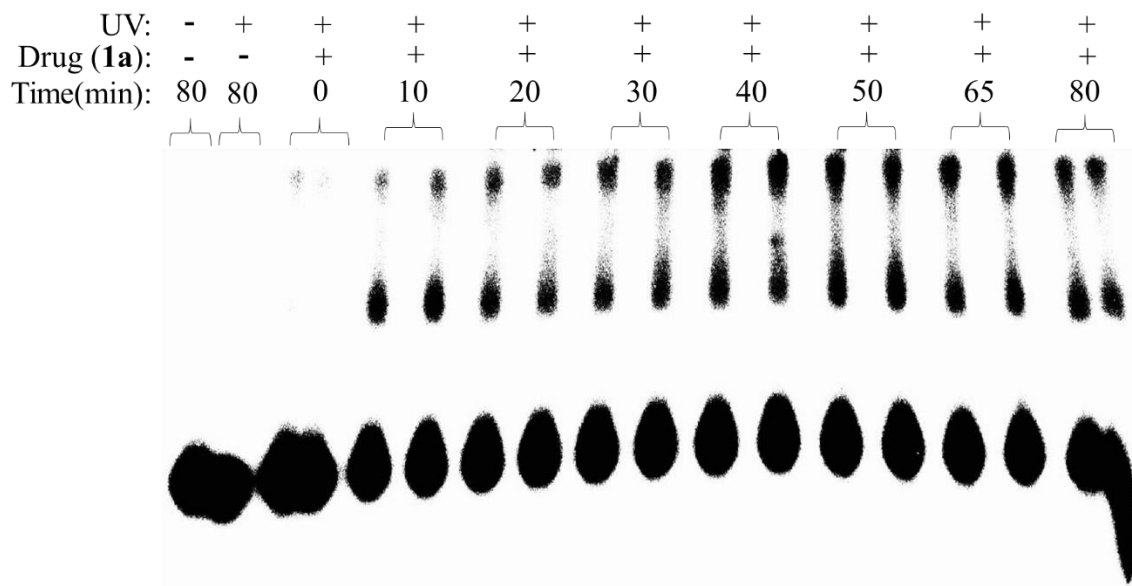
**Carbocation trapping:** To a solution of MeONH<sub>2</sub>·HCl (40 equiv) in DMF (2 mL) was added trimethylamine (44 equiv). After stirring at RT for 30 min, **1b** (1 equiv) in DMF were added. The resulting mixture was stirred for 20 min, then irradiated with 350 nm light until the starting material was consumed. The reaction was quenched with water and the mixture was extracted with dichloromethane (3V3 mL). The combined organic phases were washed with brine and dried over anhydrous Na<sub>2</sub>SO<sub>4</sub>. After removing solvent, the residue was purified by chromatography (hexane/ dichloromethane =5:1) to provide the corresponding trapping adducts **6**.

**Methods used for LCMS-IT-TOF analysis:** The separation of the reaction mixture was conducted on an ACQUITY CSH C18 column (2.1 mm 50 mm, 1.7 mm particle size) using gradient: 0–2.0 min 30–60% MeCN in A, 2.0–3.0 min 60–90% MeCN in A, 3.0–4.0 min 90% MeCN in A, 4.0–4.3 min 90–30% MeCN in A, 4.3–6.0 min 30% MeCN in A, at a flow rate of 0.4 mLmin<sup>-1</sup> [Solution A: 0.1% (v/v) formic acid in water].

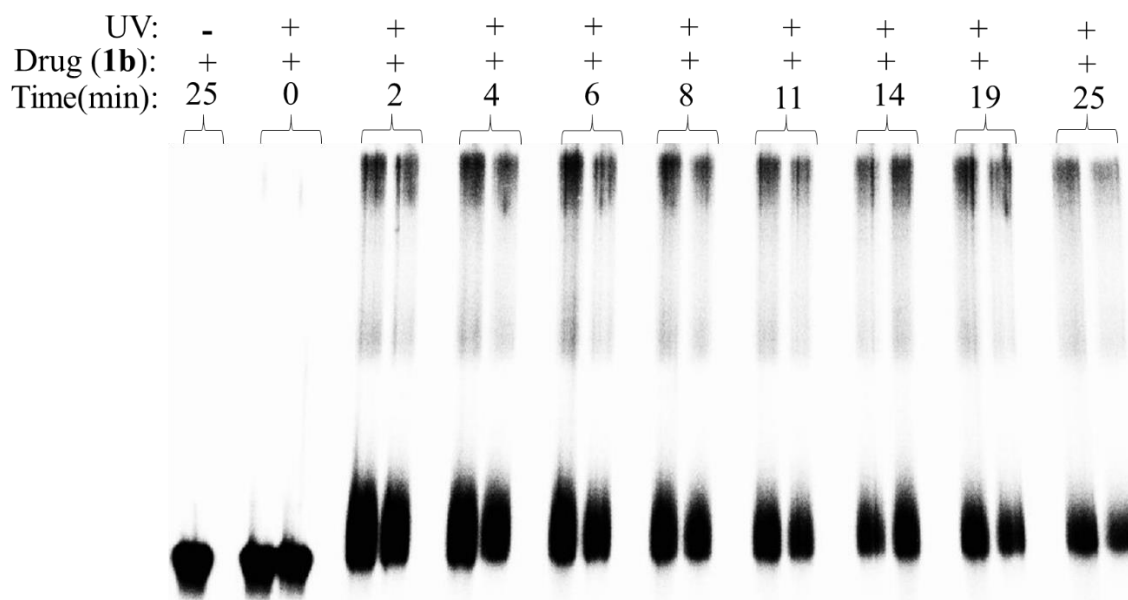
## 2.6 Reference

- (1) Kumar, C. V.; Asuncion, E. H. DNA Binding Studies and Site Selective Fluorescence Sensitization of an Anthryl Probe. *J. Am. Chem. Soc.* **1993**, *115* (19), 8547–8553. <https://doi.org/10.1021/ja00072a004>.
- (2) Aathimanikandan, S. V.; Sandanaraj, B. S.; Arges, C. G.; Bardeen, C. J.; Thayumanavan, S. Effect of Guest Molecule Flexibility in Access to Dendritic Interiors. *Org. Lett.* **2005**, *7* (14), 2809–2812. <https://doi.org/10.1021/ol050579b>.
- (3) Rivlin, N.; Brosh, R.; Oren, M.; Rotter, V. Mutations in the P53 Tumor Suppressor Gene: Important Milestones at the Various Steps of Tumorigenesis. *Genes & Cancer* **2011**, *2* (4), 466–474. <https://doi.org/10.1177/1947601911408889>.
- (4) Ozaki, T.; Nakagawara, A. Role of P53 in Cell Death and Human Cancers. *Cancers* **2011**, *3* (1), 994–1013. <https://doi.org/10.3390/cancers3010994>.
- (5) Wang, Y.; Liu, S.; Lin, Z.; Fan, Y.; Wang, Y.; Peng, X. Photochemical Generation of Benzyl Cations That Selectively Cross-Link Guanine and Cytosine in DNA. *Org. Lett.* **2016**, *18* (11), 2544–2547. <https://doi.org/10.1021/acs.orglett.6b00755>.
- (6) Wang, Y.; Lin, Z.; Fan, H.; Peng, X. Photoinduced DNA Interstrand Cross-Link Formation by Naphthalene Boronates via a Carbocation. *Chemistry – A European Journal* **2016**, *22* (30), 10382–10386. <https://doi.org/10.1002/chem.201601504>.
- (7) Maxam, A. M.; Gilbert, W. Sequencing End-Labeled DNA with Base-Specific Chemical Cleavages. *Methods Enzymol* **1980**, *65* (1), 499–560. [https://doi.org/10.1016/s0076-6879\(80\)65059-9](https://doi.org/10.1016/s0076-6879(80)65059-9).
- (8) Maxam, A. M.; Gilbert, W. A New Method for Sequencing DNA. *Proceedings of the National Academy of Sciences* **1977**, *74* (2), 560–564. <https://doi.org/10.1073/pnas.74.2.560>.
- (9) Paul, B.; Mukherjee, A.; Bhuyan, D.; Guha, S. Construction of Unsymmetrical Bis-Urea Macrocyclic Host for Neutral Molecule and Chloride-Ion Binding. *Journal of Heterocyclic Chemistry* **2021**, *58* (10), 2033–2038. <https://doi.org/10.1002/jhet.4329>.
- (10) Collins, C. J.; Lanz, M.; Goralski, C. T.; Singaram, B. Aminoborohydrides. 10. The Synthesis of Tertiary Amine–Boranes from Various Benzyl Halides and Lithium N,N-Dialkylaminoborohydrides. *J. Org. Chem.* **1999**, *64* (7), 2574–2576. <https://doi.org/10.1021/jo982176d>.

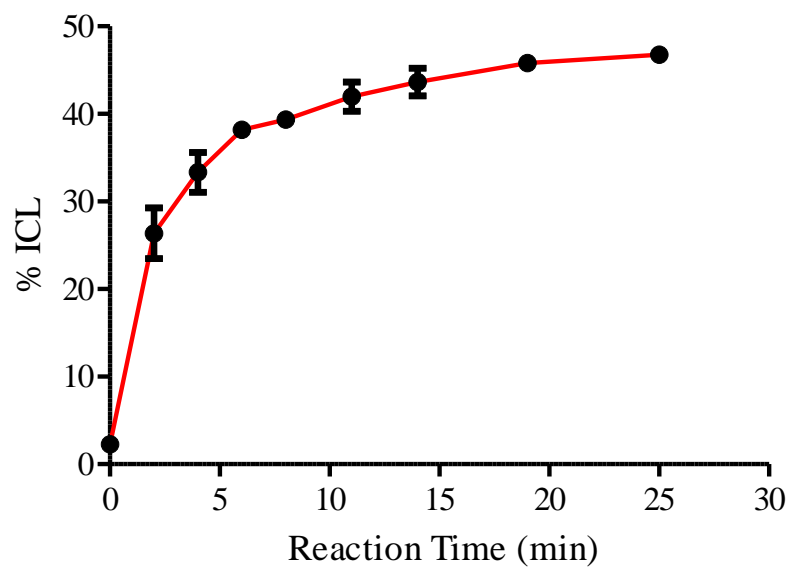
## 2.7 Appendix A: Phosphor Image Autoradiograms



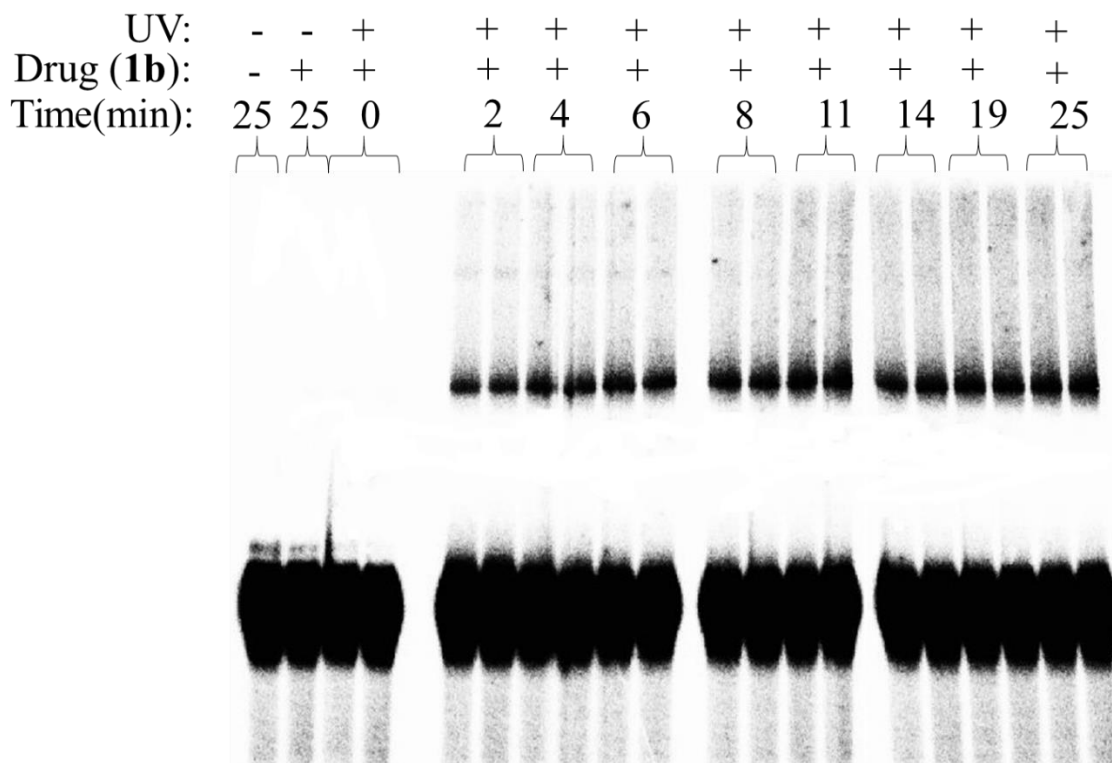
The rate of ICL formation of duplex **3** for **1a** upon photo-irradiation. **1a** at time points 0, 10, 20, 30, 40, 50, 65, 80 min. [**1a**] = 800  $\mu$ M. Reaction mixtures were photo-irradiated under UV (350 nm), duplicates was done at each time point.



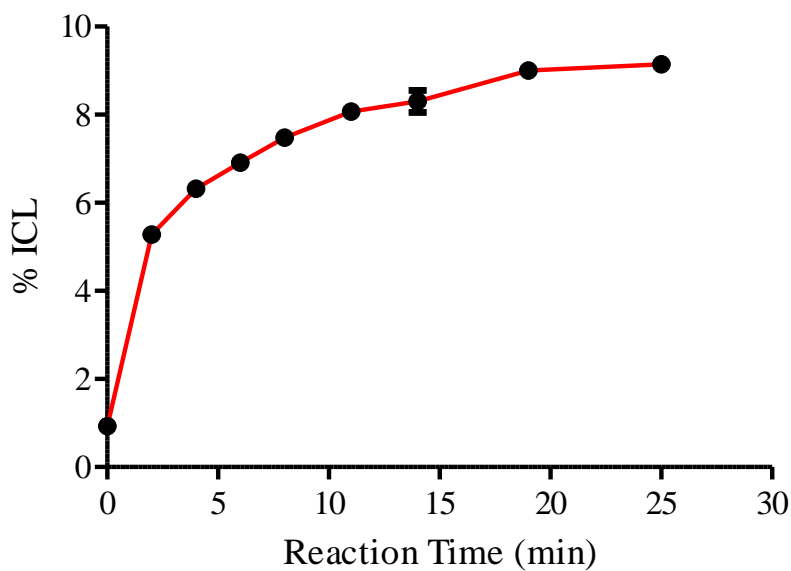
**1b** in H<sub>2</sub>O system



The rate of ICL formation of duplex **3** for **1b** upon photo-irradiation. **1b** at time points 0, 2, 4, 6, 8, 11, 14, 19, 25 min. [**1b**] = 500  $\mu$ M. Reaction mixtures were photo-irradiated under UV (350 nm), duplicates was done at each time point.



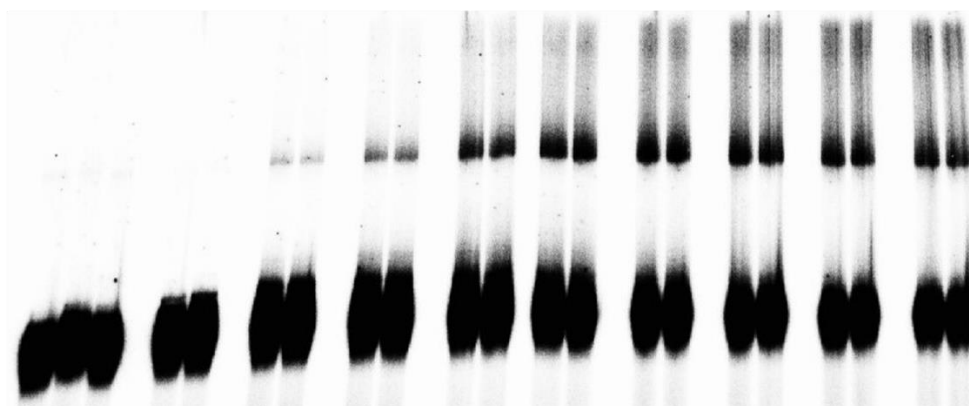
**1b** in H<sub>2</sub>O:DMSO system



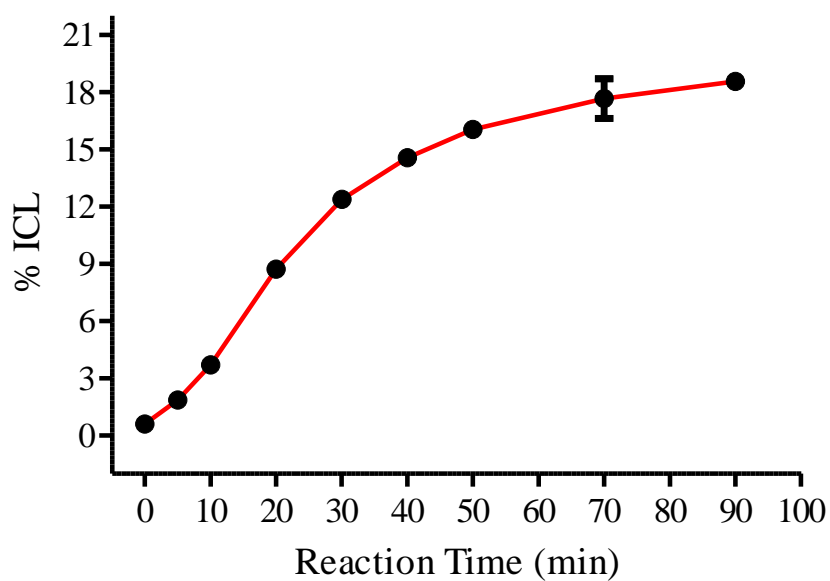
The rate of ICL formation of duplex **3** for **1b** upon photo-irradiation. **1b** at time points 0, 2, 4, 6, 8, 11, 14, 19, 25 min. [**1b**] = 500  $\mu$ M and aqueous: organic ratio (v/v) = 14: 6. Reaction mixtures were photo-irradiated under UV (350 nm), duplicates was done at each time point.



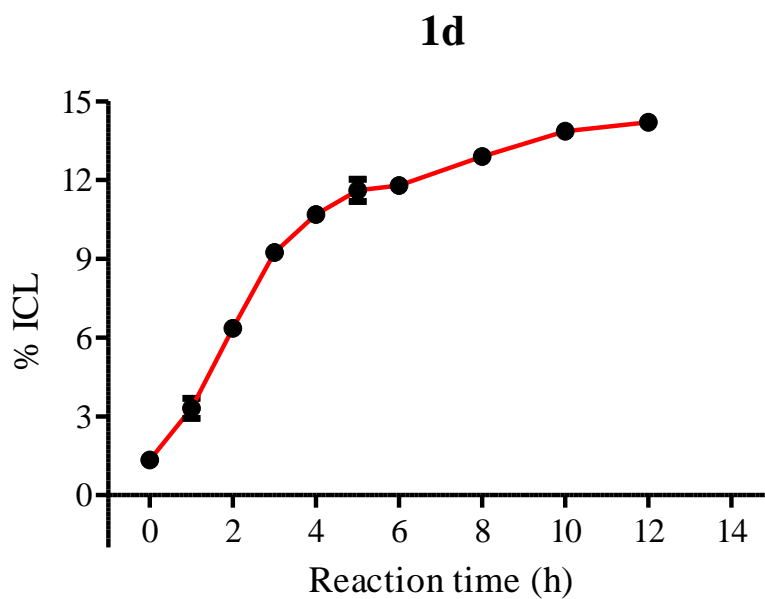
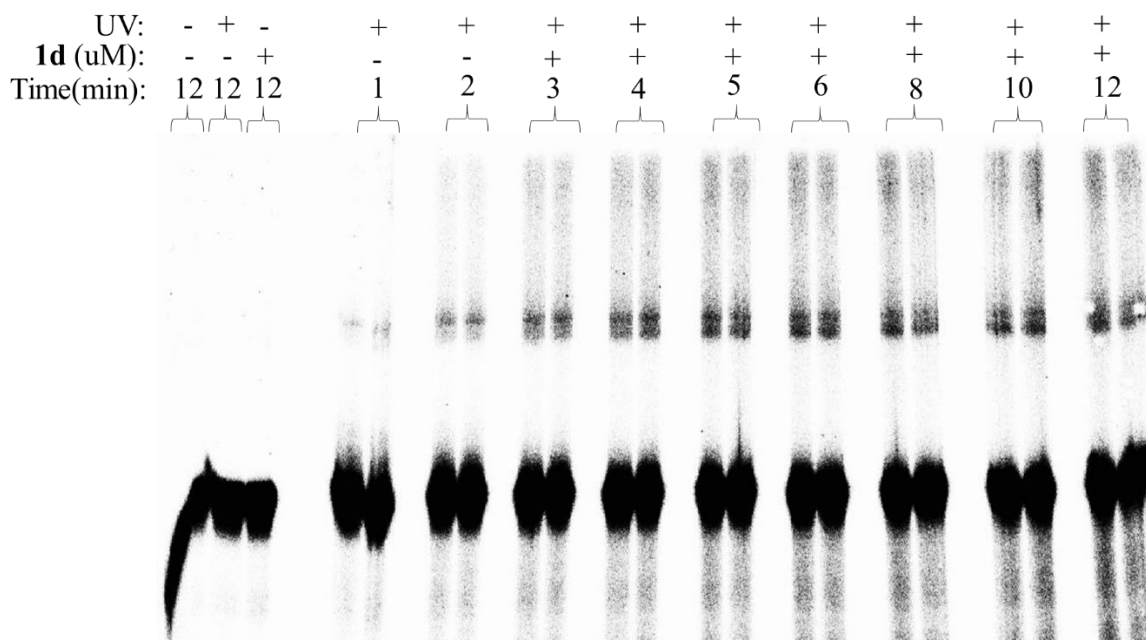
|                     |    |    |    |   |   |    |    |    |    |    |    |    |
|---------------------|----|----|----|---|---|----|----|----|----|----|----|----|
| UV:                 | -  | +  | -  | + | + | +  | +  | +  | +  | +  | +  | +  |
| Drug ( <b>1c</b> ): | -  | -  | +  | + | + | +  | +  | +  | +  | +  | +  | +  |
| Time(min):          | 90 | 90 | 90 | 0 | 5 | 10 | 20 | 30 | 40 | 50 | 70 | 90 |



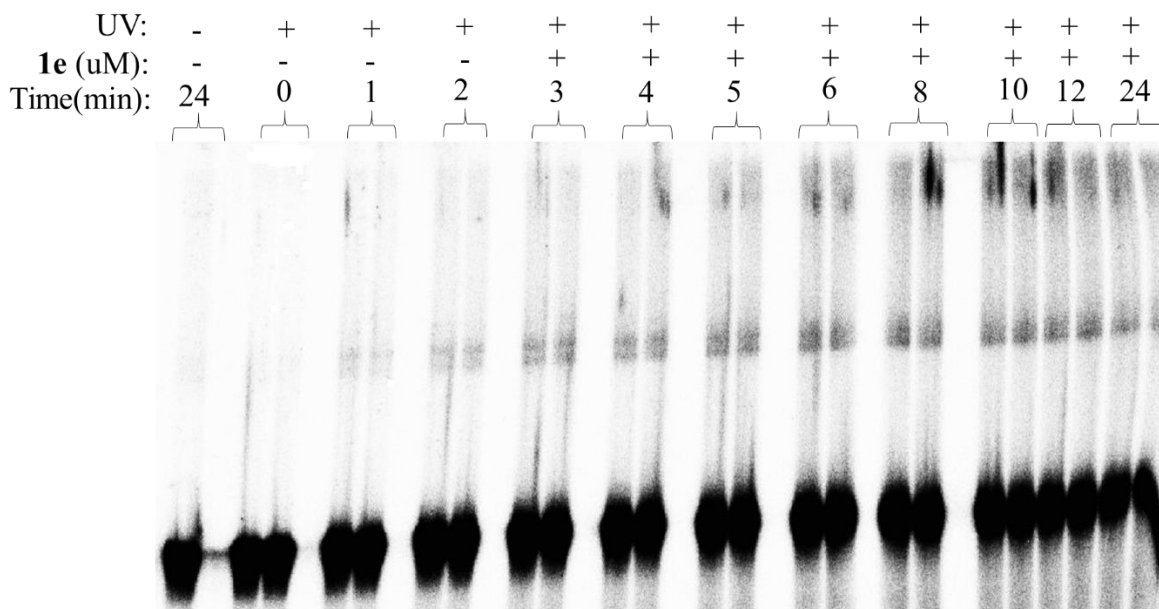
**1c**



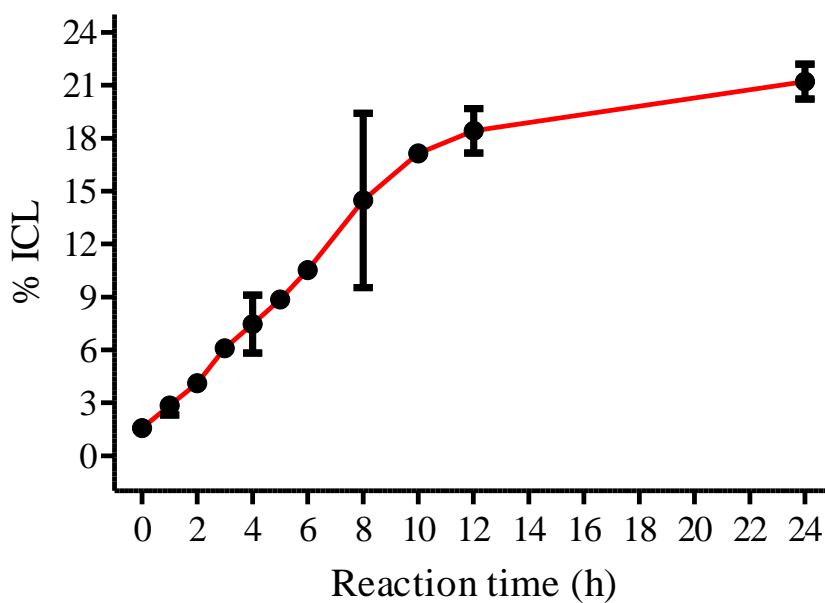
The rate of ICL formation of duplex **3** for **1c** upon photo-irradiation. **1c** at time points 0, 5, 10, 20, 30, 40, 50, 70 and 90 min. [**1c**] = 400  $\mu$ M. Reaction mixtures were photo-irradiated under UV (350 nm), duplicates was done at each time point.



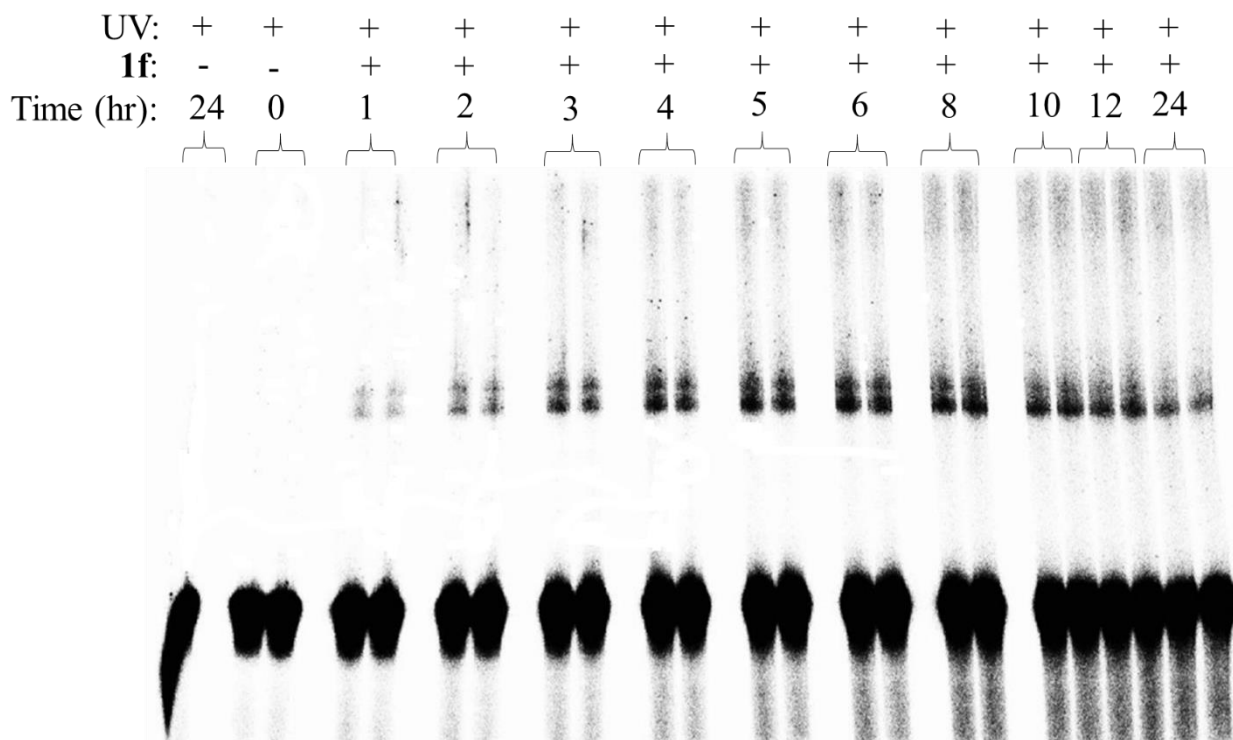
The rate of ICL formation of duplex **3** for **1d** upon photo-irradiation. **1d** at time points 0, 1, 2, 3, 4, 5, 6, 8, 10 and 12 h. [**1d**] = 500  $\mu$ M. Reaction mixtures were photo-irradiated under UV (350 nm), duplicates was done at each time point.



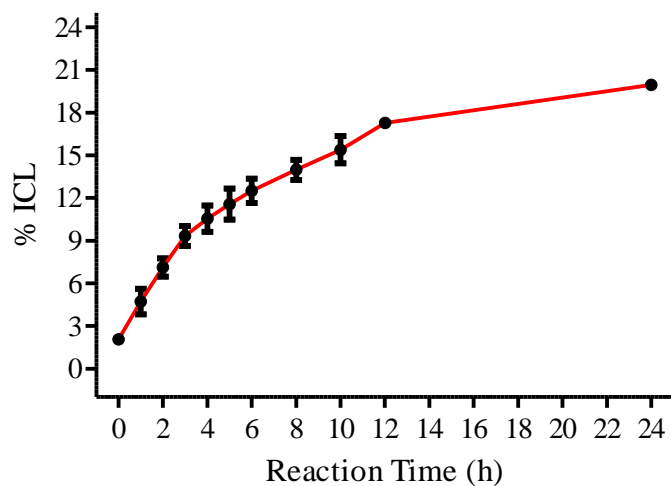
**1e**



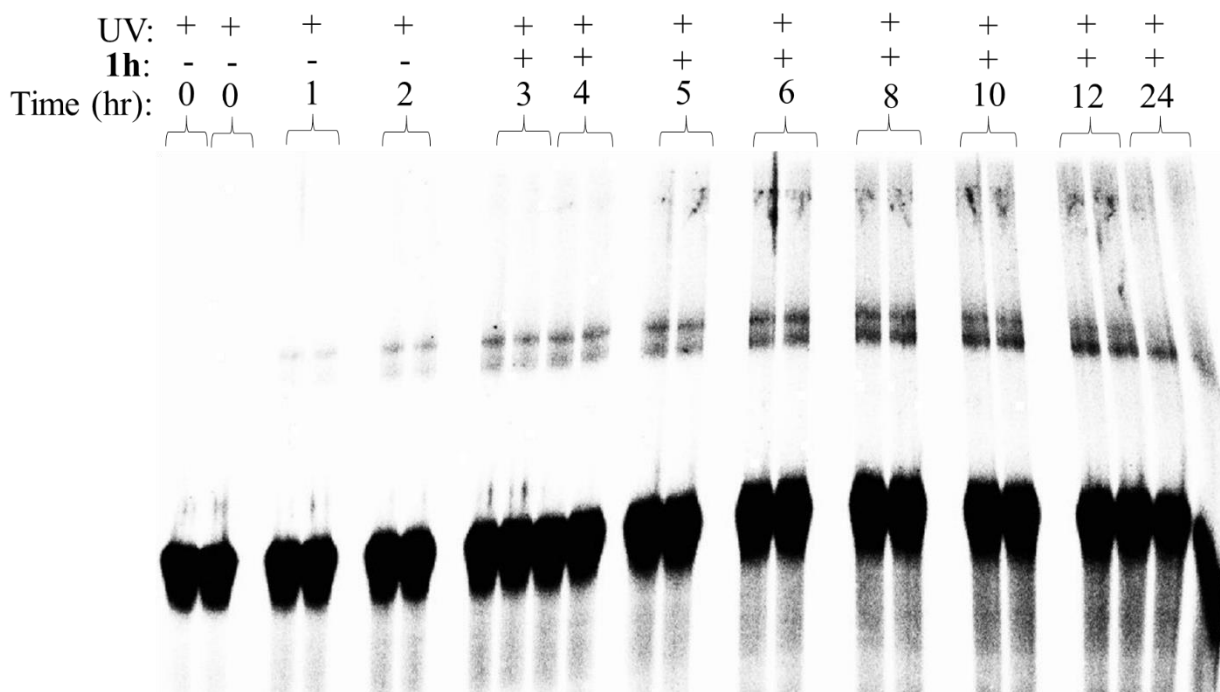
The rate of ICL formation of duplex **3** for **1e** upon photo-irradiation. **1e** at time points 0, 1, 2, 3, 4, 5, 6, 8, 10, 12, 24. Concentration of [**1e**] = 500  $\mu$ M. Reaction mixtures were photo-irradiated under UV (350 nm), duplicates were done at each time point.



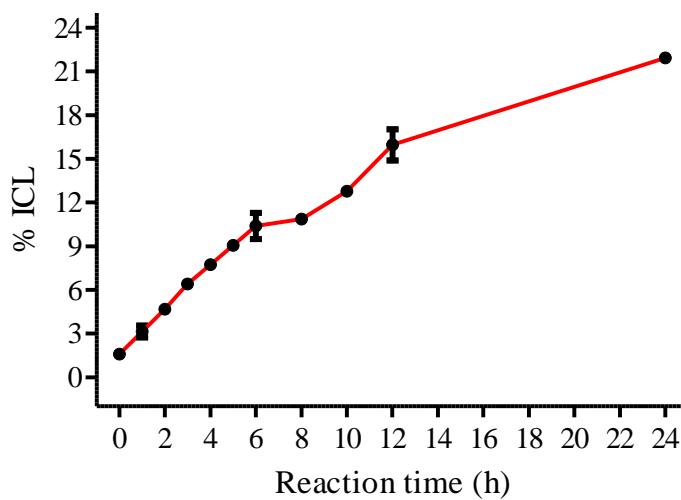
**1f**



The rate of ICL formation of duplex **3** for **1e** upon photo-irradiation. **1e** at time points 0, 1, 2, 3, 4, 5, 6, 8, 10, 12, 24. Concentration of [**1e**] = 500  $\mu$ M. Reaction mixtures were photo-irradiated under UV (350 nm), duplicates were done at each time point.

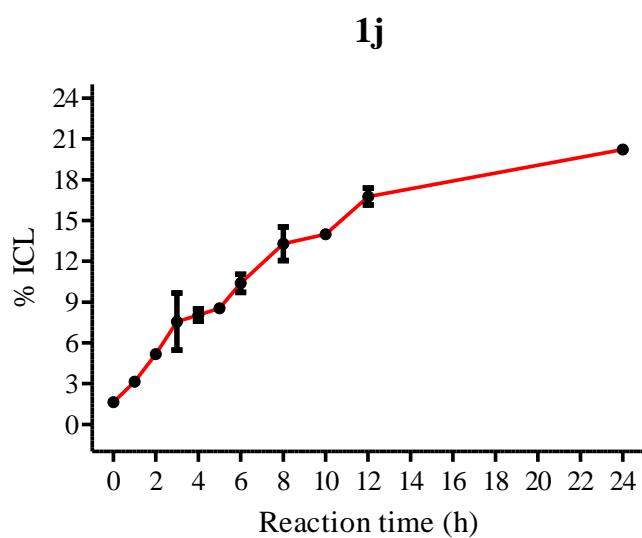
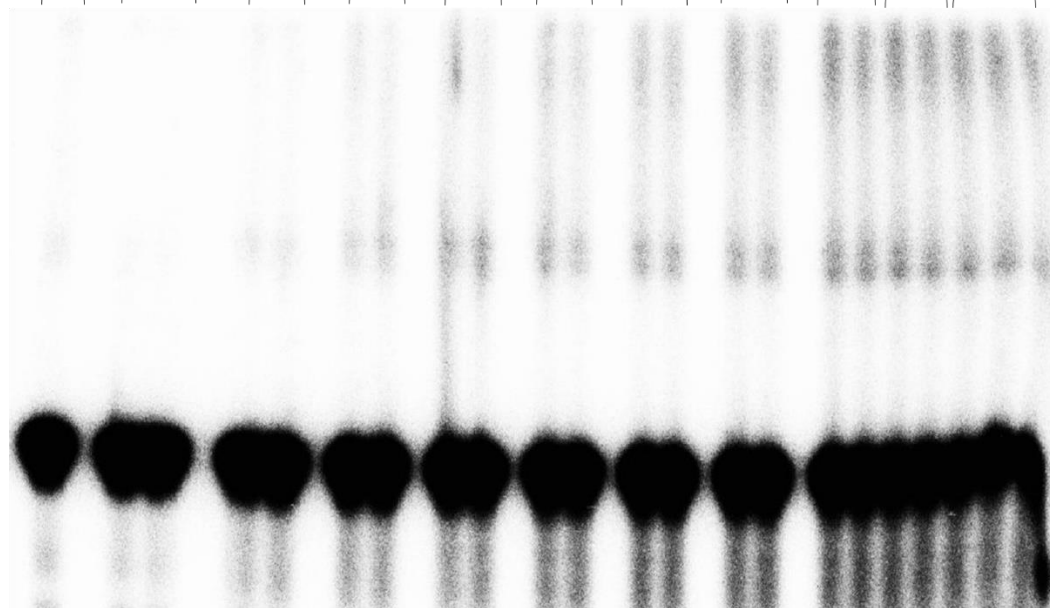


**1h**



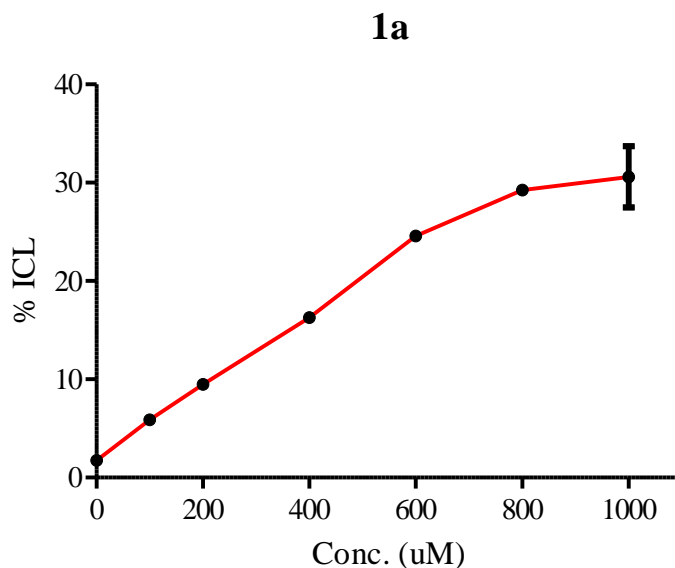
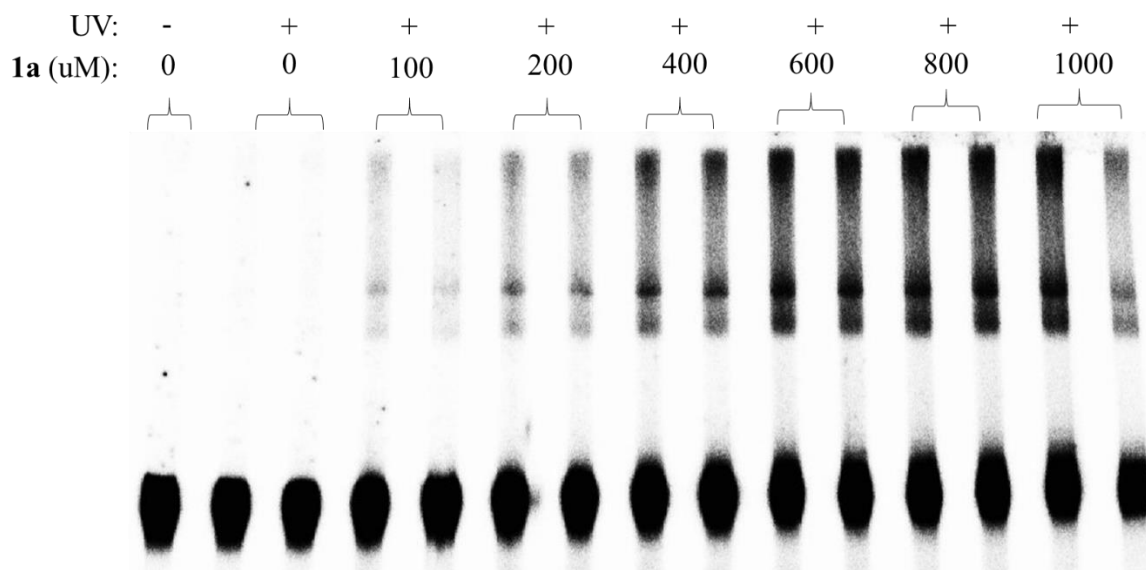
The rate of ICL formation of duplex **3** for **1e** upon photo-irradiation. **1e** at time points 0, 1, 2, 3, 4, 5, 6, 8, 10, 12, 24. Concentration of [**1e**] = 500  $\mu$ M. Reaction mixtures were photo-irradiated under UV (350 nm), duplicates were done at each time point.

|            |   |   |   |   |   |   |   |   |   |    |    |
|------------|---|---|---|---|---|---|---|---|---|----|----|
| UV:        | + | + | + | + | + | + | + | + | + | +  | +  |
| <b>1j:</b> | - | - | - | + | + | + | + | + | + | +  | +  |
| Time (hr): | 0 | 0 | 1 | 2 | 3 | 4 | 5 | 6 | 8 | 10 | 12 |

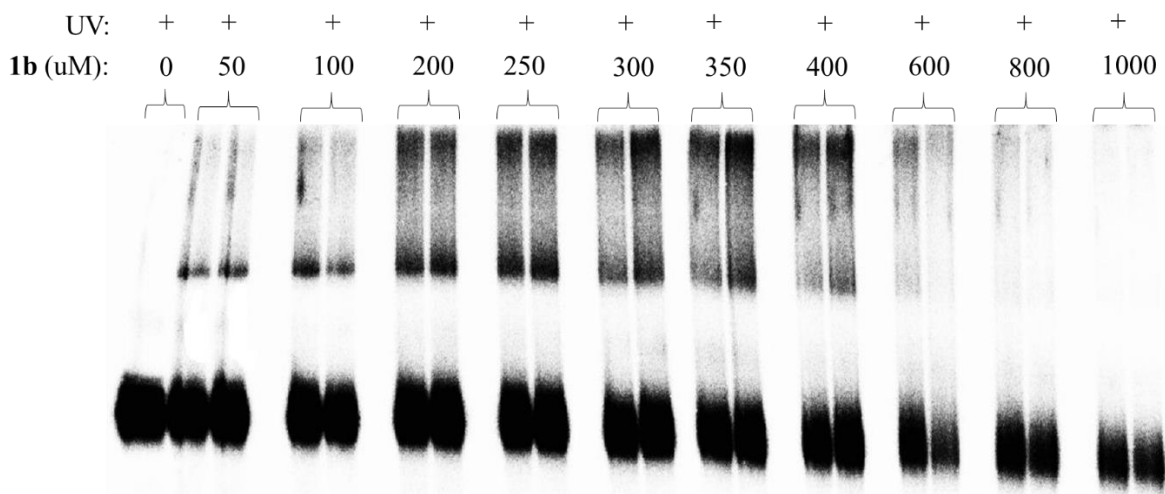


The rate of ICL formation of duplex **3** for **1e** upon photo-irradiation. **1e** at time points 0, 1, 2, 3, 4, 5, 6, 8, 10, 12, 24. Concentration of [**1e**] = 500  $\mu$ M. Reaction mixtures were photo-irradiated under UV (350 nm), duplicates were done at each time point.

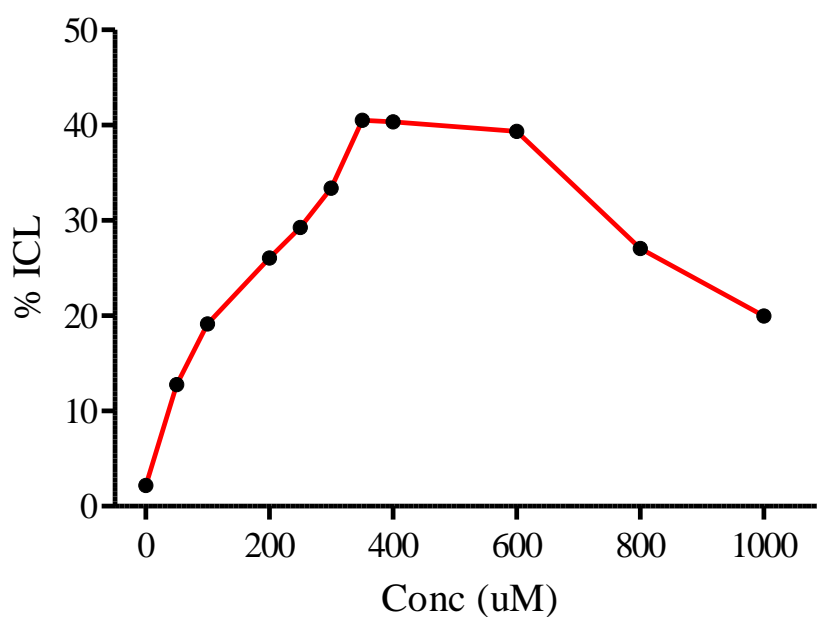
### Concentration dependent DNA ICL formation S



The concentration dependence of ICL formation of duplex **3** for **1a** upon photo irradiation. Phosphor image autoradiogram of 20% denaturing PAGE analysis of **1a** under varying concentration. 0, 100  $\mu$ M, 200  $\mu$ M, 300  $\mu$ M, 400  $\mu$ M, 500 $\mu$ M, 600  $\mu$ M, 800 $\mu$ M and 1000 $\mu$ M. Reaction mixtures were photo-irradiated under UV (350 nm) for 55 min.

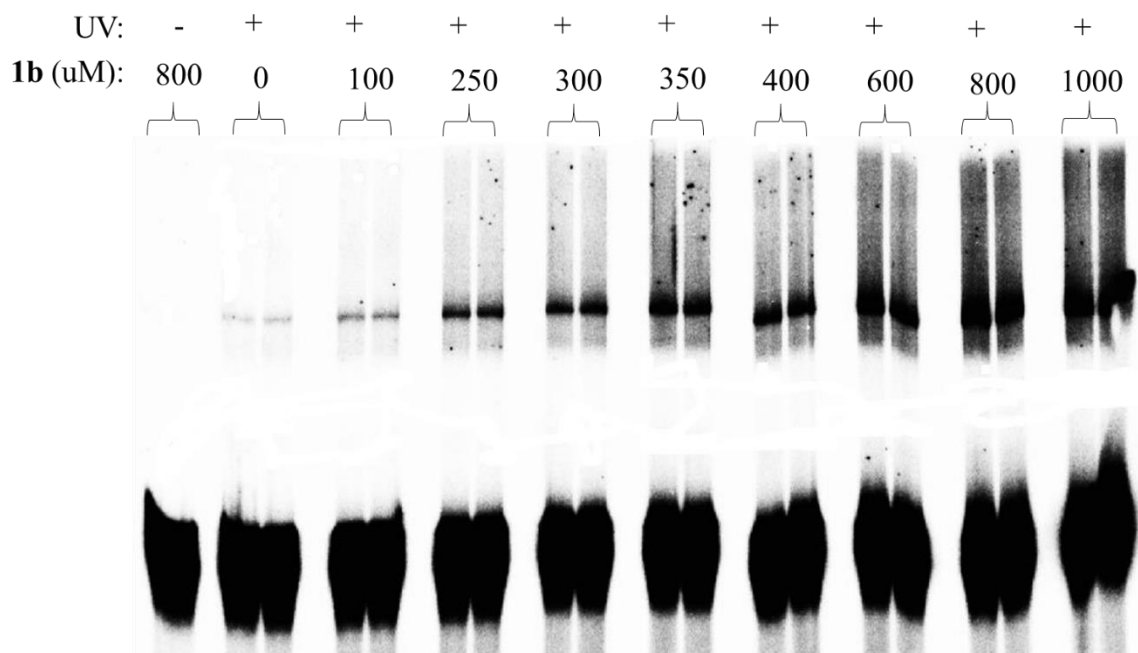


### **1b** in Water

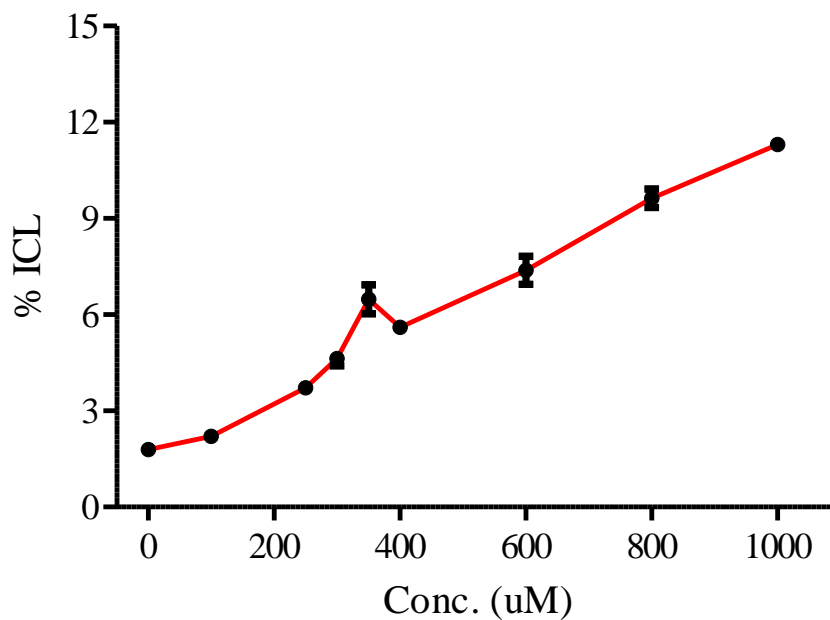


The concentration dependence of ICL formation of duplex **3** for **1b** (dissolved in H<sub>2</sub>O) upon photo irradiation. Phosphor image autoradiogram of 20% denaturing PAGE analysis of **1b** under varying concentration. 0, 50  $\mu$ M, 100  $\mu$ M, 200  $\mu$ M, 250  $\mu$ M, 300  $\mu$ M, 350  $\mu$ M, 400  $\mu$ M, 600  $\mu$ M, 800 $\mu$ M and 1000 $\mu$ M. Reaction mixtures were photo-irradiated under UV (350 nm) for 5 min.

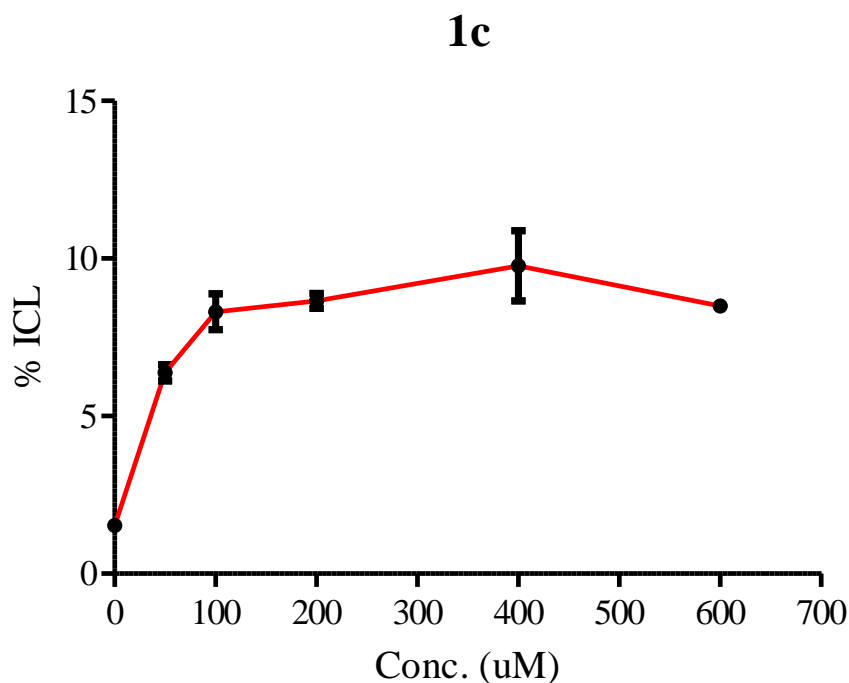
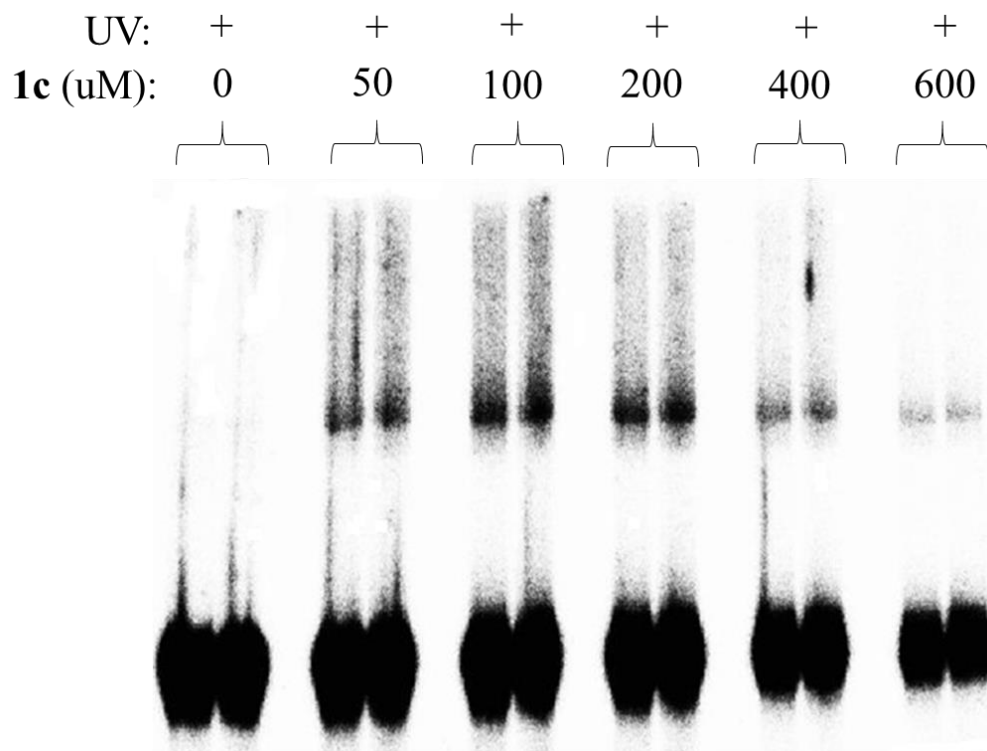




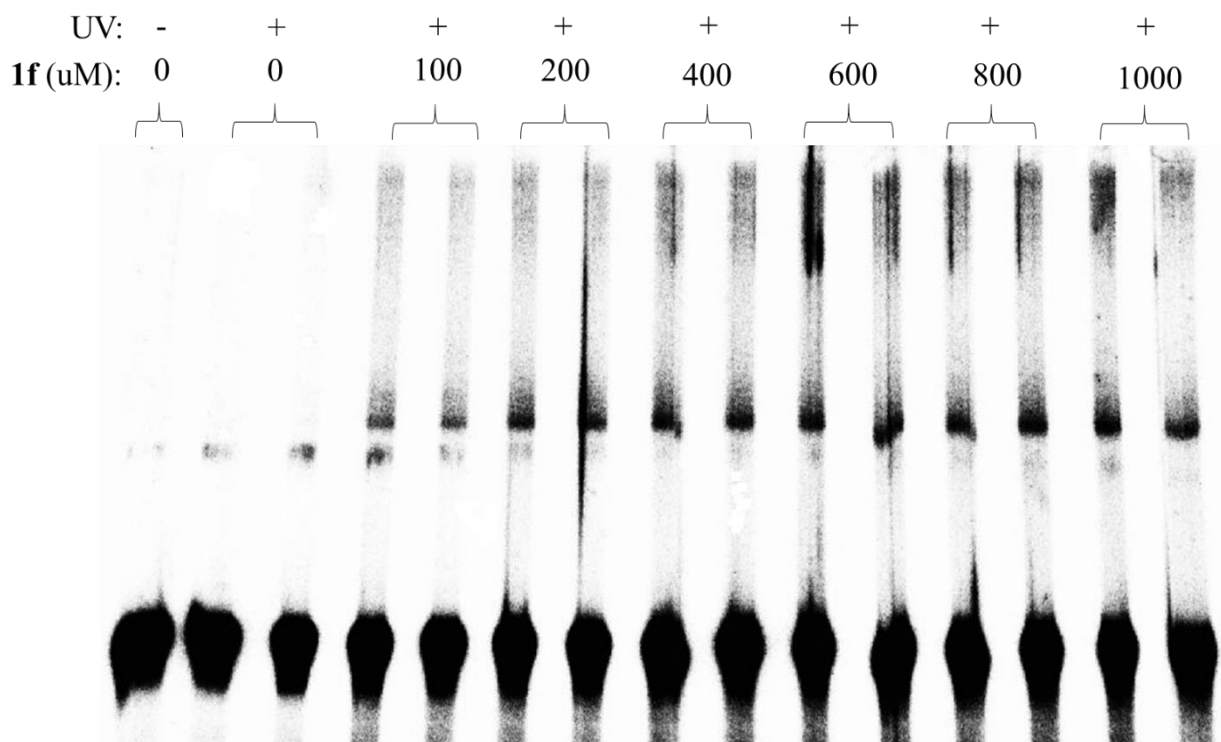
### **1b** dissolved in DMSO



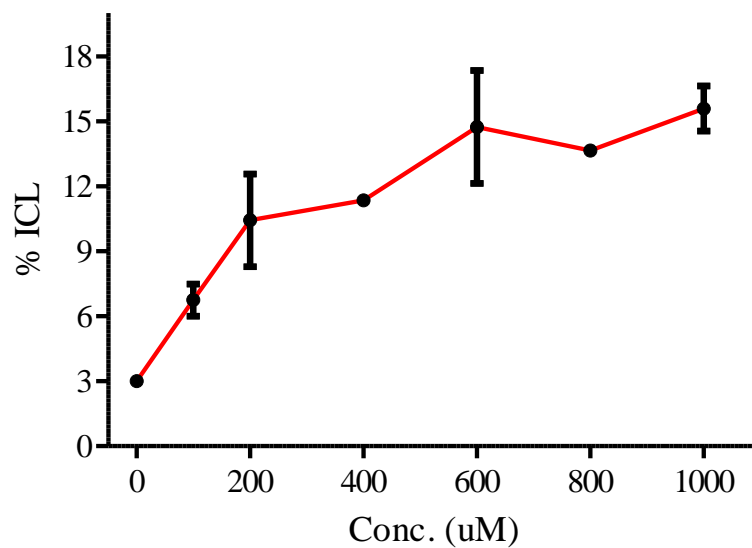
The concentration dependence of ICL formation of duplex **3** for **1b** (dissolved in DMSO) upon photo irradiation. Phosphor image autoradiogram of 20% denaturing PAGE analysis of **1b** under varying concentration. 0, 100  $\mu$ M, 250  $\mu$ M, 300  $\mu$ M, 350  $\mu$ M, 400  $\mu$ M, 600  $\mu$ M, 800 $\mu$ M, 1000 $\mu$ M. Reaction mixtures were photo-irradiated under UV (350 nm) for 20 min.



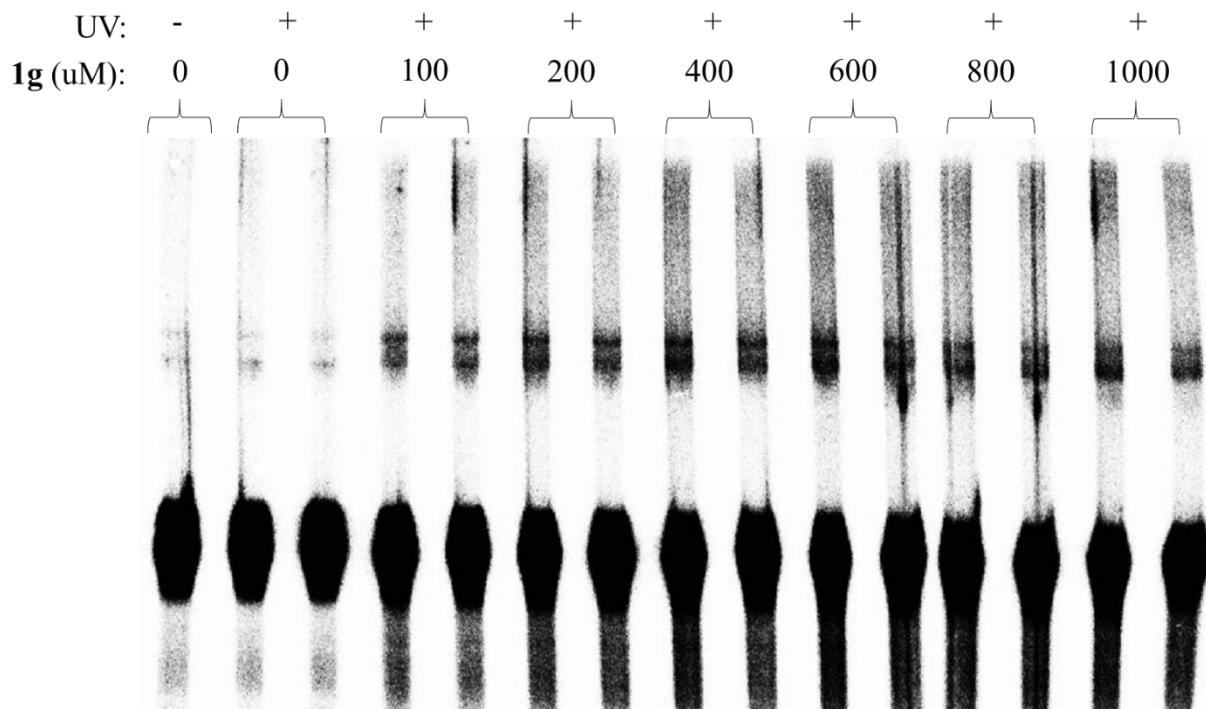
The concentration dependence of ICL formation of duplex **3** for **1c** upon photo irradiation. Phosphor image autoradiogram of 20% denaturing PAGE analysis of **1c** under varying concentration. 0, 50  $\mu$ M, 100  $\mu$ M, 200  $\mu$ M, 400  $\mu$ M, 600  $\mu$ M. Reaction mixtures were photo-irradiated under UV (350 nm) for 50 min.



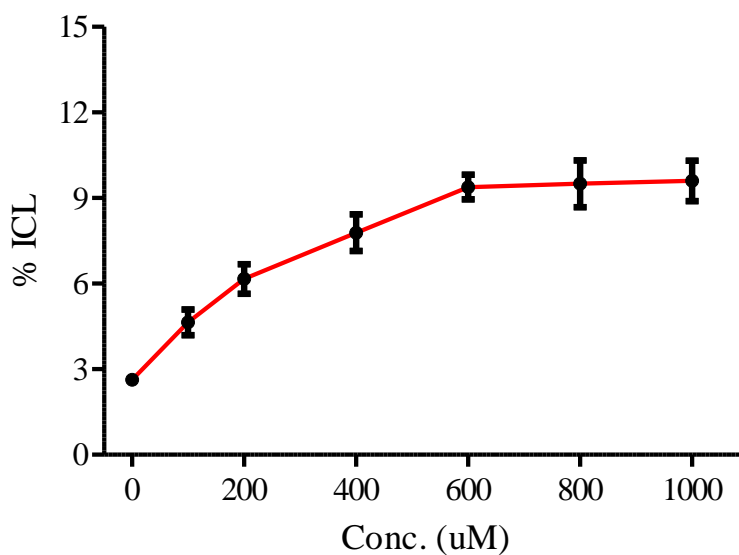
**1f**



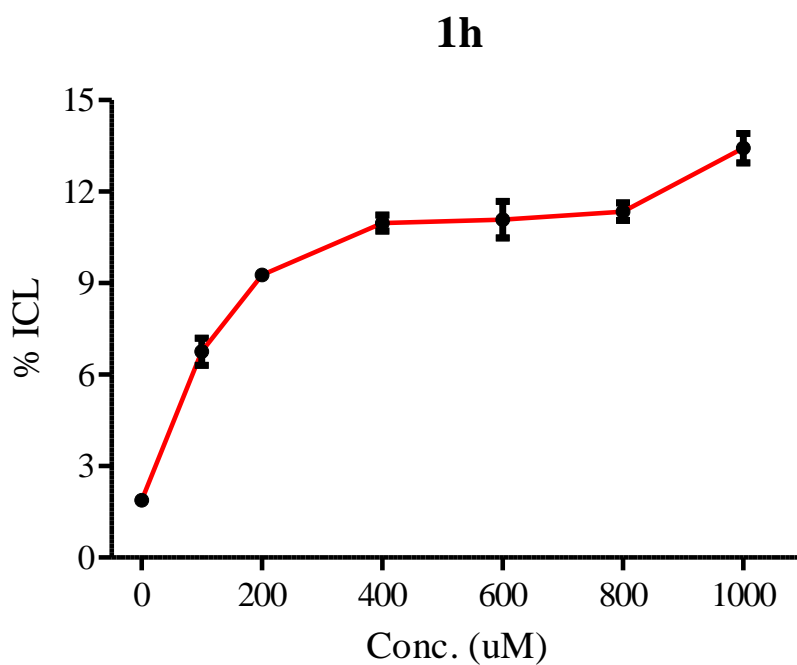
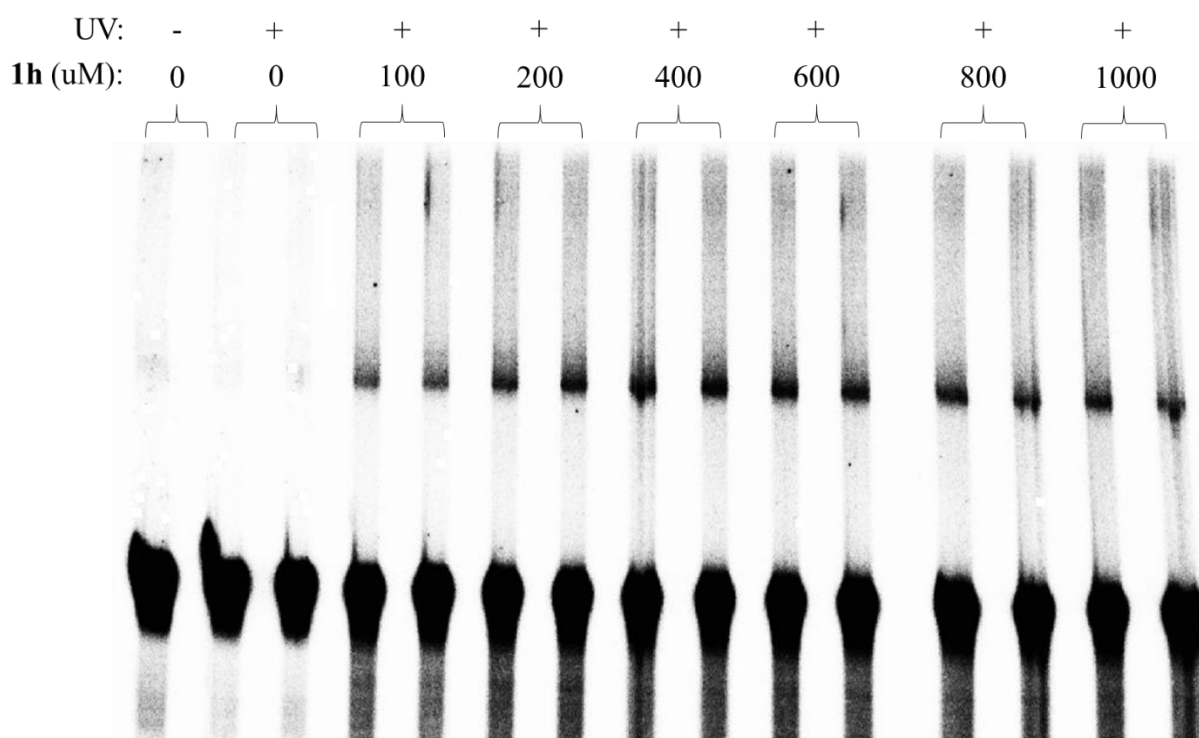
The concentration dependence of ICL formation of duplex **3** for **1c** upon photo irradiation. Phosphor image autoradiogram of 20% denaturing PAGE analysis of **1c** under varying concentration. 0, 50  $\mu\text{M}$ , 100  $\mu\text{M}$ , 200  $\mu\text{M}$ , 400  $\mu\text{M}$ , 600  $\mu\text{M}$ . Reaction mixtures were photo-irradiated under UV (350 nm) for 50 min.



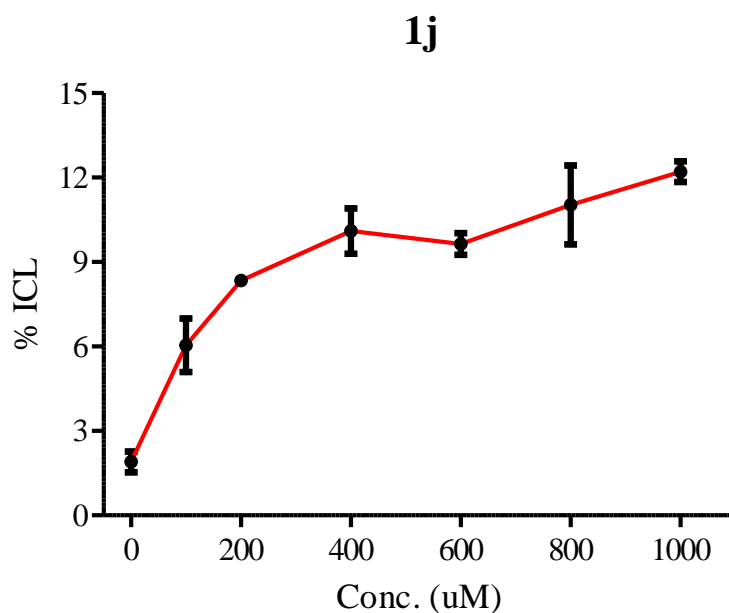
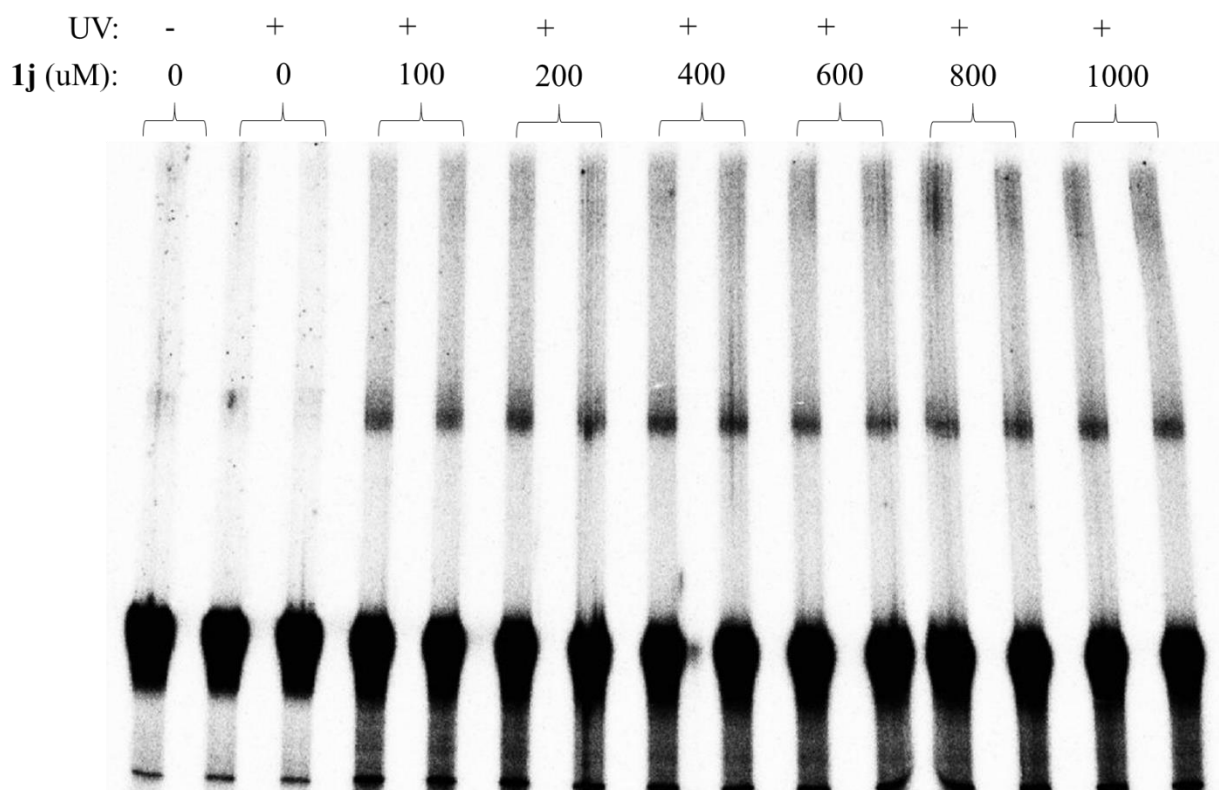
**1g**



The concentration dependence of ICL formation of duplex **3** for **1c** upon photo irradiation. Phosphor image autoradiogram of 20% denaturing PAGE analysis of **1c** under varying concentration. 0, 50  $\mu$ M, 100  $\mu$ M, 200  $\mu$ M, 400  $\mu$ M, 600  $\mu$ M. Reaction mixtures were photo-irradiated under UV (350 nm) for 50 min.



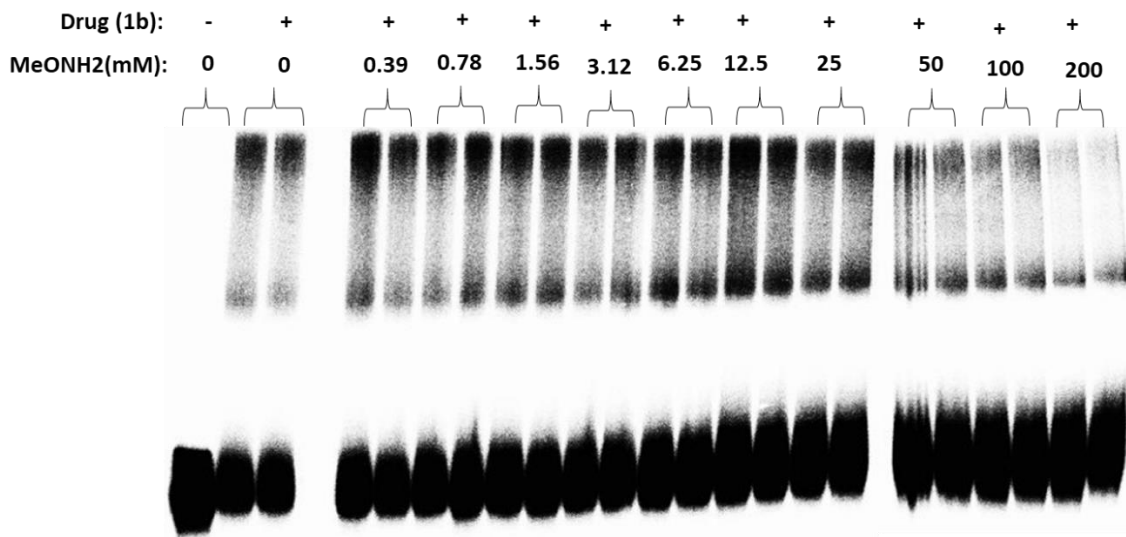
The concentration dependence of ICL formation of duplex **3** for **1c** upon photo irradiation. Phosphor image autoradiogram of 20% denaturing PAGE analysis of **1c** under varying concentration. 0, 50  $\mu$ M, 100  $\mu$ M, 200  $\mu$ M, 400  $\mu$ M, 600  $\mu$ M. Reaction mixtures were photo-irradiated under UV (350 nm) for 50 min.



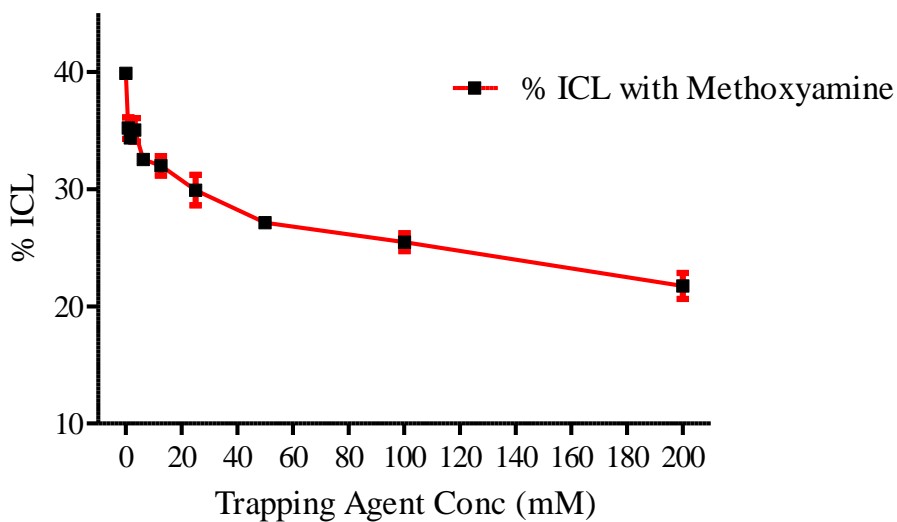
The concentration dependence of ICL formation of duplex **3** for **1c** upon photo irradiation. Phosphor image autoradiogram of 20% denaturing PAGE analysis of **1c** under varying concentration. 0, 50  $\mu\text{M}$ , 100  $\mu\text{M}$ , 200  $\mu\text{M}$ , 400  $\mu\text{M}$ , 600  $\mu\text{M}$ . Reaction mixtures were photo-irradiated under UV (350 nm) for 50 min.

### MeONH<sub>2</sub> trapping:

Lane 1: UV only. Lanes 2-21: with UV and compounds; MeONH<sub>2</sub> concentration: lane 2,3: 0, lane 4,5: 780 μM, lane 6,7: 1.56mM, lane 8,9: 3.12mM, lane 10,11: 6.25mM, lane 12,13: 12.5mM, lane 14,15: 25mM, lane 16,17: 50mM, lane 18,19: 100mM, lane 20,21: 200mM.



**1b**

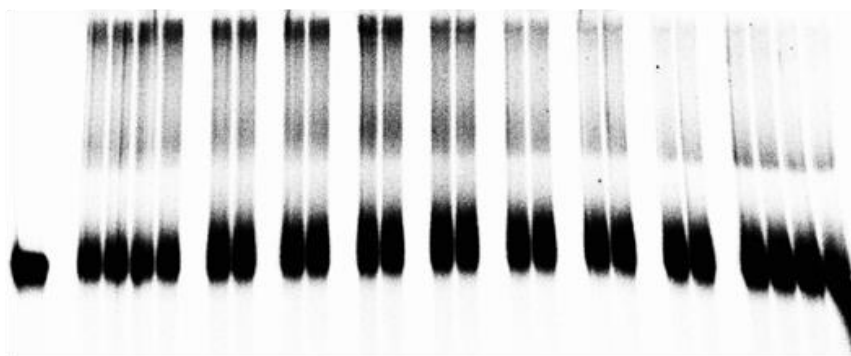



Carbocation trapping with ICL formation of duplex 3 for 1b at optimized conditions: 350 μM. 5 min.

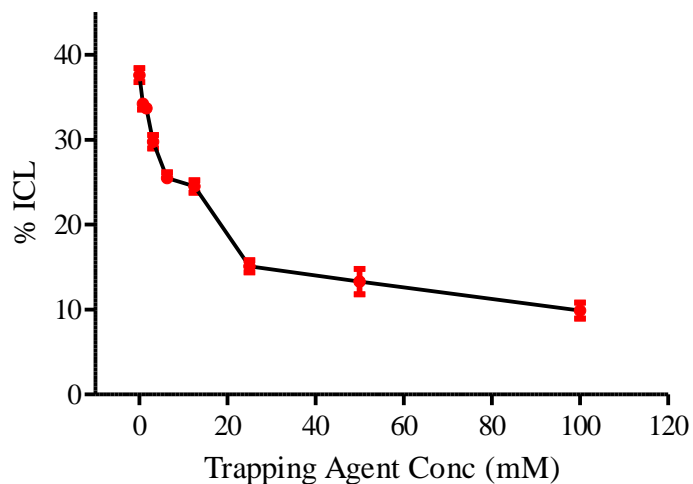
### BME trapping:

Lane 1: UV only. Lane 2-21 with UV and compounds; BME concentration: lane 2,3: 0, lane 4,5: 190  $\mu$ M, lane 6,7: 390  $\mu$ M, lane 8,9: 780  $\mu$ M, lane 10,11: 1.56 mM, lane 12,13: 3.12 mM, lane 14,15: 6.25 mM, lane 16,17: 12.5 mM, lane 18,19: 25 mM, lane 20,21: 50 mM, lane 22,23: 100 mM.

|            |     |   |      |      |      |      |      |      |      |    |    |     |
|------------|-----|---|------|------|------|------|------|------|------|----|----|-----|
| Drug (1b): | -   | + | +    | +    | +    | +    | +    | +    | +    | +  | +  |     |
| BME(mM):   | DNA | 0 | 0.19 | 0.39 | 0.78 | 1.56 | 3.12 | 6.25 | 12.5 | 25 | 50 | 100 |



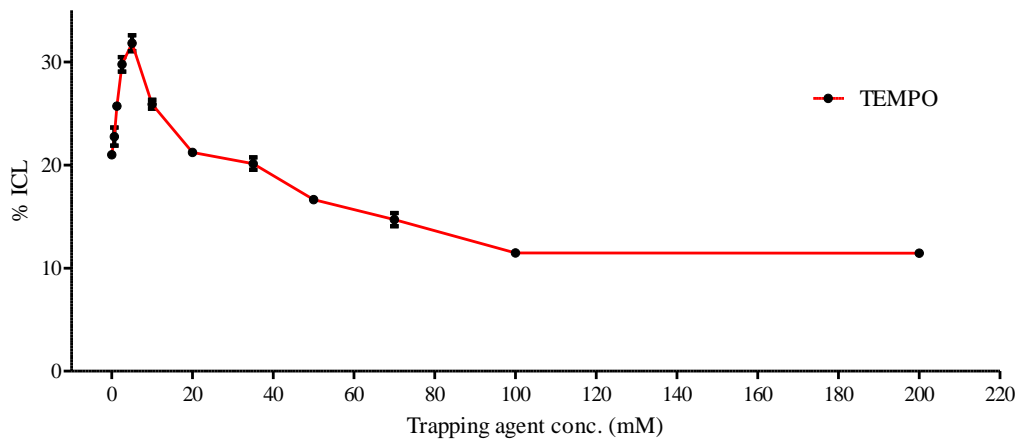
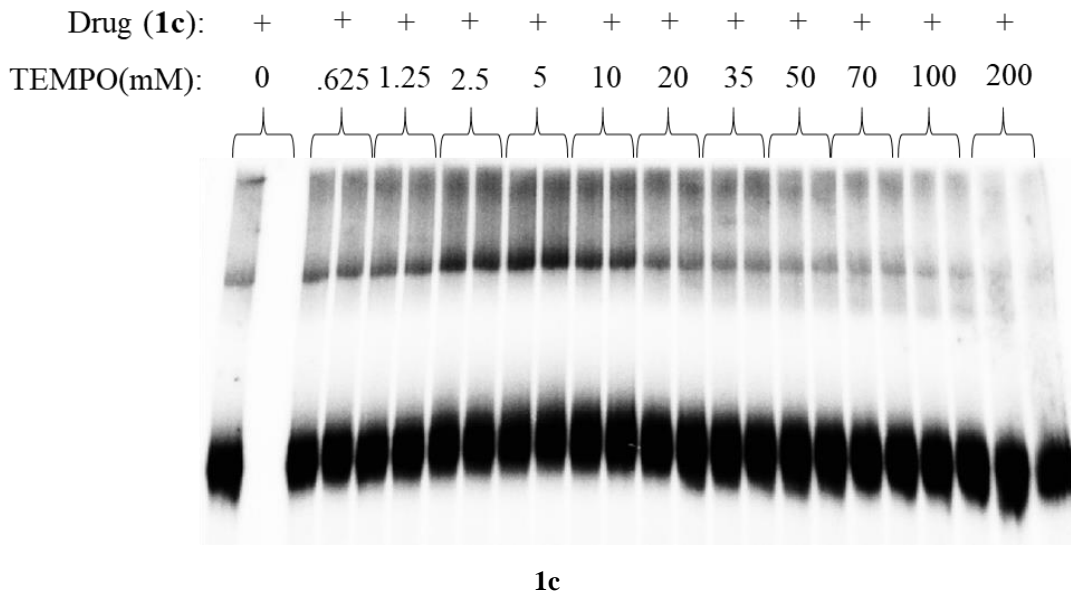
**1b**



Carbocation and/or radical trapping with ICL formation of duplex **3** for **1b** at optimized conditions: 350  $\mu$ M. 5 min

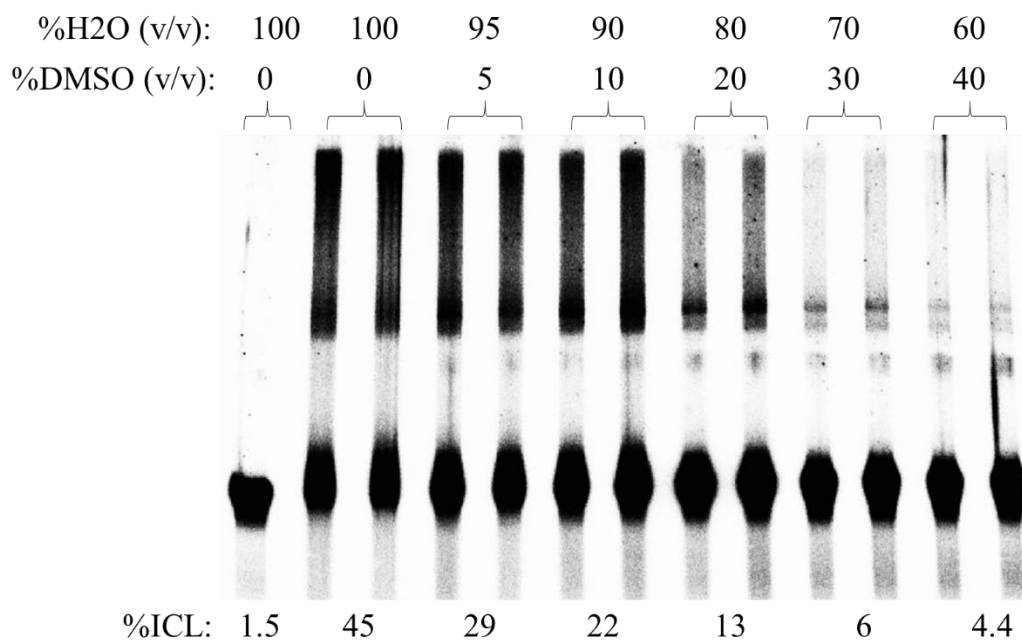


TEMPO trapping: lane **1**: UV only. Lane **2-24** with UV and compounds; TEMPO concentration: lane **2**: 0, lane **3,4**: 625  $\mu$ M, lane **5,6**: 1.25 mM, lane **7,8**: 2.5 mM, lane **9,10**: 5 mM, lane **11,12**: 10 mM, lane **13,14**: 20 mM, lane **15,16**: 35 mM, lane **17,18**: 50 mM, lane **19,20**: 70 mM, lane **21,22**: 100 mM, lane **23,24**: 200 mM.



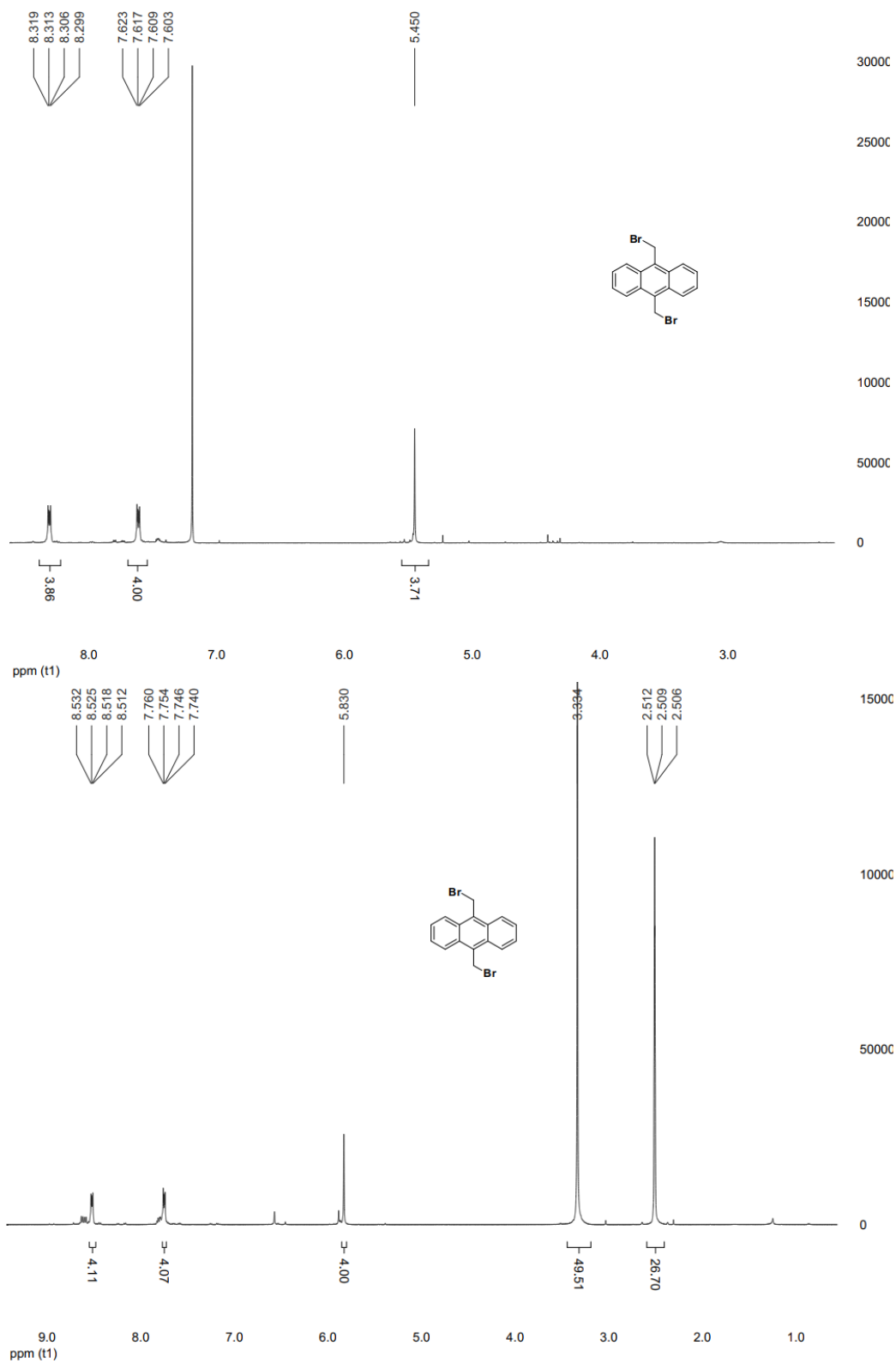
TEMPO trapping with ICL formation of duplex **3** for **1c** at optimized conditions: 350  $\mu$ M. 5 min

### Organic Solvent Ratio dependent ICL formation study of **1b**

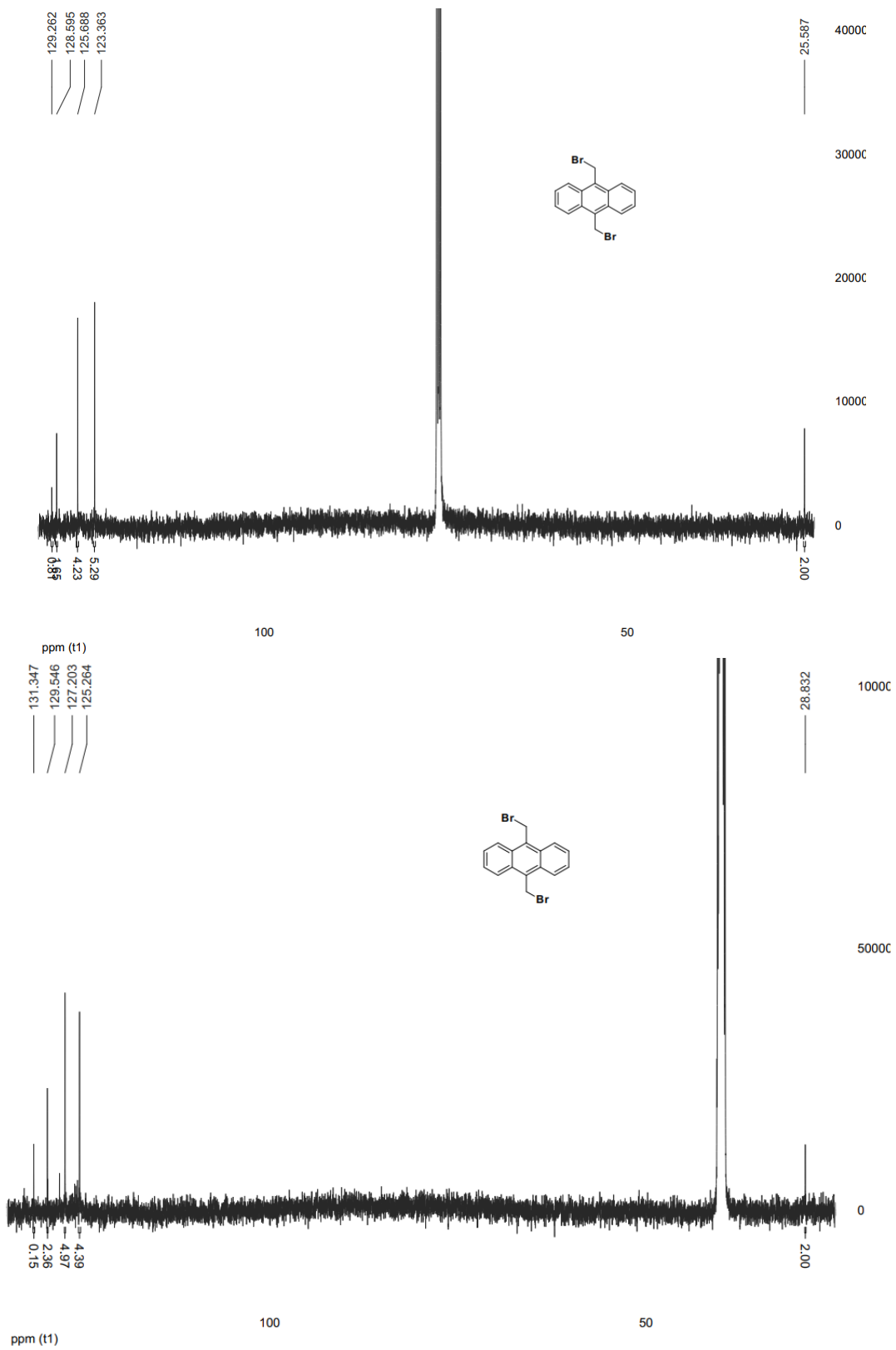


Photoinduced DNA ICL formation for **1b**. lane 1: DNA without drug but with UV irradiation at 350 nm; Lane 2,4,6: DNA with the drug (optimal concentration) but no UV irradiation at 350 nm for optimal time; lane 3,5,7: DNA with the drug (optimal concentration) upon 350 nm irradiation for optimal time; lane 3: **1b** (ICL yield, 40 %); lane 5: **1a** (ICL yield, 10.9 %); lane 7: **1c** (ICL yield, 11.3 %). DNA ICL yields were obtained by duplicate experiments and shown as average  $\pm$  standard deviation.

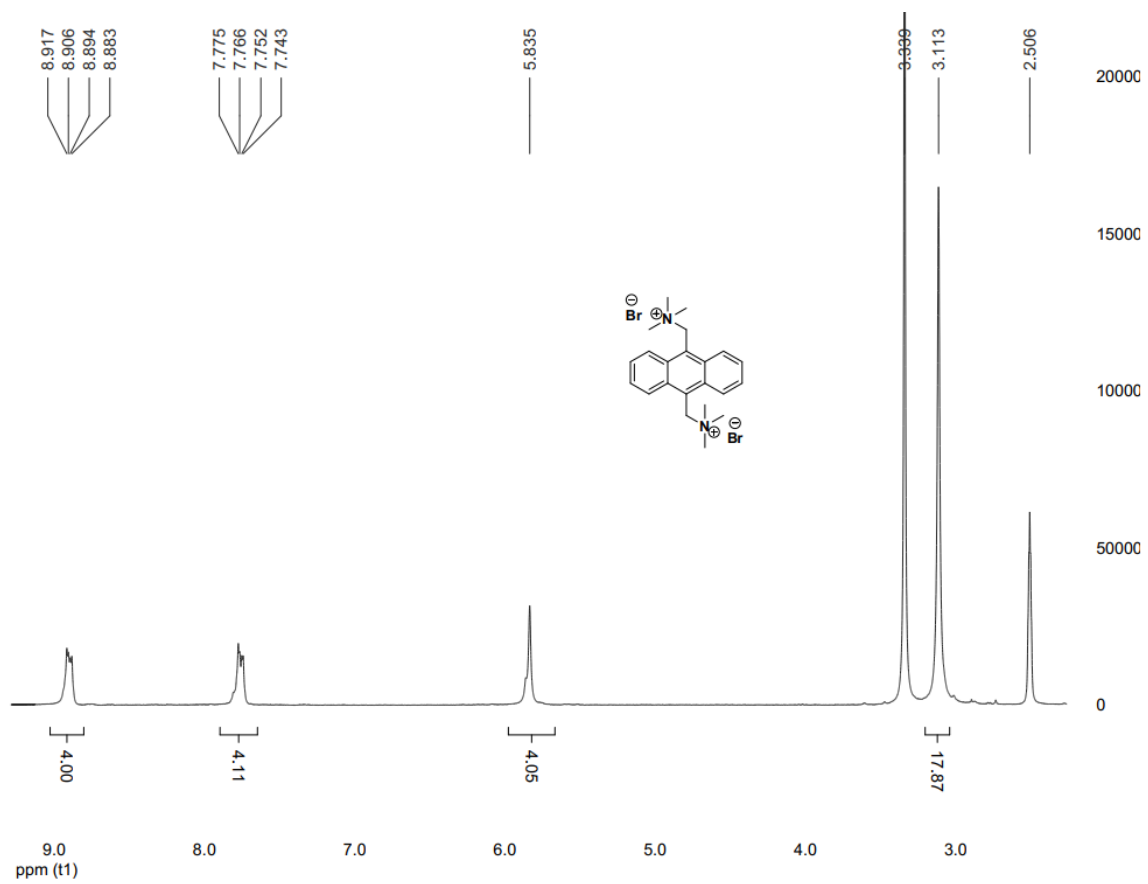
## 2.8 Appendix B: Characterization of compounds



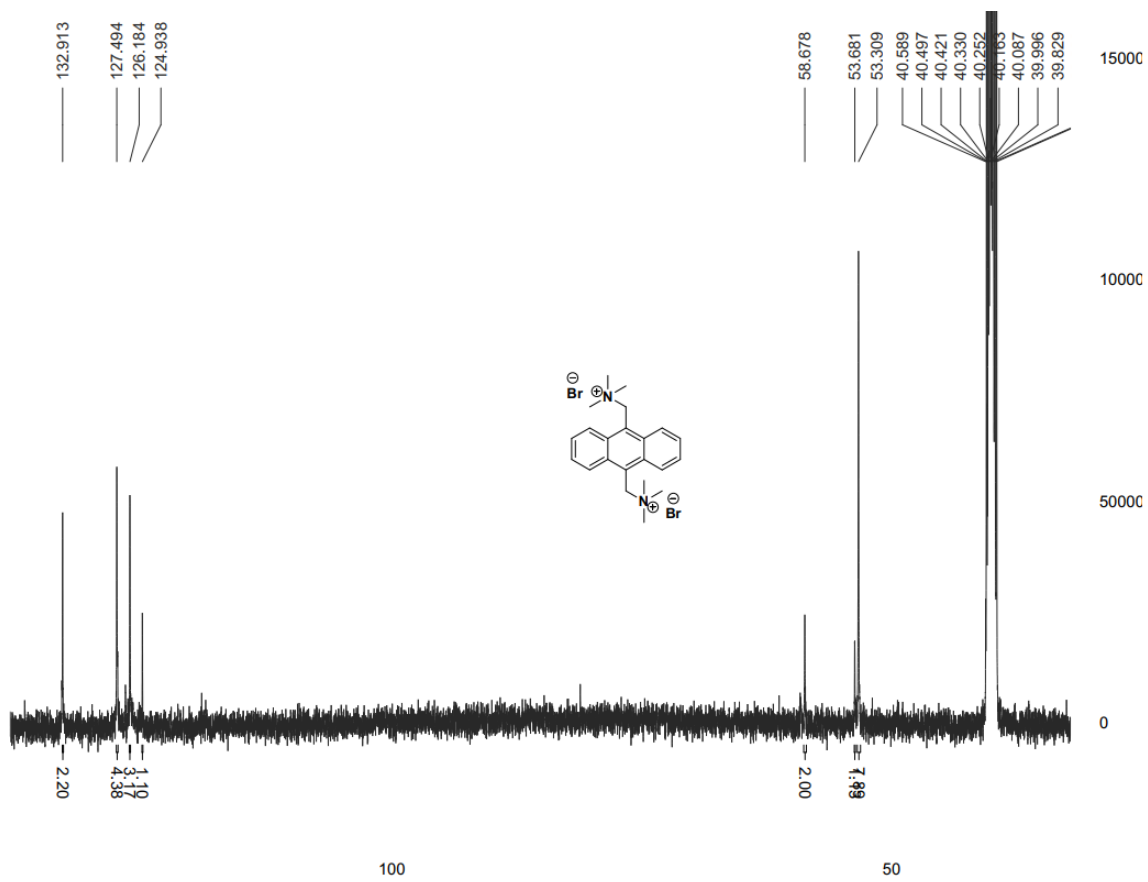
$^1\text{H}$  NMR (500 MHz, CDCl<sub>3</sub>-*d*, DMSO-*d*<sub>6</sub>) spectrum of compound **1a**.



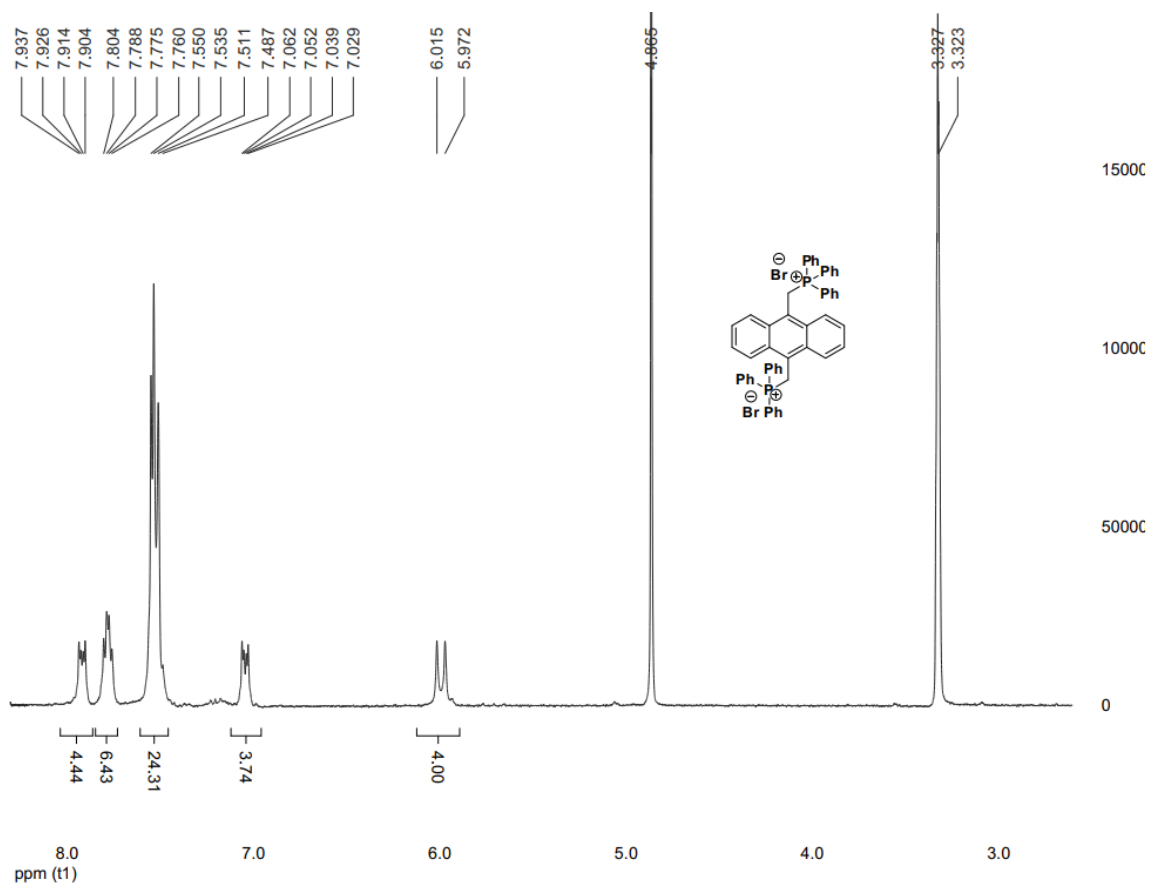
$^{13}\text{C}$  NMR (500 MHz, CDCl<sub>3</sub>-*d*, DMSO-*d*<sub>6</sub>) spectrum of compound **1a**.



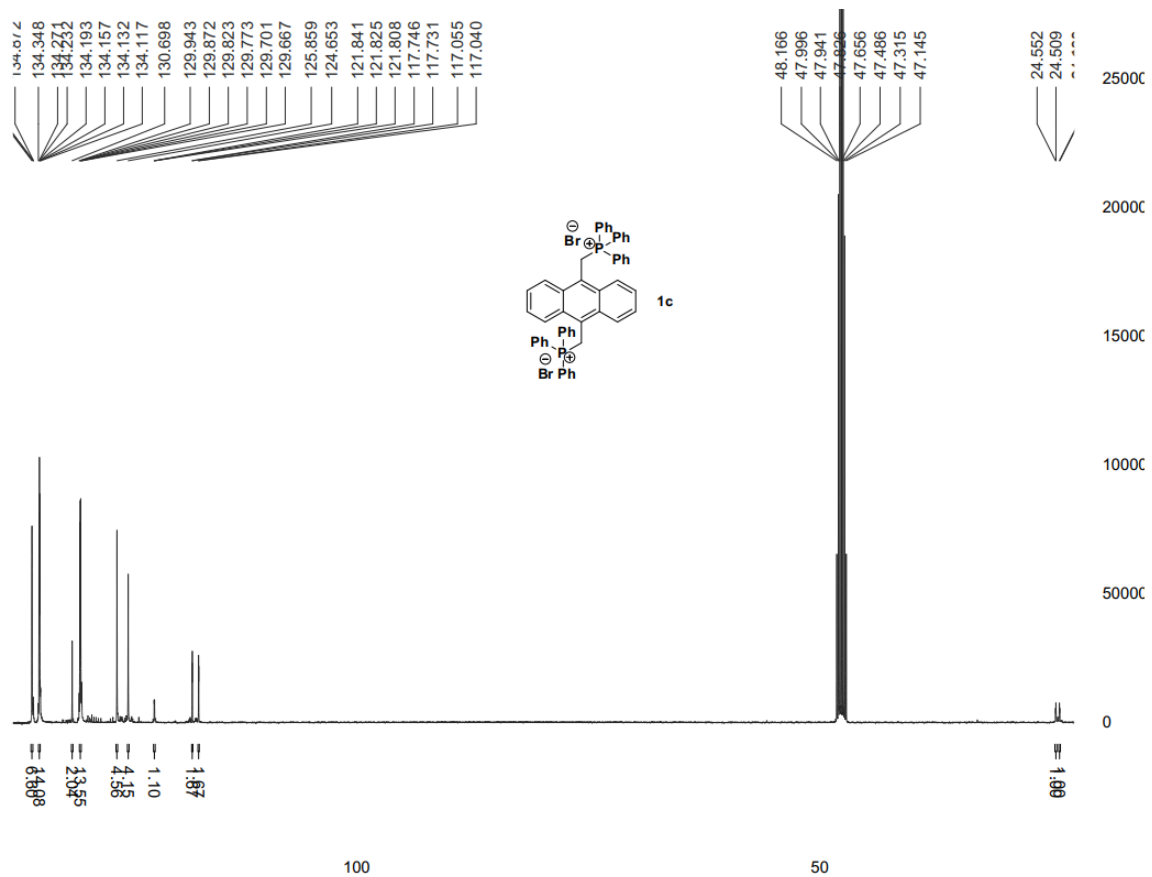
<sup>1</sup>H NMR (500 MHz, DMSO-*d*<sub>6</sub>) spectrum of compound **1b**.



$^{13}\text{C}$  NMR (500 MHz, DMSO-*d*<sub>6</sub>) spectrum of compound **1b**.

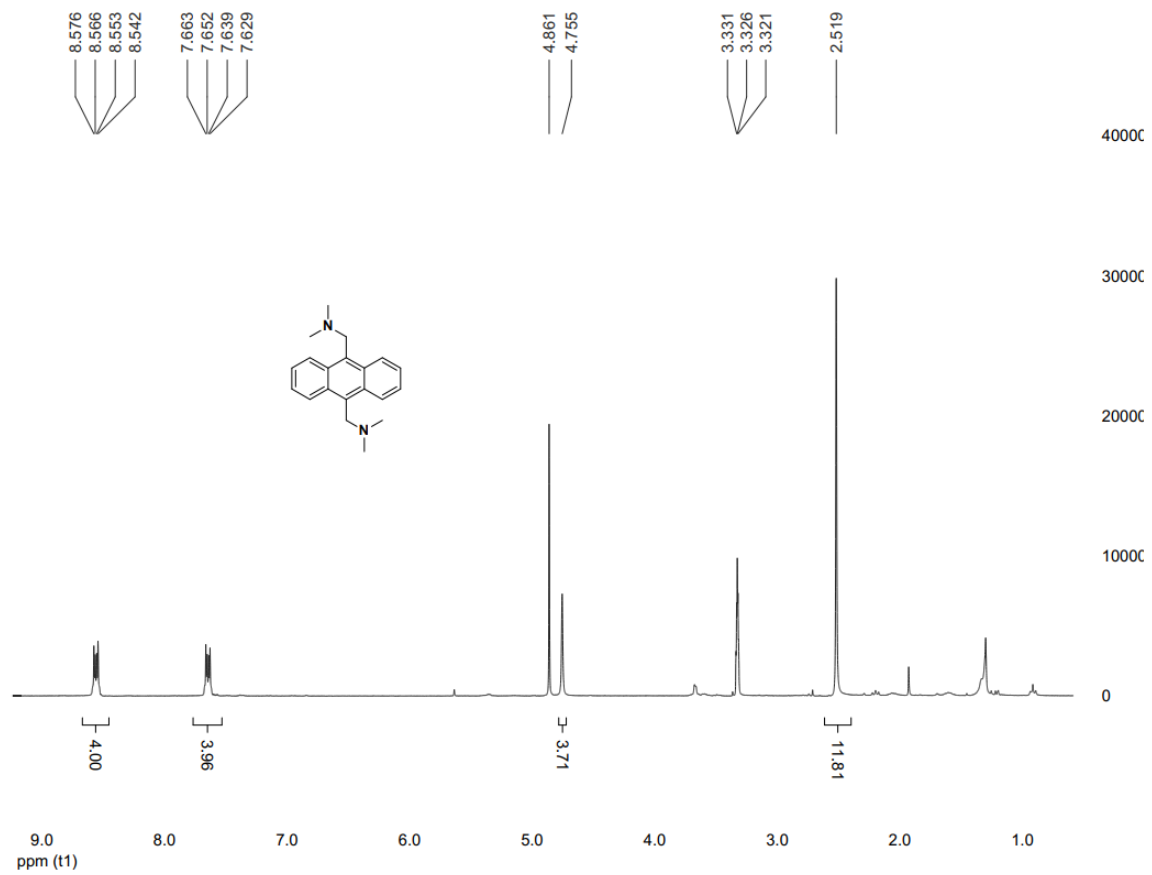


$^1\text{H}$  NMR (500 MHz, MeOD-*d*) spectrum of compound **1c**.

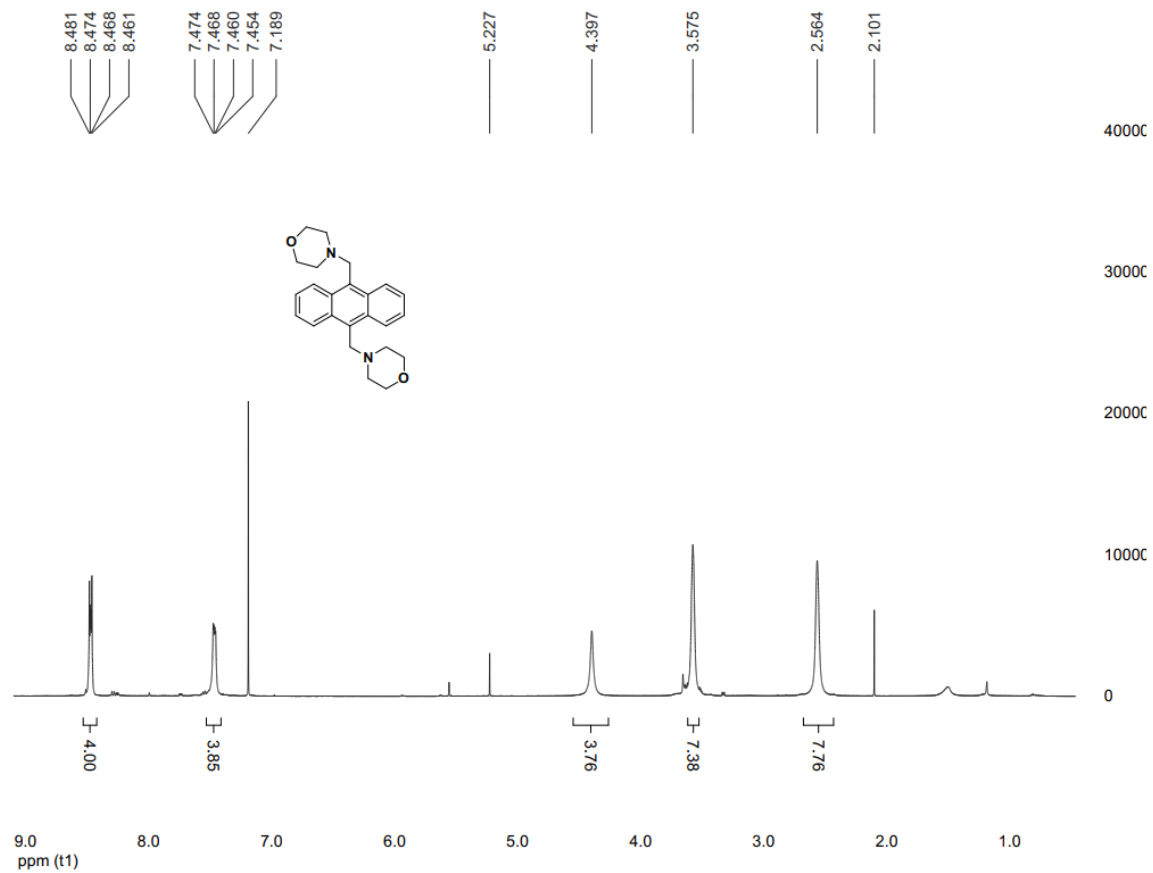


<sup>13</sup>C NMR (500 MHz, MeOD-*d*) spectrum of compound **1c**.

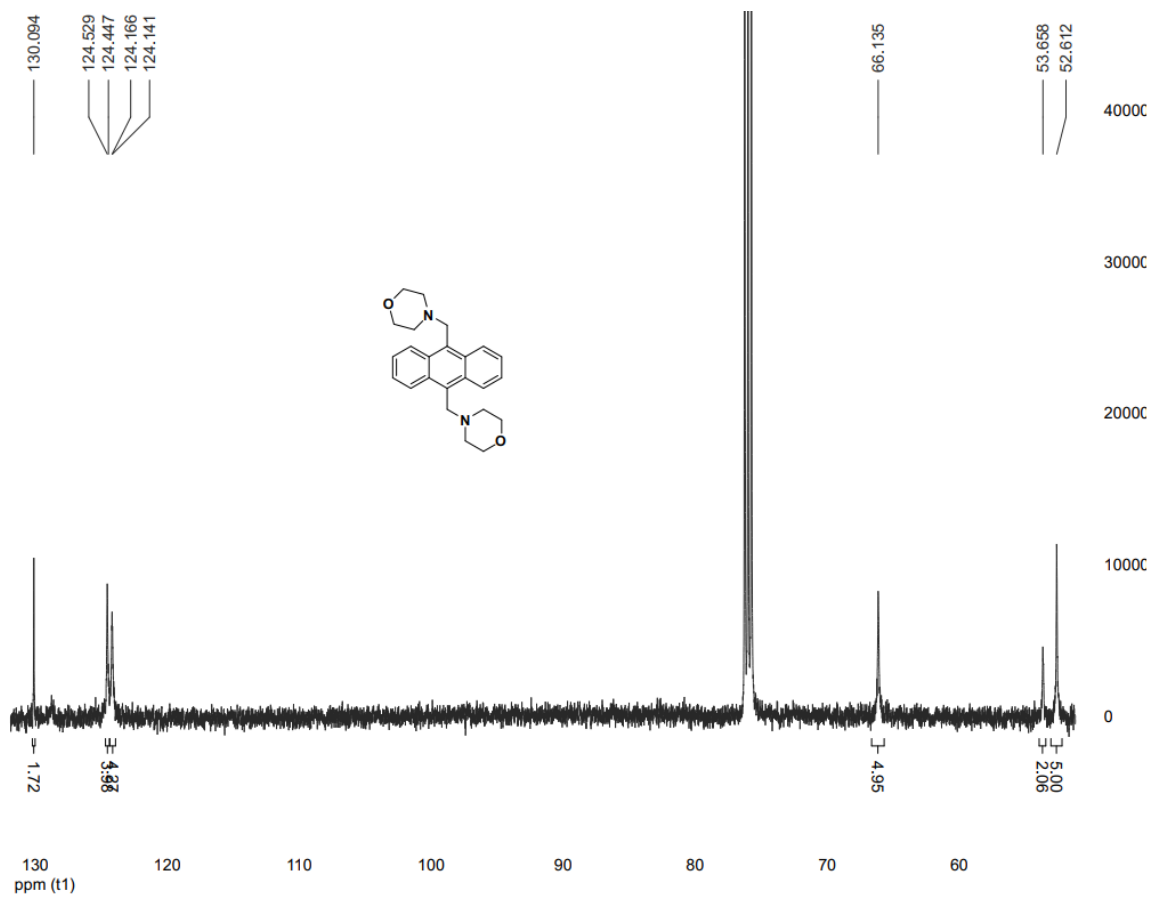




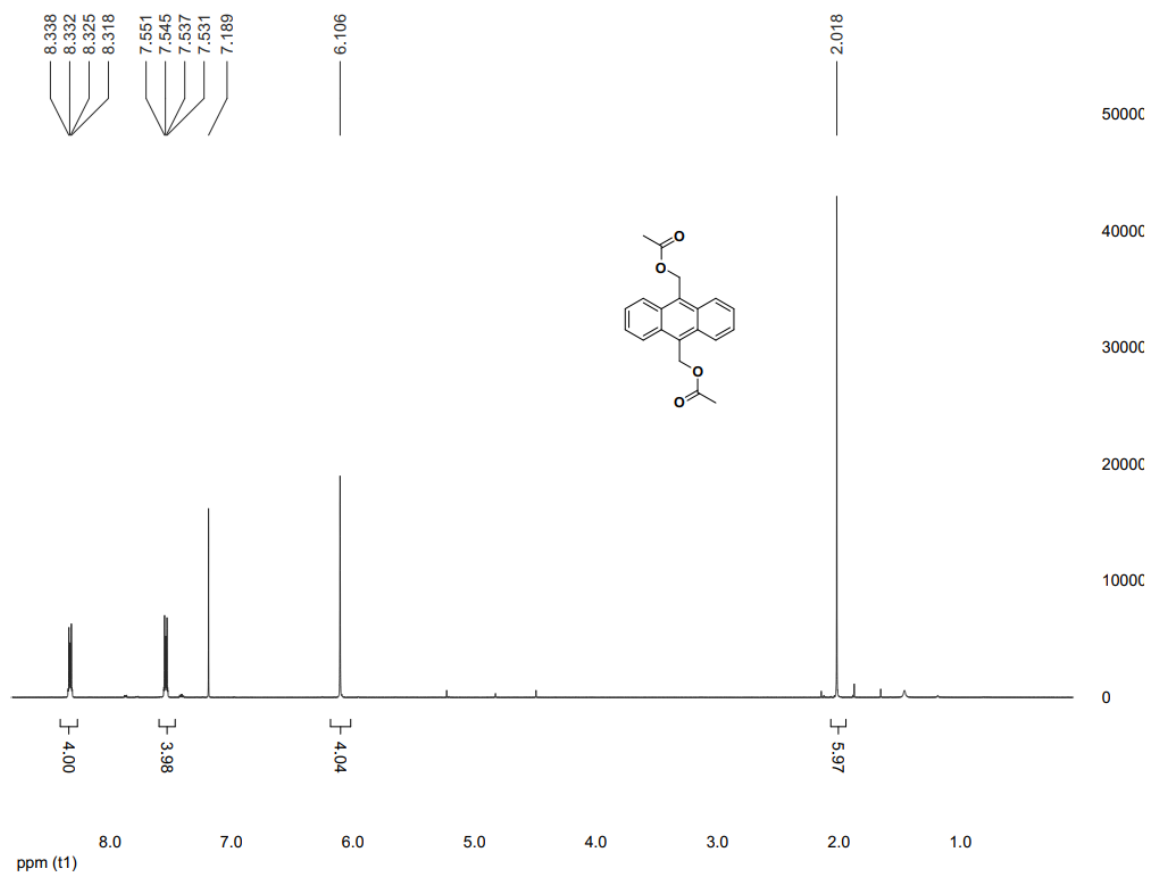
$^1\text{H}$  NMR (500 MHz,) spectrum of compound **1d**.



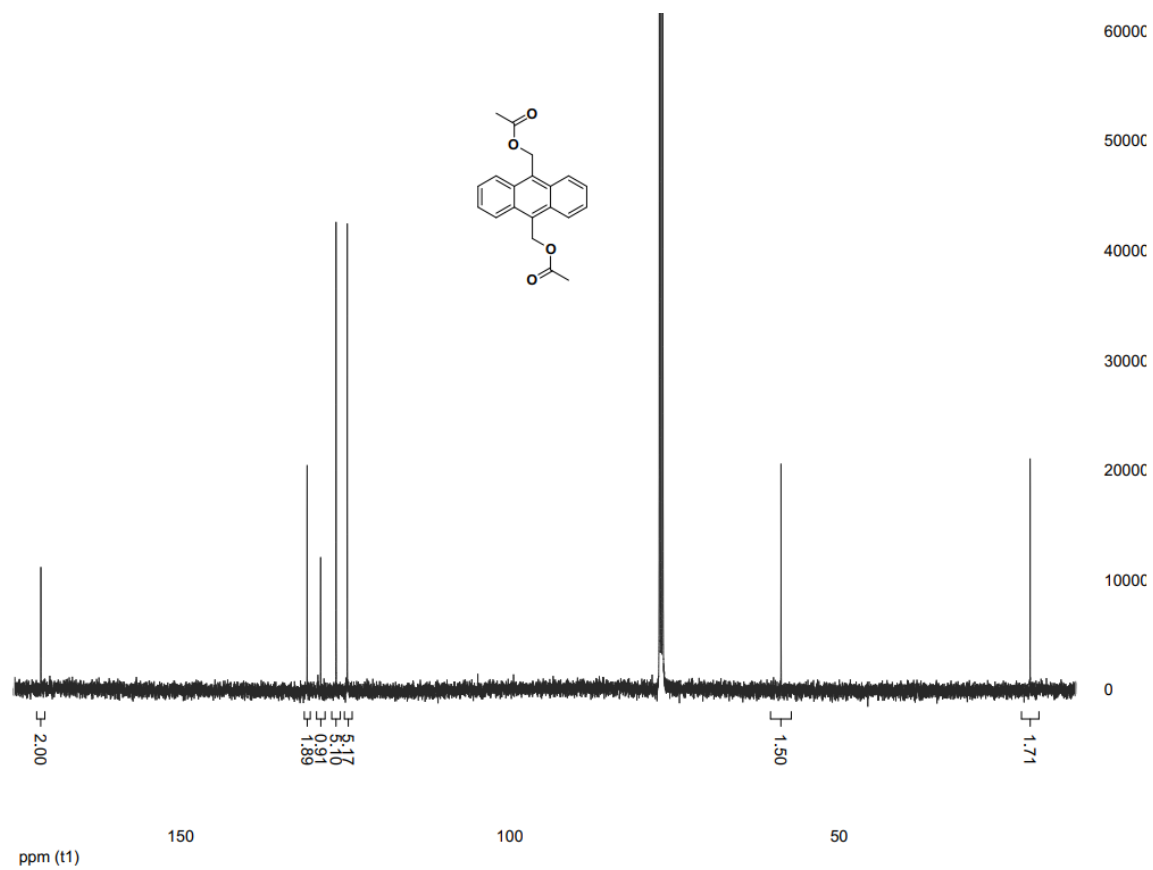
<sup>1</sup>H NMR (500 MHz, DMSO-*d*<sub>6</sub>) spectrum of **1e**.



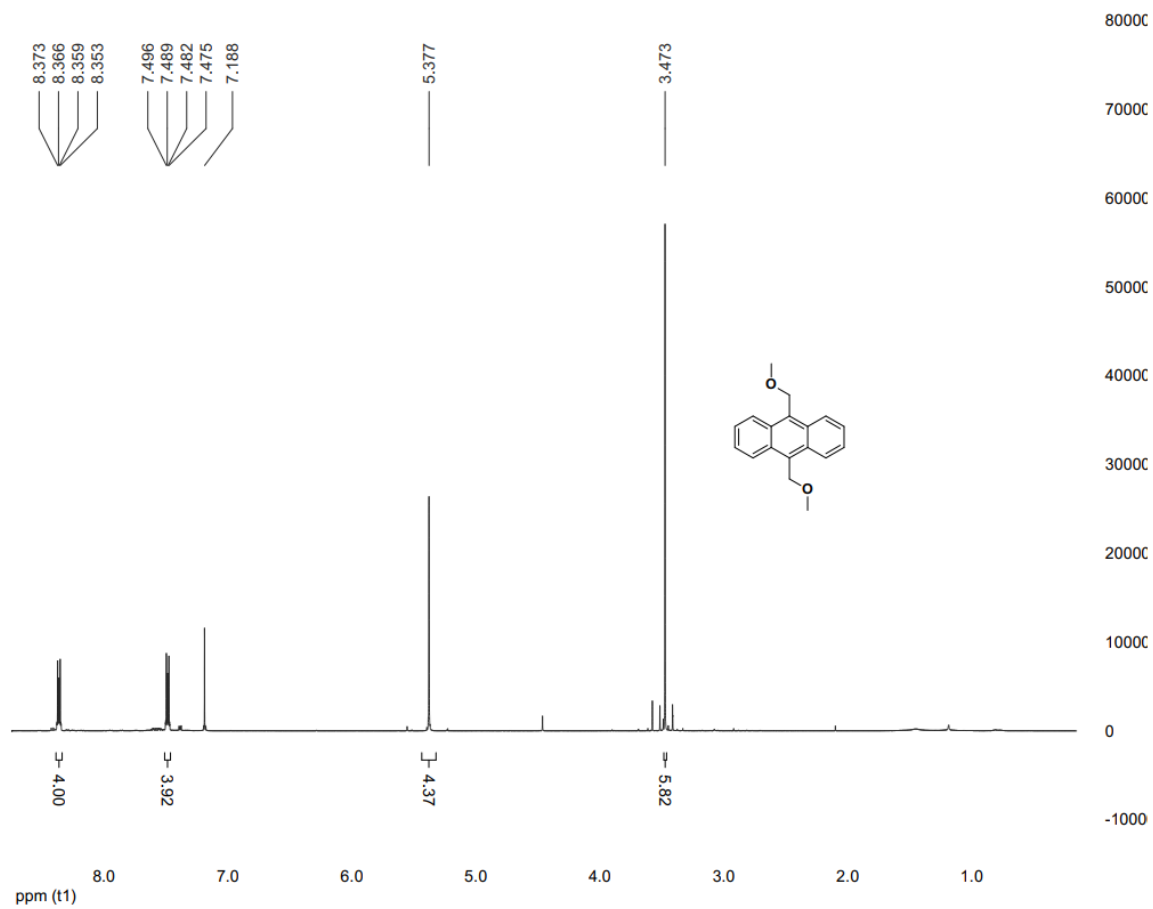
$^{13}\text{C}$  NMR (500 MHz,  $\text{DMSO-}d_6$ ) spectrum of **1e**.



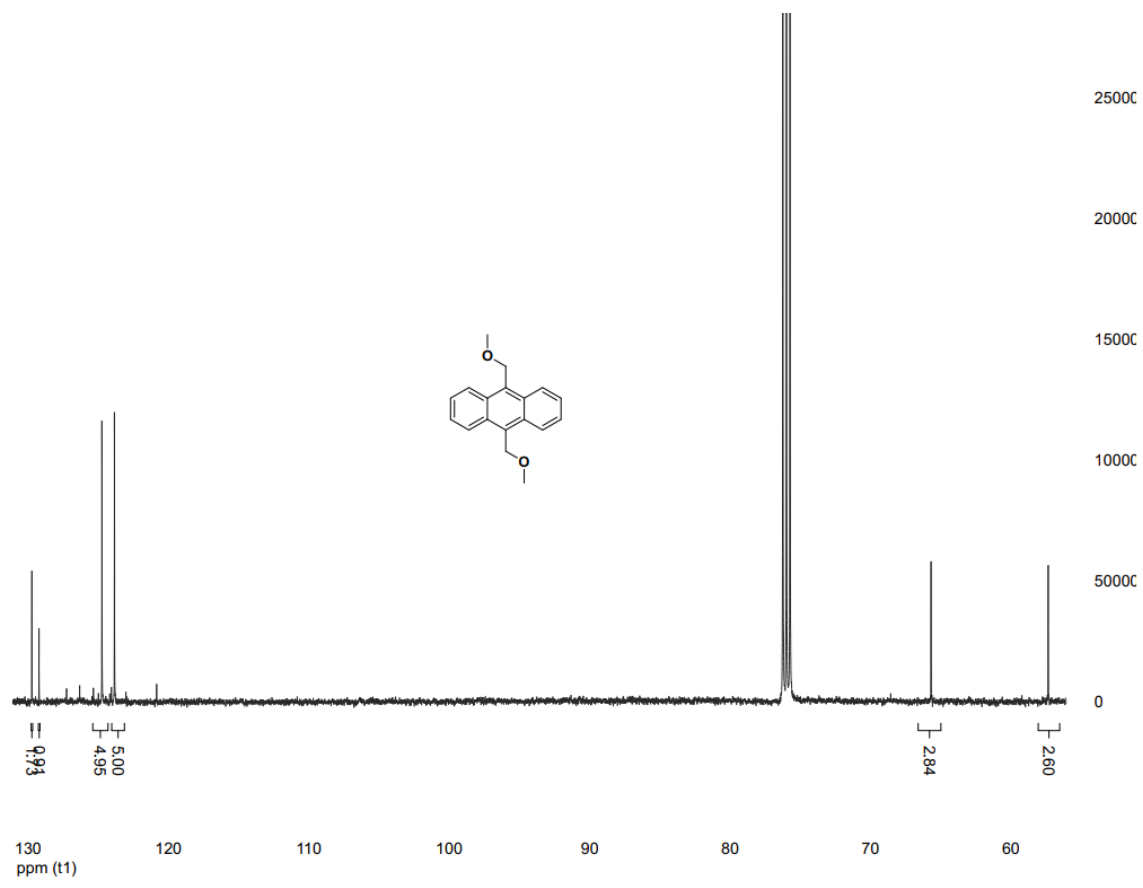
<sup>1</sup>H NMR (500 MHz, CDCl<sub>3</sub>-*d*) spectrum of **1f**



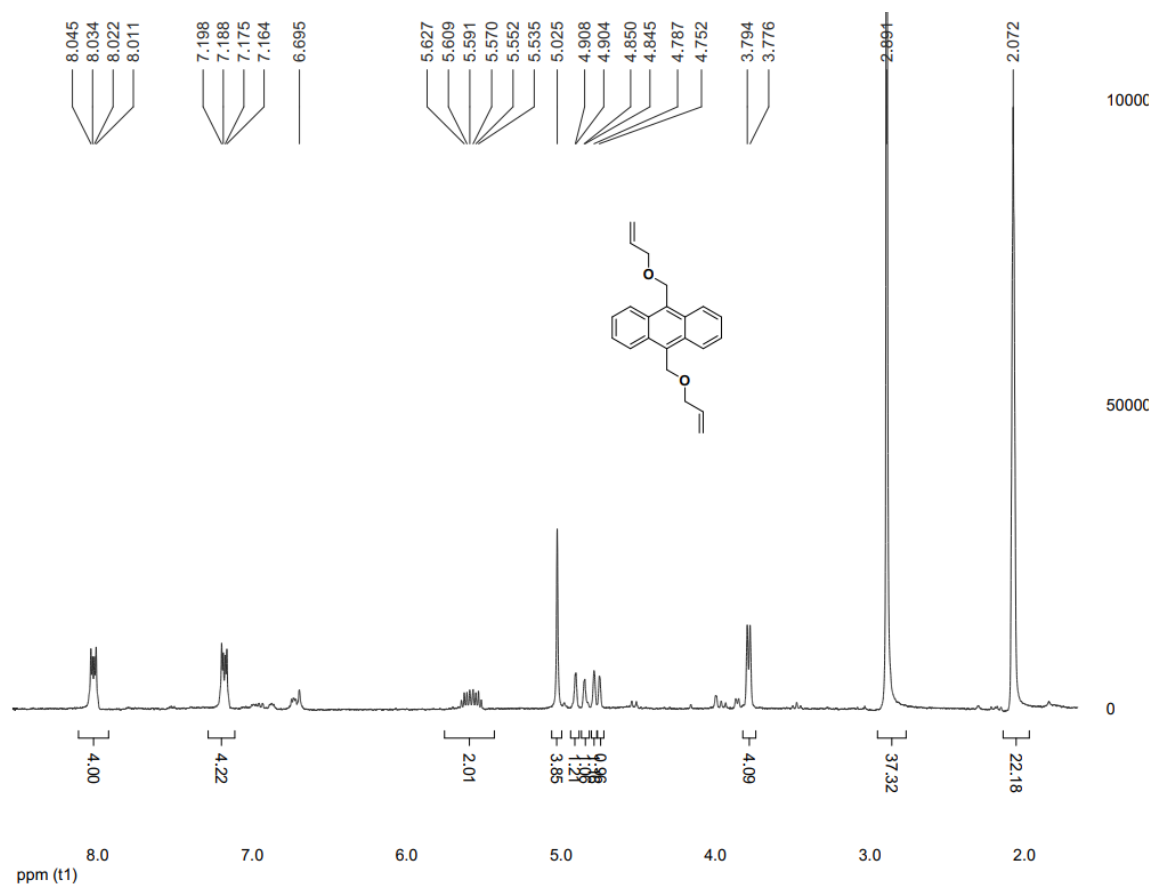
$^{13}\text{C}$  NMR spectrum of (500 MHz,  $\text{CDCl}_3-d$ ) spectrum of **1f**



<sup>1</sup>H NMR (500 MHz, CDCl<sub>3</sub>-d) spectrum of **1h**

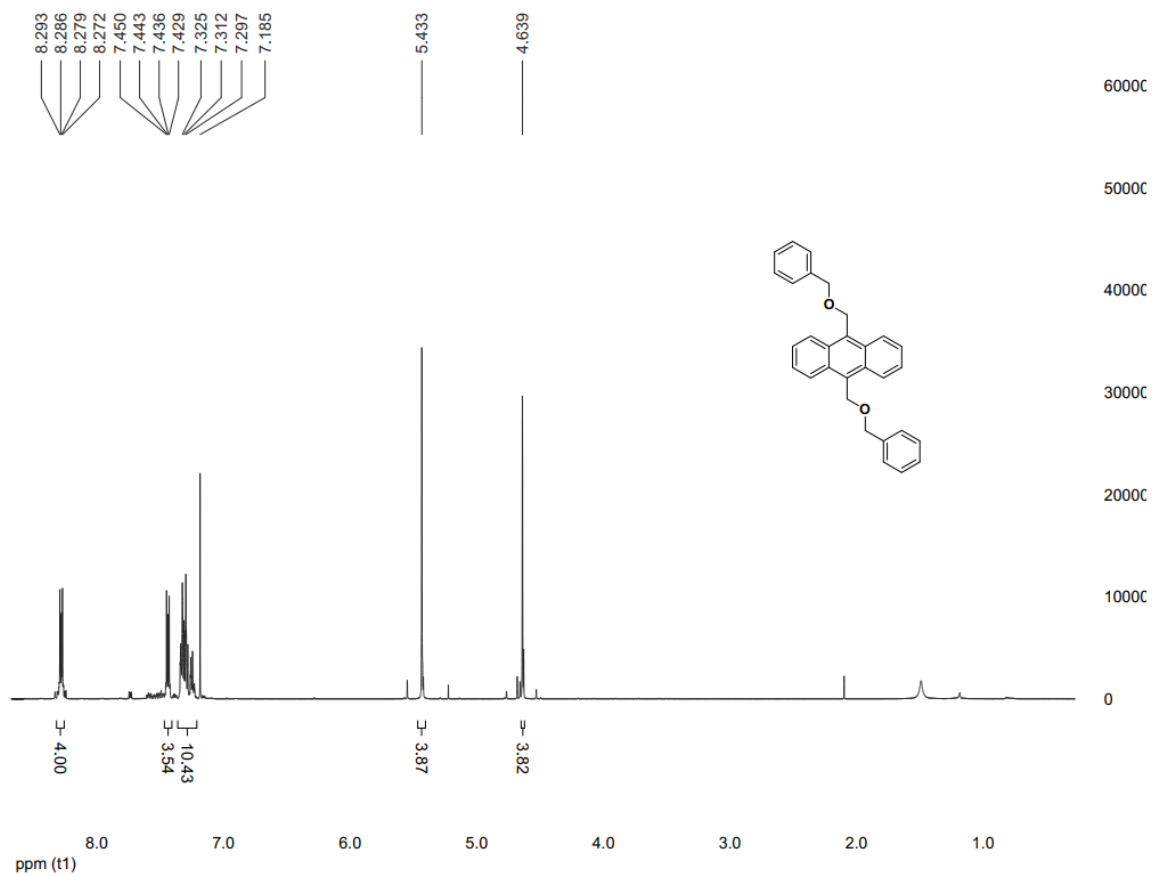


$^{13}\text{C}$  NMR (500 MHz,  $\text{CDCl}_3-d$ ) spectrum of **1h**

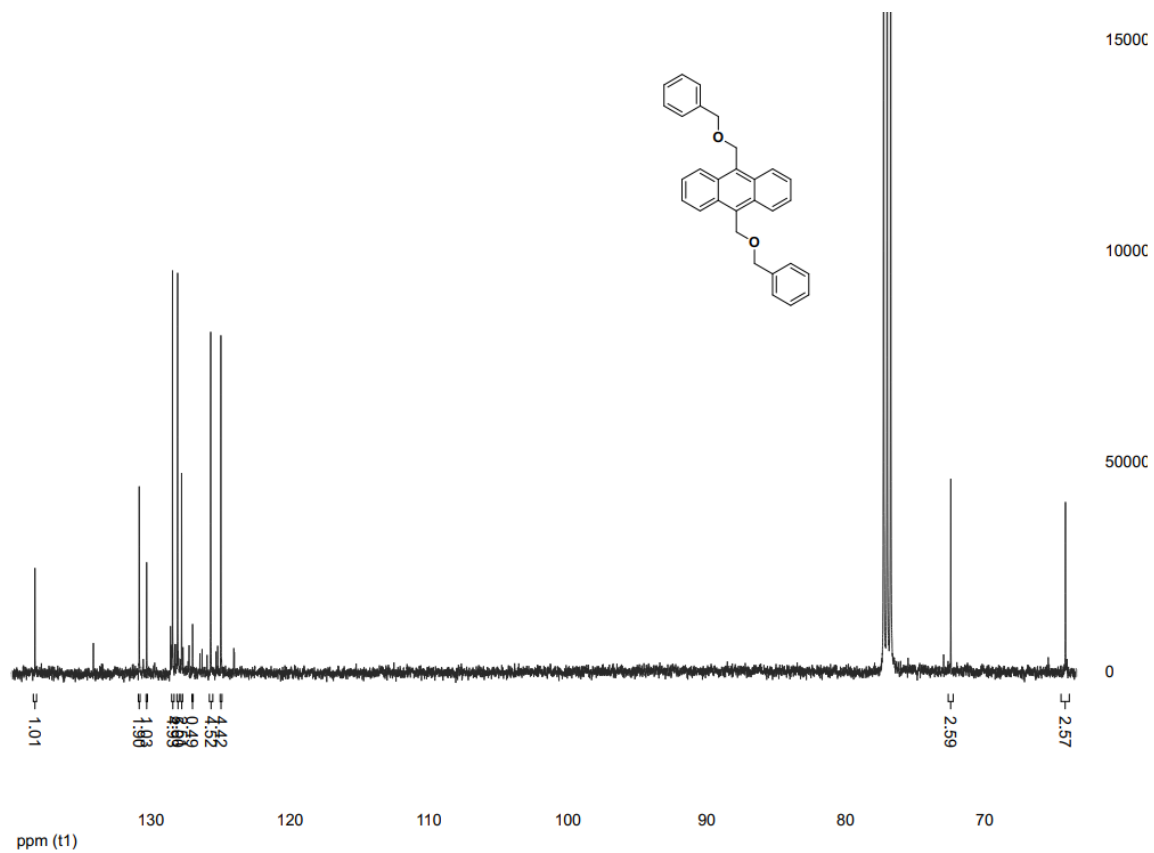


$^1\text{H}$  NMR (500 MHz, ) spectrum of **1i**

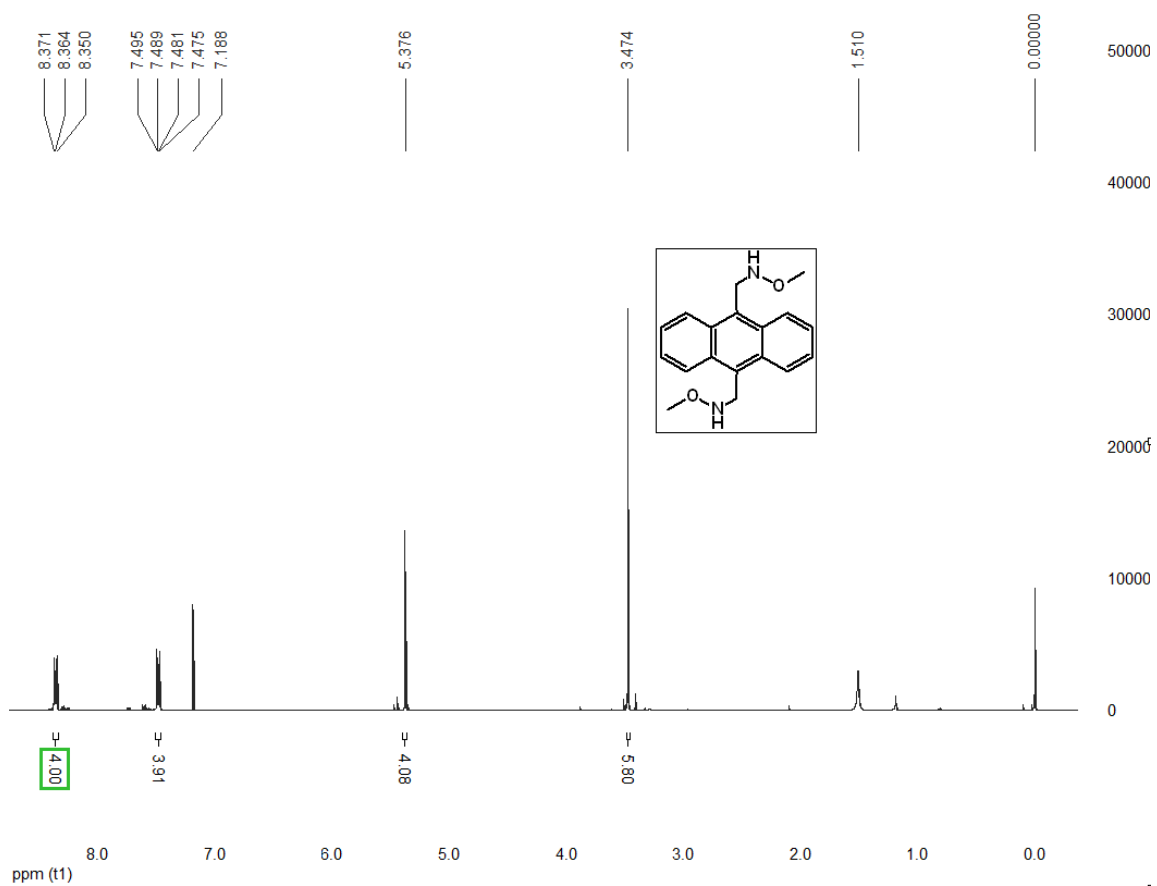




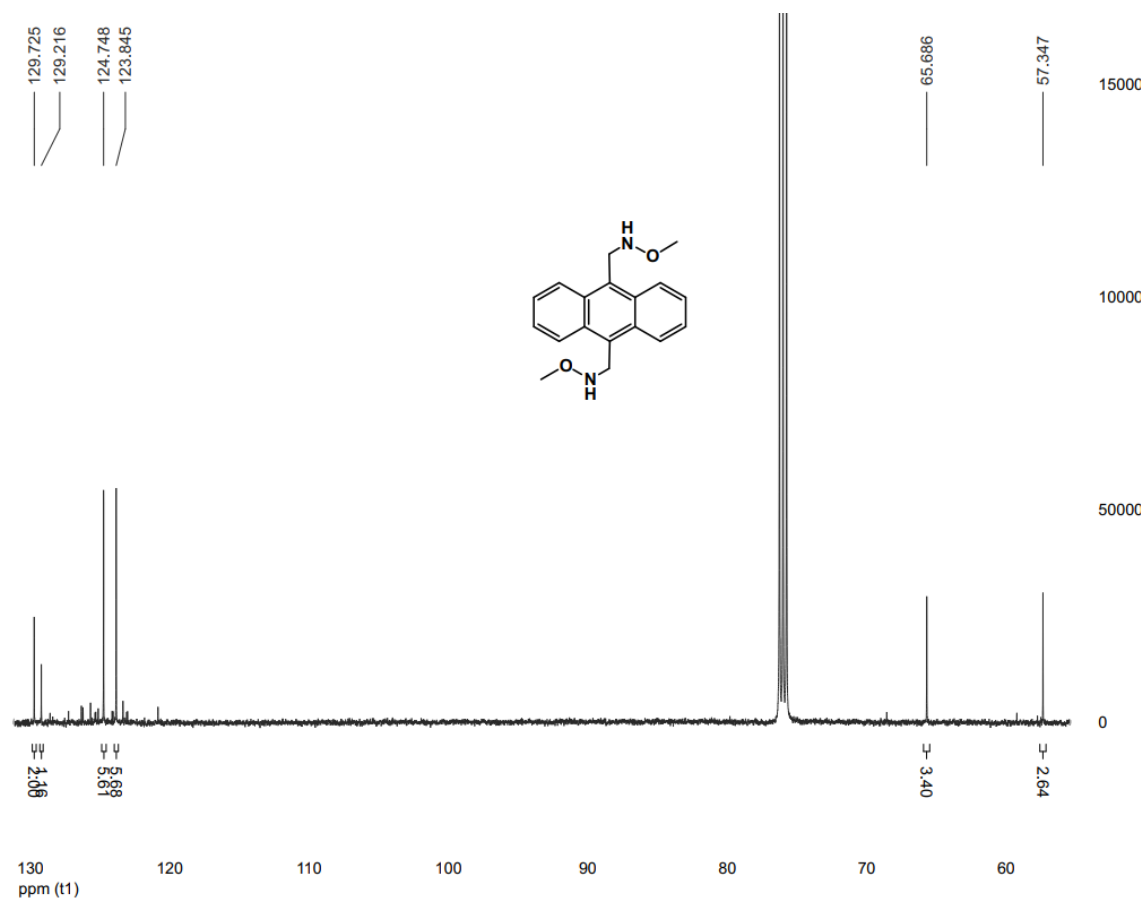
$^1\text{H}$  NMR (500 MHz,  $\text{CDCl}_3-d$ ) spectrum of **1j**



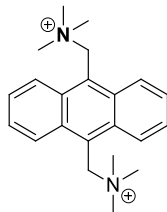
$^{13}\text{C}$  NMR (500 MHz,  $\text{CDCl}_3-d$ ) spectrum of **1j**



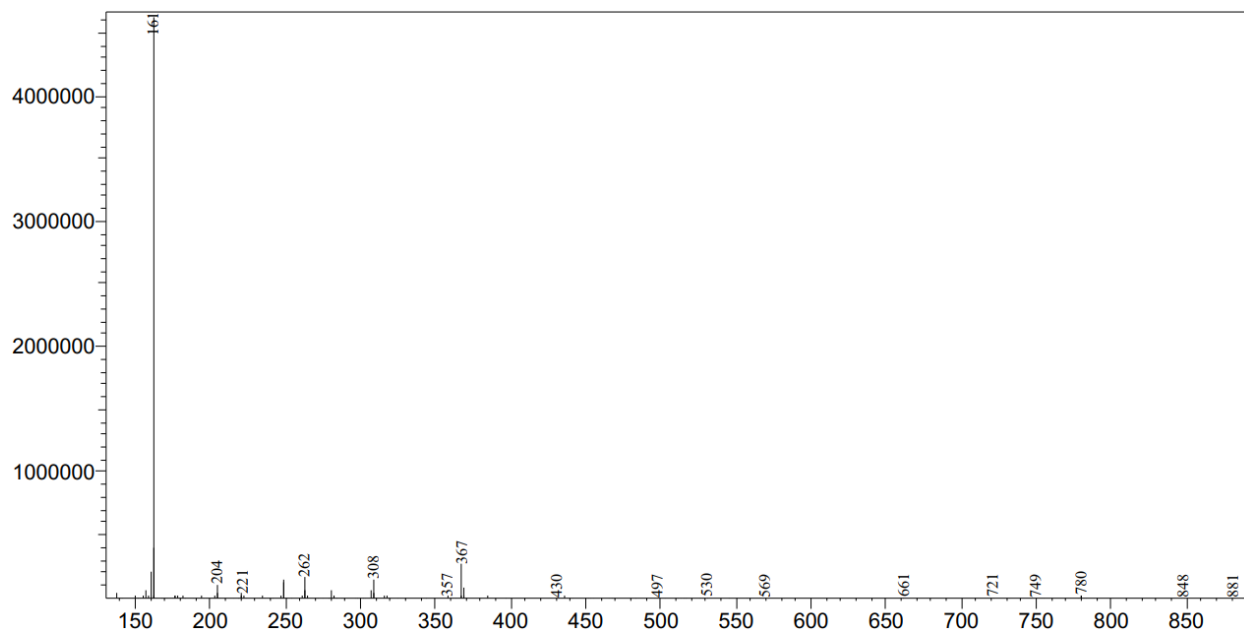
$^1\text{H}$  NMR (500 MHz,  $\text{CDCl}_3$ -*d*) spectrum of adduct **6**.



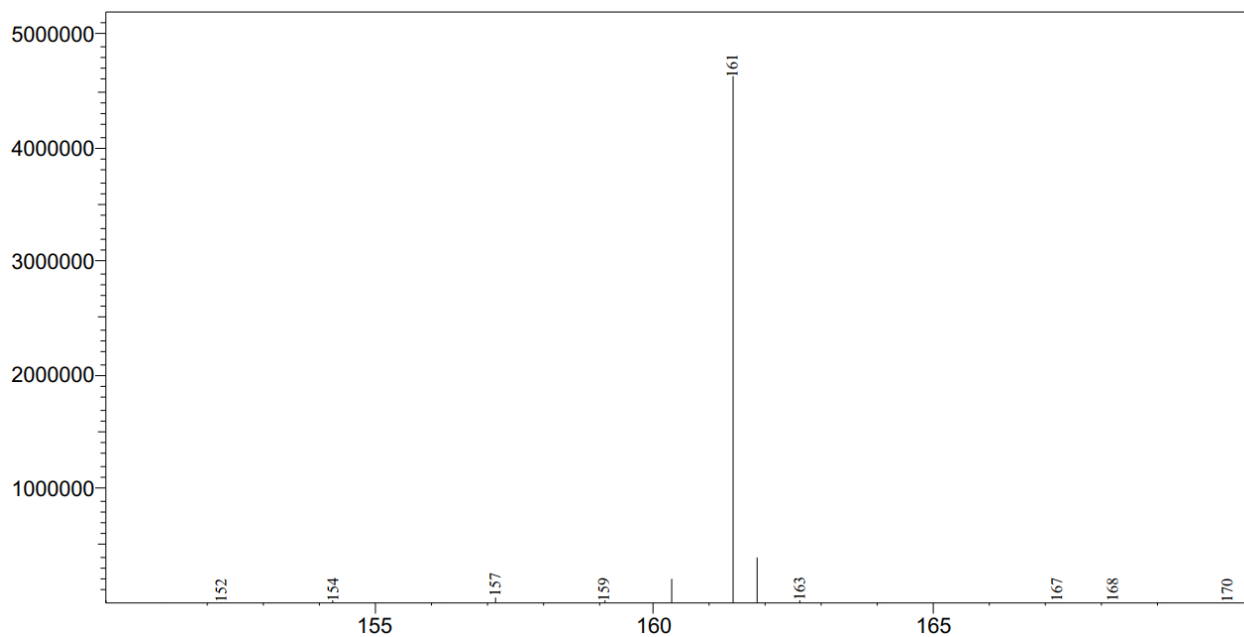
<sup>13</sup>C NMR (500 MHz, CDCl<sub>3</sub>-d) spectrum of compound 6.



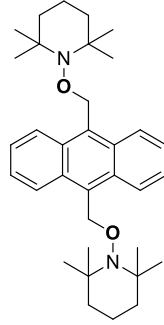
Scan (E+) Ret. Time: [0.157->0.333]-[0.423->5.923] Scan#: [95->201]-[255->3555]



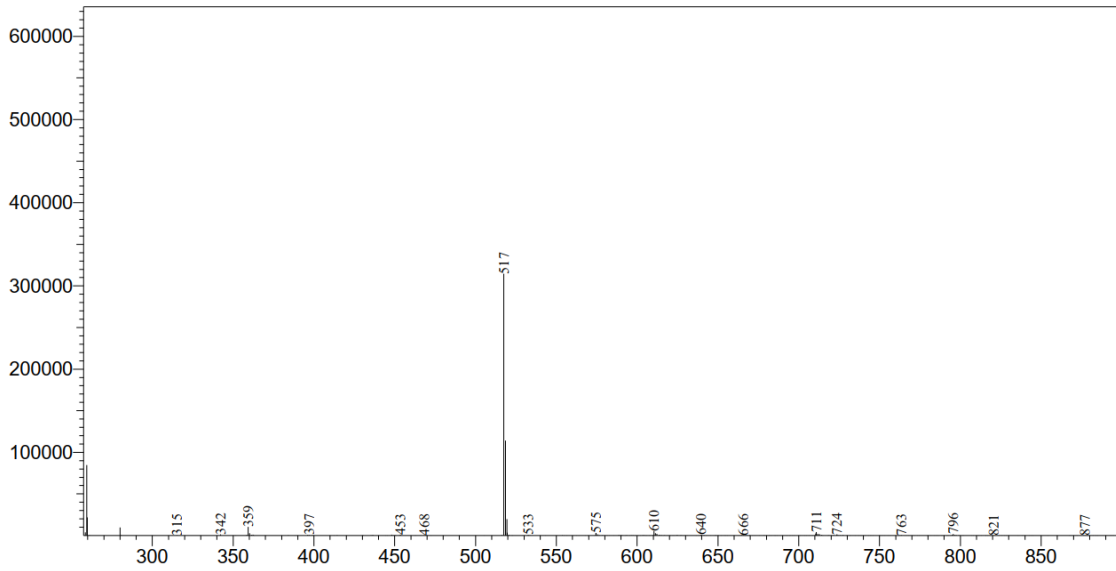
Measured Region for 161 m/z



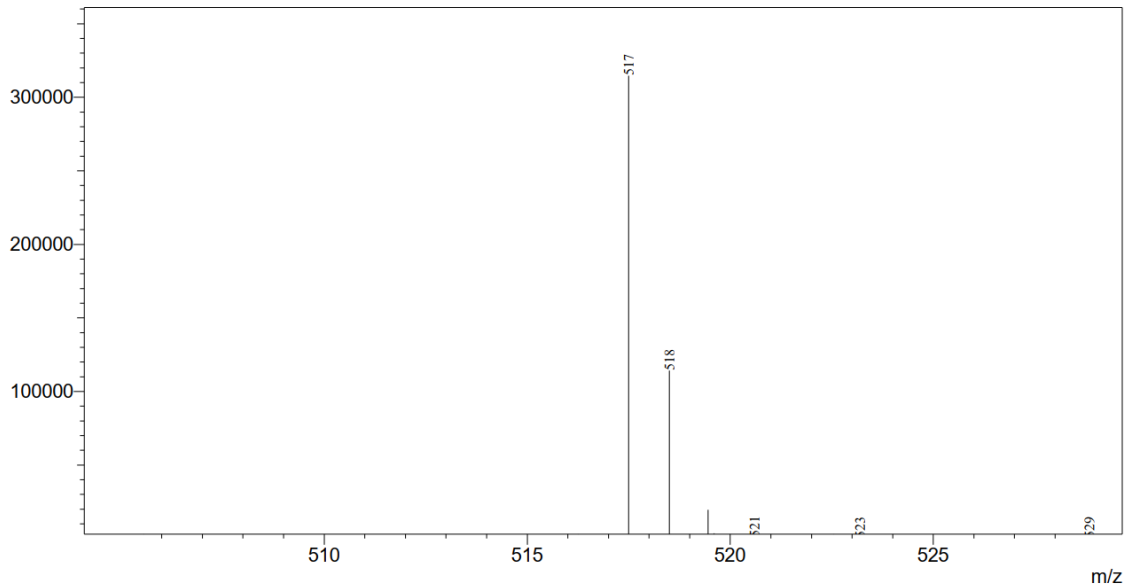
ESI-MS analysis of compound **1b**



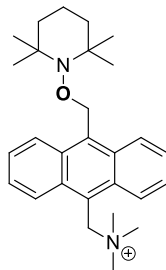
Scan (E+) Ret. Time: [14.807->15.137]-[0.150->14.730] Scan#: [8885->9083]-[91->8839]



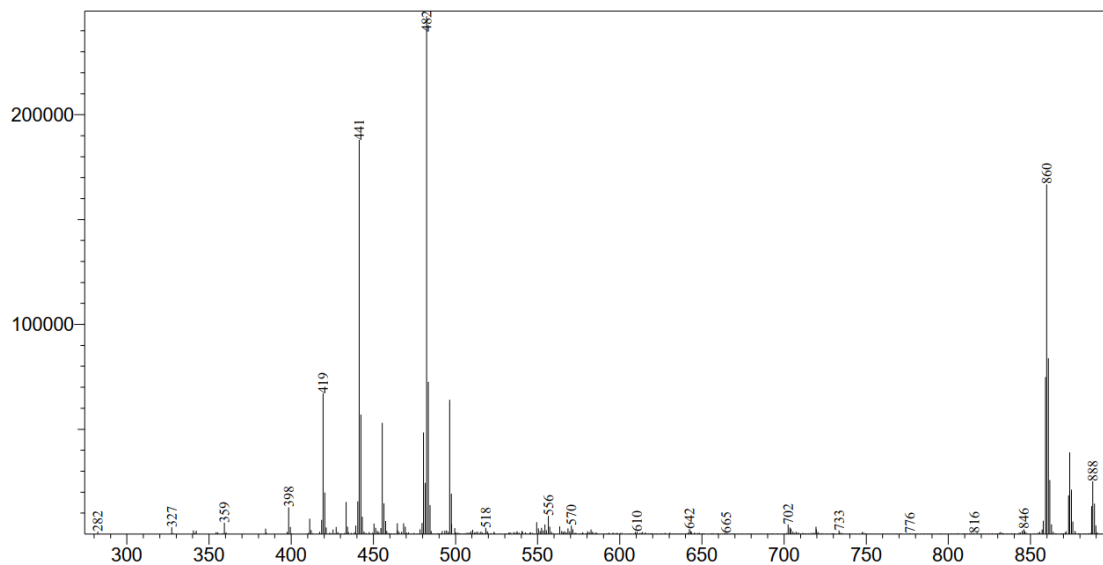
Measured Region for 517 m/z



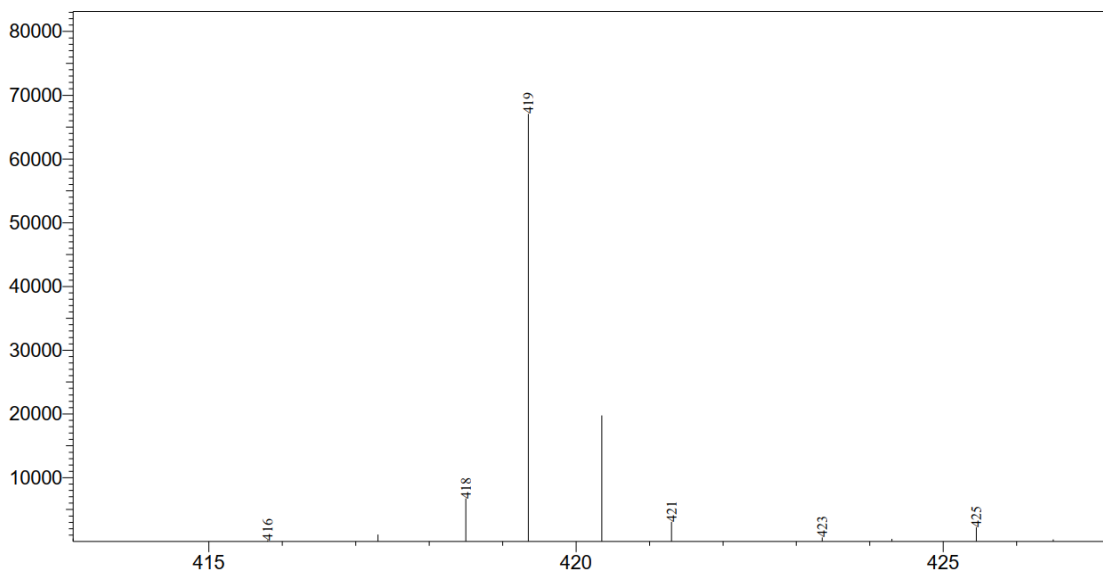
ESI-MS analysis of TEMPO trapping di-adduct with compound **1b**



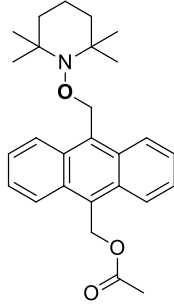
Scan (E+) Ret. Time: [13.467->13.897]-[0.073->13.087 Scan#: [8081->8339]-[45->7853]



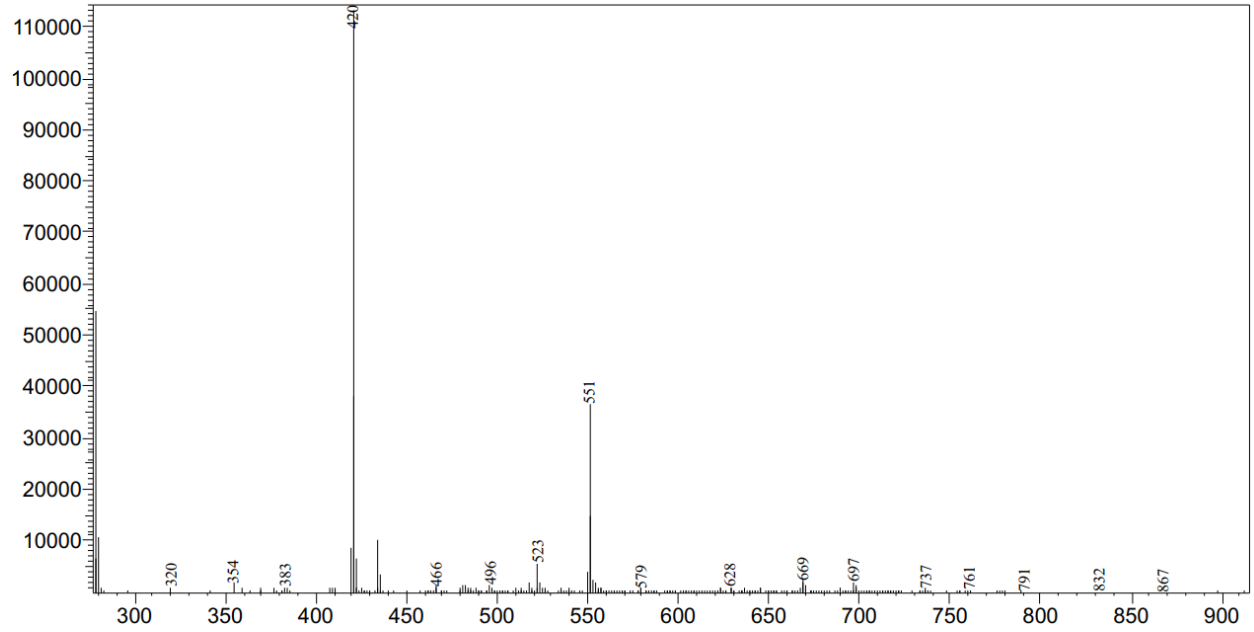
Measured Region for 419.62 m/z



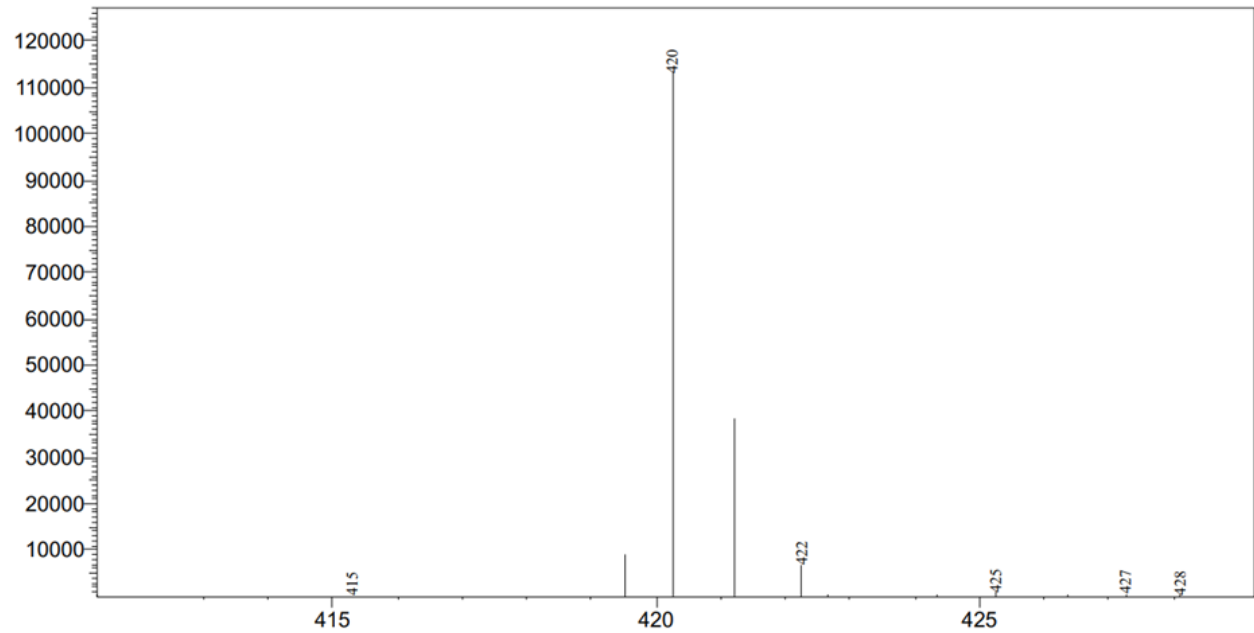
ESI-MS analysis of TEMPO trapping mono-adduct with compound **1b**



Scan (E+) Ret. Time: [13.007->13.553]-[0.200-12.717] Scan#: [7805->8133]-[121->7631]

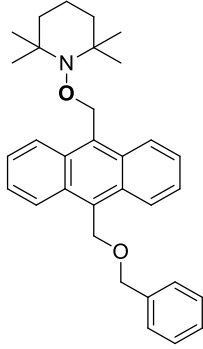


Measured Region for 420.25 m/z

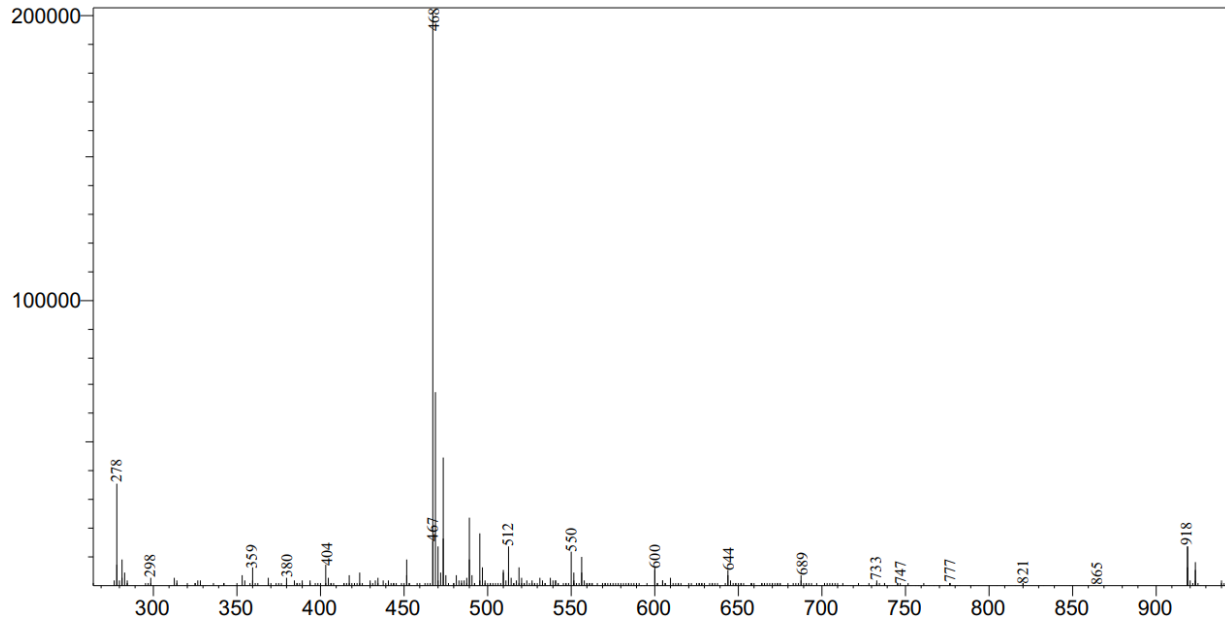


Anthracene Acetate Analogue TEMPO Mono-Adduct Spectrum 11-2-21

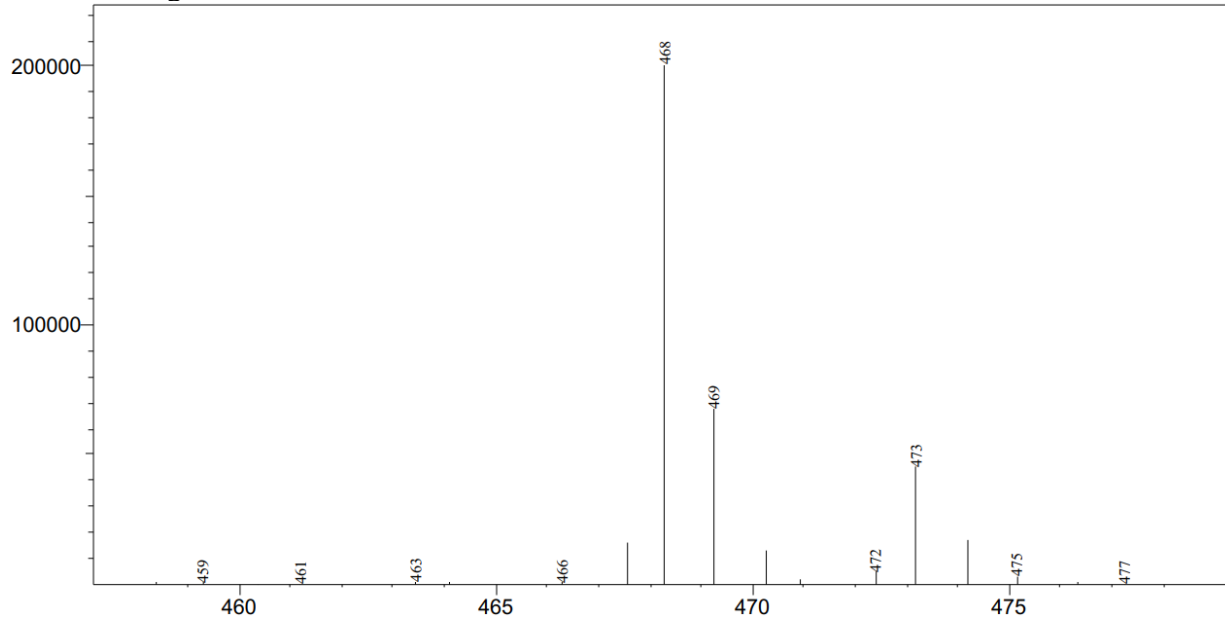




Scan (E+) Ret. Time: [11.853->12.660]-[0.170->11.737] Scan#: [7113->7597]-[103->7043]



Measured Region for 468.28 m/z



Anthracene Benzyloxymethyl Analogue TEMPO Mono-Adduct Spectrum 11-2-21

## Chapter 3. *In vivo* efficacy and selectivity of hydrogen peroxide

### activated DNA interstrand cross-linking agents

#### 3.1 Introduction

##### 3.1.1 Reactive oxygen species as activator for prodrug

There are various types of DNA ICL agents available for the treatment of various types of cancer diseases, such as cisplatin, mitomycin C, nitrogen mustards, psoralens, etc<sup>1,2</sup>. However, these traditional DNA ICL agents lack of selectivity towards cancer cells, which is why they show serious side effects. One way to reduce the toxicity of these agents is to make DNA alkylating agents that can only be activated in tumor specific conditions. Various strategies have been employed for inducing DNA ICL formation under tumor specific condition. Our group focuses on exploiting the differences between tumor and normal cells for developing inducible DNA cross-linking agents that can selectively attack and kill tumor cells.

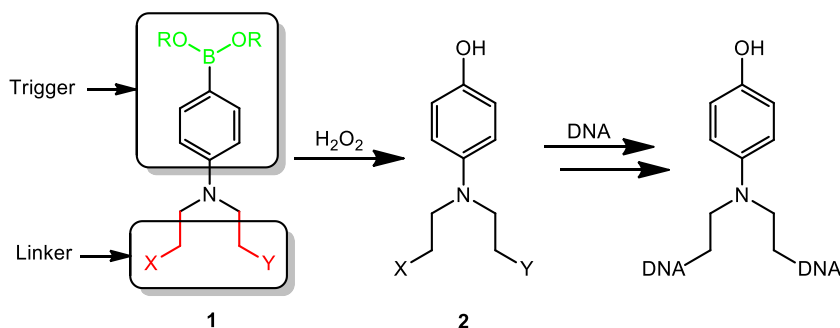
Cancer cells have an intrinsically high rate of metabolic rate. Due to the increased metabolisms and mitochondria malfunction, cancer cells produce high level of reactive oxygen species (ROS) including hydroxyl radical (OH•), superoxide radical anions (O<sub>2</sub><sup>•-</sup>) and hydrogen peroxide<sup>3,4</sup>.

Among different ROS, H<sub>2</sub>O<sub>2</sub> is relatively stable with a longer half-life and higher intracellular concentration. Various ROS probes have been employed to measure the level of endogenous H<sub>2</sub>O<sub>2</sub>, the most stable ROS, which indicated that many different types of human tumor cell lines produced large amounts of H<sub>2</sub>O<sub>2</sub>. It has been assessed that the concentrations of H<sub>2</sub>O<sub>2</sub> can be up to 100-fold higher in cancer cells than in healthy cells<sup>5-9</sup>. To improve the selectivity and specificity of cytotoxic agents against cancer cells, H<sub>2</sub>O<sub>2</sub>-activated anticancer prodrugs have been designed and developed<sup>10,11</sup>. Boronate esters and boronic acids selectively react with H<sub>2</sub>O<sub>2</sub> and thus make an ideal target for the activation of prodrugs<sup>12</sup>. A number of arylboronic acid- and

ester-based prodrugs have been developed, including prodrugs of DNA alkylating agents<sup>13-19</sup>, aminoferrocene analogues<sup>20-22</sup>, estrogen receptor regulators<sup>23,24</sup>, antitumor nitric oxide<sup>25,26</sup>, and theranostic prodrugs<sup>27,28</sup>. Many of these prodrugs showed *in vitro* cytotoxicity and selectivity toward cancer cells. However, only a few reports have discussed *in vivo* efficacy and selectivity<sup>16,20,28</sup>.

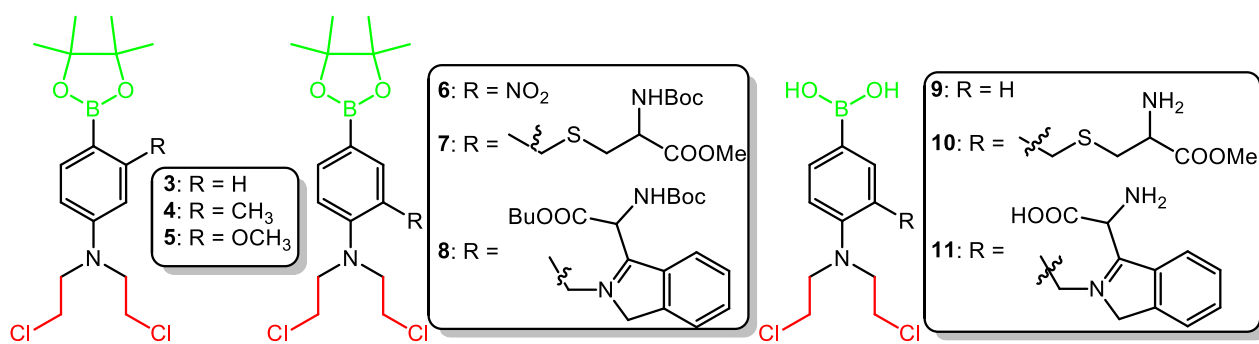
### 3.1.2 H<sub>2</sub>O<sub>2</sub>-Activated Nitrogen Mustard Precursors

Recently, our group reported two classes of H<sub>2</sub>O<sub>2</sub>-activated DNA cross-linking agents, including quinone methide precursors<sup>13,14,19</sup> and nitrogen mustard analogues<sup>15-19</sup>, that contained a boronic acid or boronate ester as a ROS-responsive trigger unit (Scheme 3-1). The electron-withdrawing property of boronates mask the reactivity of the DNA alkylating functional group while allow its selective activation by H<sub>2</sub>O<sub>2</sub> (**1** → **2**) (Scheme 3-1). These prodrugs can be activated in the presence of H<sub>2</sub>O<sub>2</sub> to release nitrogen mustards that directly cross-link DNA at the dG/dC sites. DNA ICL assay indicated that these novel prodrugs showed good activity and selectivity toward H<sub>2</sub>O<sub>2</sub>. Furthermore, they selectively inhibit cancer cell growth, but normal cells were less affected. These results demonstrated that the arylboronates can effectively mask the cytotoxicity of nitrogen mustards while allow the activation by H<sub>2</sub>O<sub>2</sub><sup>18</sup>.



**Scheme 3-1.** Activation of H<sub>2</sub>O<sub>2</sub>-triggered alkylating agents.

Previously, the DNA cross-linking activities and selectivity's of **3–11** were investigated using a 49-mer DNA duplex, that contained one consensus sequence for nitrogen mustards. ICL formation and yields were analyzed via denaturing polyacrylamide-gel electrophoresis (PAGE) with phosphor image analysis (Image Quant 5.2). Most of the compounds (**3–6** and **9–11**, 1.0 mM) induced very few DNA ICLs (1.5–15%) in the absence of H<sub>2</sub>O<sub>2</sub> (1.5 mM), whereas addition of H<sub>2</sub>O<sub>2</sub> greatly enhanced their cross-linking yields<sup>16</sup> (up to 65%). It was found that the compounds with weak donating groups, such as **4**, had increased selectivity (defined as the ratio of the DNA-ICL yield with H<sub>2</sub>O<sub>2</sub> to that without H<sub>2</sub>O<sub>2</sub>). On the other hand, compounds with strong donating groups (**5**) or strong withdrawing groups (**6**) had decreased selectivity. Thus it was concluded that a strong donating group offsets the deactivating effect of the boronic acid or ester group, leading to an increased cross-linking yield (8% for **5**) in the absence of H<sub>2</sub>O<sub>2</sub>. A withdrawing group, e.g. NO<sub>2</sub> suppresses the reactivity of the liberated compound, causing low enhancement of the H<sub>2</sub>O<sub>2</sub>-induced cross-linking efficiency (9% for **6**). These results showed that the electronic effects could tune the cross-linking ability and selectivity of the ROS-inducible DNA alkylating agents.



**Scheme 3-2.** Chemical structures of modified aromatic nitrogen mustards **3–11**.

Wenbing et al. also investigated compounds with amino acid side chains (**7**, **8**, **10**, and **11**). Surprisingly, very low DNA-ICL yields (less than 5%) were reported for **7** and **8**, both with and

without H<sub>2</sub>O<sub>2</sub>. The low DNA-cross-linking capability is thought to be caused by the steric hindrance of the Boc group preventing **7** and **8** from effectively interacting with the major or minor grooves of DNA. Further investigation showed that removal of the Boc group led to compounds (**10** or **11**) with greatly enhanced DNA-ICL formation. Thus, in addition to electronic properties, steric hindrance significantly affects the ICL formation of these compounds. These results further indicated that a strong electron-donating group or an amino acid side chain (**5**, **10**, and **11**) slightly increased the DNA-ICL yield in the absence of H<sub>2</sub>O<sub>2</sub>.

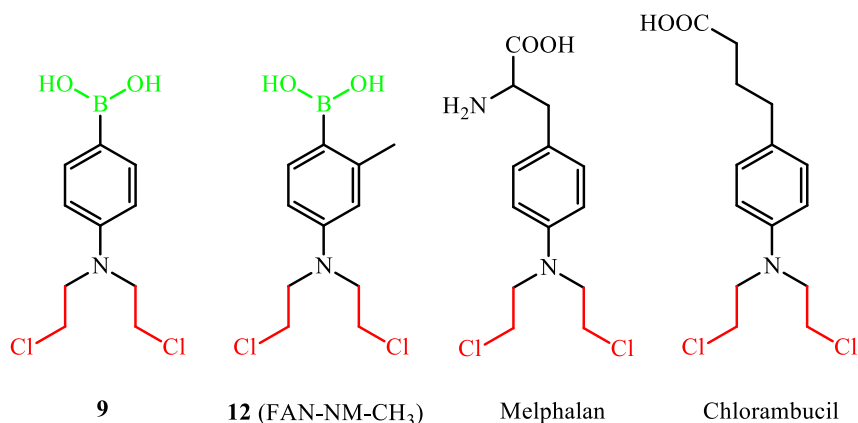
Table 3-1 summarizes the biophysical properties, selectivity, and cytotoxicity of all various modified nitrogen mustards **3-11**.

| Compound  | R                   | % ICL yield | Selectivity | Cytotoxicity in Human Cancer Cell Line | GI <sub>50</sub> |
|-----------|---------------------|-------------|-------------|--|------------------|
| <b>3</b>  | n/a                 | High        | High        | Significant growth inhibition          | Highest          |
| <b>4</b>  | Weak donating       | High        | High        | Significant growth inhibition          | <3               |
| <b>5</b>  | Strong donating     | medium      | medium      | Significant growth inhibition          | n/a              |
| <b>6</b>  | Strong withdrawing  | Low         | Low         | No cytotoxicity                        | n/a              |
| <b>7</b>  | a.a. with BOC group | Low         | Low         | No cytotoxicity                        | n/a              |
| <b>8</b>  | a.a. with BOC group | Low         | Low         | No cytotoxicity                        | n/a              |
| <b>9</b>  | n/a                 | High        | High        | Significant growth inhibition          | <4               |
| <b>10</b> | a.a. BOC free       | medium      | medium      | Most Significant growth inhibition     | Lowest           |
| <b>11</b> | a.a. BOC free       | medium      | medium      | No cytotoxicity                        | n/a              |

**Table 3-1.** Biophysical properties of **3-9** compared with cytotoxicity and GI<sub>50</sub>.

All previous observations showed that H<sub>2</sub>O<sub>2</sub>-activated DNA cross-linking agents are selective anticancer prodrug candidates for triple negative breast cancer (TNBC) treatment, although a detailed mechanism for the ROS activation of these prodrugs in cancer cells is yet to be determined. It was reported that TNBC cells exhibit intrinsically higher H<sub>2</sub>O<sub>2</sub> levels in association

with the downregulation and decreased bioactivity of catalase<sup>9</sup>. Generally, human breast epithelial cells produce very little ROS and regulate their metabolism normally. On the other hand, the production of H<sub>2</sub>O<sub>2</sub> regulates the growth of aggressive breast cancer cells. Since aromatic nitrogen mustard **9** (CWB-20145) and its methyl analogue **12** (FAN-NM-CH<sub>3</sub>) exhibited the best biological and physicochemical properties, we investigated their pharmacokinetics and in vivo therapeutic efficacy and selectivity using a cell line-derived xenograft model of TNBC.



**Scheme 3-3.** Structure of antitumor agent **12** with control drug Chlorambucil and Melphalan.

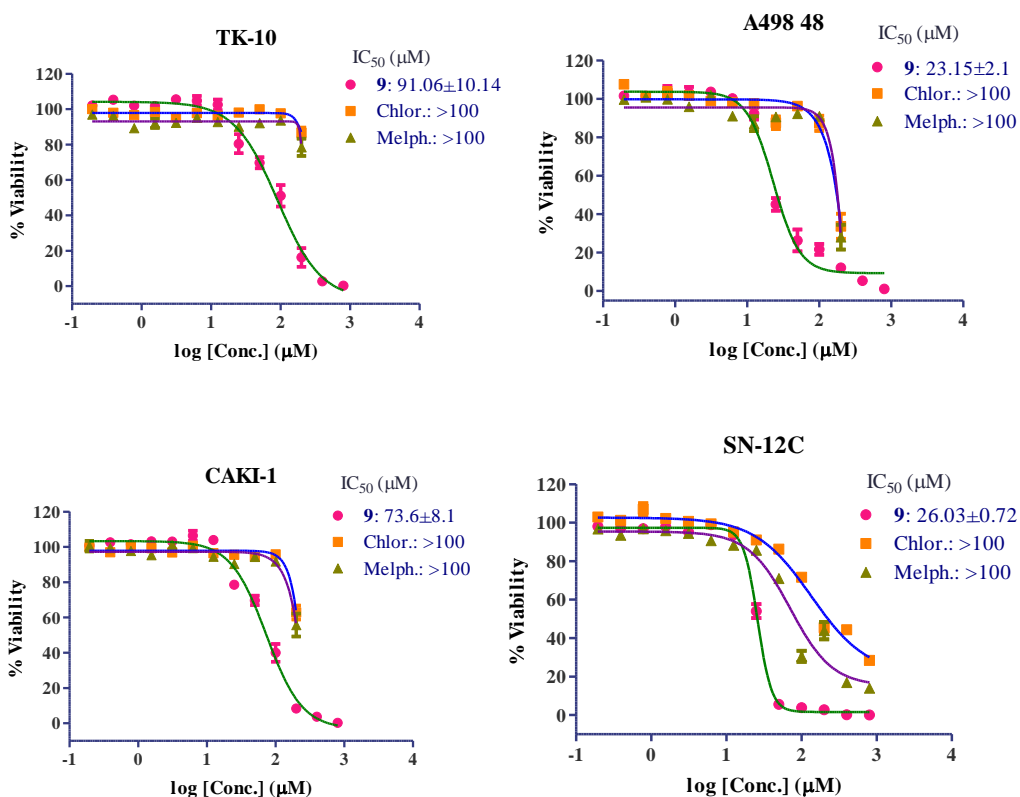
## 3.2 *In-vitro* toxicity study

### 3.2.1 Concentration Dependent Cytotoxicity Study.

#### **Compound 12 is more Cytotoxic than Chlorambucil or Melphalan in Human Breast Cancer and Renal Cancer Cell Lines.**

Previously, the cytotoxicity of **9** was tested against 60 human cancer cell lines at the National Cancer Institute (NCI) Developmental Therapeutics Program, which showed that **9** has a significant cytotoxicity in several cancer cell lines. Here, we determined the cytotoxicity of **12** with breast cancer MDA-MB-468 cells and renal cancer cell lines including UO-31, A498, SN12C, TK-10, and CAKI-1. The results are depicted in Figure 3-1. The dose-dependent cytotoxicity study (after 48 h in the presence of compound concentrations ranging from 0.195 to 200  $\mu$ M) showed

that **12** is more effective in killing cancer cells than chlorambucil and melphalan. For example, the half-maximal inhibitory concentration ( $IC_{50}$ ) of **12** for MDA-MB-468 is 3.1  $\mu\text{M}$ , which is one tenth that of chlorambucil ( $IC_{50} = 34.4 \mu\text{M}$ ) and one-sixteenth that of melphalan ( $IC_{50} = 48.7 \mu\text{M}$ ). Similarly, the  $IC_{50}$  of **12** for UO-31 is 48.94  $\mu\text{M}$ , while those of chlorambucil and melphalan were higher than 100  $\mu\text{M}$ . Similar results were obtained with A498, SN12C, TK-10, and CAKI-1 cells. It is important to note that, the introduction of a methyl group in **12** showed improved potency. For example, **12** is four-fold more potent than **9** for the MDA-MB-468 cell line ( $IC_{50} = 3.1 \mu\text{M}$  for **12** vs 16.7  $\mu\text{M}$  for **9**). Similarly, lower  $IC_{50}$  values were observed for **12** than **9** in other cell lines, including A498, SN12C, TK-10, and CAKI-1. Collectively, these data suggest that a methyl group greatly improved anticancer effect.



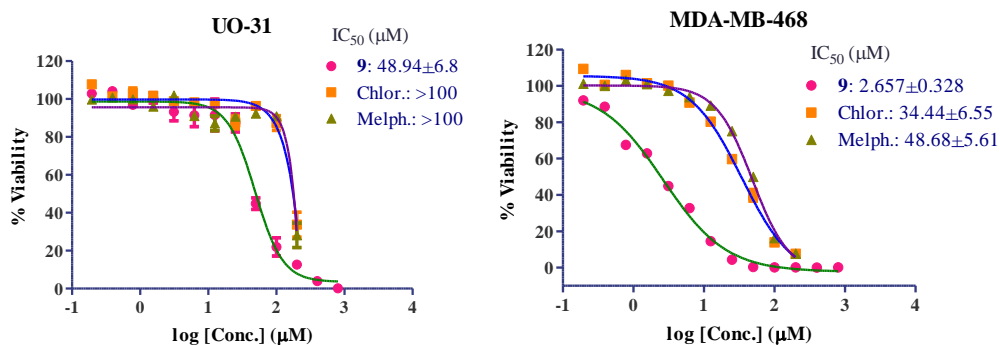


**Figure 3-1.** Cellular toxicity of **12**, chlorambucil, and melphalan in (A) MDA-MB-468, (B) UO-31, (C) A498, (D) SN12C, (E) CAKI-1, and (F) TK-10 when incubated for 48 h with concentrations ranging from 0.195 to 200 μM (n = 4, IC<sub>50</sub> values were determined by a nonlinear regression). The significance was determined by one-way ANOVA followed by a Tukey test to compare all pairs of columns (n = 4, (\*) P < 0.05, (\*\*\*) p < 0.0001).

### 3.2.2 Time Dependent Cytotoxicity Study.

The time-dependent cytotoxicity of **12** was assessed with MDA-MB-468 over the period of 4 days (Figure 3-2). The cells were treated with 10 or 20 μM of **12** respectively. Only a 42% viability was observed for the MDA-MB-468 cells after a 24 h exposure of **12** (20 μM). Similarly, 10 μM **12** led to a 65% viability at 24 h and 29% at 48 h for the MDA-MB-468 cells. It was observed<sup>29</sup> that MDA-MB-468 cells are more sensitive to **12** than to **9**. Finally, our findings indicate that the cytotoxicity of **12** is time-dependent and exhibits a long-lasting effect on the viability of cancer cells.



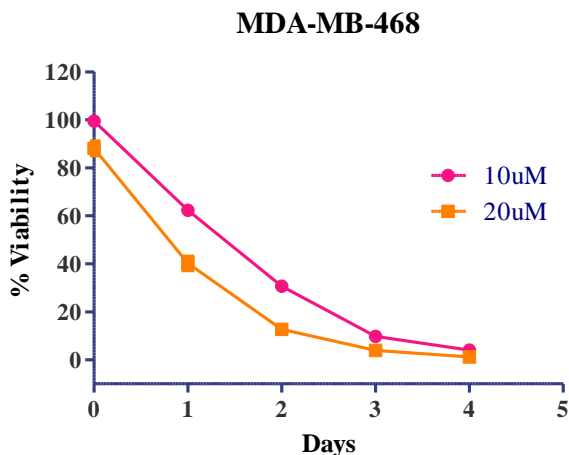


**Figure 3-2.** Time-dependent toxic response of MDA-MB-468 cells when incubated with 10 or 20  $\mu\text{M}$  of **12** ( $n = 4$ ). The significance was determined by one-way ANOVA followed by a Tukey test to compare all pairs of columns ( $n = 4$ , (\*)  $P < 0.05$ , (\*\*\*)  $p < 0.0001$ ).

### 3.2.3 MDA-MB-468 Cell Produced a High Level of $\text{H}_2\text{O}_2$ .

Cytotoxicity study established that the MDA-MB-468 cell was particularly sensitive towards these  $\text{H}_2\text{O}_2$ -activated prodrugs. So we investigated if there's a correlation between the efficacy of these prodrugs and  $\text{H}_2\text{O}_2$  level. Previously, Sen and coauthors reported that several breast cancer cell lines, including the MDA-MB-468 cell line, showed greatly increased  $\text{H}_2\text{O}_2$  production rates than normal human breast epithelial cells, which is associated with the downregulation and decreased bioactivity of catalase in TNBC cells. Increased  $\text{H}_2\text{O}_2$  production leads to an increased proliferation of aggressive TNBC cells. Here, we determined  $\text{H}_2\text{O}_2$  level produced by MDA-MB-468 cells using the Amplex Red hydrogen peroxide assay kit (Invitrogen, A22188). To quantify the  $\text{H}_2\text{O}_2$  released from MDA-MB-468 cells, we first prepared a  $\text{H}_2\text{O}_2$  standard curve. Approximately 2.0-2.5  $\mu\text{M}$   $\text{H}_2\text{O}_2$  was detected with  $(25-50) \times 10^3$  MDA-MB-468 cells after being incubated at  $37^\circ\text{C}$  for 5 h (Figure 3-3). It is to be noted that the actual  $\text{H}_2\text{O}_2$  concentration of the cell samples is two-fold higher due to the prepared cell samples mixed with an equal amount of Amplex Red reagent before the assay.

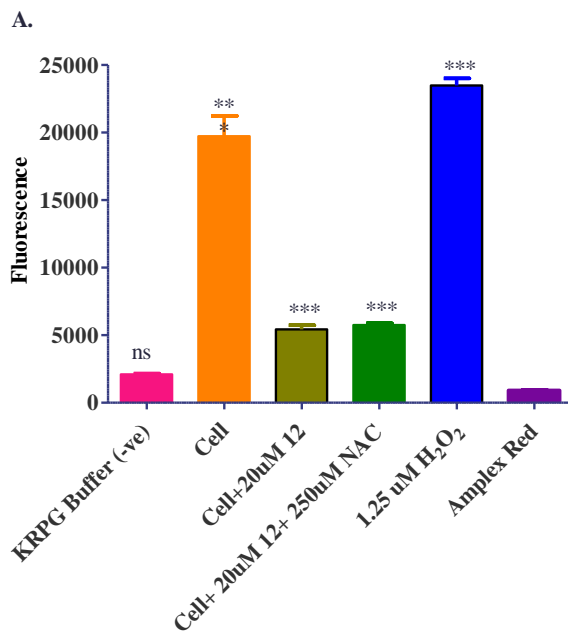


**Figure 3-3.** H<sub>2</sub>O<sub>2</sub> level released from MDA-MB-468 cells as measured by Amplex Red (data are represented as mean  $\pm$  SD from three independent experiments) (Note: as the prepared samples mixed with an equal amount of Amplex Red reagent before the assay, the final H<sub>2</sub>O<sub>2</sub> concentrations are two-fold lower). The significance was determined by one-way ANOVA followed by Dunnett to compare all columns (n = 6), (\*) P < 0.05, (\*\*\*) p < 0.0001 vs control (Amplex Red only).

#### 3.2.4 Cytotoxicity inhibition study using ROS blocker.

Given that the H<sub>2</sub>O<sub>2</sub>-activated prodrugs can be converted to the active forms in the presence of H<sub>2</sub>O<sub>2</sub>, we postulated that blocking the ROS production by N-acetyl cysteine (NAC) would inhibit the cytotoxicity of these agents. To test our hypothesis, we incubated MDA-MB-468 cells with **12** in the presence or absence of NAC and measured the end points such as cytotoxicity. On one hand, our data showed that, in the presence of NAC (250-500  $\mu$ M), the apoptosis induced by **12** (20  $\mu$ M) was slightly decreased (Figure 3-4). On the other hand, a much lower H<sub>2</sub>O<sub>2</sub> level was detected in the cells treated with **12** alone or with **12**/NAC (Figure 3-3). Collectively, the data suggested that **12** functions through ROS-dependent mechanisms.

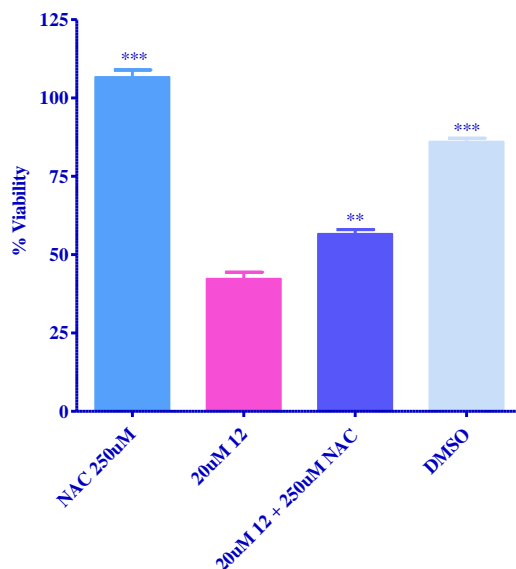


**Figure 3-4.** Toxic response of MDA-MB-468 cells when incubated with NAC (250 µM), **12** (20 µM), **12** (20 µM) + NAC (250 µM), and DMSO (control). Data are represented as mean ± SD from three independent experiments. The significance was determined by one-way ANOVA followed by Dunnett to compare all columns (n = 4), (\*) P < 0.05, (\*\*\*) p < 0.0001 vs 20 µM **12**.

### 3.3 *In-vitro* efficacy and selectivity of ROS-activate prodrugs

#### 3.3.1 Safety Study with CD-1 Mice

**One dose treatment.** The CD-1 mice were injected ip with one dose of nitrogen mustard precursor **12** and observed for one week. Five different doses of **12** were tested (20, 40, 60, 80, and 100 mg/kg) . All mice survived after seven days. No obvious toxicity was observed for mice treated with 20 mg/kg dose, where the weight of mice slightly increased, which was similar to the control mice (Figure 3-5). However, obvious weight loss was observed with the mice treated with 40 mg/kg or higher doses. The mice weight significantly decreased next day after drug treatment, while the mice weight slightly increased when the injection was discontinued. Chlorambucil, however, induced death at 80 mg/kg for all animals.

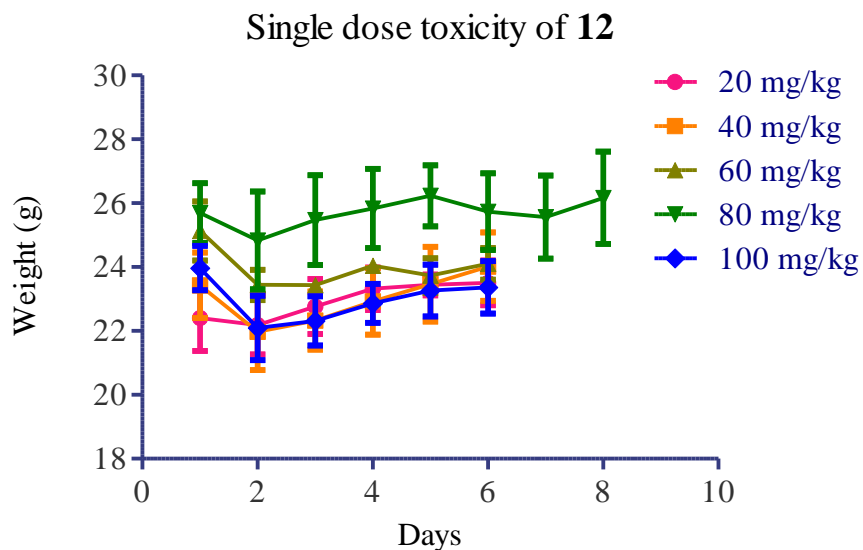


**Figure 3-5.** The results of one dose treatment for compound **12**.

**Five dose treatments:** Single dose toxicity study demonstrated that ROS-activated prodrug **12** are less toxic than chlorambucil. Then a repeated-dose toxicity study was conducted to determine the safe dose for further *in vivo* efficacy study. The mice were injected with six different dosages of compound **12** (5 mg/kg, 10 mg/kg, 20 mg/kg, 30 mg/kg, 40 mg/kg, and 50 mg/kg) and each dose with seven continuous injections within seven days. All mice treated with lower dosages (10 and 20 mg/kg) of **12** survived after seven days (**Figure 3-6**). Mice treated with 10 mg/kg dose had no obvious weight loss in the first three days, weight loss was observed beginning the 5<sup>th</sup> day, while obvious weight loss was observed on the 7<sup>th</sup> day. Mice treated with 20 mg/kg dosage showed obvious weight loss from the 3<sup>rd</sup> day. Mice treated with higher dose (40 mg/kg, 50 mg/kg) of compound **12** showed obvious weight loss and euthanized on the sixth and fourth day respectively.

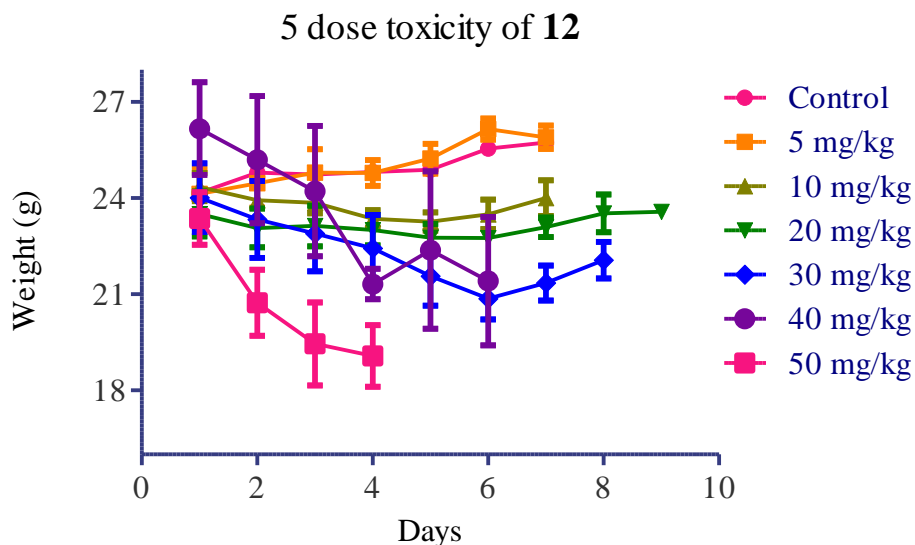


**Figure 3-6.** The results of five injections per week for compound **12**.

Chlorambucil induced death at a 40 mg/kg repeated dose on day 3. All mice treated daily with 40 mg/kg and 50 mg/kg **12** survived. Thus, ROS-activated prodrug **12** showed a better safety profile than chlorambucil. No obvious weight loss was observed for mice treated with **12** at all three doses (5.0, 10, and 20 mg/kg) (Figure 3-6). More importantly, a slight increase of body weight was observed for mice treated with 5.0 mg/kg of **12** which was similar to control mice. Thus, a dose of 5.0 mg/kg was used for the following *in vivo* efficacy study.

### 3.4 *In vivo* efficacy study with athymic nude mice xenografted with breast cancer cell line MDA-MB-468

To investigate the *in vivo* efficacy of **12**, the human breast cancer xenografts were established by a subcutaneous implant of MDA-MB-468 cancer cells in athymic nude mice. Tumors developed in all mice within one week. The mice were divided into two groups that were treated with either vehicle or **12** (5 mg/kg). The mice was injected with **12** daily except for weekend. The size of tumors and the weight of mice were measured weekly. The data are presented in Figure 3-6. It was found that **12** greatly inhibited the tumor growth *in vivo*, evidenced by 94.6% of calculated tumor growth inhibition rate [IR (%) = [1 - (mean volume of treated tumors)/(mean volume of control

tumors)]  $\times 100$ ] and 80% of tumor shrinkage. After nine weeks of treatment, the mean volume for **12**-treated tumors was only  $46.3 \pm 17.7 \text{ mm}^3$ , that is, 5.4% of the mean volume of the control tumors.

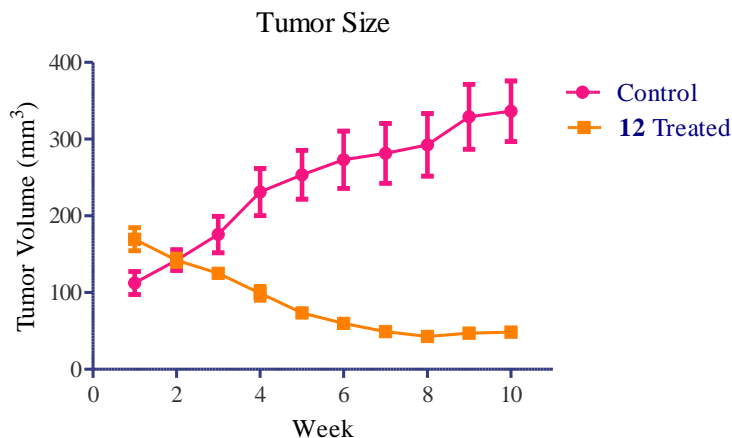


**Figure 3-6.** In vivo evaluation of a daily treatment of **12** in athymic nude mice. The volume of tumors for control and **12**-treated mice from 1<sup>st</sup> to 9<sup>th</sup> week (5 mg/kg). Time-dependent tumor growth measured by caliper. The mice were administered IP with vehicle, **12** at a dose of 5 mg/kg.

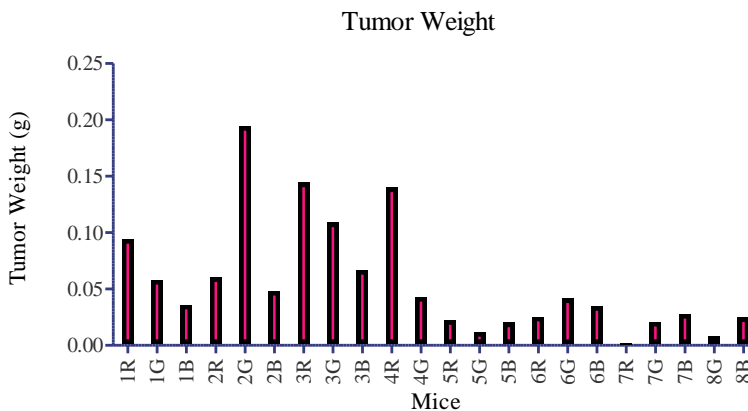


**Figure 3-7.** Final harvested tumor weight for control and **12**-treated mice after 9-week's treatment.

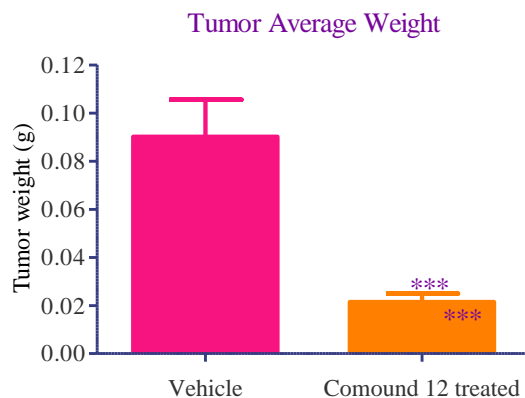


**Figure 3-8.** The mean of tumor weights at the end of treatment. Data are expressed as mean  $\pm$  SD ( $n = 8$ ), (\*\*\*)  $p < 0.001$  vs control group.

The tumors were excised and weighed on the first day of week nine. The weight of tumors in the control group ranged from 100 to 370 mg, while those of **12**-treated mice were  $17.3 \pm 7.4$  mg. The results demonstrated that **12** effectively inhibited the tumor growth for MDA-MB-468 xenografts with a dosage of 5.0 mg/kg.

The two groups of athymic nude mice under an *in vivo* efficacy study were also monitored for symptoms of toxicity including changes in body weight, loss of appetite, reduced activity levels, treatment-related mortality, and changes (color and weight) in kidney, liver, spleen, and heart. Our observation suggested that the IP administration of **12** (5 mg/kg) for nine weeks (five injections per week) induced neither animal death nor weight loss. The **12**-treated mice showed a similar increase in body weight as compared to the control group (Figure 3-9). Together, the *in vivo* investigation demonstrated that ROS-activated prodrug **12** potently suppressed the tumor growth without affecting normal tissues in the mice.

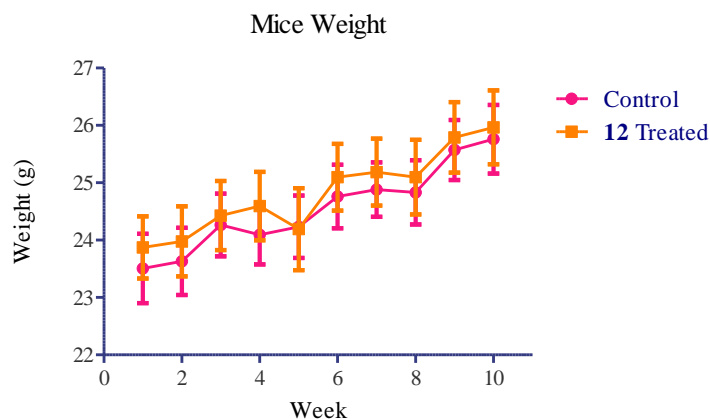


**Figure 3-9.** Body weight of mice for control and **12**-treated mice from 1<sup>st</sup> to 9<sup>th</sup> week (5 mg/kg).

### 3.4.1 Pharmacokinetics and Stability.

**Blood Plasma pharmacokinetics and LC-MS/MS analysis.** The conversion of prodrug **12** was investigated in mice (Figure 3-10) as well as in the presence of liver microsomes (Figure 3-10).

Initially, we investigated the conversion of **12** in mice over a period of 2 h (Figure 3-11). The blood concentrations of **12** were quantified by LC-MS/MS following a single intraperitoneal injection of 10 mg/kg (Figure 3-10). Compound **12** was readily detected in plasma with a  $t_{\max}$  of ~3 min. The presence of a methyl group in **12** greatly increased the half-life to 8.84 min from 4.92 min for **9**. The rate of transformation for **9** in the blood was fast ( $0.141 \text{ min}^{-1}$ ), which is 2 times faster than that of **12** ( $0.078 \text{ min}^{-1}$ ). Compound **12** showed an area under the curve (AUC) of 16253 ng·min/mL, which is higher than that of **9** (10883 ng·min/mL). The data suggested that a methyl group greatly increases the half-life and duration of the prodrugs.



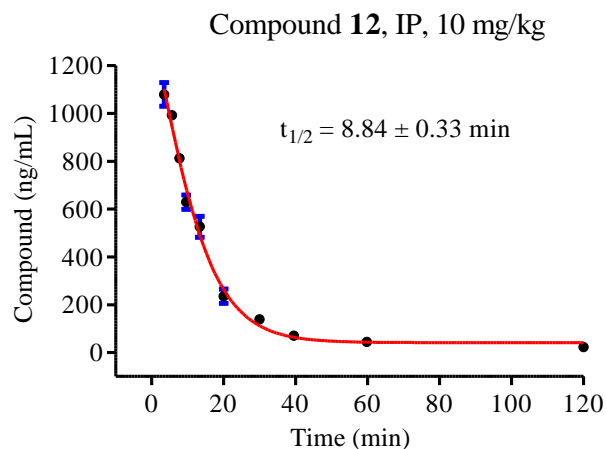


**Figure 3-10.** Pharmacokinetic profile of **12**. Plasma pharmacokinetic analysis of **12** in CD-1 mice following a single IP dose of 10 mg/kg. All experiments were conducted twice in triplet.

**Microsomal Stability Assay.** The conversion of prodrug **12** was investigated in mice as well as in the presence of liver microsomes (Figure 3-11). The *in vitro* microsomal stability studies revealed that prodrug **12** is significantly more stable in human microsome ( $t_{1/2} = 59.38$  min for **12**) than in mouse microsome ( $t_{1/2} = 23.49$  for **12**) (Figure 3-11).

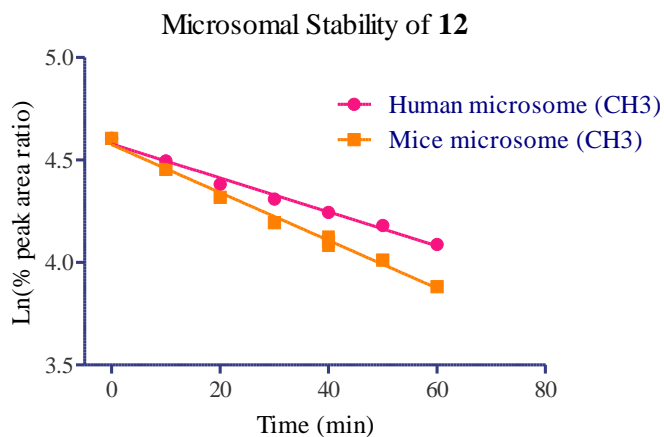


**Figure 3-11.** Pharmacokinetic profile of **12**. Stability of prodrug **12** in the presence of human and mice microsomes. All experiments were conducted twice in triplicate.

**Liver Pharmacokinetics and LC-MS/MS Analysis.**

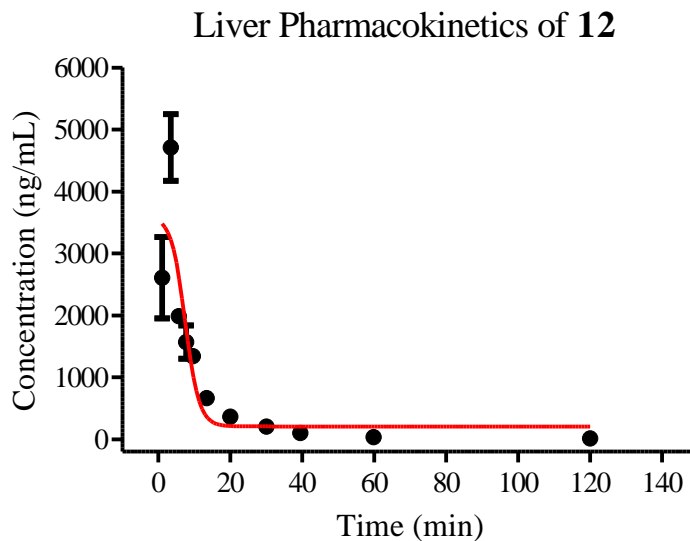


**Figure 3-12.** Pharmacokinetic profile of **12**. Liver pharmacokinetics analysis of **12** in CD-1 mice following a single IP dose of 10 mg/kg. All experiments were conducted twice in triplet.

Transformation of prodrug **12** in liver was also investigated in mice over a period of two hours. Liver concentration of **12** was quantified similarly using LC-MS/MS following IP injection. Compound **12** reached maximum concentration with a  $t_{max}$  of ~ 4min. Half-life was found to be approximately 9.5 min.

**Brain Pharmacokinetics and LC-MS/MS Analysis.**

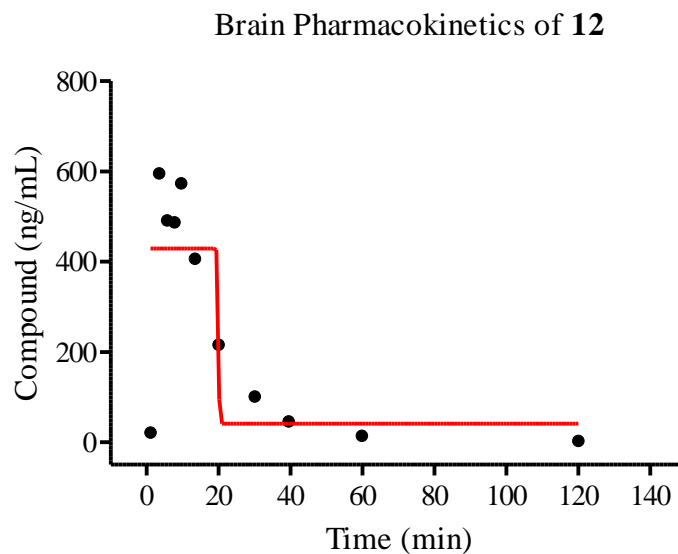
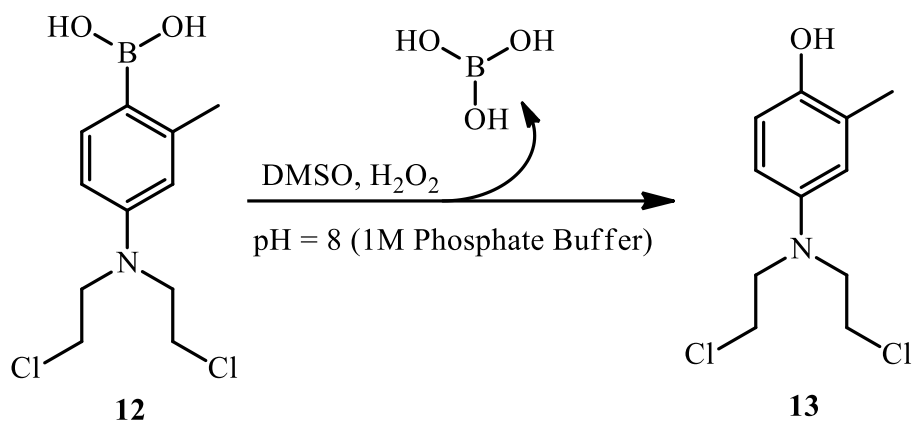


**Figure 3-13.** Pharmacokinetic profile of **12**. Brain pharmacokinetics analysis of **12** in CD-1 mice following a single IP dose of 10 mg/kg. All experiments were conducted twice in triplet.

Penetration of prodrug **12** in brain tissue was also investigated in mice over a period of two hours. Brain concentration of **12** was quantified similarly using LC-MS/MS following IP injection. Compound **12** reached maximum concentration with a  $t_{max}$  of ~ 4min in brain which was very similar to blood and liver. However, half-life was found to be approximately 25 min which is relatively higher than blood and liver. This led us believe it to be a potential compound for brain tumor-related treatment. However, more study and investigation are required for detailed mechanism.

#### 3.4.2 Detection of Drug Metabolites in Cell Culture.

**Synthesis of Activated Phenol 13.** In order to provide direct evidence for the activation of these ROS-activated prodrugs by  $H_2O_2$  in cancer cells, we determined the possible metabolites in cell cultures as well as in cells. We first synthesized the activated form **13** by oxidative deboronation of **12**, then used **13** as an internal standard.

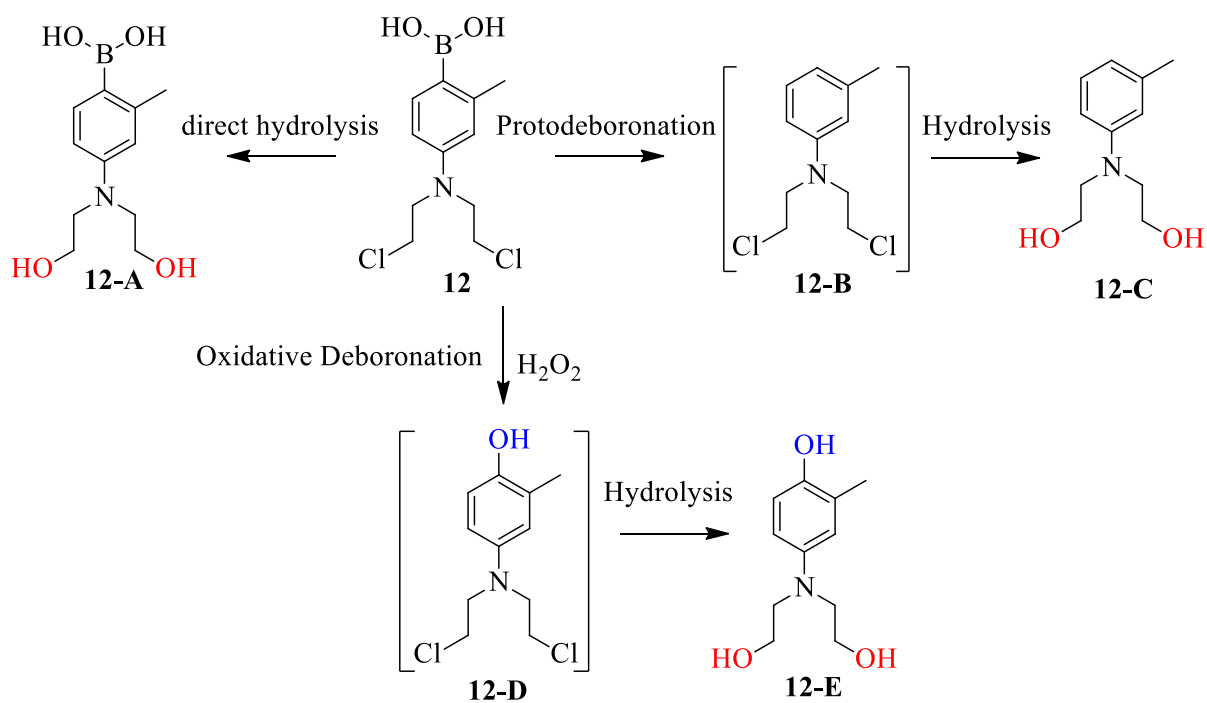


**Scheme 3-4.** Activation of **12** by  $\text{H}_2\text{O}_2$

The reaction of **12** (200  $\mu\text{mol}$ ) with  $\text{H}_2\text{O}_2$  (100  $\mu\text{mol}$ ) was carried out in a mixture of 400 mM deuterated potassium phosphate buffer (pH 8.0) (30  $\mu\text{L}$ ) and DMSO (2ml). In the presence of  $\text{H}_2\text{O}_2$ , oxidative deboronation of **12** occurred yielding alkylating agent **13**, which was characterized by NMR (See appendix). The conversion of **12** to **13** was fast that almost 80% of **12** was transformed to **13** within 30 min, and >95% of **13** was formed after 2 h, which showed that the aryl boronates developed in this work are efficient  $\text{H}_2\text{O}_2$ -responsive trigger units. Overall, the prodrugs developed in this work are sensitive to  $\text{H}_2\text{O}_2$  under physiological conditions.

In an effort to provide direct evidence for the selective transformation of a boronic acid prodrug to the phenol analogue, we used mass spectroscopy to analyze the transformed adducts obtained from a cell culture. Approximately 1–2 million cells were treated with 20  $\mu\text{M}$  prodrug **12** and incubated at  $37^\circ\text{C}$  for 2, 4, 6, 12, and 24 h. Then, the cell culture media and cells were separated, and the cells were trypsinized, extracted with MeOH, and analyzed by mass spectroscopy.

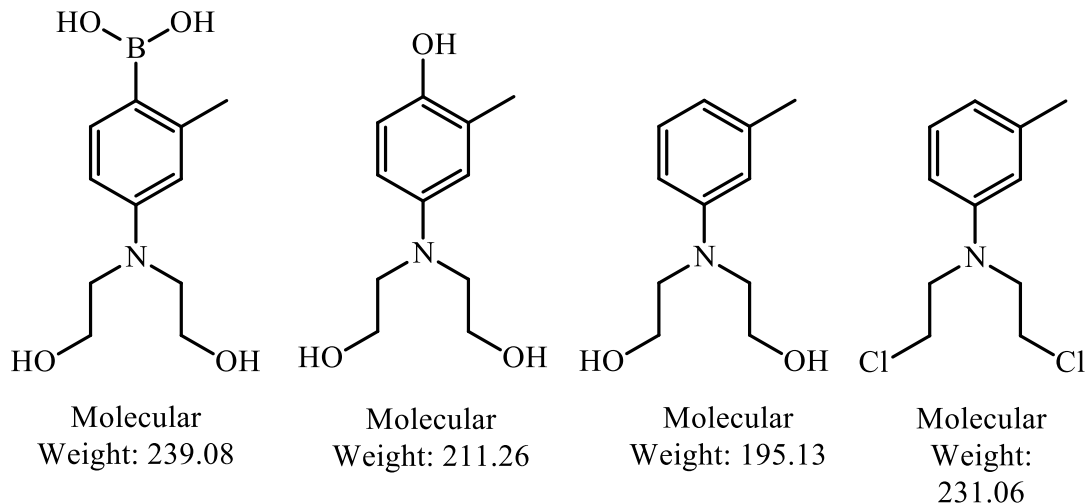
**Other possible metabolites/ transformed product:**



**Scheme 3-5.** Possible way of **12** metabolism.

There could be several transformed product of compound **12**: Hydrated **11**, Hydrated activated **12**, Protodeboronated **12**, protodeboronated and activated **12**. Compound **11** was detected with the samples incubated for 2, 4, and 6 h but disappeared after 6 h of incubation, which suggested that **12** was completely transformed to other products (Appendix). We easily detected hydrated **12** and protodeboronated **12**. The activated phenol form, however, was not detectable by mass spectrometry. It is possible that an attempt to detect activated phenol did not succeed for a number of reasons: (a) It's possible that phenol is too active to be detected; (b) It is possible that the conversion yield is low since the level of  $\text{H}_2\text{O}_2$  in cells is lower than that used in DNA cross-linking studies; (c) other transformation products are possible, including hydrolysis, reactions, or association with cellular metabolites and/or biomolecules within the cells. All these would make the detection of prodrug transformation more difficult. Collectively, these data suggest that the MDA-MB-468 cell does produce a high level of  $\text{H}_2\text{O}_2$  and that **12** may function through ROS-

dependent mechanisms, but the detailed mechanism of function has not been fully understood yet.



**Scheme 3-6.** Possible metabolites of **12** other than activated metabolite.

### 3.5 Conclusion

A central goal of cancer treatment is to selectively target tumor cells. To develop safer cancer treatments, it is necessary to utilize the unique biological processes of cancer cells. ROS-responsive trigger has shown to successfully induce the production of a cytotoxin to kill cancer cells and offers a therapeutic advantage, as cancer cells have an increased level of ROS in comparison to healthy cells<sup>5,30-32</sup>. Many ROS-activated anticancer prodrugs have been investigated, but few showed in vivo efficacy or selectivity<sup>16,20,27</sup>. Here, Using a xenograft mouse model, we demonstrated the therapeutic utility of a ROS-activated DNA interstrand cross-linking agents. Some of the most widely used anticancer drugs are DNA-alkylating agents such as cyclophosphamide, chlorambucil, and bendamustine. They are effective against fast-dividing cancer cells because they interfere with DNA replication and transcription, stall mitosis, and/or induce apoptosis. However, many nonmalignant cells, such as those in bone marrow, the lining of the mouth and intestines, and hair follicles, also divide rapidly. This is why, most DNA-targeting anticancer drugs have serious side effects, including weight and hair loss, nausea and vomiting,

fatigue, low blood-cell counts, easy bruising or bleeding, and the risk of cardiotoxicity. Luckily, their side effects due to their toxicity are controllable as it is dose-limiting. Nevertheless, in the absence of improved agents, alkylating agents are still needed for cancer treatments. However, more selective DNA-targeting agents are needed to reduce unwanted side effects.

The *in vivo* evaluation suggested that ROS-activated DNA cross-linking agent, FAN-NM-CH<sub>3</sub> (**12**) which is the methyl analogue of CWB-20145 (**9**), showed an improved *in vivo* efficacy and selectivity in comparison with the clinically used DNA alkylation agents chlorambucil and melphalan. In addition to being more toxic than chlorambucil and melphalan in several cancer cell lines, FAN-NM-CH<sub>3</sub> had improved *in vivo* efficacy, safety, and reduced side effects. It led to a significant tumor shrinkage in mice xenografted with the MDA-MB-468 cell line (up to 80% shrinkage in tumor size) without any obvious signs of general toxicity. In comparison with the parent compound CWB-20145 (**9**), its methyl analogue FAN-NM-CH<sub>3</sub> showed improved drug-like properties (e.g., increased duration time and absorption) and a superior *in vivo* efficacy with a favorable safety profile. The results of this study provide valuable guidance for further designing compounds with drug-like properties that may eventually be used as therapeutics in humans.

Most important finding of this study is that, it indicated that FAN-NM-CH<sub>3</sub> are most effective against TNBC cells, such as MDA-MB-468 cells. TNBC is one of among different subtypes of breast cancers. It is particularly difficult to treat and has a poor prognosis since it lacks estrogen receptors, progesterone receptors, and HER2<sup>33,34</sup>. Patients with triple-negative tumors have largely been bypassed out of the treatment revolution that has transformed many breast cancers. Because of the absence of a recognizable therapeutic target, cytotoxic chemotherapy remains the only systemic treatment option<sup>35-39</sup> for TNBC. FAN-NM-CH<sub>3</sub> showed increased *in vivo* efficacy and selectivity toward TNBC cells, which may lead to a selective chemotherapy with phenyl boronic

acid-modified DNA cross-linking prodrugs as a new treatment option for patients with TNBC. Although the *in vivo* mechanism of function for this type of molecule is yet to be fully understood, a high level of H<sub>2</sub>O<sub>2</sub> was detected with TNBC cells, such as the MDA-MB-468 cell, which might be one of the factors that accounted for an improved efficacy and selectivity of these molecules toward TNBC cells. In normal cells with low levels of H<sub>2</sub>O<sub>2</sub>, these prodrugs are unlikely to be activated, but they should activate specifically in cancer cells under oxidative stress, as the presence of electron-withdrawing boronic acid masked the toxicity of alkylating effectors. However, a correlation between ROS levels and efficacy and selectivity *in vivo* has not yet been established, but it is under investigation.

In conclusion, Our results here demonstrate a more potent and selective drug candidate FAN-NM-CH<sub>3</sub> (**12**) that is effective *in vivo* following our earlier development of ROS-activated DNA alkylating agents. It has improved *in-vivo* efficacy and selectivity, along with reduced side effects and improved pharmacokinetic properties. As FAN-NMCH<sub>3</sub> has a promising therapeutic activity and selectivity against TNBC cells, the H<sub>2</sub>O<sub>2</sub>-activated cross-linking agents may be useful in the treatment of TNBC patients and warrant further clinical evaluation. Currently, we are studying metabolites, exploring the correlation between *in vivo* efficacy and ROS level, understanding signal transduction pathways, and assessing immune toxic effects of this novel class of compounds in addition to investigating the potential for FAN-NM-CH<sub>3</sub> to serve as an Investigational New Drug.

### 3.6 Experiment protocol

#### 3.6.1 Protocol for cell preparation

Everything must be done in biosafety hood. The hood was sprayed down with 70% ethanol and cleaned. 16 of big flasks (150 cm<sup>2</sup>), full of cancer cells, were prepared before xenograft mice study.



The matrigel was stored in ice and put in 2-8°C overnight before xenograft mice study. The media and trypsin (HyClone, cat #: SH30042.01) was pre-warmed at 37°C and 25°C respectively for 30 min before the assay.

### **Breast cancer cell line MDA-MB-468**

Media component: 500 mL of L-15 Leibovitz media (cat #: SH30525.01), 50 mL of Fetal bovine serum (MIDSCI Cat#: S01520HI), 5 mL of NEAA (HyClone, cat #: SH30238.01), 5 mL of Penicillin (HyClone, cat #: SV30010). Note: don't need CO<sub>2</sub> for growth (small incubator without CO<sub>2</sub>, "VENT" flask)

Preparation of cancer cells in 16 big flasks:

- i. The media and trypsin (HyClone, cat #: SH30042.01) was pre-warmed at 37°C and 25°C respectively for 30 min before the assay. Media component: 500mL of L-15 Leibovitz media (cat #: SH30525.01), 50mL of fetal bovine serum (MIDSCI Cat#: S01520HI), 5mL of NEAA (HyClone, cat #: SH30238.01), 5mL of penicillin (HyClone, cat #: SV30010).
- ii. Coating: add 3.0 mL matrigel solution (0.5 mL matrigel + DMEM/High modified 200 mL) and spread to the whole bottom of the flask, incubate the flask at 37°C for 10 min. Then, remove the matrigel by aspiration.
- iii. Pretreat the flask: prewash the flask with 5.0 mL media and remove the media, then add 25 mL media in the flask; meanwhile, quickly thaw the cancer cells at 37°C within 1-2 minutes (Note: cells can easily die at r.t. in DMSO).
- iv. One flask cell growth: transfer the cells to the pre-washed flask (150 cm<sup>2</sup>) with about 25.0 mL media and incubate the cells at 37°C for about 2-7 days (the cells are spreading in the bottom of the flask).
- v. Remove the media in the flask with MDA-MB-468 cell lines by aspiration and 5 mL media

was added to wash the bottom of the flask, remove the media carefully not touching the bottom.

- vi. Add trypsin (SH 30042.01, Hyclone) (4 mL) to the flask and incubate at 37°C for 5min.
- vii. Homogenization of cells solution by pipetting the solution up and down 10 times in the corner of the flask.
- viii. Transfer 1 mL solution into four new flasks (150 cm<sup>2</sup>) which were pre-treated with 3 mL of matrigel solution (VWR cat #: 47743-715) (Step ii, coating), and add 25 mL media to the flask for cells growing.
- ix. Three to seven days later, prepare 16 big flasks of cells by repeating step i to v on every flask which is full cancer cells. The total approximate time is two to three weeks.

#### **Renal cancer cell line (UO-31, SN-12C, A-498, CAKI-1, TK-10)**

Media component: 500 mL of RPMI 1640, 1X with L-glutamine media (VWR cat #: 45000-396), 50 mL of Fetal bovine serum (MIDSCI Cat#: S01520HI), 5 mL of Penicillin (HyClone, cat#: SV30010). Note: CO<sub>2</sub> is necessary for cell growth (big incubator with CO<sub>2</sub>, flask: not vent). Other renal cancer cell lines in our lab use the same method for growth.

- i. One flask cell growth: transfer the cells to the flask (don't need coating) (150 cm<sup>2</sup>) with about 25.0 mL media and incubate the cells at 37°C for about 2-7 days (the cells are spreading in the bottom of the flask).
- ii. Remove the media in the flask with cell lines by aspiration and 5 mL media was added to wash the bottom of the flask, remove the media carefully not touching the bottom.
- iii. Add the trypsin (SH 30042.01, Hyclone) (4 mL) to the flask and incubate at 37°C for 5 min.
- iv. Homogenize the cells solution by pipetting the solution up and down 10 times in the corner of the flask.

- v. Transfer 1 mL solution into four new flasks (150 cm<sup>2</sup>), and add 25 mL media to the flask for cells growing.
- vi. Three to seven days later, prepare 16 big flasks of cell lines by repeating step ii to v on every flask which is full cancer cell lines. The total approximate time is two to three weeks.

### 3.6.2 Protocol for cell injection to nude mice

- i. Store the matrigel on ice and stay in 2-8°C overnight before xenograft mice study.
- ii. Remove the media in the flask containing cancer cell lines by aspiration and 5 mL media was added to wash the bottom of the flask, remove the media carefully not touching the bottom. 4 flasks were done one time.
- iii. Add trypsin (6 mL) to the flask and incubate at 37°C for 10 min until all the cells detached from the bottom.
- iv. Homogenize the cells solution by pipetting the solution up and down 10 time in the corner of the flask and transfer the detached cells (4 flasks) to a 50 mL conical tube (4 X 6 mL), then wash the 4 flasks with 25 mL media, collect in the conical tube (4 X 6 mL+25 mL), total 4 conical tubes.
- v. Spin down the cells in the 4 conical tubes (1000 rpm, 5 min) and remove the media carefully.
- vi. Add 10 mL media to each conical tube mix (up and down 10 times) and combine the solution in 50 mL conical tube, centrifuge (1000 rpm, 5 min) and remove the media again.
- vii. Add 5 mL media to the cell lines, mix and divided them into 25 small tubes (150-200 uL each tube).
- viii. Spin down for (1000 rpm, 1 min) and discard half of the supernatant.
- ix. Mix the cell lines with the same volume of matrigel (100-160 uL) with pipette (keep the matrigel in ice, then put in 4°C refrigerator as the matrigel can easily solidify at room

temperature) and inject 100  $\mu$ L of the mixture to each mice.

- x. Injection: 0.1 mL of above solution was injected under skin of the mice, the inject position was on the back close to the legs.

### 3.6.3 Protocol for compound injection to nude mice

#### **Formulation:**

Vehicle: In two of 1.5 mL vials, add 75  $\mu$ L of DMSO, 712  $\mu$ L of PEG 400 and 712  $\mu$ L of PBS (1X) buffer (Cat No SH30256.01). Mix well by pipetting 10 times or shaking tube.

Drug solution (Order of adding different solutions is extremely important): (1) In two of 1.5 mL vials, add 75  $\mu$ L of drug solution (DMSO); (2) add 712  $\mu$ L of PEG400 and mix; (3) add 712  $\mu$ L of PBS (1X) (Cat No SH30256.01) and mix well (add half of it and mix, then add remaining); (4)

For a dose of 10 mg/kg, the weight of mice is 20 g in average. Compound (6 mg) was dissolved in 150  $\mu$ L of DMSO.

Injection protocol:

0.1 mL of compound solution was injected each day and 5 days/per week in the belly of the mice, the injection position was close to and under the nipple. The treatment lasts for 6-8 weeks.

### 3.6.4 Protocol for Cytotoxicity Assay

- i. The media and trypsin (HyClone, cat #: SH30042.01) was pre-warmed at 37°C and 25°C respectively for 30 min before the assay. Media component: 500 mL of L-15 Leibovitz media (cat #: SH30525.01), 50 mL of Fetal bovine serum (MIDSCI Cat#: S01520HI), 5 mL of NEAA (HyClone, cat #: SH30238.01), 5 mL of Penicillin (HyClone, cat #: SV30010).
- ii. Remove the media in the flask with MDA-MB-468 cell lines by aspiration and 5 mL media was added to wash the bottom of the flask, remove the media carefully not touching the bottom. (Thaw the cell lines from liquid nitrogen at 37°C for 1 min and immediately transfer them to a

flask with 40 mL media, replace the media the next day to remove the DMSO).

- iii. Add the trypsin (3 mL) to the flask and incubate at 37°C for 5 min.
- iv. Homogenize the cells solution by pipetting the solution up and down 10 times in the corner of the flask.
- v. Transfer 1 mL solution into a new flask (150 cm<sup>2</sup>) which was pre-treated with 3 mL of Matrigel (VWR cat #: 47743-715), and add 50 mL media to the flask for cells growing.
- vi. Transfer the rest (from step 4) to a 15 mL or 50 mL conical tube, add some media (about 5 mL depending on the density of the cell lines), pipette several times to mix them, count the cell lines by pipette 10 uL to the counter: the density equals to the number in the biggest square  $\times 10^4$  /mL. The biggest square has 1 mM x 1 mM area.
- vii. Centrifuge the conical tube and cell lines will be on the bottom. Remove the media containing trypsin without affecting the cell lines.
- viii. Add the proper volume of media by counting the density you need.

**A. For dose response**, the required number is 10000-30000 cells per well (20 uL) which is  $50 \times 10^4$  to  $150 \times 10^4$  per mL. Add the cell lines 20 uL to the “384-well white polystyrene microplates” (Corning, #3570). Centrifuge the plates. Incubate the cell lines at 37°C in the incubator (Fisher #:S04313) for 2-3 h, then add the drugs by Freedom EVO ware transfer two times with each time 100 nL and total 0.2 uL, further incubate the plate at 37°C for 18-24 h. Add 20 uL of celltiter-Glo Luminescent solution (VWR cat #: PAG7572) to each well and detect the luminescent and draw the curve.

**B. For days response**, the required number is 3000 cells per well (100 uL), which is  $3 \times 10^4$  per mL. Transfer the cell lines 100 uL to each well of 96 white plate (Corning, #3903) which was pretreated by Matrigel (10 uL). Add 0.5 uL of compounds in DMSO solution with certain

concentrations to all the wells (The final concentration in the wells was suggested as EC<sub>30</sub> obtained from dose response assay). Add 100 uL celltiter-Glo Luminescent solution to one range of the wells and detect the luminescent for day 0; The next day, add 100 uL celltiter-Glo Luminescent solution to another range of wells and detect the luminescent; ... After 5 days, draw the curve.

Note: DMSO for cell line experiments should always be below 0.1%, as it is cytotoxic at higher concentrations. Primary cell cultures are far more sensitive, so if it is primaries you are using then do a further dose/response curve (viability) at concentrations below 0.1%. 5% is very high and will be dissolving the cell membranes.

### 3.6.5 Extracellular Reactive Oxygen Species Detection Assay

The Amplex Red Hydrogen Peroxide/Peroxidase Assay Kit (#A22188, Invitrogen) was used to detect the extracellular H<sub>2</sub>O<sub>2</sub> released by MDA-MB-468 cells. 15x10<sup>3</sup>-50x10<sup>3</sup> cells per well in 96 Well Black/Clear Bottom Plate (Thermo Scientific™ Catalog: 165305) were seeded. Cells were either not treated or treated with 20 uM of **12** for 24 h. The cells were then washed twice with 1 × KRPG (Krebs–Ringer phosphate consists of 145 mM NaCl, 5.7 mM sodium phosphate, 4.86 mM KCl, 0.54 mM CaCl<sub>2</sub>, 1.22 mM MgSO<sub>4</sub>, 5.5 mM glucose, pH 7.35) and incubated for 5 h in 100μL KRPG buffer. Then, 50 μL was transferred in another 96 Well Black/Clear Bottom Plate in triplicate and mixed with an equal amount of Amplex Red reagent (50μM Amplex Red and 0,1 U/mL HRP final concentrations). After 5 h incubation at room temperature in the dark, fluorescence was measured (560ex/590em nm) on an infinite M1000 microplate reader (Tecan). Each value in the figures represents a mean of triplicate samples.

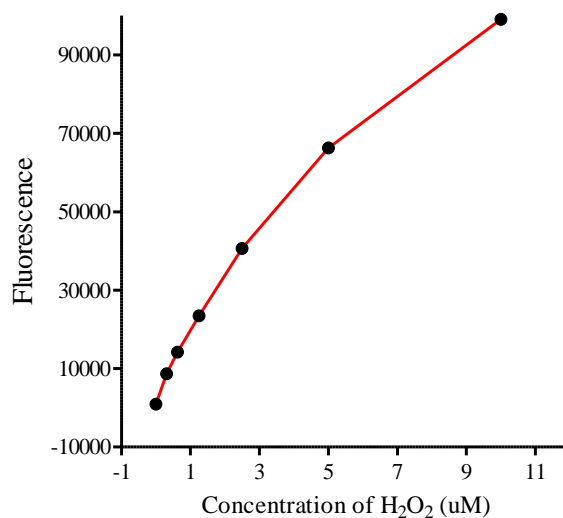


**Figure 3-16.** H<sub>2</sub>O<sub>2</sub> standard curve.

Detection of H<sub>2</sub>O<sub>2</sub> using the Amplex® Red Hydrogen Peroxide/Peroxidase Assay Kit. Reaction mixture containing 50 µM Amplex® Red reagent, 0.1 U/mL HRP and the indicated amount of H<sub>2</sub>O<sub>2</sub> in 50 mM sodium phosphate buffer, pH 7.4, was incubated at rt for 5 h and protected from light. Fluorescence was then measured with a fluorescence microplate reader using excitation at 530 ± 12.5 nm and fluorescence detection at 590 ± 17.5 nm. Background fluorescence, determined for a no-H<sub>2</sub>O<sub>2</sub> control reaction, has been subtracted from each value. Preparation of H<sub>2</sub>O<sub>2</sub> solution: dilute the appropriate amount of 20 mM H<sub>2</sub>O<sub>2</sub> working solution into 1X Reaction Buffer to produce H<sub>2</sub>O<sub>2</sub> concentrations of 0 to 20 µM, each in a volume of 50 µL. Be sure to include a no- H<sub>2</sub>O<sub>2</sub> control. As the prepared H<sub>2</sub>O<sub>2</sub> solution mixed with an equal amount of Amplex Red reagent before the assay, the final H<sub>2</sub>O<sub>2</sub> concentrations will be two-fold lower (0 to 10 µM).

### 3.6.6 Protocol for Inhibition of Cytotoxicity Study Using ROS Production Blocker

The cell line (MDA-MB-468) was transferred to a 96-well plate (Nunc™: 165306) that was pretreated with matrigel. The total number of cells was 3000 per well in 100 µL (3x10<sup>4</sup> per mL). The cells were treated with 20 µM of **12** in combination with different concentrations of N-Acetyl-

Cysteine (NAC) in water (0.5uM, 2uM, 5uM, 10uM, 50uM, 125uM, 250uM, 500uM, 1mM and 2.5mM). CellTiter-Glo reagent (100 µL) was added to the first row of the wells. The luminescence was then measured for day 0. Next, the plate was incubated at 37°C for 24 h with 100% relative humidity. CellTiter-Glo® Reagent (100 µL) was added to the second row of the wells and the luminescence was measured for 24 hours. The NAC effect was generated by plotting the percentage of viable cells against different concentrations of NAC using GraphPad Prism5 software.

### 3.6.7 Protocol for Drug Metabolite Extraction to Detect Transformation.

1. Cell count: 2,000,000 per well in 1 ml media. About 2 million MDA-MB-468 cells were seeded in a 6-well plate (about 1.0 mL growth media per cell).
2. 10mM 2uL Drug in DMSO will be added and incubated. A 10 mM solution of **12** in DMSO (2 µL) was added to each well, which was incubated at 37°C for 2, 4, 6, 12, or 24 hrs.
3. After 6 hour and 12 hour, 0.5 ml media from cell+drug, media+drug, cell+DMSO and media well will be collected and added to 0.5 ml methanol, vortexed and centrifuged at 10,000 rpm for 5 minutes.
4. Cells will be trypsinized with 0.5ml trypsin and transferred to another vial.
5. 500uL ml Methanol will be added to the trypsinized cells to deproteinize cells, vortexed, ultrasonicated for 10 min and centrifuged at 10,000 rpm for 5 minutes.
6. Supernatant layer from step 3 and 5 will be transferred to Spin-X® Centrifuge Tube Filters (vwr catalog no. 29442-760).
7. Filtered sample solution taken out for analysis in LC-MS.

### 3.6.8 Blood Pharmacokinetics and LC-MS/MS Analysis

**Internal standard: IS (133.3 ng/mL, 100 µL) in methanol (cold).**



- i. CD-1 female mice were dosed with 12 (10/mg/kg) for collecting blood (using BD 1ml TB syringe, REF 309626) after different time points (1, 3, 5, 7, 10, 13, 18, 30, 40, 60 & 120 min - 3 mice for each time point).
- ii. Blood was collected by cardiac puncture under terminal CO<sub>2</sub> anesthesia into 2 ml cryo vial tubes (Thermo scientific nunc. 368632) with 50uL of heparin (1mg/ml in water) inside and mixed for uniform mixing of heparin before chilled. The blood samples were stored in liquid nitrogen.
- iii. Blood samples were thawed on ice, vortexed, and a 100uL aliquot is taken and added to 100uL cold methanol (to deproteinize) that contains 300uL of 133.3 ng/mL I.S.
- iv. Samples are vortexed, ultra-sonicated for 10 min, centrifuged at 10,000 rpm for 5 minutes and the supernatant layer transferred to Spin-X® Centrifuge Tube Filters (vwr catalog no. 29442-760).
- v. Supernatant layer was transferred and spin filtered through 0.22um nylon centrifugal filter tubes.
- vi. 150uL of the filtered sample solution taken out for LC-MS.

### 3.6.9 Microsomal Stability Assay Protocol

#### **MAM solution:**

A: 282 µL of LCMS grade water

B: 80 µL of 0.5 M potassium phosphate buffer (pH 7.4)

C: 20 µL of NADPH A (Corning life sciences no: 451220)

D: 4 µL of NADPH B. (Corning life sciences no: 451200)

E: 4 µL of test compound (1 mM in DMSO) (see the note below)

**Internal standard: IS (300 nM, 100 µL) in acetonitrile (ice cold).**

1. MAM solution was prepared with **282**  $\mu\text{L}$  of 18.2 m $\Omega$  of water, **80**  $\mu\text{L}$  of 0.5 M potassium phosphate buffer (pH 7.4), **20**  $\mu\text{L}$  of NADPH A (Corning life sciences no: 451220), **4**  $\mu\text{L}$  of NADPH B. (Corning life sciences no: 451200), and **4**  $\mu\text{L}$  of test compound (1 mM in DMSO).
2. MAM solution was placed in the incubator (37°C) for 5 min and the reaction was initiated with addition of **10**  $\mu\text{L}$  of human or mouse microsomes (20 mg/mL) (final microsome concentration was 0.5 mg/mL) and record the time.
3. At different time points (0, 10, 20, 30, 40, 50, 60, 80, 100, 120 min), 50  $\mu\text{L}$  of the MAM solution was taken out to the conical vials with 100  $\mu\text{L}$  of ice cold internal standard o-methyl-CWB-20145 (**3**  $\mu\text{M}$  in acetonitrile) inside.
4. The solutions in conical vials were sonicated for 10 sec and spin down at 10,000 rpm for 5 minutes.
5. 100  $\mu\text{L}$  the supernatant was transferred to Spin-X HPLC filter tubes (Corning Incorporated no: 8169), centrifuged at 13,000 rpm for 5 minutes.
6. 50  $\mu\text{L}$  of the flow-through solution was dilute by LCMS grade CH<sub>3</sub>CN (466.7  $\mu\text{L}$ ) and H<sub>2</sub>O (0.1% FA) (483.3  $\mu\text{L}$ ) to 1 mL.
7. Then transfer 1 mL to glass auto sampler vial (Fischer scientific) in 2 mL (Microsolv no: 95025-WCV) and analyzed by LCMS/MS (Shimadzu 8040). All experiments were conducted in triplet.

#### 3.6.10 Liver Pharmacokinetic Assay Protocol

##### **Internal Standard: IS (100 ng/mL) in cold methanol.**

1. CD-1 female mice were dosed with FAN-NM-CH<sub>3</sub> (10/mg/kg) for collecting blood (using BD 1ml TB syringe, REF 309626) after different time points (1, 3, 5, 7, 10, 13, 18, 30, 40, 60 & 120 min - 3 mice for each time point).

2. Liver tissue were collected into 2ml cryo vial (Thermo scientific nunc. 368632), freezed in ice and stored in liquid nitrogen.
3. Whole liver tissue were thawed over ice, washed with buffer, weighed and collected on new 2 ml tube prior to homogenization.
4. Samples were homogenized and using a cole palmer LabGen 7B homogenizer (10 sec and medium speed – 4).
5. Methanol containing internal standard (100 ng/mL) was added to deproteinize according to sample weight, vortexed, ultra-sonicated for 10 min and centrifuged at 10,000 rpm for 5 minutes and the supernatant layer transferred to Spin-X® Centrifuge Tube Filters (vwr catalog no. 29442-760).
6. Supernatant was spin filtered at 10,000 rpm for 5 minutes.
7. 150uL of that filtered sample was then transferred to LC-MS vial for analysis.

#### 3.6.11 Brain Pharmacokinetic Assay Protocol

##### **Internal Standard: IS (100 ng/mL) in cold methanol.**

- i. CD-1 female mice were dosed with FAN-NM-CH3 (10 mg/kg) for collecting blood (using BD 1ml TB syringe, REF. 309626) after different time points (1, 3 , 5, 7, 10, 13, 18, 30, 40, 60 & 120 min - 3 mice for each time point).
- ii. Brain tissue were collected into 2 ml cryo vial (Thermo scientific nunc. 368632), freezed in ice and stored in liquid nitrogen.
- iii. Whole brain tissue were thawed over ice, washed and vacuum filtered with buffer (Corning 451201), weighed and collected on new 2 ml tube prior to homogenization.
- iv. Samples were homogenized and using a cole palmer LabGen 7B homogenizer (10 sec and medium speed – 4).

- v. Methanol (100 ng/mL) was added to deproteinize, vortexed, ultra-sonicated for 10 min and centrifuged at 10,000 rpm for 5 minutes and the supernatant layer transferred to Spin-X® Centrifuge Tube Filters (vwr catalog no. 29442-760).
- vi. Supernatant was spin filtered tubes at 10,000 rpm for 5 minutes.
- vii. 150 uL of that filtered sample was then transferred to LC-MS vial for analysis.

### 3.7 Reference

- (1) Rajski, S. R.; Williams, R. M. DNA Cross-Linking Agents as Antitumor Drugs. *Chem. Rev.* **1998**, *98* (8), 2723–2796. <https://doi.org/10.1021/cr9800199>.
- (2) Ralhan, R.; Kaur, J. Alkylating Agents and Cancer Therapy. *Expert Opin. Ther. Pat.* **2007**, *17* (9), 1061–1075. <https://doi.org/10.1517/13543776.17.9.1061>.
- (3) Zhou, Y.; Hileman, E. O.; Plunkett, W.; Keating, M. J.; Huang, P. Free Radical Stress in Chronic Lymphocytic Leukemia Cells and Its Role in Cellular Sensitivity to ROS-Generating Anticancer Agents. *Blood* **2003**, *101* (10), 4098–4104. <https://doi.org/10.1182/blood-2002-08-2512>.
- (4) Kamiguti, A. S.; Serrander, L.; Lin, K.; Harris, R. J.; Cawley, J. C.; Allsup, D. J.; Slupsky, J. R.; Krause, K.-H.; Zuzel, M. Expression and Activity of NOX5 in the Circulating Malignant B Cells of Hairy Cell Leukemia. *J. Immunol.* **2005**, *175* (12), 8424–8430. <https://doi.org/10.4049/jimmunol.175.12.8424>.
- (5) Szatrowski, T. P.; Nathan, C. F. Production of Large Amounts of Hydrogen Peroxide by Human Tumor Cells. *Cancer Res.* **1991**, *51* (3), 794–798.
- (6) Hole, P. S.; Zabkiewicz, J.; Munje, C.; Newton, Z.; Pearn, L.; White, P.; Marquez, N.; Hills, R. K.; Burnett, A. K.; Tonks, A.; Darley, R. L. Overproduction of NOX-Derived ROS in AML Promotes Proliferation and Is Associated with Defective Oxidative Stress Signaling. *Blood* **2013**, *122* (19), 3322–3330. <https://doi.org/10.1182/blood-2013-04-491944>.
- (7) Weinstain, R.; Savariar, E. N.; Felsen, C. N.; Tsien, R. Y. In Vivo Targeting of Hydrogen Peroxide by Activatable Cell-Penetrating Peptides. *J. Am. Chem. Soc.* **2014**, *136* (3), 874–877. <https://doi.org/10.1021/ja411547j>.
- (8) Vadukoot, A. K.; AbdulSalam, S. F.; Wunderlich, M.; Pullen, E. D.; Landero-Figueroa, J.; Mulloy, J. C.; Merino, E. J. Design of a Hydrogen Peroxide-Activatable Agent That Specifically Targets Cancer Cells. *Bioorg. Med. Chem.* **2014**, *22* (24), 6885–6892. <https://doi.org/10.1016/j.bmc.2014.10.029>.
- (9) Sen, S.; Kawahara, B.; Chaudhuri, G. Maintenance of Higher H<sub>2</sub>O<sub>2</sub> Levels, and Its Mechanism of Action to Induce Growth in Breast Cancer Cells: Important Roles of Bioactive Catalase and PP2A. *Free Radic. Biol. Med.* **2012**, *53* (8), 1541–1551. <https://doi.org/10.1016/j.freeradbiomed.2012.06.030>.
- (10) Saxon, E.; Peng, X. Recent Advances in Hydrogen Peroxide Responsive Organoborons for Biological and Biomedical Applications. *ChemBioChem* **2022**, *23* (3), e202100366. <https://doi.org/10.1002/cbic.202100366>.
- (11) Cadahía, J. P.; Previtali, V.; Troelsen, N. S.; Clausen, M. H. Prodrug Strategies for Targeted Therapy Triggered by Reactive Oxygen Species. *MedChemComm* **2019**, *10* (9), 1531–1549. <https://doi.org/10.1039/C9MD00169G>.
- (12) Yang, W.; Gao, X.; Wang, B. Biological and Medicinal Applications of Boronic Acids. In *Boronic Acids*; John Wiley & Sons, Ltd, 2005; pp 481–512. <https://doi.org/10.1002/3527606548.ch13>.
- (13) Cao, S.; Wang, Y.; Peng, X. ROS-Inducible DNA Cross-Linking Agent as a New Anticancer Prodrug Building Block. *Chem. – Eur. J.* **2012**, *18* (13), 3850–3854. <https://doi.org/10.1002/chem.201200075>.
- (14) Cao, S.; Wang, Y.; Peng, X. The Leaving Group Strongly Affects H<sub>2</sub>O<sub>2</sub>-Induced DNA Cross-Linking by Arylboronates. *J. Org. Chem.* **2014**, *79* (2), 501–508. <https://doi.org/10.1021/jo401901x>.
- (15) Chen, W.; Balakrishnan, K.; Kuang, Y.; Han, Y.; Fu, M.; Gandhi, V.; Peng, X. Reactive Oxygen Species (ROS) Inducible DNA Cross-Linking Agents and Their Effect on Cancer Cells and Normal Lymphocytes. *J. Med. Chem.* **2014**, *57* (11), 4498–4510. <https://doi.org/10.1021/jm401349g>.
- (16) Chen, W.; Fan, H.; Balakrishnan, K.; Wang, Y.; Sun, H.; Fan, Y.; Gandhi, V.; Arnold, L. A.; Peng, X. Discovery and Optimization of Novel Hydrogen Peroxide Activated Aromatic Nitrogen Mustard Derivatives as Highly Potent Anticancer Agents. *J. Med. Chem.* **2018**, *61* (20), 9132–9145. <https://doi.org/10.1021/acs.jmedchem.8b00559>.
- (17) Chen, W.; Han, Y.; Peng, X. Aromatic Nitrogen Mustard-Based Prodrugs: Activity, Selectivity, and

- the Mechanism of DNA Cross-Linking. *Chem. – Eur. J.* **2014**, *20* (24), 7410–7418. <https://doi.org/10.1002/chem.201400090>.
- (18) Kuang, Y.; Balakrishnan, K.; Gandhi, V.; Peng, X. Hydrogen Peroxide Inducible DNA Cross-Linking Agents: Targeted Anticancer Prodrugs. *J. Am. Chem. Soc.* **2011**, *133* (48), 19278–19281. <https://doi.org/10.1021/ja2073824>.
- (19) Wang, Y.; Fan, H.; Balakrishnan, K.; Lin, Z.; Cao, S.; Chen, W.; Fan, Y.; Guthrie, Q. A.; Sun, H.; Teske, K. A.; Gandhi, V.; Arnold, L. A.; Peng, X. Hydrogen Peroxide Activated Quinone Methide Precursors with Enhanced DNA Cross-Linking Capability and Cytotoxicity towards Cancer Cells. *Eur. J. Med. Chem.* **2017**, *133*, 197–207. <https://doi.org/10.1016/j.ejmech.2017.03.041>.
- (20) Daum, S.; Chekhun, V. F.; Todor, I. N.; Lukianova, N. Yu.; Shvets, Y. V.; Sellner, L.; Putzker, K.; Lewis, J.; Zenz, T.; de Graaf, I. A. M.; Groothuis, G. M. M.; Casini, A.; Zozulia, O.; Hampel, F.; Mokhir, A. Improved Synthesis of N-Benzylaminoferrocene-Based Prodrugs and Evaluation of Their Toxicity and Antileukemic Activity. *J. Med. Chem.* **2015**, *58* (4), 2015–2024. <https://doi.org/10.1021/jm5019548>.
- (21) Hagen, H.; Marzenell, P.; Jentsch, E.; Wenz, F.; Veldwijk, M. R.; Mokhir, A. Aminoferrocene-Based Prodrugs Activated by Reactive Oxygen Species. *J. Med. Chem.* **2012**, *55* (2), 924–934. <https://doi.org/10.1021/jm2014937>.
- (22) Schikora, M.; Reznikov, A.; Chaykovskaya, L.; Sachinska, O.; Polyakova, L.; Mokhir, A. Activity of Aminoferrocene-Based Prodrugs against Prostate Cancer. *Bioorg. Med. Chem. Lett.* **2015**, *25* (17), 3447–3450. <https://doi.org/10.1016/j.bmcl.2015.07.013>.
- (23) Jiang, Q.; Zhong, Q.; Zhang, Q.; Zheng, S.; Wang, G. Boron-Based 4-Hydroxytamoxifen Bioisosteres for Treatment of de Novo Tamoxifen Resistant Breast Cancer. *ACS Med. Chem. Lett.* **2012**, *3* (5), 392–396. <https://doi.org/10.1021/ml3000287>.
- (24) Liu, J.; Zheng, S.; Akerstrom, V. L.; Yuan, C.; Ma, Y.; Zhong, Q.; Zhang, C.; Zhang, Q.; Guo, S.; Ma, P.; Skripnikova, E. V.; Bratton, M. R.; Pannuti, A.; Miele, L.; Wiese, T. E.; Wang, G. Fulvestrant-3 Boronic Acid (ZB716): An Orally Bioavailable Selective Estrogen Receptor Downregulator (SERD). *J. Med. Chem.* **2016**, *59* (17), 8134–8140. <https://doi.org/10.1021/acs.jmedchem.6b00753>.
- (25) Dharmaraja, A. T.; Ravikumar, G.; Chakrapani, H. Arylboronate Ester Based Diazeniumdiolates (BORO/NO), a Class of Hydrogen Peroxide Inducible Nitric Oxide (NO) Donors. *Org. Lett.* **2014**, *16* (10), 2610–2613. <https://doi.org/10.1021/ol5010643>.
- (26) Ravikumar, G.; Bagheri, M.; Saini, D. K.; Chakrapani, H. A Small Molecule for TheraNOstic Targeting of Cancer Cells. *Chem. Commun.* **2017**, *53* (100), 13352–13355. <https://doi.org/10.1039/C7CC08526E>.
- (27) Kim, E.-J.; Bhuniya, S.; Lee, H.; Kim, H. M.; Cheong, C.; Maiti, S.; Hong, K. S.; Kim, J. S. An Activatable Prodrug for the Treatment of Metastatic Tumors. *J. Am. Chem. Soc.* **2014**, *136* (39), 13888–13894. <https://doi.org/10.1021/ja5077684>.
- (28) Kumar, R.; Han, J.; Lim, H.-J.; Ren, W. X.; Lim, J.-Y.; Kim, J.-H.; Kim, J. S. Mitochondrial Induced and Self-Monitored Intrinsic Apoptosis by Antitumor Theranostic Prodrug: In Vivo Imaging and Precise Cancer Treatment. *J. Am. Chem. Soc.* **2014**, *136* (51), 17836–17843. <https://doi.org/10.1021/ja510421q>.
- (29) Fan, H.; Zaman, M. A. U.; Chen, W.; Ali, T.; Campbell, A.; Zhang, Q.; Setu, N. I.; Saxon, E.; Zahn, N. M.; Benko, A. M.; Arnold, L. A.; Peng, X. Assessment of Phenylboronic Acid Nitrogen Mustards as Potent and Selective Drug Candidates for Triple-Negative Breast Cancer. *ACS Pharmacol. Transl. Sci.* **2021**, *4* (2), 687–702. <https://doi.org/10.1021/acspsci.0c00092>.
- (30) Brown, N. S.; Bicknell, R. Hypoxia and Oxidative Stress in Breast Cancer Oxidative Stress - Its Effects on the Growth, Metastatic Potential and Response to Therapy of Breast Cancer. *Breast Cancer Res.* **2001**, *3* (5), 323. <https://doi.org/10.1186/bcr315>.
- (31) Lim, S. D.; Sun, C.; Lambeth, J. D.; Marshall, F.; Amin, M.; Chung, L.; Petros, J. A.; Arnold, R. S. Increased Nox1 and hydrogen peroxide in prostate cancer. *The Prostate* **2005**, *62* (2), 200–207. <https://doi.org/10.1002/pros.20137>.

- (32) Pelicano, H.; Carney, D.; Huang, P. ROS Stress in Cancer Cells and Therapeutic Implications. *Drug Resist. Updat.* **2004**, *7* (2), 97–110. <https://doi.org/10.1016/j.drug.2004.01.004>.
- (33) Holliday, D. L.; Speirs, V. Choosing the Right Cell Line for Breast Cancer Research. *Breast Cancer Res.* **2011**, *13* (4), 215. <https://doi.org/10.1186/bcr2889>.
- (34) Foulkes, W. D.; Smith, I. E.; Reis-Filho, J. S. Triple-Negative Breast Cancer. *N. Engl. J. Med.* **2010**, *363* (20), 1938–1948. <https://doi.org/10.1056/NEJMra1001389>.
- (35) Brenton, J. D.; Carey, L. A.; Ahmed, A. A.; Caldas, C. Molecular Classification and Molecular Forecasting of Breast Cancer: Ready for Clinical Application? *J. Clin. Oncol.* **2005**, *23* (29), 7350–7360. <https://doi.org/10.1200/JCO.2005.03.3845>.
- (36) Chavez, K. J.; Garimella, S. V.; Lipkowitz, S. Triple Negative Breast Cancer Cell Lines: One Tool in the Search for Better Treatment of Triple Negative Breast Cancer. *Breast Dis.* **2010**, *32* (1–2), 35–48. <https://doi.org/10.3233/BD-2010-0307>.
- (37) Rouzier, R.; Perou, C. M.; Symmans, W. F.; Ibrahim, N.; Cristofanilli, M.; Anderson, K.; Hess, K. R.; Stec, J.; Ayers, M.; Wagner, P.; Morandi, P.; Fan, C.; Rabiul, I.; Ross, J. S.; Hortobagyi, G. N.; Pusztai, L. Breast Cancer Molecular Subtypes Respond Differently to Preoperative Chemotherapy. *Clin. Cancer Res.* **2005**, *11* (16), 5678–5685. <https://doi.org/10.1158/1078-0432.CCR-04-2421>.
- (38) Arnedos, M.; Bihan, C.; Delaloge, S.; Andre, F. Triple-Negative Breast Cancer: Are We Making Headway at Least? *Ther. Adv. Med. Oncol.* **2012**, *4* (4), 195–210. <https://doi.org/10.1177/1758834012444711>.
- (39) Hudis, C. A.; Gianni, L. Triple-Negative Breast Cancer: An Unmet Medical Need. *The Oncologist* **2011**, *16* (S1), 1–11. <https://doi.org/10.1634/theoncologist.2011-S1-01>.

### 3.8 Appendix A

| Tumor type    | Cell line  | IC <sub>50</sub> (μM) |              |           |
|---------------|------------|-----------------------|--------------|-----------|
|               |            | <b>12</b>             | Chlorambucil | Melphalan |
| Breast cancer | MDA-MB-468 | 2.657                 | 34.44        | 48.68     |
| Renal cancer  | UO-31      | 48.94                 | ~ 2487       | ~ 482.8   |
|               | A498       | 23.15                 | ~ 2487       | ~ 482.8   |
|               | SN12C      | 26.03                 | 134.8        | 71.03     |
|               | TK-10      | 91.06                 | ~ 209.2      | ~ 294.9   |
|               | CAKI-1     | 73.60                 | ~ 565.4      | ~ 1283    |

Summary of IC<sub>50</sub> of **12** compared with Chlorambucil and Melphalan.



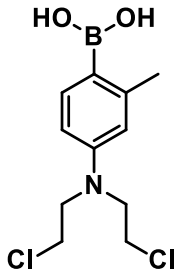
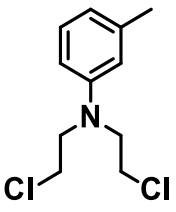
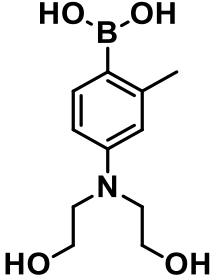
## Vehicle Treated Mice Group



## Compound **12** treated Mice Group

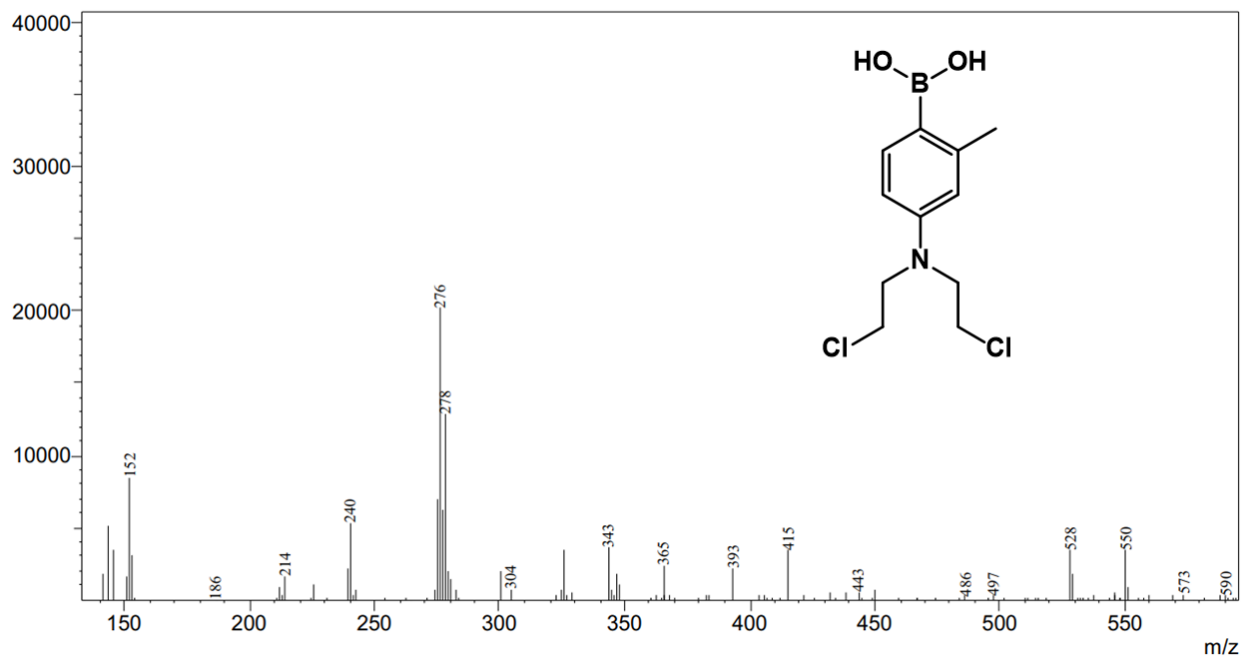


Groups of Control treated and drug (**12**) treated mice after nine weeks.

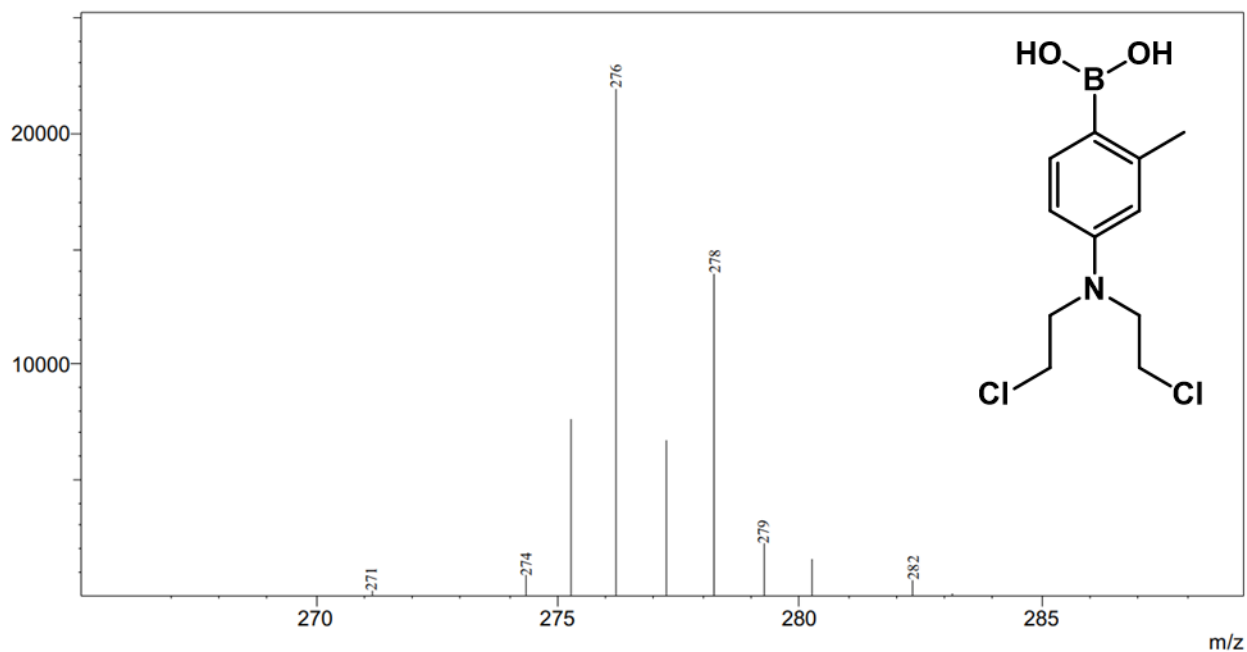
|                              |   |  |   |
|------------------------------|---|--|---|
| Incubation period:<br>6 hour |  |  |  |
| Prodrug                      | +   | -  | -   |
| Activated Drug               | -   | +  | -   |
| Media                        | -   | -  | -   |
| Media + DMSO                 | -   | -  | -   |
| Cell + DMSO                  | -   | -  | -   |
| Media + Prodrug              | +   | +  | +   |
| Cell + Prodrug               | +   | +  | +   |
| Water + Prodrug              | +   | -  | -   |

Summary of metabolite extraction study of **12**.

Event#: 1 Scan(E+) Ret. Time : [1.795->2.000]-[0.040->1.755] Scan#: [1078->1201]-[25->1054]

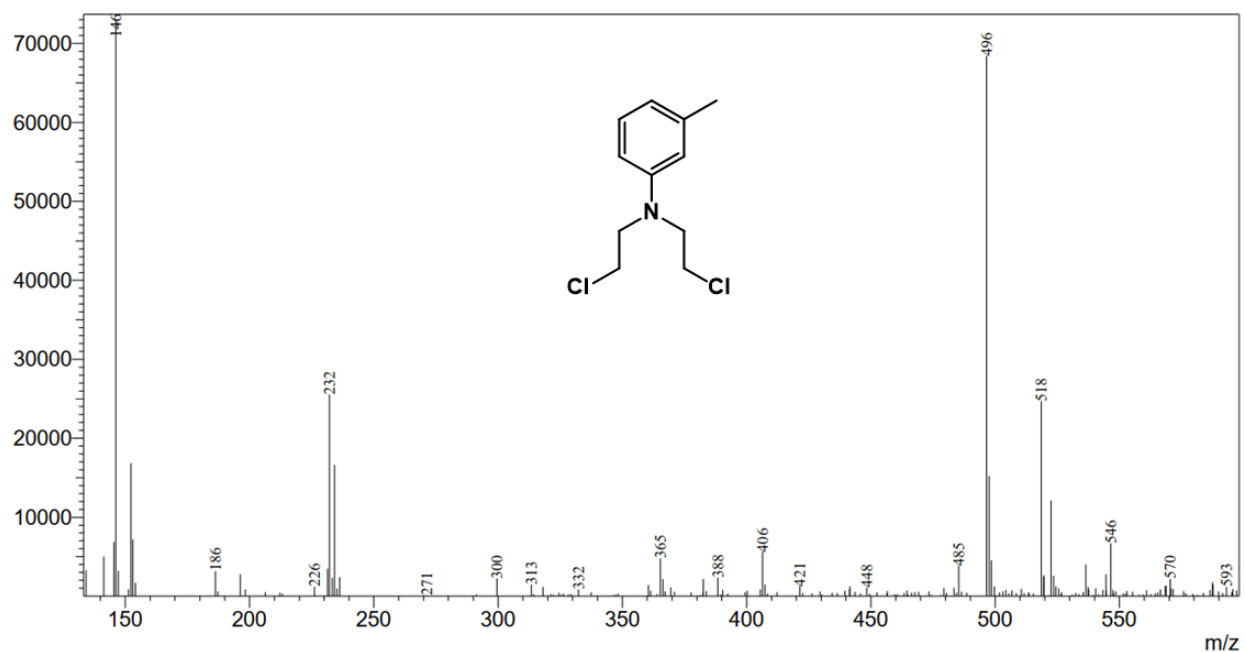


Measured region for 276 m/z



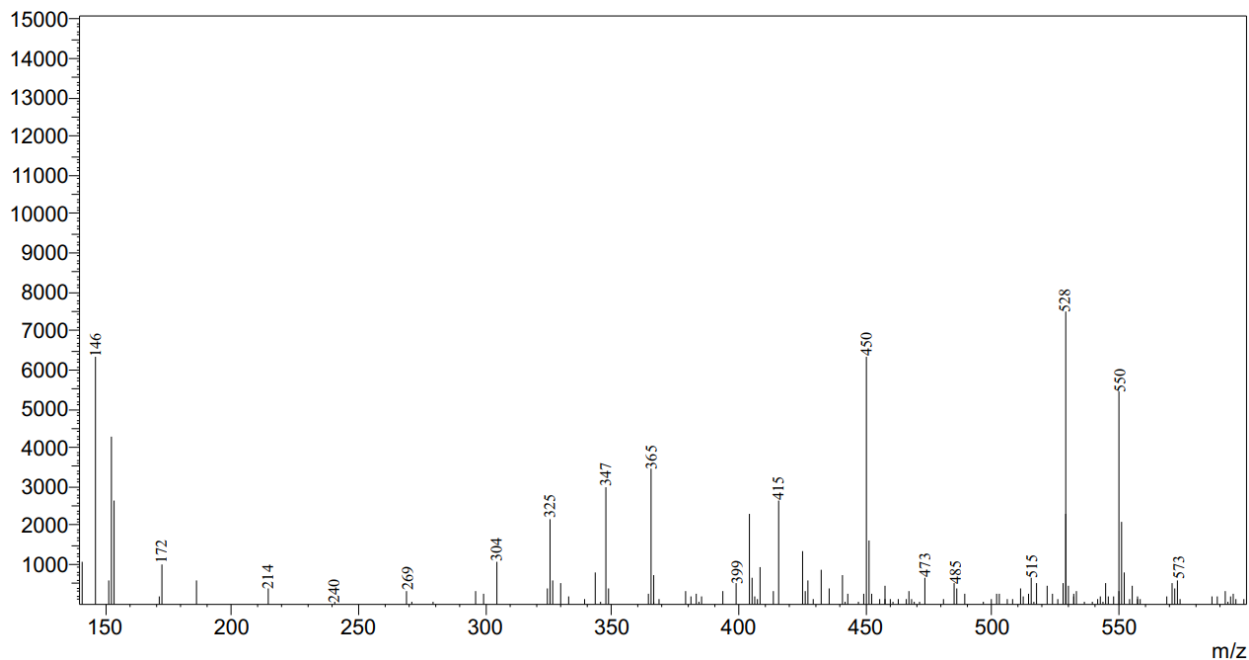
LC-MS detection of **12** in the sample obtained in cell culture media after 6 h incubation with compound **12**. Determined by an ACQUITY CSH C18 column (2.1 mm × 50 mm, 1.7 μm particle size) using gradient: 0-2.0 min 30%-60% MeCN in A, 2.0-3.0 min 60%-90% MeCN in A, 3.0-4.0 min 90% MeCN in A, 4.0-4.3 min 90%-30% MeCN in A, 4.3-6.0 min 30% MeCN in A, at a flow rate of 0.5 mL/min (Solution A: water) with 254 nm detection.

Event#: 1 Scan(E+) Ret. Time : [2.980->3.045]-[0.070->2.925] Scan# : [1789->1828]-[43->1756]



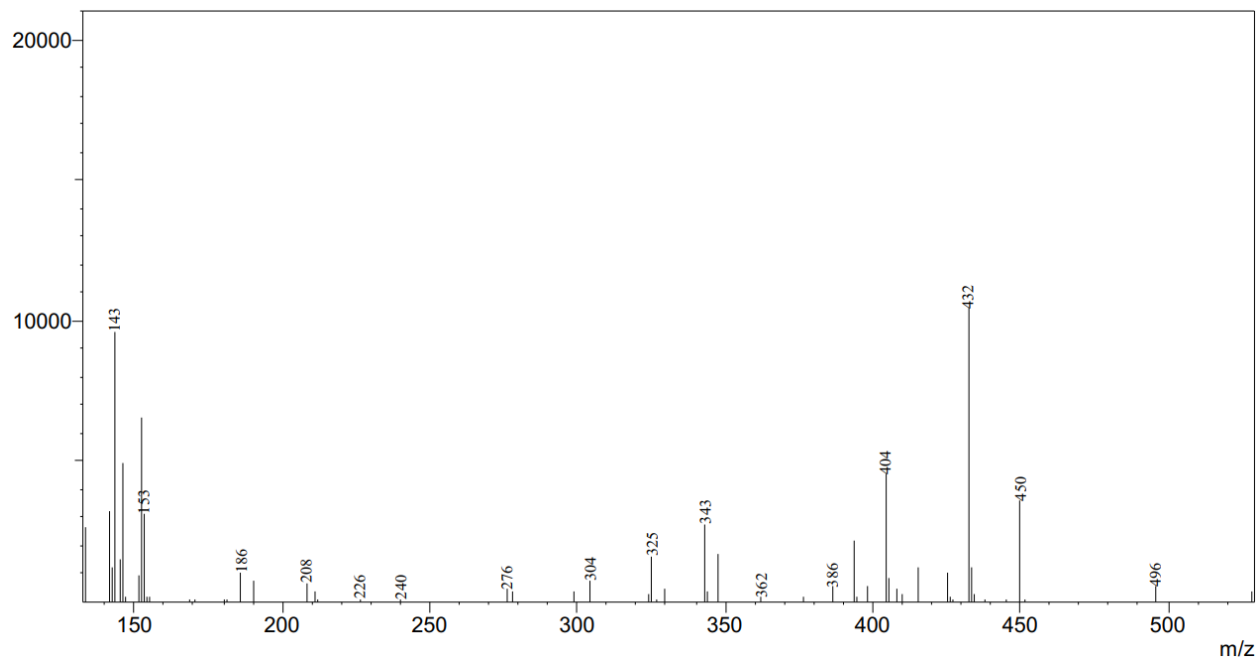
LC-MS detection of proto-deboronated **12** in the sample obtained in cell culture media after 12 h incubation with compound **12**. Determined by an ACQUITY CSH C18 column (2.1 mm × 50 mm, 1.7 μm particle size) using gradient: 0-2.0 min 30%-60% MeCN in A, 2.0-3.0 min 60%-90% MeCN in A, 3.0-4.0 min 90% MeCN in A, 4.0-4.3 min 90%-30% MeCN in A, 4.3-6.0 min 30% MeCN in A, at a flow rate of 0.5 mL/min (Solution A: water) with 254 nm detection.

Event#: 1 Scan(E+) Ret. Time : [1.810->1.990]-[0.030->1.770] Scan# : [1087->1195]-[19->1063]

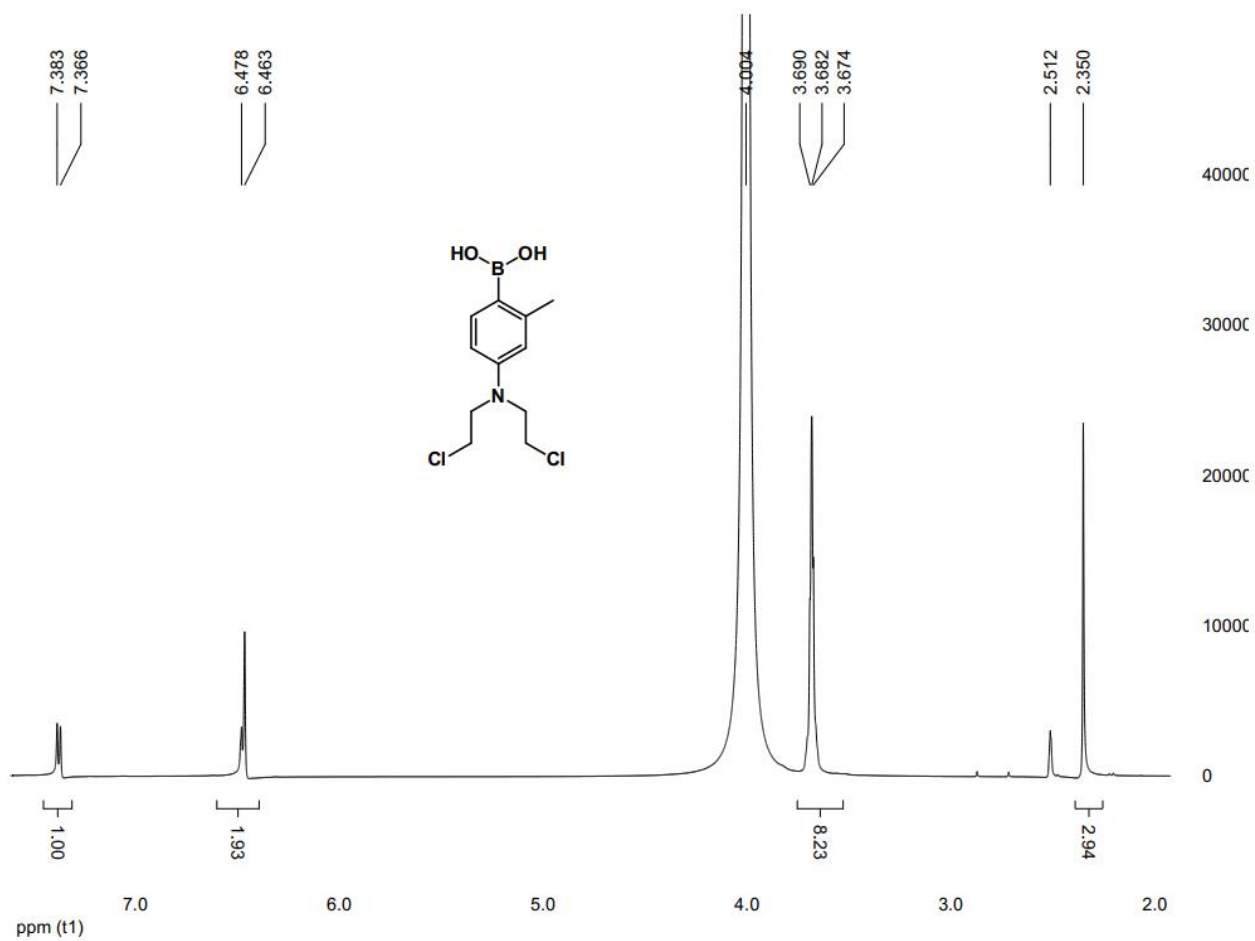


LC-MS analysis of the sample obtained in cell culture media after 12 h incubation with compound **12**. Determined by an ACQUITY CSH C18 column (2.1 mm × 50 mm, 1.7 μm particle size) using gradient: 0-2.0 min 30%-60% MeCN in A, 2.0-3.0 min 60%-90% MeCN in A, 3.0-4.0 min 90% MeCN in A, 4.0-4.3 min 90%-30% MeCN in A, 4.3-6.0 min 30% MeCN in A, at a flow rate of 0.5 mL/min (Solution A: water) with 254 nm detection.

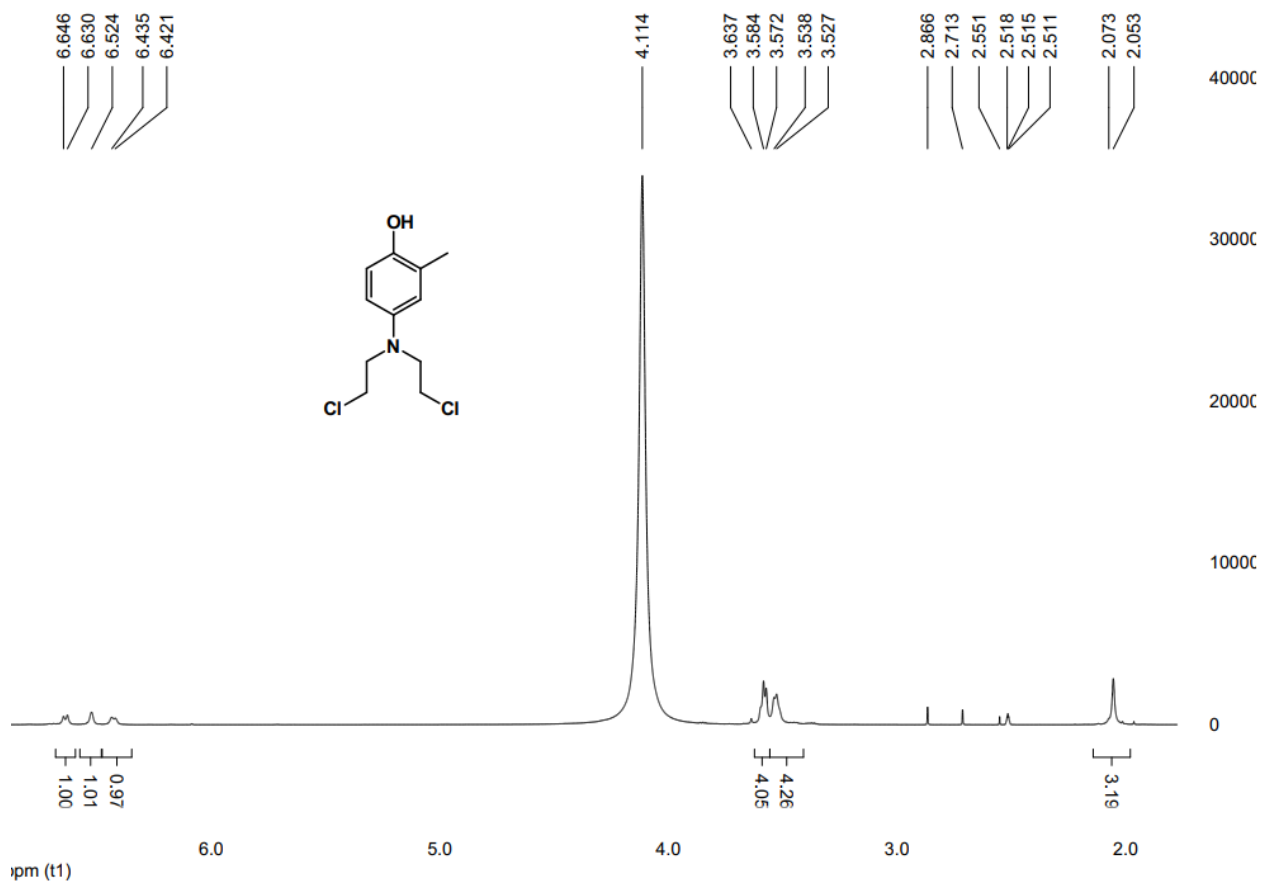
Event#: 1 Scan(E+) Ret. Time : [1.795->2.000]-[0.045->1.755] Scan# : [1078->1201]-[28->1054]



LC-MS analysis of the sample obtained from the trypsinized cells after 12 h incubation with compound **12**. Determined by an ACQUITY CSH C18 column (2.1 mm × 50 mm, 1.7 μm particle size) using gradient: 0-2.0 min 30%-60% MeCN in A, 2.0-3.0 min 60%-90% MeCN in A, 3.0-4.0 min 90% MeCN in A, 4.0-4.3 min 90%-30% MeCN in A, 4.3-6.0 min 30% MeCN in A, at a flow rate of 0.5 mL/min (Solution A: water) with 254 nm detection.



<sup>1</sup>H NMR spectrum of compound **12**.



<sup>1</sup>H NMR spectrum of compound **13**.